

ICDP DOVE Project:
Investigating the erosion and infilling of overdeepened Alpine valleys by
combining scientific drilling with geophysical exploration

Inauguraldissertation
der Philosophisch-naturwissenschaftlichen Fakultät
der Universität Bern

vorgelegt von
Sebastian Schaller
von Tentlingen (FR)

Leiter der Arbeit:
Prof. Dr. F. S. Anselmetti
Institut für Geologie & Oeschger-Zentrum für Klimaforschung
Universität Bern

Dr. M. W. Buechi
Institut für Geologie & Oeschger-Zentrum für Klimaforschung
Universität Bern

License



This work is licensed under a Creative Commons Attribution 4.0 International License
<https://creativecommons.org/licenses/by/4.0/>

ICDP DOVE Project:
Investigating the erosion and infilling of overdeepened Alpine valleys by
combining scientific drilling with geophysical exploration

Inauguraldissertation
der Philosophisch-naturwissenschaftlichen Fakultät
der Universität Bern

vorgelegt von
Sebastian Schaller
von Tentlingen (FR)

Leiter der Arbeit:
Prof. Dr. F. S. Anselmetti
Institut für Geologie & Oeschger-Zentrum für Klimaforschung
Universität Bern

Dr. M. W. Buechi
Institut für Geologie & Oeschger-Zentrum für Klimaforschung
Universität Bern

Von der Philosophisch-naturwissenschaftlichen Fakultät angenommen.

Bern, 28.02.2025

Der Dekan
Prof. Dr. Jean-Louis Reymond

Summary

The DOVE (Drilling Overdeepened Alpine Valleys) project studies the evolution of the pan-Alpine landscape during the numerous Middle and Late Pleistocene glaciations. Since glaciers often erode older records, sedimentary infills of overdeepened valleys, which are protected from subsequent glacial erosion, offer unique archives for reconstructing past glaciation, paleoclimate, and landscape evolution. Supported by the International Continental Scientific Drilling Program (ICDP), sediment cores and geophysical data from several glacially overdeepened troughs in the Northern Alpine foreland were recovered to study these processes.

Geologically, the thesis focuses on DOVE site 5068_2, where a 250-meter-thick succession of unconsolidated Quaternary sediments was recovered from the Basadingen Trough (NE Switzerland), a glacial overdeepening located in the western part of the former Rhine Glacier lobe. In the first part, the thesis focuses on reconstructing the formation history of the Basadingen Trough. Sedimentological analysis, high-resolution reflection seismic data, seismic facies analysis, and core-to-seismic correlation were combined to establish a glacio-seismic sequence stratigraphy. The valley fill was grouped into three overdeepened glacial sequences (S1–S3). These sequences reflect three separate pulses of glacial advance and retreat. A local geological 3D model was created to visualize the spatial features of these sequences. This approach overcame perspective limitations and aided in developing a local glaciation model for the Basadingen Trough.

The second focus of this thesis is the development of new approaches for the data-based and systematic investigation of glacially overdeepened valleys, adapting methods from the exploration industry. The thesis tests the potential of combining core drilling, borehole measurements, and geophysical data with advanced data analysis to improve the comparability between the different DOVE sites. Therefore, the established glacio-seismic sequence stratigraphy was developed into a more generic and adaptive model that can be applied to similar settings in formerly glaciated areas. Further, a newly developed workflow combines core drilling and borehole measurements to predict the lithology of the drilled sediments. The petrophysical and chemical borehole data-based lithoprediction was validated against core data and successfully extrapolated to a nearby borehole lacking a core, simulating an artificial core.

This study demonstrates the potential of integrating geological and geophysical datasets for systematic, data-driven investigations of glacially overdeepened valleys. The methods provide a foundation for future research in formerly glaciated landscapes, enhancing our understanding of glaciation dynamics, paleoclimate evolution, and sedimentary processes

Acknowledgment

First and foremost, I would like to extend my heartfelt thanks to the members of the DOVE Team, whose dedication and expertise made this project possible and continue to support its ongoing progress. Collaborating with you and diving into the fascinating history of the pan-Alpine landscape has been a pleasure.

I am deeply grateful to my supervisors and mentors, Prof. Dr. Flavio Anselmetti and Dr. Marius Büchi, for introducing me to the fascinating world of Quaternary geology and applied geophysical exploration and for guiding me throughout my journey as a researcher and geologist since my late bachelor studies. Your continuous encouragement, valuable professional and personal advice, and the freedom you granted me to explore various projects have guided me on my way over the past years.

I would also like to sincerely thank my co-supervisor, Prof. Dr. Fritz Schlunneger, for the interesting scientific discussions and for chairing my PhD defense. I am equally grateful to Dr. Giovanni Monegato for serving as an external referee and co-examiner during my defense.

The success of the drilling operation was only possible due to the expertise and support of many individuals and organizations. My thanks go to Fretus AG, especially the drilling crew, Juan Gonzalez, Marek Bajcura, and Joaquim Teixeira, for providing high-quality drill cores; the technical staff of the LIAG for collecting the reflection seismic data and conducting downhole logging; Katja Heeschen and the ICDP Operational Support Group for supplying the on-site MSCL scanner, the database management tool "mDis," and their thorough documentation support; Luka Seslak for his technical advice on drilling; Kim Lemke for transporting the drill cores; and all the members of the local political and private institutions and private individuals involved in the operation.

I also want to thank everyone who contributed significantly to this research. My thanks go especially to Bennet Schuster for his efforts and help with core handling, sampling, and description; Julijana Gajic and Patrizia Ruffiner for their meticulous work in processing and analyzing the TIC and TOC samples; Gerald Gabriel, Herman Bunes, and Sarah Beraus for their assistance with geophysical data processing and for facilitating my stay at the LIAG in spring 2023; Ferdinando Musso for his expertise in creating the 3D model; Stefano Fabbri for his valuable input on seismic interpretation; and David Mair and Patricio Baccera for their insights into developing wireline logging data-based lithoprediction; and to Gustaf Firla for doing the luminescence dating of the drilled sediments. I am equally grateful to Gaudenz Deplazes, Andreas Dehnert, and Erich Müller for their genuine interest in my work and for

engaging in many enriching scientific discussions. I also extend my thanks to all other members of the Geological Institute who contributed to this thesis in one way or another.

Finally, I wish to thank my dear friends, my family, and Milla for their steady support throughout this journey.

To M und m

Table of Contents

1.	Introduction and outline	3
1.1	The Quaternary	3
1.2	Glacial overdeepenings as key elements for understanding past glaciations	4
1.3	The (Northern) Alps after the MPT	6
1.3	The "Drilling Overdeepened Alpine Valley Project"(DOVE)	7
1.4	Societal relevance	9
1.5	Specific motivation and aims of the thesis	10
1.6.	Existing interpretations of the Quaternary landscape evolution around site 5068_2	11
1.7	Outline of the thesis.....	15
1.8	References	17
2.	Drilling into a deep buried valley (ICDP DOVE): a 252m long sediment succession from a glacial overdeepening in northwestern Switzerland	23
2.1	Abstract	23
2.2	Introduction	24
2.2.1	Project DOVE	25
2.2.2	Study area	26
2.3	Methods	28
2.3.1	Drilling and downhole operations.....	28
2.3.2	Core handling, description, and analysis	29
2.4	Results	32
2.4.1	Core lithologies	32
2.4.2	Lithostratigraphic units	35
2.5	Interpretation and discussion	38
2.5.1	Interpretation of depositional environment.....	38
2.5.2	Implications for glacial history	41
2.6	Summary and outlook.....	42
2.7	Further statements	43
2.7.1	Data availability.....	43
2.7.2	Sample availability	43
2.7.3	Author contributions.....	43
2.7.4	Competing interests.....	43
2.7.5	Financial support.....	44
2.7.6	Review statement	44
2.8	Acknowledgments.....	44
2.9	References	45

3.	Seismic- and core-based glacial sequence stratigraphy in an overdeepened perialpine trough in the northern Alpine foreland of Switzerland	51
3.1	Abstract	51
3.2	Introduction	52
3.2.1	Background and motivation	52
3.2.2	Study site.....	53
3.2.3	Previous work on the Basadingen Trough in the frame of the DOVE project	54
3.3	Methods	58
3.3.1	Seismic processing	58
3.3.2	Seismic facies analyses and core-to-seismic-correlation	59
3.3.3	Three-dimensional and spatial visualization and analysis of overdeepened sequences	59
3.4	Results	60
3.4.1	Seismic sequence stratigraphy and seismic facies analysis	60
3.4.2	Core-to-seismic correlation.....	62
3.4.3	3D and 2D spatial visualization of overdeepened sequences.....	65
3.5	Discussion.....	67
3.5.1	Depositional environment of the seismic sequences	67
3.5.2	Formation of the Basadingen Trough: Three overdeepened glacial sequences	70
3.5.3	The generic glacio-seismic sequence	72
3.6	Conclusion	73
3.7	Appendix	75
3.8	Further statements	75
3.8.1	Data availability.....	75
3.8.2	Competing interests.....	76
3.8.3	Funding.....	76
3.8.4	Author's contribution.....	76
3.9	Acknowledgments.....	76
3.10	References	77
4.	Wireline logging data-driven lithoprediction of unconsolidated sediments	83
4.1	Abstract	83
4.2	Introduction	84
4.2.1	Background and Motivation	84
4.2.2	Drill Site and Data Selection.....	85
4.3	Methods	88
4.3.1	Data Acquisition, Processing, and Analysis	88

4.3.2	Clustering	89
4.3.3	Classification, Evaluation, and Depth Correlation	89
4.4	Results	91
4.4.1	Data trends and impact of dimensionality reduction	91
4.4.2	Clustering Results	94
4.4.3	Lithological ground truth versus cluster-based prediction	97
4.4.4	Cross-hole correlation	97
4.5	Discussion	99
4.5.1	Importance of investigating the dataset structure	99
4.5.2	The case for dimensionality reduction	99
4.5.3	Cluster characterization and classification	100
4.5.4	Quality of cluster-based stratigraphy	102
4.5.5	Cross-hole correlation of cluster-based and core-based stratigraphies	102
4.5.6	Log catalogue	103
4.6	Conclusion	103
4.7	Appendix	105
4.7.1	Appendix Tables	105
4.7.2	Appendix Figure	108
4.8	Further statements	113
4.8.1	Data availability	113
4.8.2	Authors contribution	113
4.9	Acknowledgments	113
4.10	References	114
4.11	Digital Supplement	117
4.11.1	Tables Digital Supplement	117
4.11.2	Figures Digital Supplement	122
5.	Conclusion and outlook	129
5.1	The implications for the regional landscape evolution	129
5.2	Methodological developments	131
5.3	Practical Lessons Learned for DOVE Phase II	133
5.4	References	135
Appendix A: Drilling Overdeepened Alpine Valleys (DOVE) – Operational Report of Phase I		
Appendix B: Drilling Overdeepened Alpine Valleys (DOVE) – Explanatory remarks of Phase I		

1

Introduction and outline

1. Introduction and outline

1.1 The Quaternary

The geological period of the Quaternary, starting 2580 ka ago until today (Cohen & Gibbard, 2022), is characterized by the permanent presence of polar ice caps, the cyclic formation and decay of large northern hemisphere ice shields, and the development of glaciers and permanent ice and snow in mountainous areas all around the globe. These ice masses were in constant movement, advancing and retreating, controlled by changes in the climatic conditions. Such periodically recurrent glacial cycles left clear traces in the global marine isotope data (benthic $\delta^{18}\text{O}$; Fig. 1; Lisiecki & Raymo, 2005a), whose records allow the reconstruction of past global variations in temperature, sea level, and ice volume since the $\delta^{18}\text{O}$ correlates directly with global ice volume and inversely with the global temperature and sea level. These records further define the so-called Marine Isotope Stages (MIS), which represent either a global interglacial (warm climate with retreating glaciers; uneven MIS) or a glacial (cold climate with advancing glaciers, even MIS). The periodicity of these cycles is the product of complex overlaying cycles of orbital forcing (i.e., Milankovitch-cycles; e.g., Hinnov, 1978) and other geological and climatic factors (e.g., the position of the continents, vegetation, atmospheric composition, etc.; e.g., Maslin, 2009). In this complex system, an even minimal change in one of the individual components, so-called "tipping points", can have drastic impacts, such as the pronounced but gradual shift in the periodicity of global glacial-interglacial cycles from ~41 to 100 ka between 1250 and 700 ka ago (Fig. 1). The exact reason for this shift, recorded in the global marine isotope data, is still debated (Legrain et al., 2023). The period of this prominent shift in the periodicity of the global glacial-interglacial cycles is known as the mid-Pleistocene Climate Transition (MPT) and coincident with amplification in the reconstructed maxima and minima of the global temperature and ice volume (Fig. 1; Clark et al., 2024; Ruddiman et al., 1986). However, the global signal does not fully resolve local-to-regional variations between different areas since it is constructed from data from all around the world. Therefore, paleoclimatic archives are more sensitive to local and regional signals than global isotope records, and they need to gain more detailed insight into the local and regional variations. Promising candidates are glacially overdeepened valleys with their infill of unconsolidated terrestrial Quaternary sediments, preserving a more local paleo climatic signal.

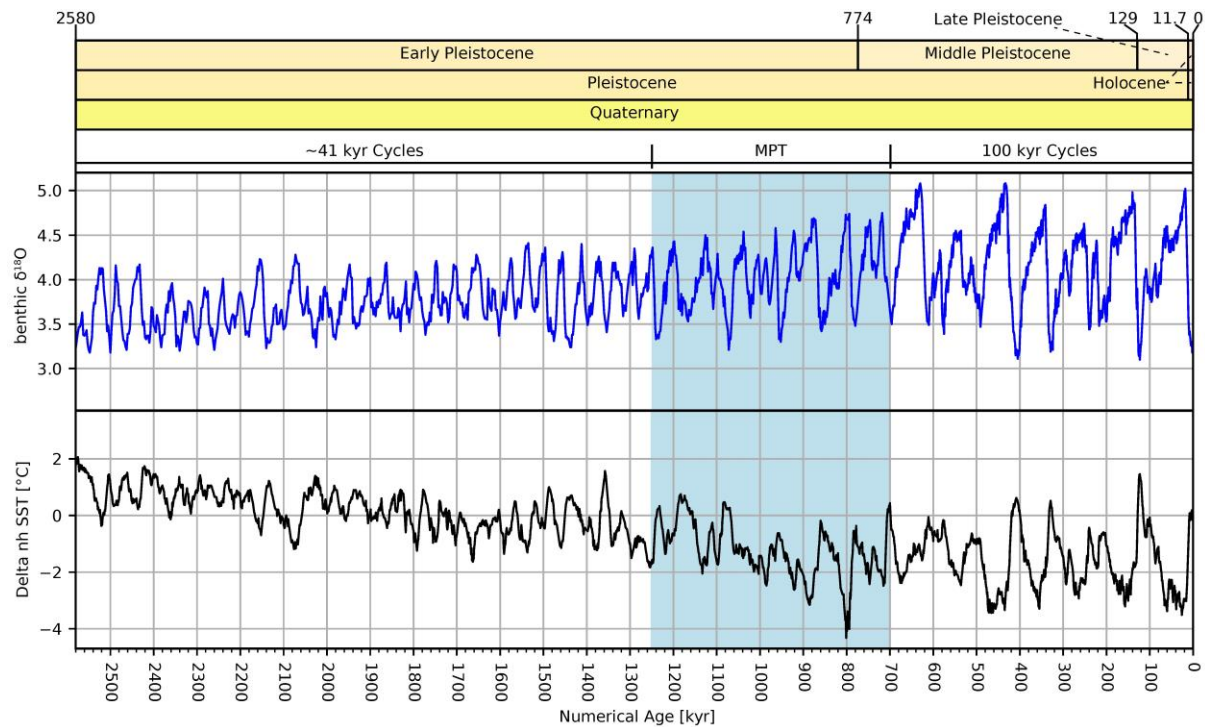


Figure 1: Overview of the stratigraphic timetable of the Quaternary period (Cohen & Gibbard, 2022), including the benthic $\delta^{18}\text{O}$ records (blue curve; after Lisiecki & Raymo, 2005b) and the reconstructed northern hemisphere sea-surface temperature (black curve; after Clark et al., 2024) together with the indicated period of the MPT and the dominant periodicity of the glacial/interglacial cycles.

1.2 Glacial overdeepenings as key elements for understanding past glaciations

Glacial overdeepened valleys and troughs occur in landscapes strongly affected by past glaciations. They are defined as structures eroded by subglacial processes reaching below the base of the lowest fluvial channels (i.e., the lowest fluvial base level) and are terminated downstream in an adverse slope (e.g., Alley et al., 2019; Cook & Swift, 2012; Kehew et al., 2012; Vegt et al., 2012). Even though these structures can reach several hundred meters below the modern surface level, they are commonly buried below the modern landscape since being refilled by sediments during deglaciation. The only direct traces on the surface are modern lakes in the mountain valleys (e.g., Lake Thun; Fabbri et al., 2018) and the foreland (e.g., Lake Constance; Schaller et al., 2022), representing the underfilled parts of these overdeepened valleys and basins, which eventually may be filled by sediments. The exact conditions leading to the initial formation or reactivation of an overdeepening are not fully understood yet. However, the occurrence and orientation of such overdeepened structures are often associated with tectonic structures, weak lithologies, and the topological forcing of ice stream flows (Preusser et al., 2010). Since the erosion and the (partial) refilling occur during a single glacial advance and retreat cycle, the valley fills remained partially protected from further glacial and fluvial erosion during later glacial advances. Therefore, these valleys can contain relatively complete or even multi-phase archives extending through several glacial cycles. A schematic

visualization of the individual stages of the development of such a stacked valley infill forming over multiple generations of erosion and refilling is displayed in Figure 2.

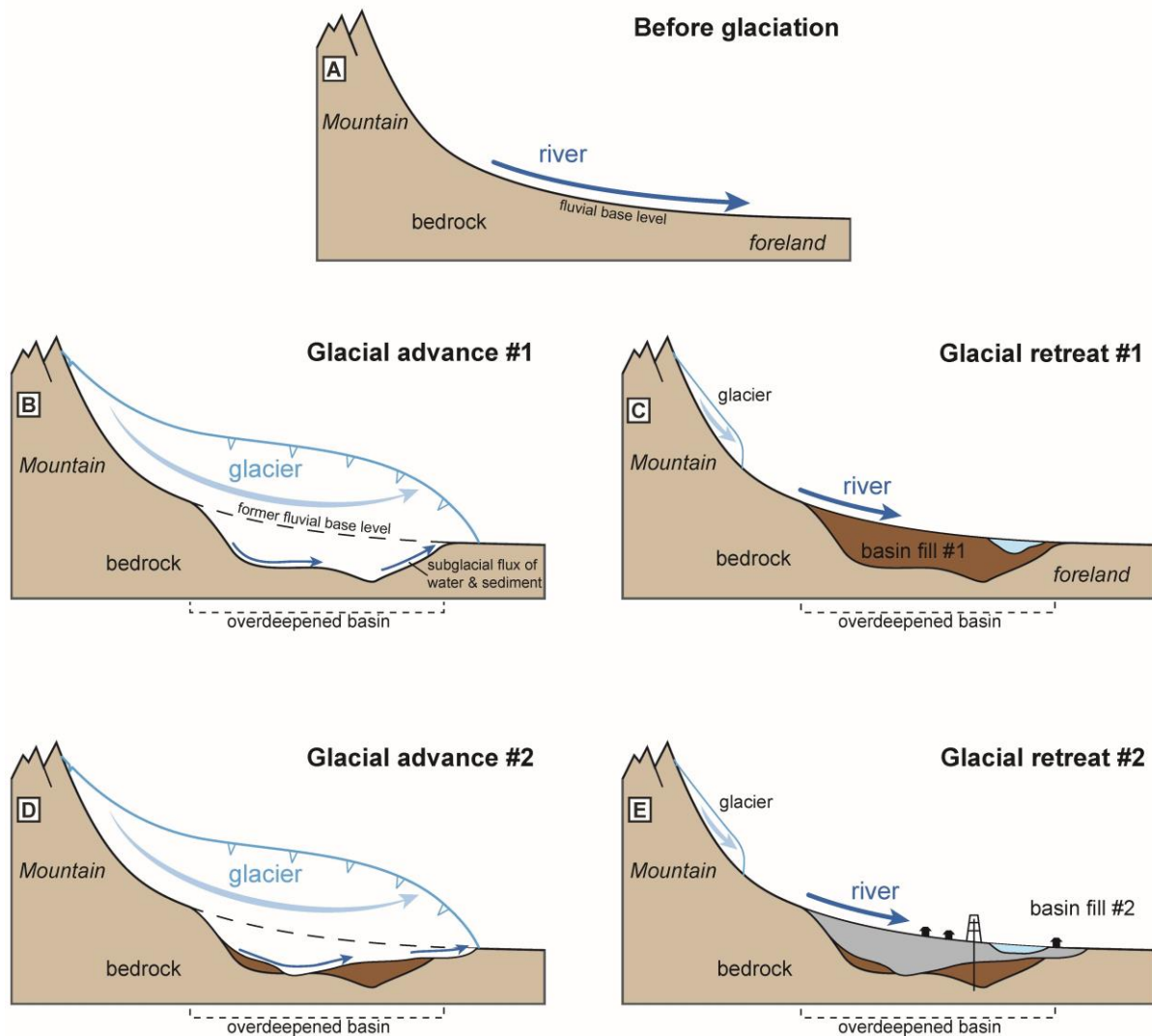


Figure 2: Schematic steps of the formation and evolution of a glacially overdeepened valley starting from a stable initial fluvial dominated landscape (A) over two glacial advances (active erosion; B and D) and retreat (active sedimentation; C and E) cycles with indicated multi-phase sedimentary infill of the basin. Further, the characteristic features of overdeepened structures are visualized: i) subglacial erosion process, ii) erosion below the fluvial base level, iii) adverse terminal slope, and iv) formation of a (temporary) lake in the underfilled parts of the valley (modified after Buechi, 2016)).

Due to their preserving character, the sedimentary infills of overdeepened valleys and troughs represent some of the most valuable terrestrial archives for understanding and reconstructing past glaciations. They are especially crucial in areas of intense past glaciation, such as the Alps, since each glacial advance tends to eliminate most traces of its preceding ones inside its area of ice extent. However, they have only moved into the focus of systematic research in the past ~10-15 years (e.g., Buechi et al., 2018, 2024; Dehnert et al., 2012; Ellwanger et al., 2011; Pomper et al., 2017; Preusser et al., 2010, 2011). This newly awakened interest in such archives was boosted by advances in dating techniques, such as cosmogenic nuclide burial and

luminescence dating. Hence, advanced dating methods, especially in combination with high-quality drill cores, represent a game changer (e.g., Dehnert et al., 2012; Fiebig et al., 2014; Schwenk et al., 2022). This combination allows for establishing an absolute chronology of a depth-controlled sedimentary profile, which is crucial for reconstructing and understanding the local glaciation history and is key to integrating the individual signals into an over-regional model. All these recent studies underline the potential and justify the significant logistical and financial effort to drill, document, and analyze these overdeepened troughs and their sediment fill.

1.3 The (Northern) Alps after the MPT

In the Alpine area, the MPT marks the onset of a phase of extensive foreland glaciations (e.g., Haeuselmann et al., 2007; Knudsen et al., 2020; Muttoni et al., 2003; Scardia et al., 2010). The Alpine glaciers tend to reach extents previously only reached by exceptionally intense pre-MPT glaciations. During such phases of extensive glaciations, numerous overdeepened troughs and valleys were carved in the (Northern) Alpine foreland (e.g., Ellwanger et al., 2011; Schlüchter, 2004). Even though the exact formation ages of these structures are still only studied punctually due to the limited amount of suitable drill cores (e.g., for the northern Alpine area: Buechi et al., 2018, 2024; Dehnert et al., 2012; Pomper et al., 2017), the studies indicate a formation during multiple glacial advance and retreat cycles. Due to the limited information, the formation and evolution of these overdeepened valleys and troughs are only resolved fragmental in the pan-Alpine area, showing many knowledge gaps in terms of i) glacial dynamic and timing of the individual glaciations and ii) environmental conditions leading to an initial formation of an overdeepened valley. Therefore, the question about the initial formation age and potential reactivations is relevant for understanding the variations in the extent and intensity between the individual glacial cycles. Recent compilations of individual regional patterns suggest a complex glacial history of the Alpine area with substantial variations in dynamics and extent of individual glaciations within the pan-Alpine area (Fig. 3; e.g., Anselmetti et al., 2022; Fiebig, 2011). The reasons for such asymmetry and asynchrony in these patterns are likely controlled or at least strongly influenced by topological aspects and local, regional, and global-scaled climate forcing such as temperature, precipitation, and circulation (e.g., Monegato et al., 2017; Spötl et al., 2021). However, without filling the main knowledge gaps, many points in the past glaciation history are left to speculation.

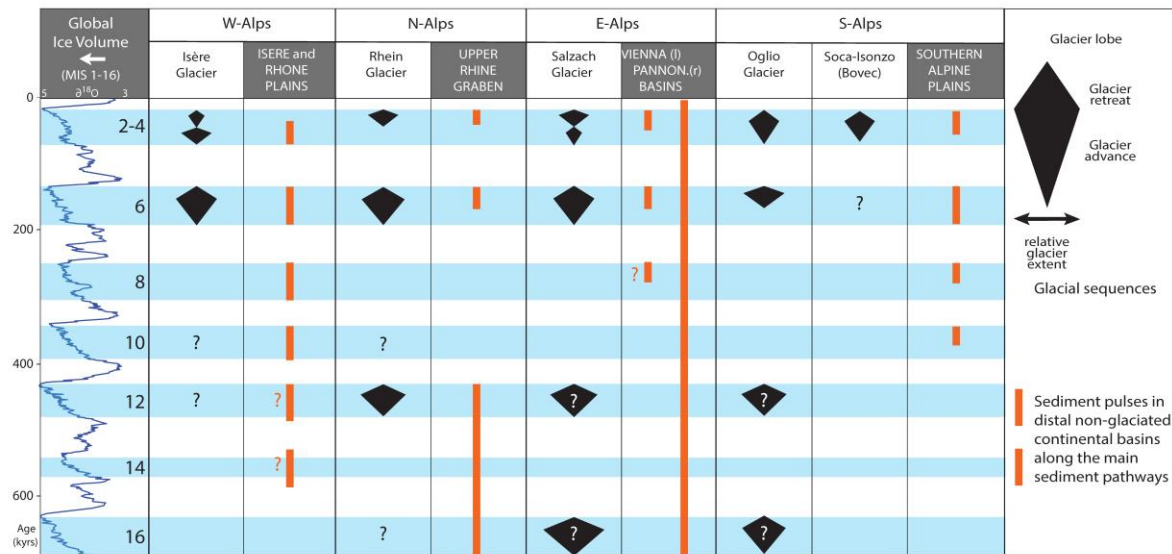


Figure 3: Compilation of the current state of knowledge of the glacial history of the pan-Alpine area during the Middle to Late Pleistocene of major glacier lobes with proposed correlation with MIS 2-16 and the benthic $\delta^{18}O$ record. Question marks indicate uncertainty in the correlation/black spots in the archives (modified after Anselmetti et al., 2022).

1.3 The "Drilling Overdeepened Alpine Valley Project"(DOVE)

Filling the main gaps in the current knowledge and enabling a better understanding of past glaciations in the pan-Alpine area during the Middle to Late Pleistocene is the primary motivation behind the International Continental Scientific Drilling Program (ICDP) project "Drilling Overdeepened Alpine Valleys" (DOVE). The project aims to quantify the assumed asymmetry in the extent and timing of past glaciations (Fig. 3) and their implications for the paleoclimate, paleolandscape, and paleoenvironmental evolution of the pan-Alpine area during the Middle to Late Pleistocene. The DOVE project uses a combined approach to investigate strategically selected glacially overdeepened valleys and troughs from ice-proximal sites around the Alpine foreland (Fig. 4) by i) executing geophysical surveys across overdeepened troughs, ii) acquiring a series of new drill cores, and iii) analyzing existing cores, which have not been fully exploited scientifically.

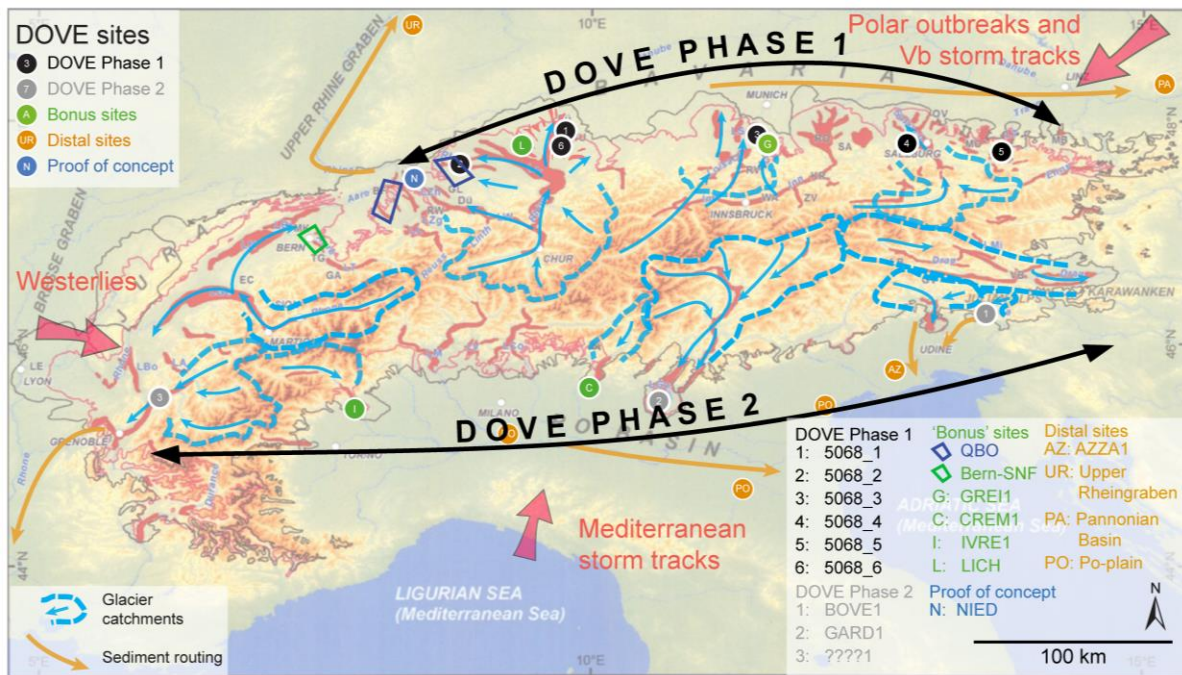


Figure 4: DOVE overview map of the pan-Alpine area with the DOVE Phase I locations (black 1-6), the planned DOVE Phase II sites (grey 1-3), and associated bonus sites (green and blue). Further, the map provides: i) the limit of the Last Glacial Maximum (LGM; pink line), ii) the maximum limit of Pleistocene glaciation (MEG; black line), iii) the location of overdeepened structures (red), iv) the direction of the major moisture sources of the pan-alpine area (red arrows), v) relevant glacial catchments of the study areas (dashed blue lines) with the main paleo-ice-flow directions (blue arrows), and vi) distal continental basins (orange circles) in the fluvial sediment pathways (arrows), providing a more continuous but indirect glaciation record (modified after Anselmetti et al., 2022; Preusser et al., 2010).

The project is divided into two phases (Fig. 4; Anselmetti et al., 2022): Phase I (started in early 2021) covers the northern and northeastern parts (Switzerland, Germany, and Austria), and Phase II (planned start for 2025/2026) the southern and western parts of the Alpine foreland (Slovenia, Italy, and France). Phase I comprises three drill cores from the former Rhine Glacier area (two newly drilled cores: 5068_1_C and 5068_2_A, and one "legacy" core: 5068_6_A), one legacy core from the former Isar-Loisach Glacier area (5068_3_A), one legacy core from the former Salzach Glacier area (5068_4_A), and one legacy core from the former Traun Glacier area (5068_5_A), a more detailed overview of the used cores is given in Table 1. The exact locations for Phase II have not yet been selected. However, it is scheduled to acquire three drillcores: one from the Bovec Glacier area (Slovenia), one from the Garda Glacier area (Italy), and one from the Rhone or Isere Glacier area (France). The DOVE project follows an integrative approach in terms of data analysis over several levels to achieve its final goal:

- | | |
|----------|--|
| Level I | The individual drill cores are analyzed following standard protocols and systematics, ensuring as much comparability as possible, and are integrated into the local geological context |
| Level II | The individual sites will be integrated into their extended regional system (i.e., the individual glacier lobes) |

- Level III The individual glacier systems are further integrated into areas of assumed similar paleoclimatic conditions, e.g., Northern Alpine area (Phase I), Southeastern Alpine Area (Phase II), and Western Alpine Area (Phase II)
- Level IV Overall DOVE synthesis and integration over the entire pan-Alpine area

Table 1: Compilation of the six drill cores included in DOVE Phase I

Nr (Fig. 4)	ICDP Borehole	IGSN	Glacier area	Country	Lat. [°] (WGS84)	Long. [°] (WGS84)	Elevation [m a.s.l.]	Length [m]	Year of Drilling
1	5068_1_C	ICDP5068 EH70001	Rhein	DE	47.9996	9.7490	588.1	164.25	2021
2	5068_2_A	ICDP5068 EH40001	Rhein	CH	47.6481	8.7533	445.1	252	2021
3	5068_3_A	ICDP5068 EHC0001	Isar- Loisach	DE	47.9710	11.4601	644	198.8	2017
4	5068_4_A	ICDP5068 EHD0001	Salzach	DE	47.8629	12.9098	445.4	136	2009
5	5068_5_A	ICDP5068 EHE0001	Traun	AT	47.6070	13.7741	714.1	880	1998
6	5068_6_A	ICDP5068 EHG0001	Rhein	DE	47.8880	9.7113	607	144	2016

1.4 Societal relevance

The relevance of systematic investigation of the formation and distribution of glacially overdeepened valleys and troughs in the densely populated Alpine Foreland goes far beyond the purely scientific motivation of the DOVE project. First, these features provide crucial insights into the paleoclimate of the Middle and Late Pleistocene, enabling more accurate reconstructions of past climatic conditions. This understanding is vital for predicting future climate change impacts and addressing related challenges in the Alpine region.

Moreover, glacial overdeepenings have critical implications for various applied fields. Understanding their formation, distribution, and geometry is essential for ensuring the long-term safety of nuclear waste repositories, managing groundwater resources, and assessing earthquake risks to critical infrastructure. These structures also play a crucial role in geothermal energy exploration and storage and supplying construction materials like gravel and sand. Additionally, subsurface knowledge is critical in planning and constructing large-scale underground infrastructure, such as railway tunnels. Historical tragedies, such as the 1908 Lötschberg Tunnel disaster in the Bernese Alps, Switzerland, illustrate the importance of profound knowledge of the geological subsurface. Workers unexpectedly encountered an overdeepened structure filled with unconsolidated Quaternary sediments and freely circulating groundwater during its construction, causing the tragic deaths of 25 miners. This example highlighted the risks of inadequate geological understanding for subsurface construction work.

1.5 Specific motivation and aims of the thesis

This thesis is integral to DOVE Phase I and is aligned with the project's core scientific motivations and goals. The study focuses on DOVE site 5068_2 (BASA) and the Basadingen Trough, a glacial overdeepened valley in Northern Switzerland (Fig. 4). The drill core 5068_2_A (BASA_A) is the first-ever ICDP drill core recovered from Swiss territory. Consequently, the primary objectives of the thesis, following Level I of the DOVE approach, are to:

- I) Recover and analyze the drill core
- II) Integrate the sedimentary archive into the local geological system
- III) Develop a local formation and evolution model for the Basadingen Trough

To achieve these aims, the thesis investigates the potential of combining (core) drilling, high-resolution reflection seismic data, and petrophysical borehole measurements for the systematic and data-driven investigation of glacially overdeepened valleys and their sedimentary infill. Even though such integrated methodologies are standard in the (energy) exploration industries (i.e., hydrocarbon, geothermal, groundwater, etc.), they were rarely applied systematically to investigate terrestrial Quaternary sediments in the past, despite the high potential for investigating subsurface geology. Therefore, establishing a systematic and data-based approach is crucial for analyzing glacial overdeepened structures and their sediments. Such an approach is especially vital to DOVE since the geometry and shape bear essential information about the formation and development of the individual overdeepenings. The combined approach aims to achieve this by surpassing the individual components' limitations and maximizing the information gained from the subsurface geology by:

- I) Calibrating and linking the seismic data with high-resolution core and borehole data
- II) Investigating advanced data analysis techniques for the analysis of core and borehole datasets
- III) Integrating and up-scaling the information from the boreholes and drill cores with the seismic data into 2D or 3D

Additionally, the thesis aims to develop a conceptual formation model linking the depositional processes with the resulting morphology by incorporating direct core-based sedimentological information with seismic-based architectural elements. Such a model is crucial for a general understanding of the formation and evolution of glacially overdeepened valleys and their infill. This understanding is key for a robust and reliable comparison and correlation between the

individual DOVE sites and, therefore, for the whole project. Furthermore, this work aims to demonstrate the potential for transferring methods from the exploration industry to new geological contexts. The potential of such applications, especially in combination with advanced data analysis methods, goes beyond the specific goals of the DOVE project.

1.6. Existing interpretations of the Quaternary landscape evolution around site 5068_2

The local landscape evolution of the closer area of DOVE–Site 5068_2 (i.e., the area between the rivers Rhine and Thur; Fig. 5) during the Middle and Late Pleistocene has been intensively studied during the last ~30 years, predominantly for groundwater exploration as well as in the broader frame of the site evaluation process for the longterm radioactive waste repository of Switzerland (e.g., Buechi et al., 2024; Dieleman et al., 2022; Graf, 2009; Müller, 1995, 2013; Preusser et al., 2011)

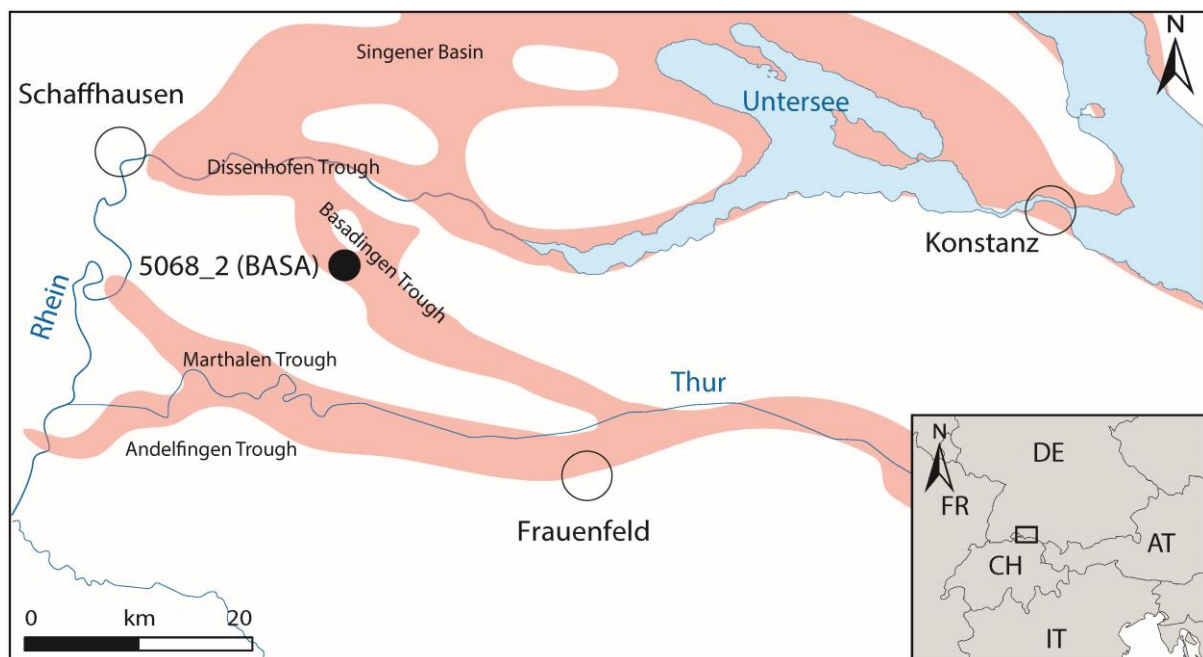


Figure 5: Overview of the surrounding area of Dove site 5068_2 with its major overdeepened troughs and basins (indicated in pale red; after Ellwanger et al., 2011).

Traces of 11 local glacial advances of the Rhine Glacier into the study area have been documented for the Middle and Late Pleistocene (Graf, 2009) and were grouped into five regional glacial periods (i.e., Möhlin Glacial, Habsburg Glacial, Hagenholz Glacial, Beringen Glacial, and Birrfeld Glacial) that are separated by interglacials (i.e., Thalgut, "Habsburg/Hagenholz", Meikirch, and Eemian). An overview of the relevant terms of Swiss stratigraphic nomenclature (i.e., Advance, Glaciation, and Glacial) is given in Graf & Burkhalter (2016). These locally defined glacial and interglacial periods can be correlated with the global marine isotope stages (e.g., Buechi et al., 2024), enabling a link between the global

and the local climate signal and setting them into a chronological context (Fig. 6), which is crucial for a regional correlation between different stratigraphic systematics. Due to the fragmented character of the direct traces of the past glaciations and limited direct age control, there are some variations and debated points between individual models for the landscape evolution (e.g., Graf, 2009; Müller, 2013; Preusser et al., 2011), such as:

- I) The timing of the Habsburg Glacial
- II) The existence of the Hagenholz Glacial
- III) The local stratigraphic interpretation of individual (glacio)-fluvial gravel deposits (i.e., Buechberg Gravel)
- IV) The exact formation period of individual glacially overdeepened valleys

However, there is a consensus about the bigger picture, the main steps of the development:

- I) The Möhlin Glacial includes the MEG-advance
- II) The existence of at least three generations of glacially overdeepenings
- III) Each glacial/interglacial transition tends to initiate a reorganization of the landscape, often leading to a change in the fluvial base level and the erosion and deposition of (glacio)fluvial gravels
- IV) The river Rhine was forced to change its path at the end of Beringen Glacial due to the closing of the Klettgau Channel at Schaffhausen

By using the regional defined nine glacials and interglacials as a framework, the local landscape evolution was condensed into ten steps (0-IX; Tabel 2), where step 0 represents the starting point of the landscape evolution after the MPT, and with the currently proposed three phases of the active formation of glacially overdeepened troughs (Step I, VII, and IX). Figure 7 gives an overview of the assumed extent of the Rhine Glacier and the active overdeepenings during the Möhlin (Step I), Habsburg (Step III), Hagenholz (Step V), Beringen (Step VII), and Birrfeld Glacials (Step IX). Based on the pre-DOVE knowledge, a working hypothesis for the DOVE site 5068_2 and the Basadingen Trough can be formulated accordingly:

- I) The Basadingen Trough, formed during the Möhlin Glacial (Step I, MIS12), built a direct connection between the rivers Rhine and Thur
- II) The trough was possibly reactivated during the Habsburg Glacial (Step III, MIS 10 or 8)
- III) was partly eroded and covered by at least one generation of glaciofluvial gravels (Buechberg Gravel; debated if it consists of one or multiple generations of gravel deposits)
- IV) The trough was not reactivated during Beringen (Step VII, MIS 6) or the Birrfeld Glacial (Step IX, MIS 5-2)

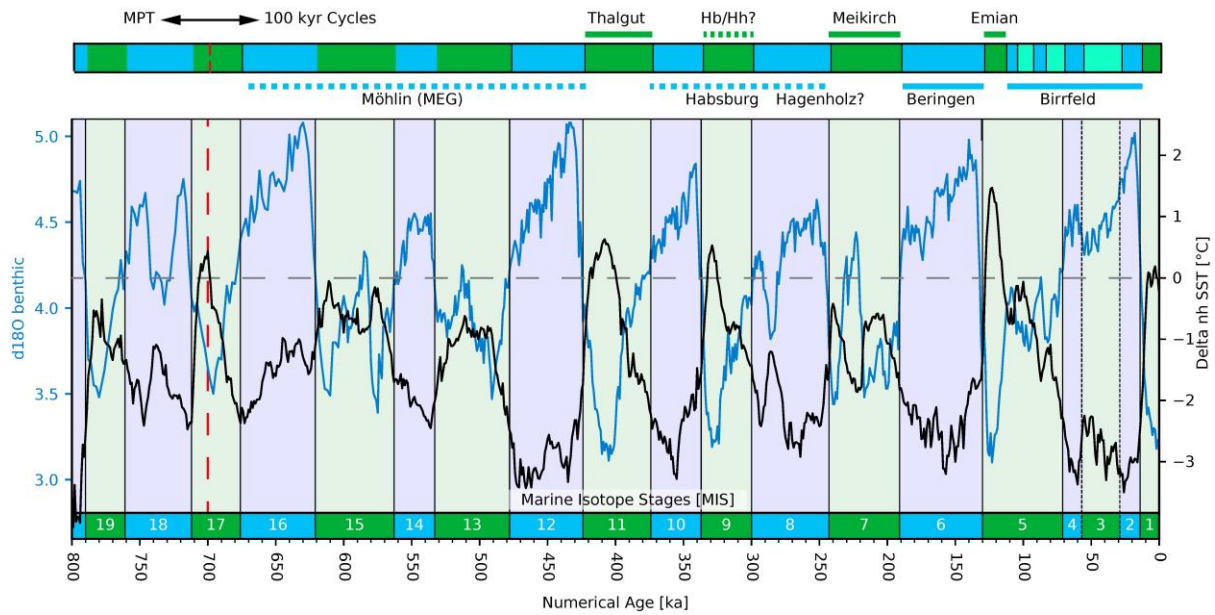


Figure 6: Correlation between the global marine isotope stages with the locally defined glacials (blue), interglacials (green), and interstadials (Turquoise) of northern Switzerland during the Middle to Late Pleistocene, uncertainties of the correlation are marked in dashed lines of the corresponding color. The global benthic $\delta^{18}\text{O}$ records (blue curve; after Lisiecki & Raymo, 2005b) and the reconstructed northern hemisphere sea surface temperature (black curve; after Clark et al., 2024) are displayed for broader context. The red dashed line marks the approximated end of the MPT, and "Hb/Hh" stands for the debated interglacial between the Habsburg and Hagenholz Glacial.

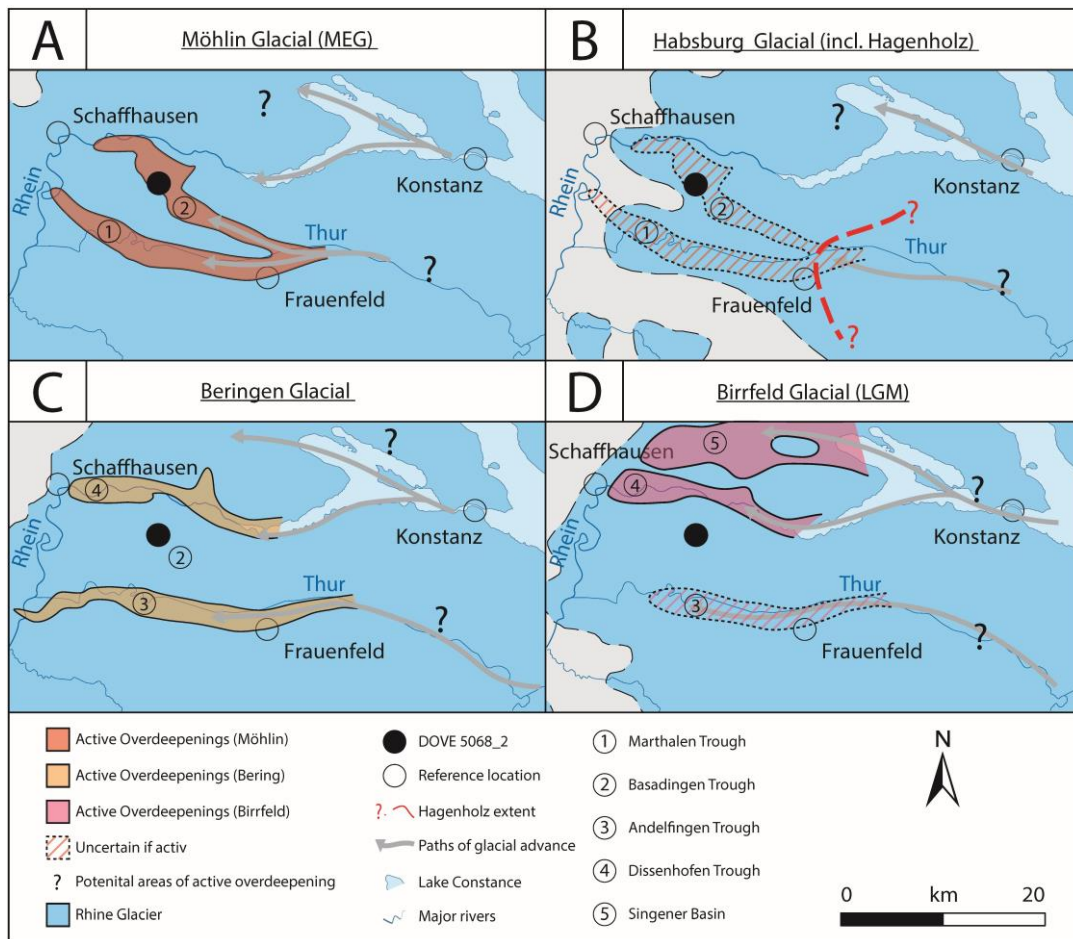


Figure 7: Overview sketches of the Middle to Late Pleistocene glaciations at the Dove site 5068_2. Showing the extent of the Rhine glacier (after Graf, 2009 and Preusser et al., 2011) and (active) overdeepenings (after Buechi et al., 2024; Graf, 2009; Müller, 2013) during the A) Möhlín Glacial (MEG), B) Habsburg Glacial (including the extent of the debated Hagenholz Glacial), C) Beringen Glacial, and D) Birrfeld Glacial (LGM).

Table 2: Condensed local landscape evolution of DOVE site 5068_2 with the correlation between the global marine isotope stages (MIS) and the local terminology for northern Switzerland

Step	Epoch	MIS
0	After the Mid-Pleistocene Transition (MPT)	>16
<ul style="list-style-type: none"> ➤ Reorganization of the regional fluvial drainage system ➤ Onset of the deposition of the "Hochterasse" (High Terrace) ➤ Unclear what happened during MIS 17 and 13, likely several complete glacial-interglacial cycles 		
I	Möhlín Glacial	16(?)–12
<ul style="list-style-type: none"> ➤ Most Extensive Glaciation (MEG) ➤ Formation of the first generation of glacially overdeepenings during the deglaciation after MEG ➤ Refilling of overdeepenings with glacial, glaciolacustrine, and lacustrine sediments during and after deglaciation 		
II	Thalgut Interglacial	11
<ul style="list-style-type: none"> ➤ Fluvial erosion of post-Möhlín landscape 		
III	Habsburg Glacial	10–8(?)
<ul style="list-style-type: none"> ➤ Possibly a second advance during the Möhlín Glacial ➤ Possible reactivation of some of the older overdeepenings ➤ Deposition and erosion of glaciofluvial gravels ➤ Development of several moraine-dammed lakes during deglaciation 		
IV	Habsburg-Hagenholz Interglacial	9?
<ul style="list-style-type: none"> ➤ Unclear if interglacial or interstadial ➤ Fluvial erosion of post-Habsburg landscape 		
V	Hagenholz Glacial	8 or early 6?
<ul style="list-style-type: none"> ➤ Possibly an early Beringen advance with only very little fragmented evidence left ➤ Glacier advance did not fully cover the study area, ➤ No evidence of active glacial overdeepenings ➤ Deposition and erosion of glacio-fluvial gravels 		
VI	Meikirch Interglacial	7
<ul style="list-style-type: none"> ➤ Fluvial erosion of post Hagenholz landscape 		
VII	Beringen Glacial	6
<ul style="list-style-type: none"> ➤ Contains likely two to three glacial (re)advances ➤ Second formation phase of glacial overdeepening ➤ Potential reactivations of overdeepenings during main advances ➤ Formation and (partial) refilling of lakes during interstadials ➤ Deposition and erosion of glacio-fluvial gravels 		
VIII	Eemian Interglacial	5e
<ul style="list-style-type: none"> ➤ The last full interglacial ➤ Onset of the deposition of the lower terrace (NT) ➤ Fluvial erosion of post-Beringen landscape 		
IX	Birrfeld Glacial	(early) 5d–2
<ul style="list-style-type: none"> ➤ Contains several glacial advances interrupted with interstadials ➤ Last Glacial Maximum (LGM) advance during MIS2 ➤ Phase of (limited) glacial overdeepening between Rhine and Thur, but intense in the modern-day Lake Constance area, (re)excavating of the lake basin ➤ Deposition of glacial tills and glacio-fluvial gravels 		
Note: blue = Glacial; green = interglacial.		

1.7 Outline of the thesis

Chapter 2 introduces the local and regional context of DOVE Site 5068_2, relating to data from the pre-drill site survey, representing the status quo during the drilling operation. This chapter presents findings from the initial core description of drill core 5068_2_A, focusing on developing a detailed lithological classification of the recovered sediments. Furthermore, it proposes a preliminary model for the evolution of the Basadingen Trough by integrating core description results with the local geological framework and pre-existing knowledge. Additionally, this chapter includes an overview of the drilling operation and the core handling workflow (sampling strategies and data handling), serving as a guideline for other DOVE sites. Chapter 2 provides the foundational background and core information for further detailed studies. This chapter is published as Schaller et al. (2023).

Chapter 3 establishes and applies a glacio-seismic sequence stratigraphy by integrating the findings from the initial core description from Chapter 2 with refined reflection seismic data from the site survey. This process includes i) updating pre-drill seismic data using a refined velocity model based on in-hole measurements ("check shots"), ii) conducting seismic facies and seismic sequence stratigraphy analysis that will be integrated with core lithologies, and iii) extrapolating these defined patterns to the second seismic line. The chapter further utilizes the concept of the glacio-seismic sequence stratigraphy to create a 3D visualization of the Basadingen Trough, leading to a refined formation history for the trough discussed within the local geological context. This chapter has been submitted and was not accepted, so it is currently revised for resubmission in December 2024 (Schaller et al., in prep a).

Chapter 4 focuses on developing and testing a workflow based on wireline logging data designed to establish an artificial lithological profile and enable data-driven stratigraphic correlation and integration with the petrophysical and chemical properties. The workflow, combining advanced dimensionality reduction techniques and hierarchical clustering, was tested on datasets from two nearby drill holes at DOVE site 5068_1, including drill core 5068_1_C. This setup enables cross-well correlation between reconstructed profiles, with the core-controlled well serving as a translation key between the reconstructed data-based profiles and the actual drilled lithology. This chapter will be submitted in early 2025 (Schaller et al., in prep. b)

Chapter 5 provides, together with a brief outlook, a comprehensive conclusion addressing i) the implications of the findings for the regional geological setting, ii) the potential applications of the developed and applied workflows, and iii) critical operational and conceptual considerations for DOVE Phase II.

Appendix A includes the DOVE Phase I Operational Report, documenting the initial data acquisition phase, covering site description, drilling operations, wireline logging, and on-site core handling and sampling protocols.

Appendix B contains the explanatory notes for the operational dataset of the ICDP project DOVE Phase I (ICDP 5068), complementing the Operational Report. This appendix provides metadata, tables, and additional information from the project database (mDIS DOVE) and supports other researchers' further data usage following the FAIR principle.

1.8 References

- Alley, R. B., Cuffey, K. M., & Zoet, L. K. (2019). Glacial erosion: Status and outlook. *Annals of Glaciology*, 60(80), 1–13. <https://doi.org/10.1017/aog.2019.38>
- Anselmetti, F. S., Bavec, M., Crouzet, C., Fiebig, M., Gabriel, G., Preusser, F., Ravazzi, C., & DOVE scientific team. (2022). Drilling Overdeepened Alpine Valleys (ICDP-DOVE): Quantifying the age, extent, and environmental impact of Alpine glaciations. *Scientific Drilling*, 31, 51–70. <https://doi.org/10.5194/sd-31-51-2022>
- Buechi, M. W. (2016). *Overdeepened glacial basins as archives for the Quaternary landscape evolution of the Alps*. <https://doi.org/10.13140/RG.2.2.17415.80802>
- Buechi, M. W., Graf, H. R., Haldimann, P., Lowick, S. E., & Anselmetti, F. S. (2018). Multiple Quaternary erosion and infill cycles in overdeepened basins of the northern Alpine foreland. *Swiss Journal of Geosciences*, 111(1–2), 133–167. <https://doi.org/10.1007/s00015-017-0289-9>
- Buechi, M. W., Landgraf, A., Madritsch, H., Mueller, D., Knipping, M., Nyffenegger, F., Preusser, F., Schaller, S., Schnellmann, M., & Deplazes, G. (2024). Terminal glacial overdeepenings: Patterns of erosion, infilling and new constraints on the glaciation history of Northern Switzerland. *Quaternary Science Reviews*, 344, 108970. <https://doi.org/10.1016/j.quascirev.2024.108970>
- Clark, P. U., Shakun, J. D., Rosenthal, Y., Köhler, P., & Bartlein, P. J. (2024). Global and regional temperature change over the past 4.5 million years. *Science*, 383(6685), 884–890. <https://doi.org/10.1126/science.adi1908>
- Cohen, K., & Gibbard, P. (2022). *Global chronostratigraphical correlation table for the last 2.7 million years v.2019 (Poster version)*. 5. <https://doi.org/10.17632/dtsn3xn3n6.5>
- Cook, S. J., & Swift, D. A. (2012). Subglacial basins: Their origin and importance in glacial systems and landscapes. *Earth-Science Reviews*, 115(4), 332–372. <https://doi.org/10.1016/j.earscirev.2012.09.009>
- Dehnert, A., Lowick, S. E., Preusser, F., Anselmetti, F. S., Drescher-Schneider, R., Graf, H. R., Heller, F., Horstmeyer, H., Kemna, H. A., Nowaczyk, N. R., Züger, A., & Furrer, H. (2012). Evolution of an overdeepened trough in the northern Alpine Foreland at Niederweningen, Switzerland. *Quaternary Science Reviews*, 34, 127–145. <https://doi.org/10.1016/j.quascirev.2011.12.015>
- Dieleman, C., Christl, M., Vockenhuber, C., Gautschi, P., Graf, H., & Akçar, N. (2022). Age of the Most Extensive Glaciation in the Alps. *Geosciences*, 12, 39. <https://doi.org/10.3390/geosciences12010039>
- Ellwanger, D., Wielandt-Schuster, U., Franz, M., & Simon, T. (2011). The Quaternary of the southwest German Alpine Foreland (Bodensee-Oberschwaben, Baden-Württemberg, Southwest Germany). *E&G Quaternary Science Journal*, 60(2/3), 306–328. <https://doi.org/10.3285/eg.60.2-3.07>
- Fabbri, S. C., Buechi, M. W., Horstmeyer, H., Hilbe, M., Hübscher, C., Schmelzbach, C., Weiss, B., & Anselmetti, F. S. (2018). A subaquatic moraine complex in overdeepened Lake Thun (Switzerland) unravelling the deglaciation history of the Aare Glacier. *Quaternary Science Reviews*, 187, 62–79. <https://doi.org/10.1016/j.quascirev.2018.03.010>
- Fiebig, M. (2011). Editorial. *E&G Quaternary Science Journal*, 60(2/3), 278–281. <https://doi.org/10.3285/eg.60.2-3.05>
- Fiebig, M., Herbst, P., Drescher-Schneider, R., Lüthgens, C., Lomax, J., & Doppler, G. (2014). Some remarks about a new Last Glacial record from the western Salzach foreland glacier basin (Southern Germany). *Quaternary International*, 328–329, 107–119. <https://doi.org/10.1016/j.quaint.2013.12.048>
- Graf, H. R. (2009). *Stratigraphie von Mittel- und Spätpleistozän in der Nordschweiz. Beiträge zur Geologischen Karte der Schweiz (N.F.)* (Vol. 168). Landesgeologie.
- Graf, H. R., & Burkhalter, R. (2016). Quaternary deposits: Concept for a stratigraphic classification and nomenclature—an example from northern Switzerland. *Swiss Journal of Geosciences*, 109(2), 137–147. <https://doi.org/10.1007/s00015-016-0222-7>
- Haeuselmann, P., Granger, D. E., Jeannin, P.-Y., & Lauritzen, S.-E. (2007). Abrupt glacial valley incision at 0.8 Ma dated from cave deposits in Switzerland. *Geology*, 35(2), 143. <https://doi.org/10.1130/G23094A>
- Hinnov, L. (1978). Milankovitch cycles. In *Sedimentology* (pp. 720–724). Springer Berlin Heidelberg. https://doi.org/10.1007/3-540-31079-7_138
- Kehew, A. E., Piotrowski, J. A., & Jørgensen, F. (2012). Tunnel valleys: Concepts and controversies — A review. *Earth-Science Reviews*, 113(1), 33–58. <https://doi.org/10.1016/j.earscirev.2012.02.002>
- Knudsen, M. F., Nørgaard, J., Grischott, R., Kober, F., Egholm, D. L., Hansen, T. M., & Jansen, J. D. (2020). New cosmogenic nuclide burial-dating model indicates onset of major glaciations in the Alps during Middle Pleistocene Transition. *Earth and Planetary Science Letters*, 549, 116491. <https://doi.org/10.1016/j.epsl.2020.116491>
- Legrain, E., Parrenin, F., & Capron, E. (2023). A gradual change is more likely to have caused the Mid-Pleistocene Transition than an abrupt event. *Communications Earth & Environment*, 4(1), 1–10. <https://doi.org/10.1038/s43247-023-00754-0>

- Lisiecki, L. E., & Raymo, M. E. (2005a). A Pliocene-Pleistocene stack of 57 globally distributed benthic $\delta^{18}\text{O}$ records. *Paleoceanography*, 20(1). <https://doi.org/10.1029/2004PA001071>
- Lisiecki, L. E., & Raymo, M. E. (2005b). *Lisiecki and Raymo 2005 Global Pliocene-Pleistocene Benthic $\delta^{18}\text{O}$ Stack* [Dataset]. <https://doi.org/10.25921/k88j-0106>
- Maslin, M. (2009). Quaternary Climate Transitions and Cycles. In V. Gornitz (Ed.), *Encyclopedia of Paleoclimatology and Ancient Environments* (pp. 841–855). Springer Netherlands. https://doi.org/10.1007/978-1-4020-4411-3_198
- Monegato, G., Scardia, G., Hajdas, I., Rizzini, F., & Piccin, A. (2017). The Alpine LGM in the boreal ice-sheets game. *Scientific Reports*, 7(1), 2078. <https://doi.org/10.1038/s41598-017-02148-7>
- Müller, E. R. (1995). Neues zur Geologie zwischen Thur und Rhein. *Mitteilungen Der Thurgauischen Naturforschenden Gesellschaft Mitt. Thurg. Natf. Ges.*, 53(1), 9–42.
- Müller, E. R. (2013). Mittelpleistozäne Schottervorkommen zwischen dem Thurtal und Schaffhausen. *Swiss Bulletin für angewante Geologie*, 18(1), 3–27. <https://doi.org/10.5169/SEALS-391135>
- Muttoni, G., Carcano, C., Garzanti, E., Ghielmi, M., Piccin, A., Pini, R., Rogledi, S., & Sciunnach, D. (2003). Onset of major Pleistocene glaciations in the Alps. *Geology*, 31(11), 989–992. <https://doi.org/10.1130/G19445.1>
- Pomper, J., Salcher, B. C., Eichkitz, C., Prasicek, G., Lang, A., Lindner, M., & Götz, J. (2017). The glacially overdeepened trough of the Salzach Valley, Austria: Bedrock geometry and sedimentary fill of a major Alpine subglacial basin. *Geomorphology*, 295, 147–158. <https://doi.org/10.1016/j.geomorph.2017.07.009>
- Preusser, F., Graf, H. R., Keller, O., Krayss, E., & Schlüchter, C. (2011). Quaternary glaciation history of northern Switzerland. *E&G Quaternary Science Journal*, 60(2/3), 282–305. <https://doi.org/10.3285/eg.60.2-3.06>
- Preusser, F., Reitner, J. M., & Schlüchter, C. (2010). Distribution, geometry, age and origin of overdeepened valleys and basins in the Alps and their foreland. *Swiss Journal of Geosciences*, 103(3), 407–426. <https://doi.org/10.1007/s00015-010-0044-y>
- Ruddiman, W. F., Raymo, M., & McIntyre, A. (1986). Matuyama 41,000-year cycles: North Atlantic Ocean and northern hemisphere ice sheets. *Earth and Planetary Science Letters*, 80(1), 117–129. [https://doi.org/10.1016/0012-821X\(86\)90024-5](https://doi.org/10.1016/0012-821X(86)90024-5)
- Scardia, G., Donegana, M., Muttoni, G., Ravazzi, C., & Vezzoli, G. (2010). Late Matuyama climate forcing on sedimentation at the margin of the southern Alps (Italy). *Quaternary Science Reviews*, 29(7), 832–846. <https://doi.org/10.1016/j.quascirev.2009.12.002>
- Schaller, S., Böttcher, M. E., Buechi, M. W., Epp, L. S., Fabbri, S. C., Gribenski, N., Harms, U., Krastel, S., Liebezeit, A., Lindhorst, K., Marxen, H., Raschke, U., Schleheck, D., Schmiedinger, I., Schwalb, A., Vogel, H., Wessels, M., & Anselmetti, F. S. (2022). Postglacial evolution of Lake Constance: Sedimentological and geochemical evidence from a deep-basin sediment core. *Swiss Journal of Geosciences*, 115(1), 7. <https://doi.org/10.1186/s00015-022-00412-1>
- Schaller, S., Buechi, M. W., Schuster, B., & Anselmetti, F. S. (2023). Drilling into a deep buried valley (ICDP DOVE): A 252\,m long sediment succession from a glacial overdeepening in northwestern Switzerland. *Scientific Drilling*, 32, 27–42. <https://doi.org/10.5194/sd-32-27-2023>
- Schaller, S., Beraus., S., Buechi, M. W., Buness, H., Schuster, B., & Anselmetti, F. S. (in Prep a). Seismic- and core-based glacial sequence stratigraphy in an overdeepened perialpine trough in the northern Alpine foreland of Switzerland.
- Schaller, S., Becerra, P., Beraus., S., Buechi, M. W., Mair, D., Sardar Abadi, M., Schuster, B., & Anselmetti, F. S. (in Prep b). Wireline logging data-driven lithoprediction of unconsolidated sediments.
- Schlüchter, C. (2004). The Swiss glacial record – a schematic summary. In *Developments in Quaternary Sciences* (Vol. 2, pp. 413–418). Elsevier. [https://doi.org/10.1016/S1571-0866\(04\)80092-7](https://doi.org/10.1016/S1571-0866(04)80092-7)
- Schwenk, M. A., Schläfli, P., Bandou, D., Gribenski, N., Douillet, G. A., & Schlunegger, F. (2022). From glacial erosion to basin overfill: A 240 m-thick overdeepening–fill sequence in Bern, Switzerland. *Scientific Drilling*, 30, 17–42. <https://doi.org/10.5194/sd-30-17-2022>
- Spötl, C., Koltai, G., Jarosch, A. H., & Cheng, H. (2021). Increased autumn and winter precipitation during the Last Glacial Maximum in the European Alps. *Nature Communications*, 12(1), Article 1. <https://doi.org/10.1038/s41467-021-22090-7>
- Vegt, P., van der, Janszen, A., & Moscariello, A. (2012). Tunnel valleys: Current knowledge and future perspectives. In M. Huuse, J. Redfern, D. P. L. Heron, R. J. Dixon, A. Moscariello, & J. Craig (Eds.), *Glaciogenic Reservoirs and Hydrocarbon Systems* (Vol. 368, p. 0). Geological Society of London. <https://doi.org/10.1144/SP368.13>

2

Drilling into a deep buried valley (ICDP DOVE): a 252m long sediment succession from a glacial overdeepening in northwestern Switzerland

Sebastian Schaller^{1,2}

MariusW. Buechi^{1,2}

Bennet Schuster^{3,1,2}

Flavio S. Anselmetti^{1,2}

¹Institute of Geological Sciences, Universität Bern,

²Oeschger Centre for Climate Change Research, Universität Bern

³Institute of Earth and Environmental Sciences, University of Freiburg

This article was published in *Scientific Drilling* on the 26 October 2023 under a Creative Commons Attribution 4.0 License: DOI: <https://doi.org/10.5194/sd-32-27-2023>

2. Drilling into a deep buried valley (ICDP DOVE): a 252m long sediment succession from a glacial overdeepening in northwestern Switzerland

2.1 Abstract

The modern Alpine landscape and its foreland were strongly impacted by the numerous glacier advance and retreat cycles during the Middle to Late Pleistocene. Due to the overall erosive character of each glaciation cycle, however, direct traces of older glaciations tend to be poorly preserved within the formerly glaciated domains of the pan-Alpine area. Nevertheless, sediments of older glaciations may occur hidden under the modern surface in buried glacially overdeepened troughs that reach below the normal level of fluvial erosion (fluvial base level). These sedimentary archives, partly dating back to the Middle Pleistocene period, are of great scientific value for reconstructing the timing and extent of extensive Alpine glaciation, paleoclimate, and paleoenvironmental changes in the past and help to better understand ongoing and future changes in the pan-Alpine area. Therefore, the International Continental Scientific Drilling Program (ICDP) project DOVE (Drilling Overdeepened Alpine Valleys) targets several of these glacial overdeepened sedimentary basins to recover their sedimentary infills. In the frame of the DOVE project, a 252 m long drill core of unconsolidated Quaternary sediments was recovered in northern Switzerland from an over 300 m deep glacially overdeepened structure (“Basadingen Trough”) formed by the former Rhine Glacier lobe system. The recovered sedimentary succession was divided into three stratigraphic units on the basis of lithological and petrophysical characteristics. The lowest unit, deposited below the fluvial base level, consists of an over 200 m thick succession of glacial to (glacio)lacustrine sediments and contains remains of possibly two glaciation cycles. Overlying this lowermost succession, an ~ 37 m thick fluvial-to-glaciofluvial gravel deposit occurs, which correlates to a locally outcropping Middle Pleistocene formation (“Buechberg Gravel Complex”). The sediment succession is capped by an ~ 11 m thick diamictic succession interpreted as the subglacial till from the later extensive glaciation, including the regional glaciation during the Last Glacial Maximum. The recovered sediment succession thus supports the proposed multi-phase origin of trough formation and its infill.

2.2 Introduction

The global marine isotope records reveal the changes in the global temperature and ice volumes during the Quaternary. This geological period is dominated by glacial–interglacial cycles, each including stadial–interstadial higher-frequency fluctuations (Lisiecki & Raymo, 2005). Further, the marine isotope records show a global shift in the periodicity from ca. 41 to 100 ka and an increase in the amplitude of the temperature and ice volume during the Middle Pleistocene climatic transition (MPT) between 1250 and 700 ka (Clark et al., 2006; Ruddiman et al., 1986). During each glacial–interglacial cycle, ice sheets grew in the polar areas as well as in mountainous areas (including the Alps), and glaciers advanced into the lowlands from where they retreated again with the onset of the next interglacial. While the last glaciation left prominent traces in the Alpine landscape (e.g., erratic blocks and side and end moraines), traces of previous glaciations often became obscured and eroded as advancing glaciers modified the overridden landscape drastically.

During extensive glaciation of the Alpine foreland, numerous glacially overdeepened troughs were eroded by subglacial processes below the fluvial base level, i.e., below the lowest fluvial channels terminating downstream with adverse slopes (e.g., Alley et al., 2019; Cook & Swift, 2012). Upon deglaciation, the troughs were refilled with sediments and, in most cases, eventually completely buried. Like this, the valley fills remained at least partially protected from subsequent glacial and fluvial erosion and therefore contain relatively complete or multi-phase archives extending through several glacial cycles (Buechi et al., 2018; Ellwanger et al., 2011; Pomper et al., 2017; Preusser et al., 2010). Therefore, these overdeepened valley fills represent some of the most valuable land-based sedimentary archives in glacial landscapes for reconstructing glacial history over multiple glaciations. They thus contribute significantly to reconstructing the glaciation history preceding the last glacial cycle in areas such as the Alps and its foreland, as shown in several case studies (Buechi et al., 2018, p. 18; Dehnert et al., 2012; Fiebig et al., 2014; Schwenk et al., 2022). These studies profited from new developments in dating methods, especially luminescence dating and cosmogenic nuclide burial dating, which allow researchers to establish an absolute chronology of those archives, which is a prerequisite for understanding and reconstructing the local-to-regional glaciation history into a broader context. On a regional scale, the onset of increased glacial erosion (Haeuselmann et al., 2007; Valla et al., 2011) and the beginning formation of overdeepened structures during the MPT have been proposed for the Alpine region at that time (e.g., Ellwanger et al., 2011; Schlüchter, 2004). The initial concept with four proposed Alpine glaciations (Penck & Brückner, 1909)

has been replaced by a scenario with ca. 15 proposed glaciations (Preusser et al., 2011). Furthermore, it has been documented that regional the glacial dynamics and extents also vary strongly inside the pan-Alpine area. For example, it is postulated that at around ca. 65 ka, the glaciers in the western Alps reached their last maximum of extension (e.g., Gribenski et al., 2021), while it is postulated that glaciers barely reached into the inner Alpine valleys in the Eastern Alps (Ivy-Ochs et al., 2008). Such asymmetry and asynchronicity can be related to many local, regional, and global factors such as topography, climate change (including temperature and precipitation), and ice dynamics (e.g., Reber & Schlunegger, 2016; Spötl et al., 2021).

All these studies also underline the potential and justify the significant logistical and financial effort to drill, document, and analyze these overdeepened troughs and their sediment fill. Besides their unique scientific value as sedimentary archives, understanding overdeepened structures is also crucial for applied aspects such as the longtime safety of nuclear waste disposal sites, groundwater reservoirs, natural hazards, and large-scale underground transportation infrastructure.

2.2.1 Project DOVE

In the frame of the International Continental Scientific Drilling Program (ICDP) project Drilling Overdeepened Alpine Valleys (DOVE), the sedimentary infill of several overdeepened troughs are targeted with the overarching goal of quantifying the proposed asymmetry in the extent and timing of the Alpine glaciations in the pan-Alpine area and their implications for the paleoclimate, paleolandscape, and paleoenvironmental evolution back to the Middle Pleistocene. A detailed overview of the DOVE project is provided in Anselmetti et al. (2022). The project seeks to achieve these goals by combining the following: i) a series of new drill cores, ii) analyzing existing drill cores, and iii) geophysical surveys across overdeepened troughs. The project is grouped into two phases: Phase I covers the northern and northeastern parts of the Alps (Switzerland, Germany, and Austria) and comprises three drill cores from the former Rhine Glacier area (ICDP Site 5068_1, TANN, IGSN (International Generic Sample Number): ICDP5068EH70001; ICDP Site 5068_2, BASA, IGSN: ICDP5068EH40001; and ICDP Site 5068_6, GAIS, IGSN: ICDP5068EHG0001; Fig. 1a), one from the former Isar-Loisach Glacier area (ICDP Site 5068_3, SCHA, IGSN: ICDP5068EHC0001), one from the former Salzach Glacier area (ICDP Site 5068_4, FREI, IGSN: ICDP5068EHD0001), and one from the former Traun Glacier area (ICDP Site 5068_5, BADA, IGSN: ICDP5068EHE0001) (Anselmetti et al., 2022). It is planned to cover the southern and western parts of the Alps

(Slovenia, Italy, and France) in Phase II (Anselmetti et al., 2022). The comparison and integration of data in Phase I will occur in several steps: i) the data of the individual drill cores will be individually analyzed and integrated into the local context; ii) the sites will be integrated into their extended regional system, e.g., the individual glacier lobes; and iii) an overall synthesis of Phase I in the northern Alps will be accomplished. Eventually, the same steps are planned for Phase II for the southern and western areas. Finally, the overall DOVE synthesis and integration over the entire pan-Alpine area will be achieved. This study represents the first step on this path and presents the results of the ICDP site 5068_2 (BASA), where the first ICDP drill core was recovered on Swiss territory (Fig. 1a and b).

2.2.2 Study area

The study area is located in the southwestern part of the former Rhine Glacier lobe and inside the proposed Most Extensive Glaciation (MEG) during the Middle Pleistocene and the Last Glacial Maximum (LGM, Fig. 1a). Previous studies have documented a dendritic pattern of overdeepenings within the footprint of the Rhine Glacier (Fig. 1a). Geometrically, these overdeepened basins appear to have a common root in the Alpine Rhine valley and the partially filled basin of Lake Constance (e.g., Cohen et al., 2018; Ellwanger et al., 2011; Fabbri et al., 2021; Keller & Krayss, 1993; Schaller et al., 2022). From this root, several overdeepened basins branch into side systems and even further distal overdeepenings (Fig. 1a). While the origin of this pattern is not fully understood, regional studies indicate that the formation of these overdeepenings did not all occur at the same time but during different glaciations (e.g., Ellwanger et al., 2011; Graf, 2009b, 2009a; Müller, 2013).

In the surroundings of the drill site, with a terrain elevation at the drill site of ~ 445 m above sea level (m a.s.l.), several parallel to partly cross-cutting bedrock overdeepenings have been detected in bedrock surface maps compiled from variably abundant drillings and geophysical data (Fig. 1b; e.g., Müller, 2013; Pietsch & Jordan, 2014). The bedrock overdeepenings, including the Basadingen Trough, reach over 300 m below the modern topography and are mainly incised into the Neogene siltstones and sandstones of the Molasse basin (mainly Upper Marine Molasse, OMM, and Lower Freshwater Molasse, USM; Hofmann, 1967; Hofmann & Hantke, 1964). The bedrock maps also reveal characteristic adverse slopes at the termini of the individual overdeepenings. At the surface, the considerable bedrock relief due to overdeepening glacial erosion is buried by younger glacial or glaciofluvial sediments (Graf, 2009b; Müller, 2013).

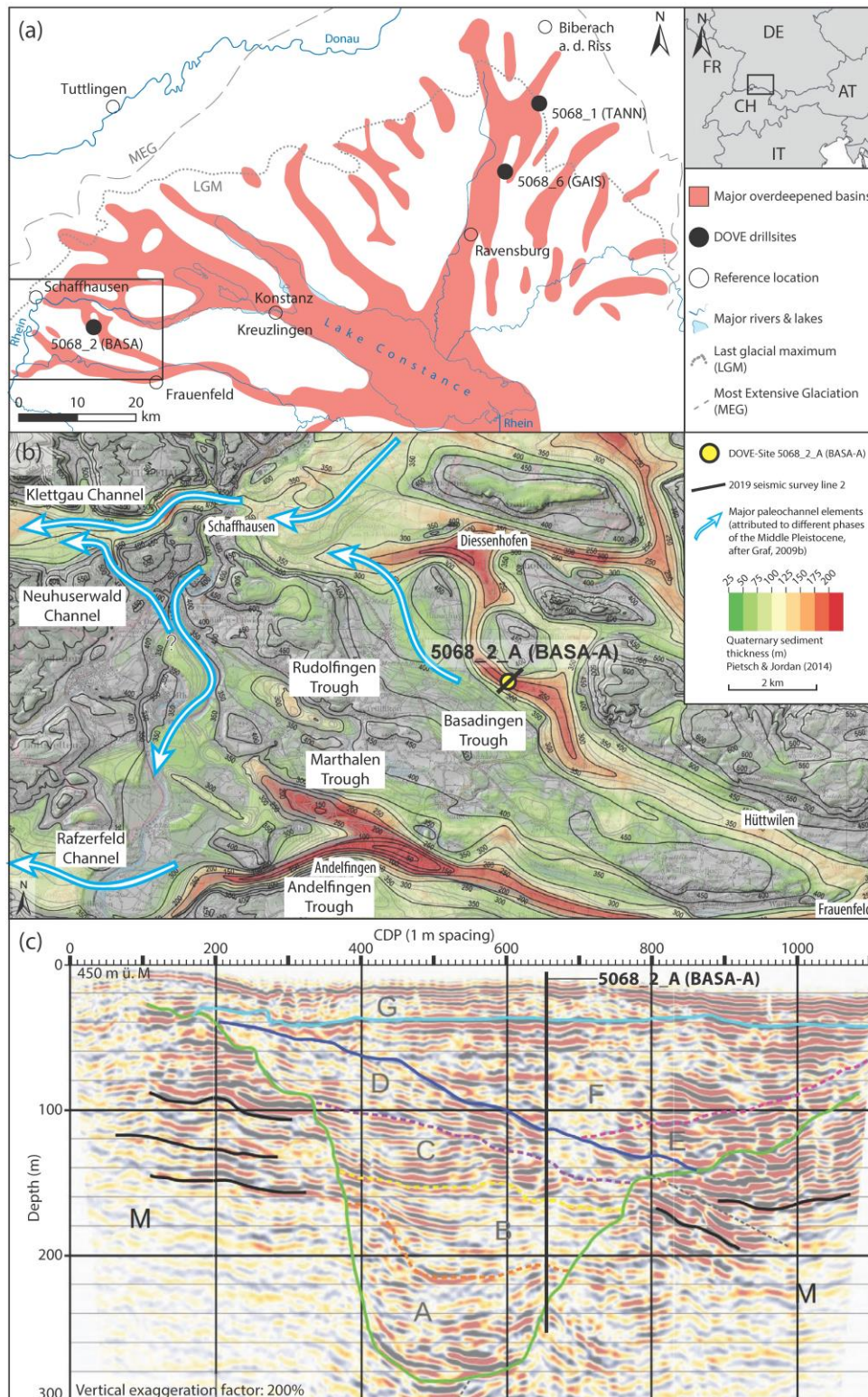


Figure 1: (a) Overview of the overdeepened systems within the former Rhine paleoglacier lobe (modified from Ellwanger et al., 2011). Extents of the Rhine Glacier during the Most Extensive Glaciation (MEG) and of the Last Glacial Maximum (LGM) and two DOVE Phase I sites: 5068_1 (TANN), 5068_2 (BASA), and 5068_6 (GAIS) are indicated. (b) Regional overview of the overdeepened system of the southwestern branch of the Rhine Glacier, including the thickness of the Quaternary sediments (Pietsch and Jordan, 2014), the postulated local Middle Pleistocene paleochannels (Graf, 2009b), the indicated DOVE site 5068_2 (BASA), and trace of the seismic line. (c) Pre-drilling interpretation of the seismic line across the Basadingen Trough (Brandt, 2020): M represents the molasse bedrock; the green line represents the outline of trough; A–G represent the stratified unconsolidated Quaternary filling with indicated potential erosional (solid lines) and internal boundaries (dashed lines); solid black lines in M represent prominent and potential continuous reflections; dashed black lines represent assumed faults; the black vertical line represents drill hole 5068_2-A (BASA-A) with predicted bedrock at ~240 m depth. Note that the final drilling depth of 252 m did not penetrate bedrock but ended in coarse (basal) sediments.

The transition from the overdeepened to non-overdeepened (fluvial) domain is an important physical process boundary for the interpretation of the erosional and depositional processes. The lowest fluvial outlet of the study area is the Klettgau fluvial paleochannel and lies at ~ 340 m a.s.l. just west of Schaffhausen. Considering this minimal fluvial base level, the erosional and depositional processes below ~ 100 m core depth have occurred in an overdeepened position and, thus, most likely in a subglacial-to-lacustrine setting. Higher values for the fluvial base level at the drill site – but with larger uncertainties – can be estimated from the highest elevations reached by the adverse slopes. Based on the base maps of the lowest fluvial gravels (“Buechberg Gravel Complex”, Middle Pleistocene; Müller, 2013), Graf (2009b) and Müller (2013) convincingly show that the lowest Pleistocene base (LPB) level gently rises to the east and reaches ~ 370 m a.s.l. at the lowest known basal contact of the gravel formation. The base map reveals a strong topography of this basal boundary surface, which lies between 390 and 400 m a.s.l. around the drill site.

As part of the drill site selection process, two closely spaced seismic cross-sections over the Basadingen Trough were acquired using an acoustic signal source with a frequency between 20 and 240 Hz, a shot-point spacing of 4 m, and a receiver spacing of 2 m (Brandt, 2020; Fig. 1c). The time-to-depth conversion of the two lines was based on the stacking velocity model, assuming velocities of ~ 2500 m s⁻¹ for bedrock and between ~ 1400 and ~ 2100 m s⁻¹ for the sedimentary infill. The use of the rather simplified velocity model may have caused some uncertainties in the time–depth conversion of the seismic data. Both lines indicate a nearly 300 m deep bedrock incision and an infill which was interpreted to be a complex stratified geometry with a major cross-cutting unconformity separating a deep and narrow structure from a broad and shallow depression. This pattern suggests a multi-phase infill history during at least two glaciation cycles, as was earlier proposed by Müller (2013) based on existing flush drillings.

2.3 Methods

2.3.1 Drilling and downhole operations

Drilling operations were conducted by a private contractor (Fretus AG, Bad Zurzach, Switzerland) between 25 May and 10 November 2021 (Fig. 2a–d). A final depth of 252 m was reached using a combined approach of percussion drilling (Düsterloh hammer) to a depth of 57 m and, below, a triple-tube core-barrel system (CSK-146 wireline diamond-coring system). Bedrock, initially predicted for ~ 240 m (Fig. 1c), could not be reached due to geotechnically

challenging sediments, loss of drilling fluid in the hole, and related technical difficulties at the final depth of 252 m. The > 12 m underestimation of Quaternary sediment thickness is likely related to uncertainties in i) the seismic velocities and/or ii) the interpretation of the deeper reflections. A total of 278 core sections with a core diameter of 104 mm and lengths between 0.1 and 1 m were recovered in opaque PVC liners. The liners had a standard length of 1 m and were only cut if the length of the nominal drilled section was < 1 m. The liners were not cut in the case of core loss, and this space was not compensated with filler material. Consequently, the quality of those sections may have suffered due to some remobilizations, especially in cases of low internal cohesion. However, since the main reason for the core loss was mobilization and/or flushing during the drilling itself, those sections were of poor quality anyway. A total recovery of $\sim 94\%$ was reached, from which $\sim 11\%$ was disturbed to the degree that it lost its internal structure. Water inflow was registered at depths of 3–4 and 10–11 m. The local groundwater table was reached at a depth of ~ 29.5 m, which remained stable during the entire drilling operation. Significant drilling-fluid losses occurred in gravel-dominated sections between 93–108 and 141–143 m and below 250 m. They represent the major technical and lithological challenges encountered during the drilling operation. For stabilizing and reducing the drilling resistance inside the drill hole, the drill hole was telescoped several times by using different casing diameters and a flushing agent consisting of water mixed with additions of biodegradable polymers and bentonite. After the completion of the drilling activities, a broad downhole wireline logging campaign was executed by the Leibniz Institute for Applied Geophysics (LIAG). After completion of the wireline logging, the drill hole was refilled with intervals of gravel, bentonite, and concrete according to governmental regulations. A detailed technical overview of the drilling and logging operations; core quality; the technical parameters, such as borehole geometry, used casings, and the applied refilling scheme is provided in the DOVE operational report (DOVE-Phase 1 Scientific Team et al., 2023a)

2.3.2 Core handling, description, and analysis

On-site core-related workflow: After recovery, the liners were sealed and labeled with section ID and driller depth. Each core section was weighed for a preliminary approximation of recovery. In parallel to the drilling campaign, p-wave velocity (will not be further considered due to poor quality), wet bulk density, magnetic susceptibility, and natural gamma radiation of each core section were measured in the field laboratory (Fig. 3) with a Geotek multi-sensor core logger (MSCL) (Geotek Limited, Daventry, Northants, UK) at a resolution of 5 mm. The core sections were stored in labeled standard-sized wooden boxes for better handling. Later,

they were brought in batches to the Institute of Geological Sciences, University of Bern, to be stored in the cooling room until the initial core description (ICD). In parallel to recovering, the fine-grained and sandy sediments were strategically sampled for noble-gas pore-water analyses (16 samples) and microbiological investigations of the deep biosphere (60 samples).



Figure 2: (a) Drill rig used from 0 to 228 mtd (meters total depth); (b) drill rig used from 228 to 252 mtd; (c) drill bit used during percussion-hammer coring to a depth of 57 mtd; and (d) diamond and hard-metal drill bit used during rotary drilling below 57 mtd (photos by Sebastian Schaller).



Figure 3: Field lab near the drill site containing the MSCL scanner (photo by Sebastian Schaller).

Off-site core-related workflow: During the ICD, each core section was cut, opened, and split lengthwise into an archive half for non-destructive analyses and a working half for invasive sampling. Complete processing of the working half was performed under red-light conditions to prevent light contamination, potentially hampering the use of optically stimulated luminescence (OSL) dating. The following work was conducted on each archive half. A high-resolution line scan was obtained, and each section was sedimentologically described and documented in a log sheet. The focus of these descriptions was on the following: i) the dominant grain size, ii) type and thickness of bedding, iii) color, iv) contacts between different beds, v) secondary sedimentary structure, vi) quality of the core section, and vii) an overview of clast lithology and morphology. Furthermore, where applicable, undrained shear strength (c'_u) and undrained uniaxial compressive strength (q'_u) were measured at 25, 50, and 75 cm section depth with a pocket vane shear tester and a pocket penetrometer. A final total depth was defined based on the observations of core quality from the ICD and the driller's top depth of each section. Depth is addressed as meters total depth (mtd) when discussing the entire sediment succession or as centimeter section depth (cmsd) when aiming for individual core sections. Based on the combined findings from the ICD, 14 sedimentary lithotypes were defined and described (Table 1). The whole sediment succession was assigned to the best-fit lithotype. Eventually, the stratigraphic succession was subdivided into three main stratigraphic units (A–C).

In addition, X-ray computed tomography (CT) images of 49 selected core sections were taken with a medical X-ray CT scanner at the Institute of Forensic Medicine, University of Bern. Systematically, 231 samples for grain-size distribution, geochemical analyses (e.g., total inorganic carbon, TIC, and total organic carbon, TOC), and potential additional investigations were taken from each working half at 50 cmsd whenever possible (sample spacing ~ 1 m). These samples were freeze-dried, and the mean water content at each position was derived from the corresponding weight differences between the three wet and dry subsamples. Furthermore, smear slides have been taken from interesting silt- and clay-rich sections.

Further, based on the line scans, samples were taken for a first screening of pollen content (31 samples), luminescence dating (22 samples), cosmogenic nuclide burial dating (2 samples), and geotechnical analyses (23 samples). After completing the ICD and the sampling campaign, the core halves were sealed in lightproof black foil, stored in standard-sized wooden boxes, labeled according to the ICDP guidelines, and brought to a commercial cooled storage facility, which serves as a temporary repository during the active DOVE Phase I (Anselmetti et al.,

2022). For further information on the curated samples, analysis, and data, see the operational dataset (DOVE-Phase 1 Scientific Team et al., 2023b) and explanatory remarks (DOVE-Phase 1 Scientific Team et al., 2023c).

Carbon analysis (organic matter and carbonate content): Total carbon (TC), nitrogen, sulfur, and total organic carbon (TOC) were analyzed from the fine fraction ($< 63 \mu\text{m}$) using a Thermo Scientific FLASH 2000 elemental analyzer (Thermo Fischer, Waltham, MA, USA). Total inorganic carbon (TIC) was derived as the differences between TC and TOC. Weight percent of carbonates (CaCO_3) and organic matter were calculated using a stoichiometrically simplified approach from TIC and TOC through multiplication with 8.3 and 1.8, respectively (Meyers & Teranes, 2001). This approach does not consider potential down-core changes in carbonate phases (i.e., dolomite/carbonate ratio). Nevertheless, it allows for a quantitative approximation of the total lithological constituents.

MSCL data processing: MSCL data were processed in five steps: i) data of empty sections of liners, representing core loss, were removed; ii) a baseline correction was applied to the corresponding magnetic susceptibility data to correct potential systematic shifts in the data (subtraction of the average of the calibration data between 0.5 and 15 cm of each measurement cycle); iii) low-density data ($< 1.5 \text{ g cm}^{-3}$), considered heavily disturbed sections, were excluded from the density log; iv) p-wave velocity data with an amplitude of 0, representing poor data quality, were excluded from the p-wave data (As the overall data quality of the p-wave data is low, p-wave-velocity values are not further presented or discussed.); v) the depth of the cleaned MSCL logs was corrected with the actual depth; and vi) the data from the uppermost and lowermost centimeter in each section were considered likely disturbed and thus excluded.

2.4 Results

2.4.1 Core lithologies

The 252 m long sediment succession was divided into 14 sedimentological lithotypes (Fig. 4). Table 1 provides an overview of these 14 defined lithotypes, including description and interpretation of the depositional environment, along with a representative core-section line scan. Figure 5 displays a composition of detailed line scans, CT scans, and the key lithotypes of 10 selected core sections.

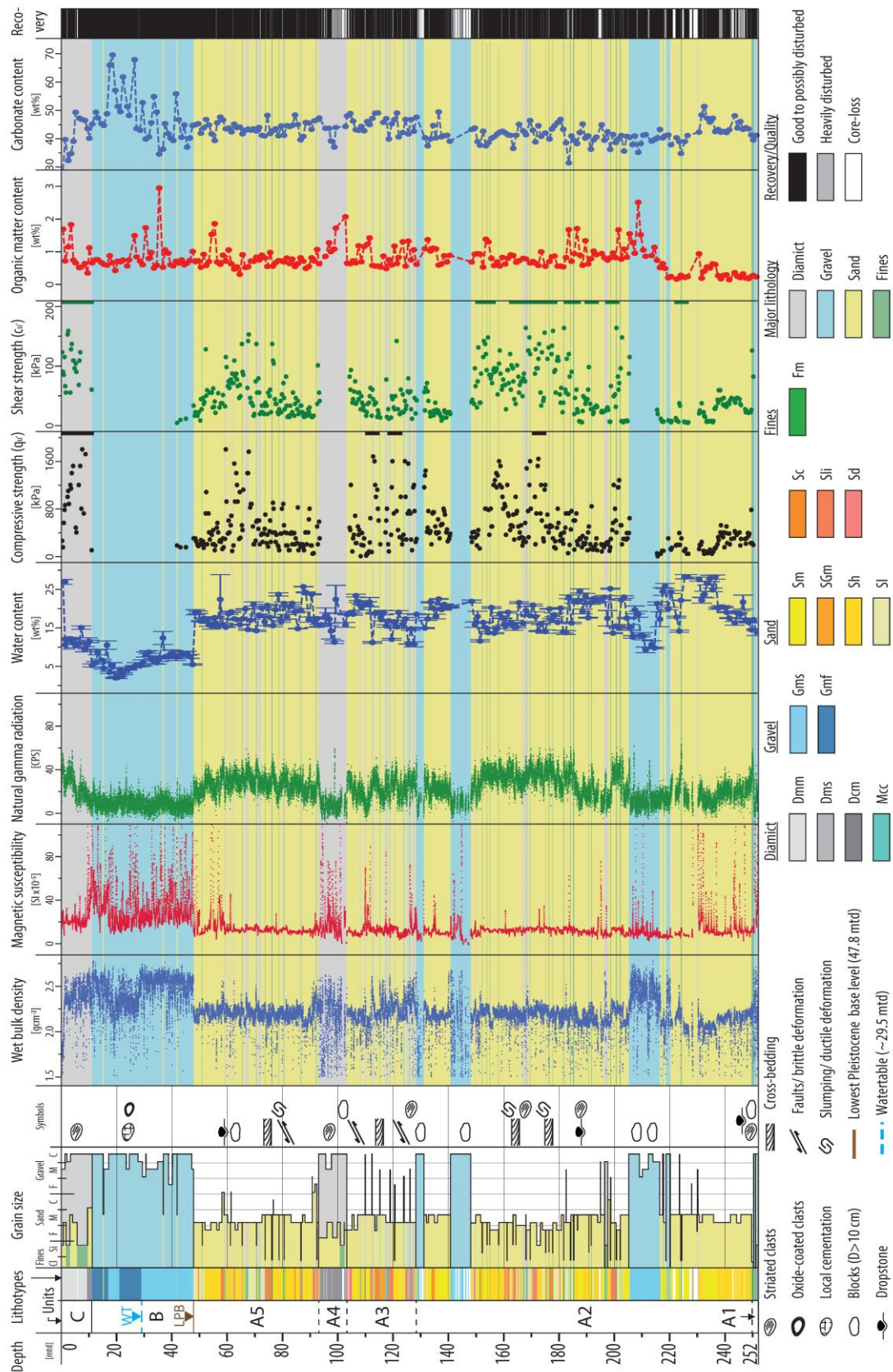


Figure 4: Lithological and petrophysical data versus depth. Columns from left to right: depth-scale [mtd], stratigraphic units (labeled with A1–A5, B, and C; WT = water table; LPB = lowest Pleistocene base level), lithotypes, dominant grain size with indicated main lithotypes, symbols of prominent observations, wet bulk density (g cm^{-3}), magnetic susceptibility ($\text{SI} \times 10^{-5}$), natural gamma radiation (CPS, counts per second), water content with indicated standard deviation (wt %), undrained uniaxial compressive strength (q'_u) (kPa), undrained shear strength (c'_u) (kPa), organic matter content (wt %), carbonate content (wt %), and the recovery. Main lithotypes are indicated as semi-transparent color codes over the plot's entire width.

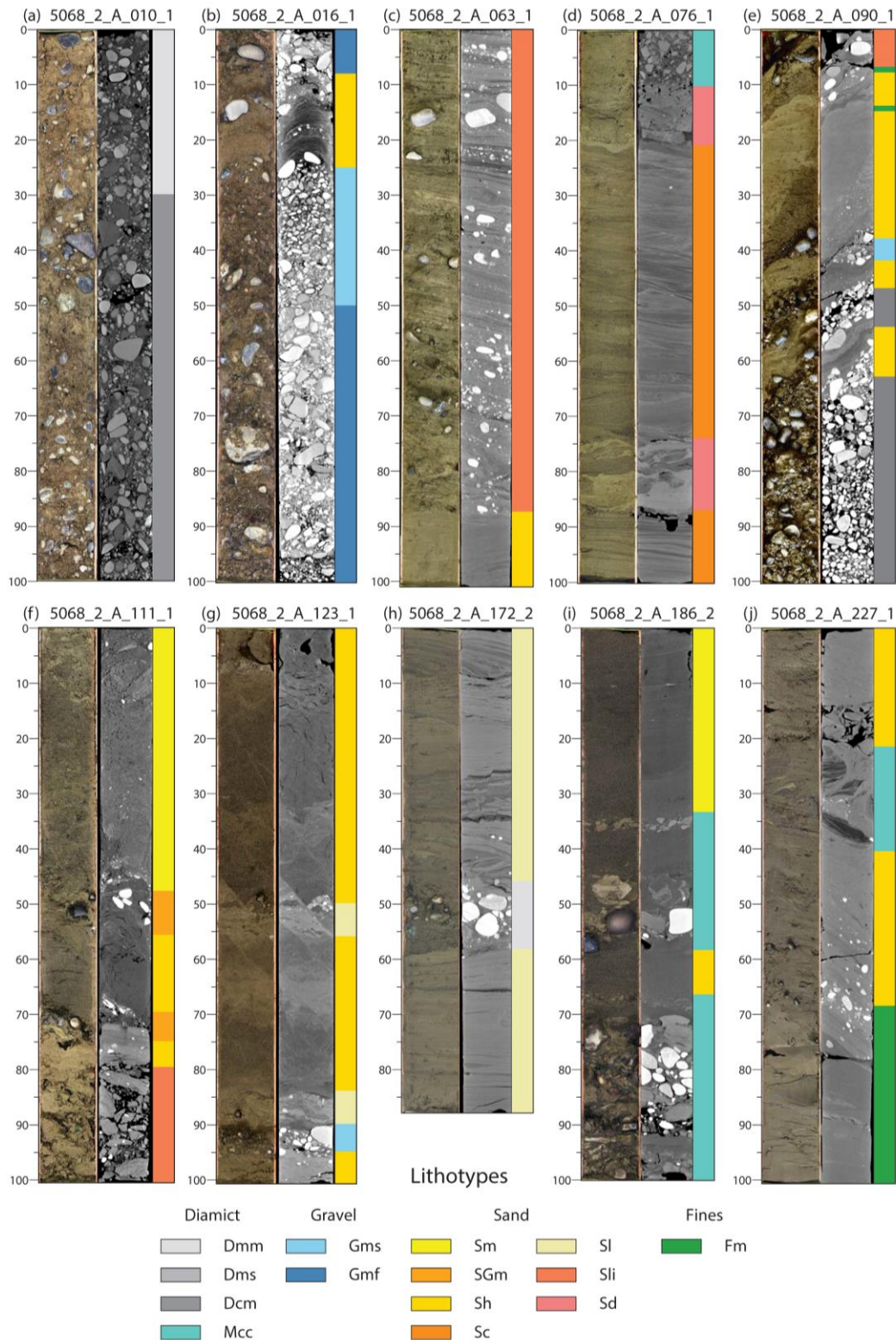


Figure 5: CT and line scans of selected representative core sections with corresponding lithotypes. Each core section is labeled at the top; the scale is in centimeter section depth (cmsd) and shows the following from left to right: line scan, CT scan, and lithotypes. The color code for the lithotypes is given at the bottom. Shown core sections from left to right are the following: (a) 5068_2_A_010_1 (9–10 mtd), (b) 5068_2_A_016_1 (15–16 mtd), (c) 5068_2_A_063_1 (58–59 mtd), (d) 5068_2_A_076_1 (74–75 mtd), (e) 5068_2_A_090_1 (93–94 mtd), (f) 5068_2_A_111_1 (111–112 mtd), (g) 5068_2_A_123_1 (122–123 mtd), (h) 5068_2_A_172_2 (182–182.88 mtd), (i) 5068_2_A_186_2 (196–197 mtd), and (j) 5068_2_A_227_1 (249–250 mtd).








2.4.2 Lithostratigraphic units

Based on the succession of the 14 endmember lithotypes (Table 1), the recovered succession (Fig. 4) was grouped into three lithostratigraphic units (A, B, and C), with Unit A containing five subunits (A1–A5). These units are briefly characterized from bottom to top.

Table 1: Colors and lithocodes of the individual lithotypes with description and interpretations. The line-scan image shows a representative core section (origin of line scan is indicated in the lower-right corner of core photos); scale is in centimeters.

Description		Interpretation	Core photo
Diamicts			
<i>Dmm</i>	Matrix-supported massive: Massive matrix-supported with isolated fine to coarse gravel clasts in a silty to sandy matrix with isolated cobbles (0-40 % clasts, 60-100 % matrix). Crudely bedded in decimeter- to meter-scale by a slight variation in matrix composition and/or in clast size and number. Beige color, many fresh striations, poorly sorted, subangular to subrounded.	i) Subglacial till (Evans et al., 2006) or ii) terrestrial or subaqueous cohesive debris flows with glacial sediment sources (Mulder and Alexander, 2001; Eyles et al., 1983).	
<i>Dms</i>	Matrix-supported stratified diamict: Matrix supported with fine to coarse gravel clasts in a massive sandy to partly silty matrix (0-40 % clasts, 60-100 % matrix), stratified into centimeter- to decimeter-scale beds by oriented but mostly isolated clasts. Beige to grey-beige color, few striations, poorly sorted, subangular to (sub)rounded.	Proximal hyperconcentrated density flow deposits (Mulder and Alexander, 2001).	
<i>Dem</i>	Clast-supported massive diamict: Massive clast-supported, fine to coarse gravel with isolated cobbles with a silty matrix with variable sand content (60-80 % clasts, 20-40 % matrix). Sometimes crudely bedded by a slight variation in matrix composition and dominant clast size. Poorly sorted, beige matrix color, striations, subangular to subrounded.	i) subglacial below or above the fluvial base level (Evans et al., 2006), or ii) glaciofluvial deposits solely above the fluvial base level (Eyles et al., 1983).	
<i>Mcc</i>	Mud-clast conglomerate: Mixture of beige to beige-brown clay chips with a variable medium to coarse gravel content (0->50%) in a grey-beige to brownish medium sandy matrix (5-80 % clasts, 20-95 % matrix). Mud clasts show partially internal structures and rounding of various degrees (subangular to rounded).	Fine lacustrine sediments, rounding indicates transportation upon reworking, eroded by subaqueous mass movements or other subaqueous events with high erosive potential (e.g., Li et al., 2017). The individual gravel content may indicate the type of event, i.e., a high content may indicate a delta collapse as source event.	
Gravels			
<i>Gms</i>	Massive to crudely bedded sandy gravel: Massive medium to coarse (partly fine) gravel, with few isolated sand layers, with little to no silt and isolated cobbles (75-80 % clasts, 20-25 % matrix). Crudely bedded by variation in clast size and number and slight variation in matrix composition, moderately to well sorted, beige to beige-brownish matrix color, (sub)rounded to well rounded.	i) Fluvial to glaciofluvial deposits (over the fluvial base level; Eyles et al., 1983) or ii) subglacial to glaciolacustrine deposits, e.g., high concentration channelized density flows in a subaqueous glacial fan system (below the fluvial base level; Eyles et al., 1983).	
<i>Gmf</i>	Massive to crudely bedded silty sandy gravel: Massive medium to coarse gravel, partly sandy, silty with isolated cobbles (75-80 % clasts, 20-25 % matrix). Crudely bedded by variations in clast size and number and slight variations in matrix composition, moderately to well sorted, brownish-reddish to brownish matrix color, (sub)rounded to well rounded, with some cementations and oxidations.	Fluvial to glaciofluvial deposits (Eyles et al., 1983), in the range of current groundwater fluctuations, leads to cementation and oxidations of clasts.	
Fines			
<i>Fm</i>	Massive clay/silt: Massive clay and silt, little sandy, only very few isolated gravel clasts (C: <1 %, M: >99 %). Partially laminated by intercalating sand laminae resulting in a cm- to dm-scaled bedding, rarely mottled by soft clasts, with some isolated drop stones, well to very well sorted, beige to grey beige, partly slightly brownish.	i) Deposited in calm states of the lake, i.e., (glacio)lacustrine background sedimentation (Leemann and Niessen, 1994). ii) the very top of a concentrated density flows event (Mulder and Alexander, 2001); or iii) very distal from the sediment source or low energy turbidity deposits (Te, Bouma 1962).	

Table 1: Continued

Description		Interpretation	Core photo
Sands			
Sm	Massive sand: Massive fine to medium sand, occasionally coarse sandy, with little to no silt and only isolated gravel clasts (<5 % clasts, >95 % matrix). Crudely bedded in decimeter- to meter-scale by a slight variation in silt content and dominant grain-size fraction, well to very well sorted, greyish-beige to brownish-beige, rarely mottled with soft clasts.	Hyperconcentrated density flow deposits (Mulder and Alexander, 2001).	
SGm	Massive sand and gravel mix: Massive mix of fine to medium sand and gravel, with little to no silt (5-60 % clasts, 40-95 % matrix). Partly centimeter- to decimeter-scale bedded by oriented clasts, moderately to well sorted, subrounded to well rounded, greyish-beige to brownish-beige.	Base of concentrated density-flow deposits, very proximal to sources, or high-energy events (Mulder and Alexander, 2001).	
Sh	Bedded sand: Bedded fine to medium sand, with variable silt content and few isolated gravel clasts (<5 % clasts, >95 % matrix). Bedded in centimeter- to decimeter-scale by a variation in silt content and dominant grain-size fraction, fining up to a massive appearance, well to very well sorted, greyish-beige to brownish-beige.	i) (Massive) hyperconcentrated density flow deposits (Mulder and Alexander 2001), more distal to the source or with less energy, or ii) (stratified) turbidity deposits (Ta; Bouma, 1962; Mulder and Alexander, 2001).	
Sl	Laminated sand: Laminated fine to medium sand with variable silt content, with few isolated clay laminae and isolated gravel clasts (<1 % clasts, >99 % matrix), laminated in millimeter- to centimeter-scale by variations in silt content and dominant grain-size fraction. Individual laminae are fining-up to massive, partially mica-rich, well to very well sorted, greyish-beige to brownish-beige, with partially reddish colors.	Distal or low-energy turbidite deposit (Tb, Td; Bouma, 1962).	
Sc	Cross-bedded sand: Cross-bedded fine to medium sand, partially silty, with isolated clay laminae and very few isolated gravel clasts (<1 % clasts, >99 % matrix). Cross-bedded in centimeter- to decimeter-scale with internal millimeter-scaled laminae, individual laminae are fining up, partly mica-rich, well to very well sorted, greyish-beige to brownish-beige, occasionally of reddish color.	Distal or low energy turbidity deposit (Tc; Bouma, 1962).	
Sil	Irregularly bedded sand, silt, and clay: Silt and clay to coarse sand, with individual gravel clasts (0-10 % clasts, 90-100 % matrix). Irregular in centimeter- to sub-decimeter-scale bedded to laminated, individual lamina/beds are mostly well-sorted and are massive to partly fining-up, partially deformed, with internal erosive contacts, with high contrast, greyish beige to brownish beige.	Stacked successions of different types of density-flow deposits, likely formed under highly variable energy conditions, possibly in cross-cutting subaquatic channel systems.	
Sd	Deformed mix of sand, silt, and clay: Strongly folded and bent mix of originally laminated to bedded sand, clay, and silt with isolated gravel clasts (<1 % clasts, >99 % matrix). Traces of slumps and dehydration structures, ductile deformed, beige to brownish beige.	i) Deformed syn- or postdepositionally by i) rapid loading and dewatering or, ii) mass movements, or iii) glaciotectionics (Evans, 2018).	

Unit A (252.00–47.75 mtd): Unit A consists of primarily sand-dominated sediments (Fig. 5c–j) intercalated by several-meter-thick gravel-dominated beds (Fig. 4). The sand-dominated successions can be distinguished and categorized into three types: i) stacked massive sandy beds with low clay and silt content (Table 1; Sm and Sh), partially separated by clay caps (Fm), and intercalated by isolated minor gravel beds (Gms) or gravel-rich sections (SGm); ii) fine-to-medium sand beds with a higher clay and silt content, thin-bedded (Sh) to laminated (Sl) and partially cross-bedded (Sc), and with isolated clay laminae (Fm); and iii) massive sand (Sm, Sh, Sl, and Sil) interbedded to intercalated with mostly centimeter-to-decimeter-scaled partly stratified beds of sand and gravel mix (SGm), massive gravel beds (Gms), and stratified (Dms) or massive diamictic (Dmm) beds. The sandy successions, in parts, show traces of

ductile deformations (Table 1; Sd, e.g., boudinage, flame structures, folding, and dewatering structures) and some brittle deformation (e.g., small-scale faults). The bases of the rather massive sandy or gravel-rich beds partially show erosive contacts, which may contain rip-up clasts (Mcc).

The gravel-dominated beds within Unit A can be further divided into two types: i) more diamictic beds (Table 1; Dcm) with a silt-rich matrix, steeply inclined beds, and, in parts, including striated and bullet-shaped clasts and ii) gravel beds (Gms) with better clast rounding, low silt and clay content, and a primarily sandy matrix. The base of Unit A (> 249.7 mtd) is built by a succession of diamictic beds with a massive dropstone-rich ~ 0.5 m thick clay bed on top (Fm; Fig. 5j). Several larger Molasse bedrock fragments and clasts with glacial striations occur in this diamictic succession. Additionally, some coarse-grained sections have a high permeability as large volumes of fluids were lost during drilling.

Over the entire Unit A, the sandy sections generally show lower density and magnetic susceptibility values and higher natural gamma values than gravelly ones (Fig. 4). Organic matter content varies between 0.5 % and 1 % except from some isolated peaks of up to 2 % in the sandy sections and a drop to nearly 0 % below 217 mtd. The carbonate content ranges between ~ 40 % and 50 %.

Unit B (47.75–11.00 mtd): Unit B consists of a succession of decimeter-to-meter-thick beds of sandy (Table 1; Gms) to partly silty (Gmf) gravel with isolated sand beds. The gravel beds are well sorted to locally moderately sorted with a clast-size range from fine to coarse gravel with some cobbles, and clasts are mostly (sub-)rounded to well-rounded. The groundwater table separates the succession of Unit B into the following: i) below ~ 29.5 mtd, constantly water saturated and with a sand-rich and silt-and-clay-poor matrix, and ii) above ~ 29.5 mtd, affected by the fluctuation of the groundwater table, with local cementations and oxide-covered clasts and a partly silt- and clay-enriched matrix (Fig. 5b). The section generally has a high density with stepwise changes above the groundwater table, high but noisy magnetic susceptibility values, and low natural gamma values (Fig. 4). Furthermore, Unit B has a low organic matter content of ~ 1 % and a highly variable carbonate content between 35 % and 65 %.

Unit C (11.00–0.00 mtd): The uppermost unit consists mainly of a massive to crudely bedded, poorly sorted, silty to partly sandy matrix-supported diamict (Table 1; Dmm; Fig. 5a) with a clast-size range from fine gravel up to cobbles and a frequent appearance of striated and/or

bullet-shaped/flat-iron-shaped clasts. A general fining-up trend occurs in the clast size together with a decrease in clast content from $\sim 80\%$ to $> 5\%$, supported by the up-core decreasing trend of the density values and the negatively corresponding natural gamma log (Fig. 4). The uppermost ~ 1 m shows an increasing level of organic matter, decalcification, signs of bioturbation, and a humus layer on its very top.

2.5 Interpretation and discussion

2.5.1 Interpretation of depositional environment

Unit A (252.00–47.75 mtd) overdeepened basin fill: The sediments of Unit A were deposited in an overdeepened setting in a clastic-dominated glacial, glaciolacustrine, or lacustrine environment. The thick, stacked succession of current and mass-movement-dominated lithotypes suggests that the overdeepening was the depocenter and dominated by fast accumulation forming deltaic or basin-floor fan systems (Table 1). In such a setting, the observed lithotype association with thick sandy successions (mainly Sm and Sh), interbedded gravels (Gms), and gravelly diamicts (Dms, Dcm, and Mcc) may be interpreted as an externally forced system driven by allogenic or autogenic processes. In the case of an autogenic endmember, the activity and proximity of the sediment influx from the glacier or rivers exert the dominant controls defining the primary sediment and energy source (e.g., Fitzsimons & Howarth, 2018; Lønne, 1995). Thus the changes in the grain-size distribution and the thickness of the bedding may represent changes in the glacier's position. However, since these energy changes are not instantaneous but occur gradually over a longer time, other processes are needed to explain the frequently observed grain-size variations. Alternatively, accumulation on proximal basin-floor fan systems is associated with considerable lateral facies variability, reflecting allogenic changes of the deposition on basin-floor fans (Fitzsimons & Howarth, 2018; Lønne, 1995). This would partly suppress the sedimentary traces of the glacial proximity-related long-term depositional environmental changes, especially the potential shift from a glaciolacustrine towards a more lacustrine regime. Nevertheless, with an increasing distance of the glacier, the dominant depositional environment will evolve from a direct glacial, via a glaciolacustrine, to a lacustrine one, which may even develop into a warm lake state until the next glacial advance will reverse the evolution (e.g., Anselmetti et al., 2022; Dehnert et al., 2012; Fitzsimons & Howarth, 2018). On the basis of these processes, the succession of depositional environments of Unit A is subdivided into five subunits (from bottom to top, A1–A5):

Subunit A1 (> 249.7 mtd): The basal diamictic succession (Table 1; Dmm, Dcm, and Fm) is interpreted as proximal, submarginal to possibly subglacial deposits, emplaced in close proximity to a glacier grounded in the deep trough. The interpretation is supported by the pervasive occurrence of striated clasts and the strongly inclined bedding, indicating glaciotectionic processes. The large number of local bedrock fragments in the basal succession indicates proximity to the bedrock surface. The succession shows similar properties to the basal sediments encountered by Dehnert et al. (2012), Buechi et al. (2017), and Schwenk et al. (2022). These deposits were also interpreted by them as ice-contact sediments at the transition to glaciolacustrine deposition. This transition is represented in the recovered sediment succession by a massive clay bed (Fig. 5j).

Subunit A2 (249.7–0128.7 mtd): This section is interpreted to have been deposited in a glaciolacustrine setting and consists of the following: i) thick to medium bedded sand-dominated hyperconcentrated to concentrated density-flow deposits (Table 1; Sm and Sh; Mulder & Alexander, 2001); ii) massive gravel-dominated beds, likely high-concentration channelized density-flow deposits (Gms), originating from a subaqueous glacial fan system (Eyles & Eyles, 1983); and iii) a succession of rather thin-bedded to laminated sands of likely turbiditic origin (Sl and Sc; Bouma, 1962; Mulder & Alexander, 2001). This turbiditic succession separates the partially interbedded sand-dominated and gravel-dominated density-flow deposits into a lower and upper succession, and the latter is terminated by a massive gravel bed. Since these sharp changes in grain size and bedding, frequently observed in this unit, are likely directly related to the flow energy, they may also indicate a lateral variation of the glacier outlet or local subaquatic channel-levee patterns along the submerged proglacial front. Thus, the long-term grain-size evolution controlled by glacier proximity is superimposed by higher-frequency changes caused by local variations in this highly dynamic setting of the glacier front. Therefore, it is unclear if the laminated to partially cross-bedded succession represents a rather lacustrine environment with a more distal-located glacier or a low-energy endmember of the lateral changing depositional system.

Subunit A3 (128.7–103.2 mtd): The succession of tightly interbedded sand (Table 1; Sh) and gravel (Gms) beds shows a partially diamictic character (Dms, Mcc, and Sil). These gravel-rich beds possibly represent slumps and subaquatic mass movements originating on unstable slopes of the rapidly infilling basin (e.g., deltas). The collapse

of these unstable slope deposits could be linked to increased sediment flux caused by increased fluvial activity (e.g., glacial outburst floods), an advancing glacial front, or even earthquake shaking. The section shows traces of likely glaciotectonic overprinting (Sd, ductile and brittle deformation structures). Further, the top contact of this succession is built by a strongly ductile deformed and/or folded sand bed (Sd).

Subunit A4 (103.2–91.0 mtd): This upper diamictic succession (Table 1; Dcm) is similar to the basal one of Subunit A1 but lacks a massive clay bed on top (Fig. 5e and 5j). The upper diamict is also interpreted as subglacial deposits, possibly representing another period of ice contact or at least ice proximity. The sharp and high-frequency changes in grain size of the diamict's top (Sil, Dcm, and Fm) indicate a partially high-energy but unstable environment. This transition is possibly related to pulsing channelized glacial meltwater outbursts that prevented the deposition of a massive clay bed here.

Subunit A5 (91.0–47.7 mtd): Subunit A5 is similar to the lower glaciolacustrine section of Subunit A2. However, the overall absence of the massive gravel beds indicates a shift to a more glaciolacustrine-to-lacustrine environment where the depositional energy was lower. Moreover, the succession shows some sections enriched in dropstones (Fig. 5c), pointing to a distal ice-contact lake environment. The whole sediment succession of Unit A is sharply cut off by the sediments of Unit B.

Unit B (47.75–11.00 mtd) fluvial gravel: The sediments of Unit B are interpreted as fluvial-to-glaciofluvial gravels (Table 1; Gms and Gmf). On the basis of the geographical and stratigraphic position, they are correlated with the local gravel formation “Buechberg Gravel Complex”, which also covers the surrounding areas and is interpreted as a Middle Pleistocene advance gravel (Graf, 2009b; Müller, 2013). Further, the relief of the contact surface between Unit A and Unit B indicates a strong fluvial erosion of the former top sediments of Unit A during the deposition of the gravels of Unit B (see Sect. 2 “Study area”; Graf, 2009b; Müller, 2013).

Unit C (11.00–0.00 mtd) glaciogenic diamicts: The sediments of Unit C are interpreted as a subglacial till and associated glaciogenic diamicts (Table 1; Dmm and Dcm). This interpretation is supported by the following: i) the high density and consolidation; ii) the diamictic texture (e.g., Evans, 2018; Evans et al., 2006); iii) the abundance of fresh traces of direct ice-contact transportation (e.g., striated and/or bullet-shaped clasts, e.g., Evans, 2018; Evans et al., 2006); and iv) the stratigraphic position. As the drill site is located within the LGM

extent of the former Rhine Glacier (Fig. 1a), at least the upper part, if not all of Unit C, was emplaced during the LGM glaciation (Birrfeld glaciation). Alternatively, the lower parts of Unit C may have been emplaced during earlier glaciations that reached the area, e.g., during MIS6 (Beringen glaciation, e.g., Müller, 2013; where MIS represents marine isotope stage). However, a clear unconformity was not observed in the recovered diamicts.

2.5.2 Implications for glacial history

Assuming that each glacial cycle may have left glacial deposits behind, the two diamictic deposits (Subunits A1 and A4) encountered in an overdeepened position may indicate the presence of at least two glacial sedimentary sequences within Unit A with a sequence boundary between ~ 103 and 91 mtd (Subunit A4). This interpretation is supported by the presence of glaciotectionic deformations and pressure-related dewatering structures between 128.7–103.2 mtd (Subunit A3), which may have been caused by an overriding glacier during a next glacial cycle. The postulated glacial sequence boundary potentially coincides with the depth of a prominent erosive discontinuity observed in the seismic data (solid dark blue line in Fig. 1c; Brandt, 2020). This coincidence supports the interpretation that a second glacier advance is documented in the upper part of the Basadingen Through, which apparently eroded more into the width while not removing the deeper basin fill. Future age constraints will place these successions in the context of the marine isotope stages.

Since the whole succession of Unit A was deposited mostly under glacial to glaciolacustrine conditions, the lack of a significant amount of clay- and silt-rich glaciolacustrine background sediments (Fm) has been rather surprising. This disparity may be explained by either of the following: i) no considerable amount of such sediments were deposited since the accommodation space was quickly filled by the sandy and gravelly sediments or ii) they were eroded after deposition as a former presence is at least indicated by the occurrence of mud-clast conglomerates (Mcc, rich in clay and silt rip-up clasts). Likely, both processes may have acted together in the assumed high-energy and clastic-dominated glaciolacustrine environment.

In addition to the lack of fine-grained glaciolacustrine deposits, the absence of the fine-grained interstadial/interglacial lacustrine deposits is likely explained by the following: i) the possibility that the lake never developed such a state as it became rapidly filled in late glacial periods, ii) by cold and/or short interstadials, or iii) if deposited initially they were eroded during the next glacial advance. In the case of the proposed lower glacial cycle below 103.2 mtd, the first or second case may apply since the observed increased appearance of

diamictic slumps and subaquatic mass-movement deposits between 128.7–103.2 mtd may indicate a rapid glacial readvance after a short interstadial. However, in the case of the proposed upper cycle, the third explanation might act since at least its top was eroded to a certain degree by the overlying gravels of Unit B. Based on these observations, the proposed lower cycle may be, even if not completely preserved, at least more complete than the proposed upper cycle.

However, the existence of such significant “cold” or “warm” lacustrine deposits can not be ruled out for the whole Basadingen Trough since i) this observation is only based on information from one drill hole; ii) the assumed highly variable depositional environment; and iii) due to possible spatial effects, which may impact the probability of local accumulation of such deposits (e.g., subaquatic channels or subaquatic deltas).

The overlying gravels and tills of Units B and C are documenting the glaciation history after the filling of the trough. The gravels of Unit B document the presence of a glacier upstream of the drill site on at least one occasion before it was covered at least once again during the LGM advance of the Rhine Glacier. Whether more than one glacial cycle is preserved in Units B and C, as suggested by Graf (2009b) and Müller (2013), will be addressed with the planned geochronological analysis.

2.6 Summary and outlook

The proposed complex based on seismic data, possibly multi-phase sedimentary fill of the Basadingen Trough (Fig. 1c; Anselmetti et al., 2022; Brandt, 2020), is fully supported by the drilled and recovered succession, even though the bedrock, predicted at ~ 240 m, was not reached with the final depth of 252 m. It is currently unclear if this is due to an inaccurate identification of the bedrock reflection or to an inaccurate velocity model. Analyzing the vertical seismic profile (VSP) will reveal more details on the bedrock's location. However, the appearance of cobble-sized freshwater molasse fragments indicates the nearby occurrence of the bedrock contact. A first correlation of the drilled succession with the seismic interpretation indicates the coincidence of the glacial depositional sequence at ~ 103 mtd or ~ 340 m a.s.l. with the seismic sequence boundary (Figs. 1c and 4; Brandt, 2020), indicating that the Rhine Glacier advanced over the upper part of the Basadingen Trough at that time. This pattern further supports the sedimentary succession's proposed multi-phase origin in at least two glacial cycles (Anselmetti et al., 2022). Furthermore, the lacustrine (overdeepened) character of the sediments of Subunit A5 indicates a higher fluvial base level at that time, as was proposed by Graf (2009b) and Müller (2013).

Upcoming correlations of seismic, wireline, and core data will help to establish a robust model of the evolution of the Basadingen Trough. The systematical correlation and characterization of the sedimentological core properties with the extended geophysical and geochemical dataset will refine the definition of glacial sequence stratigraphy that can eventually be dated by the planned geochronological data. This will contribute to the understanding of the local and regional glaciation history, the formation of overdeepenings in the Alpine foreland, and (within the context of DOVE) glaciation and landscape evolution of the Alps.

2.7 Further statements

2.7.1 Data availability

The DOVE operational dataset is published under <https://doi.org/10.5880/ICDP.5068.001> (DOVE-Phase 1 Scientific Team et al., 2023b) together with the operational report (DOVE-Phase 1 Scientific Team et al., 2023a) and the explanatory remarks (DOVE-Phase 1 Scientific Team et al., 2023c). Information on the project and the data is also available on the ICDP DOVE project website: <https://www.icdp-online.org/projects/by-continent/europe/dove-switzerland>.

2.7.2 Sample availability

IGSNs are assigned to the hole and sample material; samples are available upon request; for further information, see the operational dataset (Dove-Phase 1 Scientific Team et al., 2023b) and the operational report (DOVE-Phase 1 Scientific Team et al., 2023a).

2.7.3 Author contributions

SS served as the leading drill site geologist during the drilling operation, had the lead in the ICD, analyzed the data, and was the main author of the paper with the support of FSA and MWB. BS helped as a substitute drill site geologist and contributed substantially to the ICD. MWB and FSA organized the drilling campaign, operated as substitute drill site geologists, provided support and advice for SS during the drilling operation and the ICD, and provided significant scientific input to the paper as part of their role as PhD supervisors of SS. All authors approved the text and the figures.

2.7.4 Competing interests

The contact author has declared that none of the authors has any competing interests.

2.7.5 Financial support

This research has been supported by the ICDP, the Deutsche Forschungsgemeinschaft (DFG, grant nos. KR2073/3-1, BU 2467/1-2, GA749/5-1, BU 2467/3-1, BU 3894/2-1, BU 3894/3-1, and PR 957/6-1), Nagra, ENSI, LGRB, LFU, LIAG, BOKU Vienna, and University of Bern.

2.7.6 Review statement

This paper was edited by Nadine Hallmann and reviewed by Bernd Wagner and Pierre Dietrich.

2.8 Acknowledgments

We are grateful for continuing support of the International Scientific Continental Drilling Program (ICDP), including the ICDP Operational Support Group for providing the on-site MSCL scanner and the database management tool “mDis”. We acknowledge the tremendous effort of the drilling company, Fretus AG, in particular the drilling crew (Juan Gonzalez, Marek Bajcura, Joaquim Teixeira) for providing us with high-quality drill cores, as well as the technical staff of LIAG, who assisted with the seismic pre-site surveys and the downhole logging. Further, we acknowledge the strong support by the members of the Bürgergemeinde Basadingen-Schlattingen, the members of the Jagdgesellschaft Hegi Belzhalden, the local inhabitants, the involved services of the political community Basadingen-Schlattingen, and the Canton of Thurgau. A special thanks goes to Luka Seslak (our technical drilling consultant), Julijana Gajic, Patrizia Ruffiner (for processing and analyzing the TIC and TOC samples), Kim Lemke (for core transport and support on the drill site), and to the whole DOVE science team for their effort to make this project happen and for keeping it running.

2.9 References

- Alley, R. B., Cuffey, K. M., & Zoet, L. K. (2019). Glacial erosion: Status and outlook. *Annals of Glaciology*, 60(80), 1–13. <https://doi.org/10.1017/aog.2019.38>
- Anselmetti, F. S., Bavec, M., Crouzet, C., Fiebig, M., Gabriel, G., Preusser, F., Ravazzi, C., & DOVE scientific team. (2022). Drilling Overdeepened Alpine Valleys (ICDP-DOVE): Quantifying the age, extent, and environmental impact of Alpine glaciations. *Scientific Drilling*, 31, 51–70. <https://doi.org/10.5194/sd-31-51-2022>
- Bouma, A. H. (1962). *Sedimentology of some Flysch deposits: A graphic approach to facies interpretation*. Elsevier. <http://lib.ugent.be/catalog/rug01:000978747> (last access: 21 September 2023)
- Brandt, A. C. (2020). *Erkundung des alpinen, glazial-übertieften Basadingen-Beckens mithilfe von P-Wellen-Seismik [BSc thesis]*. Leibniz Universität Hannover.
- Buechi, M. W., Frank, S. M., Graf, H. R., Menzies, J., & Anselmetti, F. S. (2017). Subglacial emplacement of tills and meltwater deposits at the base of overdeepened bedrock troughs. *Sedimentology*, 64(3), 658–685. <https://doi.org/10.1111/sed.12319>
- Buechi, M. W., Graf, H. R., Haldimann, P., Lowick, S. E., & Anselmetti, F. S. (2018). Multiple Quaternary erosion and infill cycles in overdeepened basins of the northern Alpine foreland. *Swiss Journal of Geosciences*, 111(1–2), 133–167. <https://doi.org/10.1007/s00015-017-0289-9>
- Clark, P. U., Archer, D., Pollard, D., Blum, J. D., Rial, J. A., Brovkin, V., Mix, A. C., Pisias, N. G., & Roy, M. (2006). The middle Pleistocene transition: Characteristics, mechanisms, and implications for long-term changes in atmospheric pCO₂. *Quaternary Science Reviews*, 25(23–24), 3150–3184. <https://doi.org/10.1016/j.quascirev.2006.07.008>
- Cohen, D., Gillet-Chaulet, F., Haeberli, W., Machguth, H., & Fischer, U. H. (2018). Numerical reconstructions of the flow and basal conditions of the Rhine glacier, European Central Alps, at the Last Glacial Maximum. *The Cryosphere*, 12(8), 2515–2544. <https://doi.org/10.5194/tc-12-2515-2018>
- Cook, S. J., & Swift, D. A. (2012). Subglacial basins: Their origin and importance in glacial systems and landscapes. *Earth-Science Reviews*, 115(4), 332–372. <https://doi.org/10.1016/j.earscirev.2012.09.009>
- Dehnert, A., Lowick, S. E., Preusser, F., Anselmetti, F. S., Drescher-Schneider, R., Graf, H. R., Heller, F., Horstmeyer, H., Kemna, H. A., Nowaczyk, N. R., Züger, A., & Furrer, H. (2012). Evolution of an overdeepened trough in the northern Alpine Foreland at Niederweningen, Switzerland. *Quaternary Science Reviews*, 34, 127–145. <https://doi.org/10.1016/j.quascirev.2011.12.015>
- DOVE-Phase 1 Scientific Team, Anselmetti, F. S., Beraus, S., Buechi, M. W., Buness, H., Burschil, T., Fiebig, M., Firla, G., Gabriel, G., Gegg, L., Grelle, T., Heeschen, K., Kroe-mer, E., Lehne, C., Lüthgens, C., Neuhuber, S., Preusser, F., Schaller, S., Schmalzfuss, C., Schuster, B., Tanner, D. C., Thomas, C., Tomonaga, Y., Wieland-Schuster, U., and Wonik, T. (2023a). Drilling Overdeepened Alpine Valleys (DOVE) – Operational Report of Phase 1, (ICDP Operational Report), GFZ German Research Centre for Geosciences, Potsdam, 70 pp., <https://doi.org/10.48440/ICDP.5068.001>
- DOVE-Phase 1 Scientific Team, Anselmetti, F. S., Beraus, S., Buechi, M. W., Buness, H., Burschil, T., Fiebig, M., Firla, G., Gabriel, G., Gegg, L., Grelle, T., Heeschen, K., Kroe-mer, E., Lehne, C., Lüthgens, C., Neuhuber, S., Preusser, F., Schaller, S., Schmalzfuss, C., Schuster, B., Tanner, D. C., Thomas, C., Tomonaga, Y., Wieland-Schuster, U., and Wonik, T. (2023b). Drilling Overdeepened Alpine Valleys (DOVE) – Operational Dataset of DOVE Phase 1, GFZ Data Services [data set], <https://doi.org/10.5880/ICDP.5068.001>
- DOVE-Phase 1 Scientific Team, Anselmetti, F. S., Beraus, S., Buechi, M. W., Buness, H., Burschil, T., Fiebig, M., Firla, G., Gabriel, G., Gegg, L., Grelle, T., Heeschen, K., Kroe-mer, E., Lehne, C., Lüthgens, C., Neuhuber, S., Preusser, F., Schaller, S., Schmalzfuss, C., Schuster, B., Tanner, D. C., Thomas, C., Tomonaga, Y., Wieland-Schuster, U., and Wonik, T. (2023c). Drilling Overdeepened Alpine Valleys (DOVE) – Explanatory remarks on the operational dataset, ICDP Operational Dataset – Explanatory Remarks, GFZ German Research Centre for Geosciences, Potsdam, 34 pp., <https://doi.org/10.48440/ICDP.5068.002>
- Ellwanger, D., Wieland-Schuster, U., Franz, M., & Simon, T. (2011). The Quaternary of the southwest German Alpine Foreland (Bodensee-Oberschwaben, Baden-Württemberg, Southwest Germany). *E&G Quaternary Science Journal*, 60(2/3), 306–328. <https://doi.org/10.3285/eg.60.2-3.07>
- Evans, D. (2018). Till: A Glacial Process Sedimentology. In *Till: A Glacial Process Sedimentology* (p. 390). John Wiley & Sons. <https://doi.org/10.1002/9781118652541>
- Evans, D. J. A., Phillips, E. R., Hiemstra, J. F., & Auton, C. A. (2006). Subglacial till: Formation, sedimentary characteristics and classification. *Earth-Science Reviews*, 78(1), 115–176. <https://doi.org/10.1016/j.earscirev.2006.04.001>
- Eyles, C. H., & Eyles, N. (1983). Glaciomarine model for upper Precambrian diamictites of the Port Askaig Formation, Scotland. *Geology*, 11(12), 692–696. [https://doi.org/10.1130/0091-7613\(1983\)11<692:GMFUPD>2.0.CO;2](https://doi.org/10.1130/0091-7613(1983)11<692:GMFUPD>2.0.CO;2)
- Fabbri, S. C., Affentranger, C., Krastel, S., Lindhorst, K., Wessels, M., Madritsch, H., Allenbach, R., Herwegh, M., Heuberger, S., Wieland-Schuster, U., Pomella, H., Schwestermann, T., & Anselmetti, F. S. (2021). Active Faulting in Lake

- Constance (Austria, Germany, Switzerland) Unraveled by Multi-Vintage Reflection Seismic Data. *Frontiers in Earth Science*, 9. <https://www.frontiersin.org/articles/10.3389/feart.2021.670532>
- Fiebig, M., Herbst, P., Drescher-Schneider, R., Lüthgens, C., Lomax, J., & Doppler, G. (2014). Some remarks about a new Last Glacial record from the western Salzach foreland glacier basin (Southern Germany). *Quaternary International*, 328–329, 107–119. <https://doi.org/10.1016/j.quaint.2013.12.048>
- Fitzsimons, S., & Howarth, J. (2018). Chapter 9—Glaciolacustrine Processes. In J. Menzies & J. J. M. van der Meer (Eds.), *Past Glacial Environments* (Second Edition) (pp. 309–334). Elsevier. <https://doi.org/10.1016/B978-0-08-100524-8.00009-9>
- Graf, H. R. (2009a). Stratigraphie und Morphogenese von frühpleistozänen Ablagerungen zwischen Bodensee und Klettgau. *E&G Quaternary Science Journal*, 58(1), 12–54. <https://doi.org/10.3285/eg.58.1.02>
- Graf, H. R. (2009b). Stratigraphie von Mittel- und Spätpleistozän in der Nordschweiz. *Beiträge zur Geologischen Karte der Schweiz* (N.F.) (Vol. 168). Landesgeologie.
- Gribenski, N., Valla, P. G., Preusser, F., Roattino, T., Crouzet, C., & Buoncristiani, J.-F. (2021). Out-of-phase Late Pleistocene glacial maxima in the Western Alps reflect past changes in North Atlantic atmospheric circulation. *Geology*, 49(9), 1096–1101. <https://doi.org/10.1130/G48688.1>
- Haeuselmann, P., Granger, D. E., Jeannin, P.-Y., & Lauritzen, S.-E. (2007). Abrupt glacial valley incision at 0.8 Ma dated from cave deposits in Switzerland. *Geology*, 35(2), 143. <https://doi.org/10.1130/G23094A>
- Hofmann, F. (1967). Erläuterungen zu: Geologischer Atlas der Schweiz—1052 Andelfingen [Atlasblatt 52]. Schweiz. Geol. Komm.
- Hofmann, F., & Hantke, R. (1964). Erläuterungen zu Blatt 1032 Diessenhofen des geologischen Atlas der Schweiz. Schweiz. Geol. Komm.
- Ivy-Ochs, S., Kerschner, H., Reuther, A., Preusser, F., Heine, K., Maisch, M., Kubik, P. W., & Schlüchter, C. (2008). Chronology of the last glacial cycle in the European Alps. *Journal of Quaternary Science*, 23(6–7), 559–573. <https://doi.org/10.1002/jqs.1202>
- Keller, O., & Krayss, E. (1993). The rhine-linth glacier in the upper wurm: A model of the last alpine glaciation. *Quaternary International*, 18, 15–27. [https://doi.org/10.1016/1040-6182\(93\)90049-L](https://doi.org/10.1016/1040-6182(93)90049-L)
- Leemann, A., & Niessen, F. (1994). Holocene glacial activity and climatic variations in the Swiss Alps: Reconstructing a continuous record from proglacial lake sediments. *The Holocene*, 4(3), 259–268. <https://doi.org/10.1177/095968369400400305>
- Li, S., Li, S., Shan, X., Gong, C., & Yu, X. (2017). Classification, formation, and transport mechanisms of mud clasts. *International Geology Review*, 59, 1609–1620. <https://doi.org/10.1080/00206814.2017.1287014>
- Lisiecki, L. E., & Raymo, M. E. (2005). A Pliocene-Pleistocene stack of 57 globally distributed benthic $\delta^{18}\text{O}$ records. *Paleoceanography*, 20(1). <https://doi.org/10.1029/2004PA001071>
- Lønne, I. (1995). Sedimentary facies and depositional architecture of ice-contact glaciomarine systems. *Sedimentary Geology*, 98(1), 13–43. [https://doi.org/10.1016/0037-0738\(95\)00025-4](https://doi.org/10.1016/0037-0738(95)00025-4)
- Meyers, P. A., & Teranes, J. L. (2001). Sediment Organic Matter. In W. M. Last & J. P. Smol (Eds.), *Tracking Environmental Change Using Lake Sediments: Physical and Geochemical Methods* (pp. 239–269). Springer Netherlands. https://doi.org/10.1007/0-306-47670-3_9
- Mulder, T., & Alexander, J. (2001). The physical character of subaqueous sedimentary density flows and their deposits. *Sedimentology*, 48(2), 269–299. <https://doi.org/10.1046/j.1365-3091.2001.00360.x>
- Müller, E. R. (2013). Mittelpleistozäne Schottervorkommen zwischen dem Thurtal und Schaffhausen. *Swiss Bulletin für angewante Geologie*, 18(1), 3–27. <https://doi.org/10.5169/SEALS-391135>
- Penck, A., & Brückner, E. (1909). *Die Alpen im Eiszeitalter*. Tauchnitz.
- Pietsch, J., & Jordan, P. (2014). Digitales Höhenmodell Basis Quartär der Nordschweiz – Version 2014 und ausgewählte Auswertungen (Technical report 14–02; Nagra Arbeitsbericht NAB). <https://nagra.ch/downloads/arbeitsbericht-nab-14-02/>
- Pomper, J., Salcher, B. C., Eichkitz, C., Prasicek, G., Lang, A., Lindner, M., & Götz, J. (2017). The glacially overdeepened trough of the Salzach Valley, Austria: Bedrock geometry and sedimentary fill of a major Alpine subglacial basin. *Geomorphology*, 295, 147–158. <https://doi.org/10.1016/j.geomorph.2017.07.009>
- Preusser, F., Graf, H. R., Keller, O., Krayss, E., & Schlüchter, C. (2011). Quaternary glaciation history of northern Switzerland. *E&G Quaternary Science Journal*, 60(2/3), 282–305. <https://doi.org/10.3285/eg.60.2-3.06>
- Preusser, F., Reitner, J. M., & Schlüchter, C. (2010). Distribution, geometry, age and origin of overdeepened valleys and basins in the Alps and their foreland. *Swiss Journal of Geosciences*, 103(3), 407–426. <https://doi.org/10.1007/s00015-010-0044-y>
- Reber, R., & Schlunegger, F. (2016). Unravelling the moisture sources of the Alpine glaciers using tunnel valleys as constraints. *Terra Nova*, 28(3), 202–211. <https://doi.org/10.1111/ter.12211>

- Ruddiman, W. F., Raymo, M., & McIntyre, A. (1986). Matuyama 41,000-year cycles: North Atlantic Ocean and northern hemisphere ice sheets. *Earth and Planetary Science Letters*, 80(1), 117–129. [https://doi.org/10.1016/0012-821X\(86\)90024-5](https://doi.org/10.1016/0012-821X(86)90024-5)
- Schaller, S., Böttcher, M. E., Buechi, M. W., Epp, L. S., Fabbri, S. C., Gribenski, N., Harms, U., Krastel, S., Liebezeit, A., Lindhorst, K., Marxen, H., Raschke, U., Schleheck, D., Schmiedinger, I., Schwalb, A., Vogel, H., Wessels, M., & Anselmetti, F. S. (2022). Postglacial evolution of Lake Constance: Sedimentological and geochemical evidence from a deep-basin sediment core. *Swiss Journal of Geosciences*, 115(1), 7. <https://doi.org/10.1186/s00015-022-00412-1>
- Schlüchter, C. (2004). The Swiss glacial record – a schematic summary. In *Developments in Quaternary Sciences* (Vol. 2, pp. 413–418). Elsevier. [https://doi.org/10.1016/S1571-0866\(04\)80092-7](https://doi.org/10.1016/S1571-0866(04)80092-7)
- Schwenk, M. A., Schläfli, P., Bandou, D., Gribenski, N., Douillet, G. A., & Schlunegger, F. (2022). From glacial erosion to basin overfill: A 240 m-thick overdeepening–fill sequence in Bern, Switzerland. *Scientific Drilling*, 30, 17–42. <https://doi.org/10.5194/sd-30-17-2022>
- Spötl, C., Koltai, G., Jarosch, A. H., & Cheng, H. (2021). Increased autumn and winter precipitation during the Last Glacial Maximum in the European Alps. *Nature Communications*, 12(1), Article 1. <https://doi.org/10.1038/s41467-021-22090-7>
- Valla, P. G., Shuster, D. L., & van der Beek, P. A. (2011). Significant increase in relief of the European Alps during mid-Pleistocene glaciations. *Nature Geoscience*, 4(10), 688–692. <https://doi.org/10.1038/ngeo1242>

3

Seismic- and core-based glacial sequence stratigraphy in an overdeepened perialpine trough in the northern Alpine foreland of Switzerland

Sebastian Schaller^{1,2}

Bennet Schuster^{3,1,2}

Sarah Beraus⁴

MariusW. Buechi^{1,2}

Bennet Schuster^{3,1,2}

Hermann Bunes⁴

Flavio S. Anselmetti^{1,2}

¹Institute of Geological Sciences, Universität Bern,

²Oeschger Centre for Climate Change Research, Universität Bern

³Institute of Earth and Environmental Sciences, University of Freiburg

⁴LIAG Institute for Applied Geophysics

After the initial rejection of an older version of this manuscript by a different journal, this version was (re)submitted in late December by the *Swiss Journal of Geoscience*.

3. Seismic- and core-based glacial sequence stratigraphy in an overdeepened perialpine trough in the northern Alpine foreland of Switzerland

3.1 Abstract

In the context of a project of the International Continental Scientific Drilling Program (ICDP) (DOVE; Drilling Overdeepened Alpine Valleys), a series of boreholes were drilled into buried overdeepened glacial troughs in the central and eastern part of the northern Alpine foreland. The sedimentary records of these overdeepenings, reaching back to the Middle Pleistocene, are essential archives for paleoclimate and key to better understanding past glaciations and landscape evolution. As part of the project, an over 250 m long succession of unconsolidated Quaternary sediments was recovered from the Basadingen Trough (ICDP 5068_2, NE Switzerland), belonging to the NW part of the former Rhine Glacier's foreland lobe. The drill site is positioned on a high-resolution 2D seismic line, serving as the basis for a seismic sequence and facies analysis. Acoustic wire-line logging data (vertical seismic profile - VSP) directly links the sediment succession with the seismic data, allowing the establishment of a detailed and unifying seismic- and core-based glacial sequence stratigraphy. Based on this stratigraphy, the overdeepened valley fill could be grouped into three overdeepened glacial sequences (S1–S3), reflecting three pulses of glacial advance and retreat.

Furthermore, a 3D model of a segment of the Basadingen Trough was created by combining the 2D seismic lines with the local geological information, visualizing the shape of the initial bedrock incision, the multiphase trough-infill architecture, and the overlying non-overdeepened cover. The model helps overcome inherent limitations in two-dimensional representations. A generic model for a glacio-seismic sequence is developed that underlines the benefits of combining complementary geological and geophysical data in these highly complex depositional settings. The close link of these sequences to glacial advance-retreat cycles contributes to the development of a local glaciation model, as shown for the Basadingen Trough. This approach can be applied to other similar settings in formerly glaciated areas.

3.2 Introduction

3.2.1 Background and motivation

The Quaternary is characterized by its recurrent glacial and interglacial cycles characterized by global variations in temperature, sea level, and ice volume well-defined in the global marine isotope or ice-core records (Lisiecki & Raymo, 2005; Pol et al., 2010). These archives indicate a pronounced but gradual shift in the periodicity of global glacial-interglacial cycles from ~41 to 100 ka between 1250 and 700 ka ago during the Mid-Pleistocene Climate Transition (MPT), along with amplification of temperature and ice-volume changes (Clark et al., 2006; Ruddiman et al., 1986). As a result of this shift, the global ice sheets of the polar and mountain regions tended to reach beyond the maxima of previous Quaternary glacial extents (e.g., Berger et al., 1999). While the last glaciation (Marine Isotope Stage 2; MIS2) left numerous traces of glaciogenic landforms in the modern Alpine and perialpine landscape, traces of older glaciation are scarce due to the erosive nature of each glacial advance and retreat cycle.

In the Alpine area, the MPT marks the onset of a phase of extensive foreland glaciations (e.g., Haeuselmann et al., 2007; Knudsen et al., 2020; Muttoni et al., 2003; Scardia et al., 2010). During these phases of extensive glaciations, numerous overdeepened troughs and valleys were carved in the Alpine foreland (e.g., Ellwanger et al., 2011; Schlüchter, 2004). Glacially overdeepened troughs and valleys are structures formed by subglacial processes that eroded below the fluvial base level, forming incisions terminating downstream with adverse slopes (e.g., Alley et al., 2019; Cook & Swift, 2012; Kehew et al., 2012; Vegt et al., 2012). Parts of these troughs remained underfilled and are forming modern perialpine lakes, while other parts were completely filled with sediments during and after deglaciation. The infill of these troughs was at least partially protected from subsequent fluvial or glacial erosion. Consequently, they contain sediments from one or even several glacial cycles and are among the most valuable land-based sedimentary archives for reconstructing glacial history across multiple glaciations in glaciated areas (e.g., Buechi et al., 2018, 2024; Ellwanger et al., 2011; Pomper et al., 2017; Preusser et al., 2010). They have proven their value for reconstructing the glacial history preceding the last glaciation of the Alps and their foreland in several case studies (Buechi et al., 2018; Dehnert et al., 2012; Fiebig et al., 2014; Schwenk et al., 2022). These studies suggest a complex glacial history of the Alpine area with substantial variations in dynamics and extent of individual glaciations (Fiebig, 2011). In the case of the last glaciation, for example, it is postulated that the glaciers in the western Alps reached their maximum extent at ~65 ka (Gribenski et al., 2021), a time when the glaciers in the eastern Alps barely reached the inner

Alpine valleys (Ivy-Ochs et al., 2008). Local, regional, and global factors such as topography and climate (including temperature, precipitation, and circulation patterns) may be responsible for such asymmetry and asynchrony (e.g., Monegato et al., 2017; Spötl et al., 2021). Furthermore, besides their scientific value as paleoclimate archives, understanding the formation, distribution, and geometry of overdeepened structures is critical for applied issues such as the long-term safety of nuclear waste disposal sites, groundwater reservoirs, natural hazards, geothermal energy storage and production, and large-scale underground transportation infrastructure.

The "Drilling Overdeepened Alpine Valleys" (DOVE) project, supported by the International Continental Scientific Drilling Program (ICDP), aims to expand our current knowledge of glacier dynamics during the Middle to Late Pleistocene in the Alpine area by systematically drilling and studying glacially overdeepened valleys (Anselmetti et al., 2022). The project aims to achieve its goals by i) geophysical surveys across overdeepened troughs, ii) combining a series of new drill cores, and iii) analyzing existing cores that were scientifically not fully exploited. Geophysical surveys such as reflection seismic (e.g., Kirkham et al., 2021, 2024) or gravimetry (e.g., Bandou et al., 2023) play a critical role in the investigation of overdeepened valleys due to their ability to detect spatial features in the geological underground. This is vital for the DOVE project since their geometry and shape are essential for understanding and reconstructing their individual formation history and detecting systematic regional formation patterns. However, since geophysical surveys will only return a physical parameter, their value is critically enhanced by directly linking with the actual geology, especially in the context of unconsolidated (Quaternary) sediments, via drill core and outcrop data (e.g., Nitsche et al., 2001; Spitzer et al., 2003). Therefore, this study aimed to test the potential of the combination of high-resolution reflection seismic data with borehole and sediment-core data to i) improve the understanding of the formation and evolution of the Basadingen Trough, ii) the local landscape evolution during the Middle to Late Pleistocene, and iii) condensing the local findings into a generic formation model for glacially overdeepened structures.

3.2.2 Study site

Previous studies suggest the presence of a spatially complex network of glacial overdeepenings in the former Rhine Glacier area (Fig. 1A). Although this overdeepened system originates predominantly from the partially filled Lake Constance Basin as a common root (e.g., Cohen et al., 2018; Ellwanger et al., 2011; Fabbri et al., 2021; Keller & Krayss, 1993; Schaller et al., 2022), the origin of this pattern is still not fully understood. Formation during several

glaciations has been proposed (e.g., Buechi et al., 2024; Ellwanger et al., 2011; Graf, 2009a, 2009a; Müller, 2013), making this area an ideal target for the DOVE project (Fig. 1A; Anselmetti et al., 2022; Schaller et al., 2023).

The complex relationships between the individual overdeepenings are also observed on a smaller scale (Fig. 1B) in the southwestern part of the former Rhine Glacier lobe, west of Lake Constance, and between Schaffhausen and Frauenfeld. Several parallel running and possibly cross-cutting overdeepenings have been identified in the bedrock surface (e.g., Müller, 2013; Pietsch & Jordan, 2014). In this area, the Middle Pleistocene fluvial drainage system was controlled by the lowest fluvial outlet with an elevation of ~340 m above sea level (m a.s.l.) at the entrance of the Klettgau fluvial paleochannel west of Schaffhausen (Fig. 1B). This elevation marks the lowest Pleistocene base level relevant to the study area (LPB; Buechi et al., 2024; Graf, 2009b; Müller, 2013). The overdeepenings were incised deeply below this LPB into the bedrock, which consists of Neogene siltstones and sandstones of the Molasse Basin, mainly Upper Marine Molasse (OMM) and Lower Freshwater Molasse (USM; Hofmann, 1967; Hofmann & Hantke, 1964). The top of this complex system of overdeepened valleys with its sedimentary infill was later modified during several phases of (glacial)-fluvial or glacial erosion and deposition (Graf, 2009b; Müller, 2013; Schaller et al., 2023). This study focuses on the Basadingen Trough, where the bedrock incision reaches over 300 m below the modern surface topography.

3.2.3 Previous work on the Basadingen Trough in the frame of the DOVE project

In 2019, during the site-selection process for the DOVE project, two high-resolution reflection seismic profiles were acquired across the Basadingen Trough by the LIAG Institute for Applied Geophysics (Fig. 1C). A first interpretation of the seismic data was made using a simplified stacking-velocity model, assuming velocities of ~2500 ms⁻¹ for the bedrock and between ~1400 and ~2100 ms⁻¹ for the sedimentary infill, leaving some room for uncertainty (Brandt, 2020). This initial interpretation indicated an over 300 m deep bedrock incision with a complex stratified infill along both lines, supporting the earlier multiphase infill history proposed by Müller (2013).

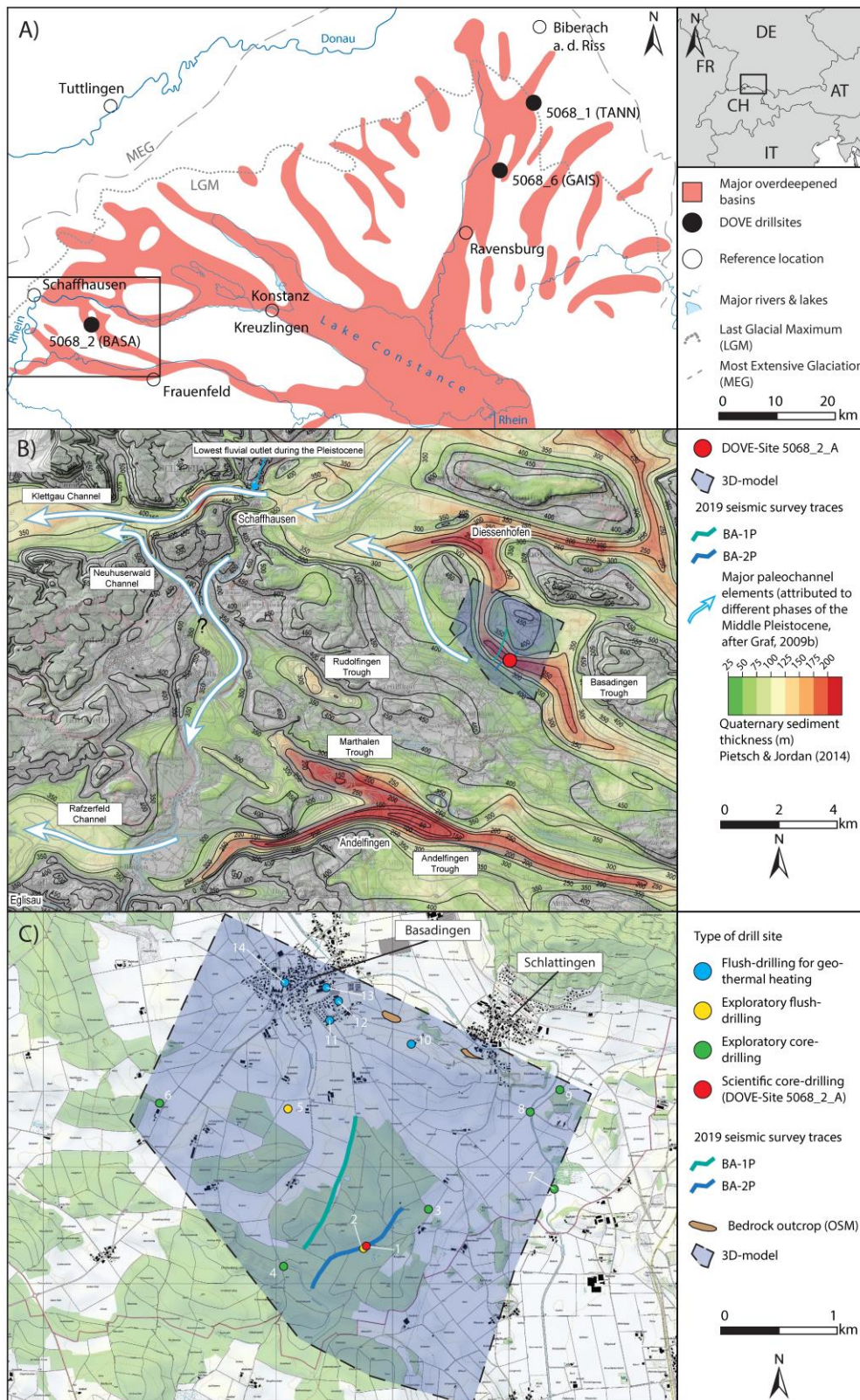


Figure 1: (A) Extension of the overdeepened valley system of the former Rhine Glacier area (modified from Ellwanger et al., 2011; Schaller et al., 2023). The three DOVE "Phase 1" drill sites 5068_1 (TANN), 5068_2 (BASA), and 5068_6 (GAIS), located within the area reached by the Rhine Glacier during the Most Extensive Glaciation (MEG) and partially during the Last Glacial Maximum (LGM), are indicated. (B) Zoom on the southwestern branch of the overdeepened system of the Rhine Glacier with the Quaternary sediment thickness (Pietsch & Jordan, 2014), the postulated local Middle Pleistocene paleochannels (Graf, 2009b), location of the DOVE Site 5068_2 (BASA; 445 m a.s.l.; WSG84: 47.6481°, 8.75327°), the two seismic lines and the 3D model perimeter. (C) 3D model perimeter with the indication of the type and location of the used input data (seismic lines, cores, and flush drilling profiles (1-14) and bedrock outcrops; background map: 1:10'000 Landeskarte V.2023; ©swisstopo).

Based on this initial interpretation, the DOVE drill site 5068_2_A (445 m a.s.l.; WSG84: 47.6481°, 8.75327°) was selected (Fig. 1B and C; Anselmetti et al., 2022; Schaller et al., 2023), and a 252 m long drill core consisting of unconsolidated Quaternary sediments was drilled and recovered between May and October 2022. Based on lithological and petrophysical characteristics, the recovered sedimentary sequence was divided into three major lithostratigraphic units: A, B, and C (Fig. 2). Unit A was additionally divided into five subunits, A1–A5. The three main units are briefly characterized from bottom to top: i) Unit A, deposited below the fluvial basal level in overdeepened position, consists of an over 200 m thick succession of glacial to (glacio)lacustrine sediments (for examples see Fig. 3); ii) Unit B is built up by a 37 m thick fluvial to glaciofluvial gravel deposit; and iii) Unit C consists of an 11 m thick diamictic succession interpreted as the subglacial till of later extensive glaciation, including the regional glaciation during the Last Glacial Maximum (LGM). The recovered sediment sequence supports the trough's proposed multiphase formation history. Following the completion of drilling in October, a downhole wire-line logging campaign was carried out by LIAG in November 2022. A detailed description of the drilling operation, the results of the initial core description, and a first interpretation and embedding into the local context are provided in Schaller et al. (2023) and the corresponding operational report (DOVE-Phase 1 Scientific Team et al, 2023a).

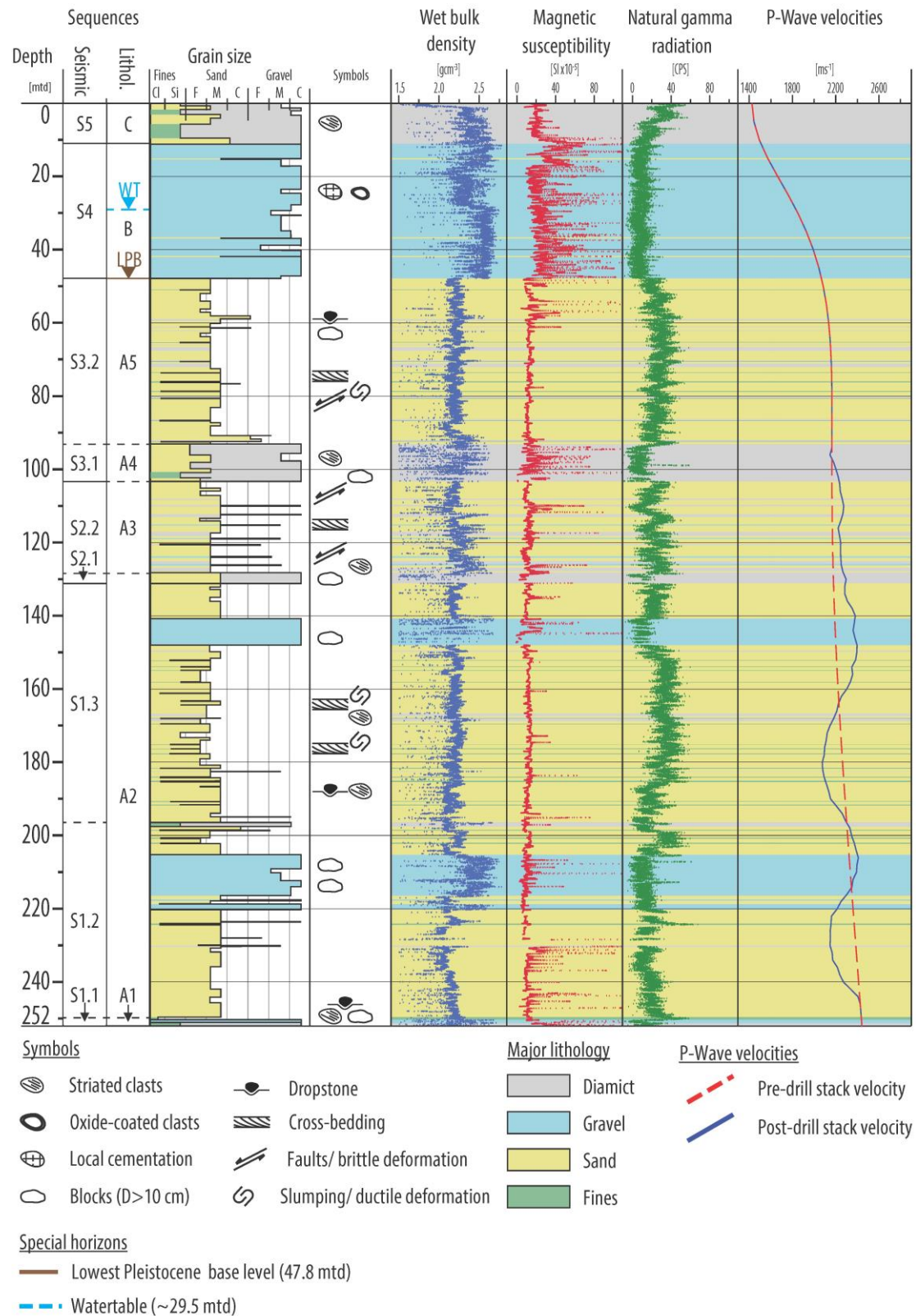


Figure 2: Core log of 5068_2_A with lithostratigraphic units and seismic sequences. Columns from left to right: depth-scale [mtd] (0 mtd = 0 m below ground level or 445 m above sea level) seismic sequences (S1–S5) with subsequences (S1.1–3, S2.1–2, and S3.1–2), lithostratigraphic units (A1–A5, B, and C), dominant grain size with primary lithologies, symbols of prominent observations, wet bulk density [gcm^{-3}], magnetic susceptibility [$\text{SI} \times 10^{-3}$], natural gamma radiation [CPS, counts per second], and the original seismic stacking velocities and VSP-corrected P-wave stack velocity [ms^{-1}] (modified after Schaller et al., 2023).

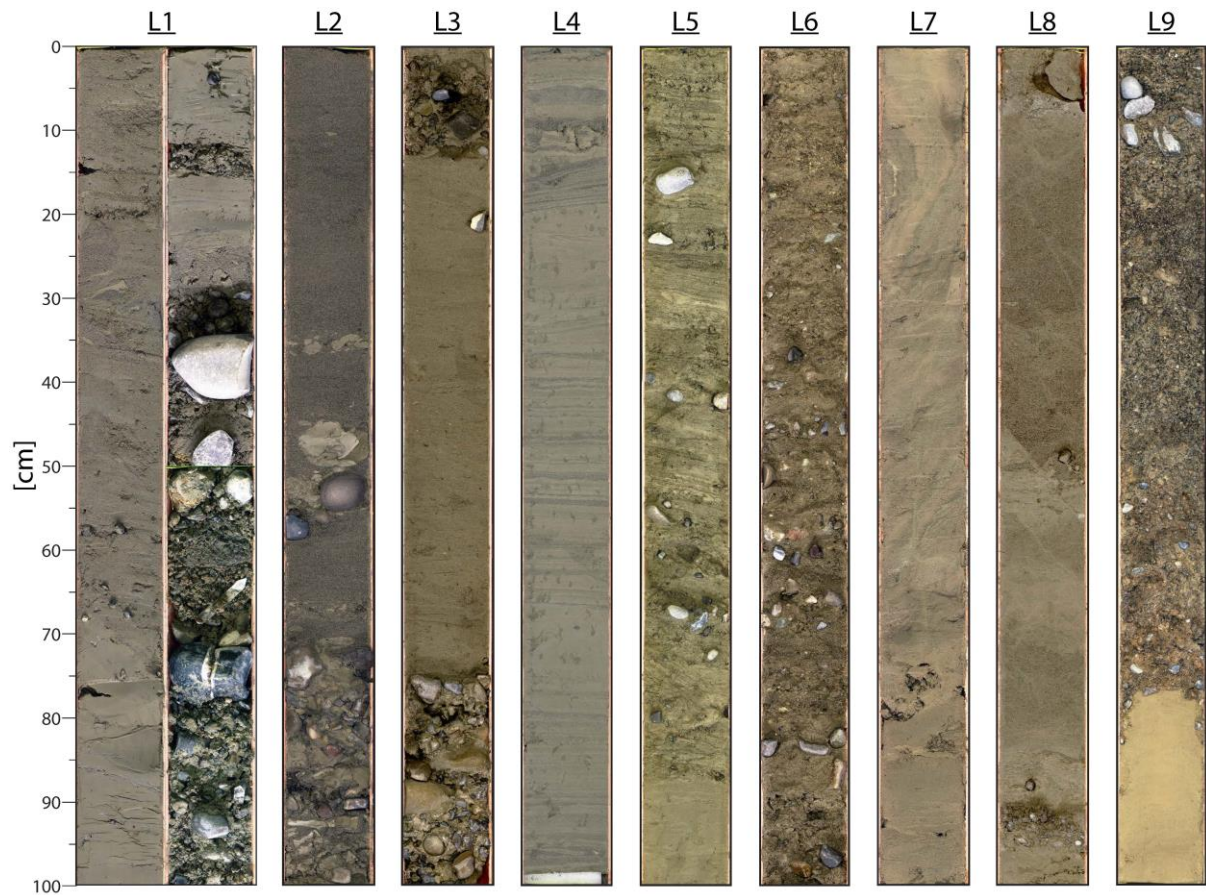


Figure 3: Core examples of key elements of the lithostratigraphic (sub)units or (sub)units boundaries of the overdeepened basin fill (Unit A) with the corresponding depth of origin in m below ground level in drill core 5068_2_A. L1 (~249-251 m) contact between subglacial (A1) and glaciolacustrine sediments (A2); L2 (~196-197 m) and L3 (~140-141 m) interlayered glaciolacustrine gravel and sand deposits (A2); L4 (~ 179-180 m) and L5 (~ 58-59 m) laminated lacustrine deposits (A2 and A5); L6 (115.5-116.5 m) clastic delta deposits (A3); L7 (~ 104-105 m) soft deformed deposits (A3); L8 (~ 123-124 m) brittle deformed deposits (A3); and L9 (~47-48 m) contact between overdeepened lacustrine basin fill (A5) and non-overdeepened (glacio)fluvial cover (B).

3.3 Methods

3.3.1 Seismic processing

A vertical seismic profile (VSP) was obtained in the open hole between 106 and 246 m depth with receiver intervals of 2 m using a digital three-component borehole geophone. Since the multi-layered steel casing could not be removed during the logging campaign, only three measurements with a spacing of 8 m between 82 and 106 m were acquired through the innermost layer of the steel casing. Both an S-wave and a P-wave electrodynamic vibrator were used as a source with exciting frequencies from 20 to 200 Hz. Data processing included correlation, vertical stacking, and rotation of the S-wave data into transversal/radial coordinates. Clear arrivals could be picked from the P-wave on the vertical component. The slowness was filtered in the depth domain using a triangular smoother with a halfwidth of 12 m. The P-wave arrival times between 82 and 246 m were combined with the previously used stacking velocities above 82 and below 246 m at the drill location into an updated velocity

model, which was further smoothed with a halfwidth of 20 m to avoid distortion of seismic waveforms due to abrupt velocity changes during depth conversion of the seismic data. The time-depth conversion of the seismic data from the 2019 survey crossing the drill site (see Section Previous work), obtained by using a hydraulic vibro-source with a frequency between 20 and 240 Hz, a shot-point spacing of 4 m, and a receiver spacing of 2 m (Brandt, 2020), was updated with the new velocity model.

3.3.2 Seismic facies analyses and core-to-seismic-correlation

In a first step, based on reflection amplitude, shape, continuity, and geometry (e.g., Mitchum et al., 1977), a seismic facies analysis was performed on the two required seismic lines crossing the Basadingen Trough (BA-1P and 2P; Fig. 1C). Based on prominent unconformities, the succession was further grouped into seismo-stratigraphic sequences. Most seismic facies were continuous along the major unconformities, so they mostly coincide with the seismic sequences (e.g., Mitchum et al., 1977), primarily characterized by a single dominant seismic facies. The seismic sequences of the well-controlled line BA-2P (Fig. 1C) were depth-correlated via the VSP data to the existing core data and lithologies (see Section Previous work). Further, they were compared and assigned to corresponding depositional environments. The defined pattern of the well-controlled seismic line was compared and correlated with the seismic interpretation of the second line. Based on both lines, a schematic and simplified model (“line drawing”) for a glacio-seismic sequence of an overdeepened valley fill was established, summarizing the observed seismic characteristics. All seismic interpretations were made with SMT Kingdom Suite 2020.

3.3.3 Three-dimensional and spatial visualization and analysis of overdeepened sequences

The 3D model of a part of the Basadingen Trough and the major Quaternary sequence boundaries were created using MOVE v.2019 (PE Limited). The model was constructed based on a grid of systematically laid profiles that integrated the existing data: i) the Dove drill core 5068_2_A and 13 existing drillings (Nr 1-14 in Fig. 1C), ii) mapped bedrock outcrops (Fig. 1C), iii) the two interpreted seismic profiles (BA-1P and 2P; Fig. 1C), iv) the proposed extent and dimensions of a local gravel unit (Müller; 2013), v) the local topography, and vi) the bedrock-elevation model. A detailed overview of the input data is provided in Tables A1 and A2. The uncertainties of the model are lowest around and between the two seismic lines and at the used drill sites. The uncertainties around the used drill sites are inversely correlated with the resolution and quality of the applied drilling techniques and recovered information (Fig. 1C), from low to very high resolution: i) flush drilling for geothermal heating (~5-10 m), ii)

explorative flush drilling (~1 m), iii) explorative core drilling (~0.1 m), and iv) scientific core drilling (~cm). Further, the bedrock horizon was fitted to the regional bedrock model at its outer boundaries, ensuring a smooth fit. The recent digital elevation model was also used for the topography horizon. Further spatial analysis of the modeled sequence horizons, such as topography and sediment thickness of the individual sequences, were done in QGIS v.3.14 using standard raster-calculation functions.

3.4 Results

3.4.1 Seismic sequence stratigraphy and seismic facies analysis

Overall, the seismic data of the Basadingen Trough display three major elements: i) the incised bedrock, ii) the Quaternary filling of the incision, and iii) the horizontally bedded Quaternary cover. These three elements can be well discerned by differences in their VSP-modified stacking velocities (Fig. 4). The steep bedrock incisions of down to ~250 (Fig. 5) and ~310 m below ground level (m b.g.l.; Fig. 6) for Line BA-1P and BA-2P, respectively, and a horizontally bedded cover of 40-50 m thickness can be well recognized in the contrasting velocity pattern. In the case of line BA-1P, the detailed outline of the steep western side of the bedrock incision is uncertain and thus marked by a dashed line. The horizontal velocity contrasts within the valley fill below ~105 m result from horizontally extrapolated high and low-velocity zones from the VSP data (Figs. 2 and 4).

Based on seismic unconformities and seismic facies analysis, eight types of seismic facies were distinguished (Facies I–VIII; Table 1) in the seismic data. This succession can be further grouped into six major seismic sequences bounded by unconformities (S0–S5). S0 corresponds to the bedrock, S1–S3 to the Quaternary valley fill, and S4 and S5 to the horizontally bedded Quaternary cover (Figs. 5 and 6). The bedrock (S0) and the Quaternary valley fill (S1–S3) can be further divided into subsequences (S0.1–0.2, S1.1–1.3, S2.1–2.2, and S3.1–3.2), which consist of one or two of the initially defined seismic facies (Figs. 5B and 6B). The bases of each of the three major seismic sequences of the Quaternary valley fill (S1–S3) consist of a relatively thin subsequence of Facies III (S1.1, S2.1, and S3.1, turquoise colored in Figs. 5B and 6B). These subsequences show a sharp unconformity at the base, defining the major sequence boundaries.

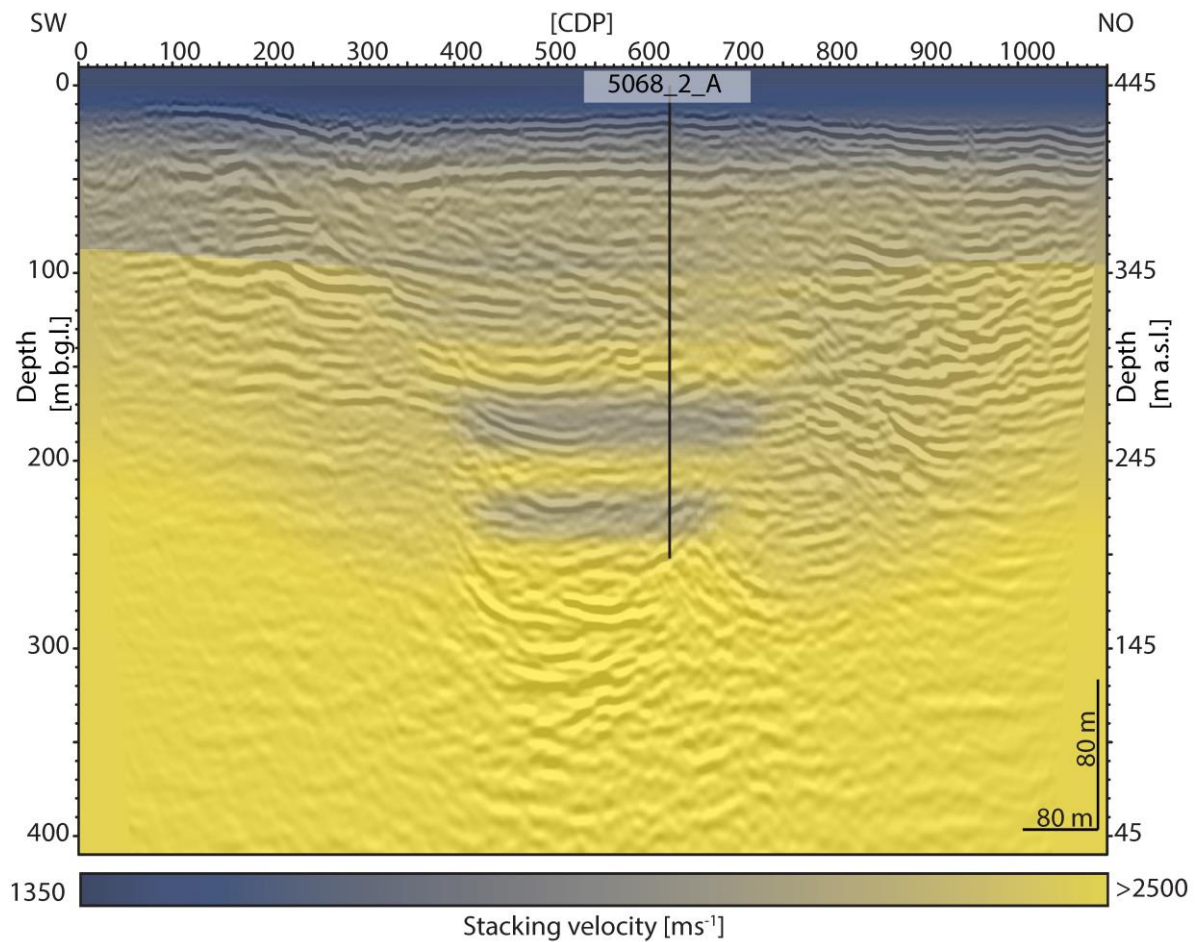


Figure 4: Color-coded P-wave stacking velocity model of depth converted reflection seismic Line BA-2P after integrating in-hole check-shot data from the VSP with indicated well trace of 5068_2_A. The P-wave velocity values range between 1350 and 2500 ms^{-1} and the depth scale is given in m b.g.l (left side) and m. a.s.l. (right side).

Table 1: Seismic facies description

Label	Description
I	Medium amplitude, long wavelength, medium transparent to transparent, cut-and-fill, and partly chaotic reflections
II	High amplitude, long wavelength, medium transparent, continuous but wavy reflections
III	High to partly medium amplitude, long wavelength, medium transparent, cut-and-fill, and partly chaotic reflections
IV	Medium to partly high amplitude, medium transparent, strong cut-and-fill, and partly chaotic reflections
V	Medium amplitude, medium transparent to partly transparent, horizontal parallel continuous reflections with onlaps
VI	Medium amplitude, medium transparent, continuous parallel dipping reflections
VII	Medium amplitude, medium transparent to partly transparent, chaotic/deformed reflections
VIII	Medium to partly high amplitude, continuous parallel reflections, partly chaotic

Note: Background color of the labels represents the later used color code of the seismic facies

3.4.2 Core-to-seismic correlation

The correlation between the seismic facies, the seismic sequences, the drilled sediment succession, and the bulk density core log shows an overall good match between the seismic interpretation and the major lithologies of the drill-core (i.e., Diamict, Gravel, Sand, and Fines; Fig. 5B). A detailed correlation between the seismic stratigraphy with the lithological stratigraphy (lithostratigraphic Units A1-5, B, and C) and its petrophysical properties (e.g., wet bulk density, magnetic susceptibility, and natural gamma radiation) is displayed in Figure 2. Further, a comparison between original P-wave stacking velocities and the VSP-corrected stacking velocity model at the drill location (Fig. 2) displays a good match between the density/grain-size trends, showing higher velocities in the gravel-rich and lower velocities in the sand-dominated beds. The correlation between the lithostratigraphic units and the seismic sequences is described in detail in the following section.

S0: This sequence represents the unit below and to the sides of the prominent deep incision, showing a steep southwestern flank and, in the upper half, a more gently rising northeastern flank. The sequence can be further divided into two subsequences with a gradual transition between: i) the lower part, S0.1, represented by Facies I, and ii) the upper part, S0.2, consisting of Facies II. The upper boundary of S0 to the overlaying strata shows a discontinuous reflection pattern, representing a prominent unconformity, especially at the more gently dipping parts of the flanks. No direct lithological correlation is possible since this sequence was not drilled during the DOVE project.

S1: Sequence S1 fills up the lower steep and narrow half of the basin and is terminated on both seismic lines at the top by a discontinuity with a concave incision on the northeastern side. This sequence can be further divided into three subsequences, S1.1-3: i) the basal subsequence S1.1 is represented by Facies III with a sharp, wavy, slightly southwest dipping unconformity at the top and is correlated with the clast-rich diamictic sediments of lithostratigraphic Unit A1 (L1); ii) the middle subsequence S1.2, represented by Facies IV, is correlated with sand- and gravel-dominated sediments (L2), and shows a sharp and slightly concave top; and iii) the uppermost subsequence S1.3 consisting of Facies V, which is correlated with bedded to laminated fine sands (L4). The sediments correlating with S1.2 and 1.3 are combined in lithostratigraphic Unit A2.

S2: Layers within S2 are dipping from southwest to northeast. In the northeast, the steep part of the basin passes to the more gently sloping flank with a sharp and wavy top contact to the

overlying sequence. S2 is composed of two subsequences, S2.1 and S2.2: i) S2.1 is represented by a thin horizontal layer of Facies III, coinciding with clast-rich diamictic sediments belonging to the very top part of lithostratigraphic Unit A2, overlain by: ii) subsequence S2.2, consisting of a combination of Facies VI and VII and showing a general southwest to northeast dipping trend. Facies VI was not directly cored. Facies VII is correlated with a recovered sequence of interlayered sandy and diamictic/gravelly sediments with traces of post-sedimentary deformation forming lithostratigraphic Unit A3 (L6, L7, and L8).

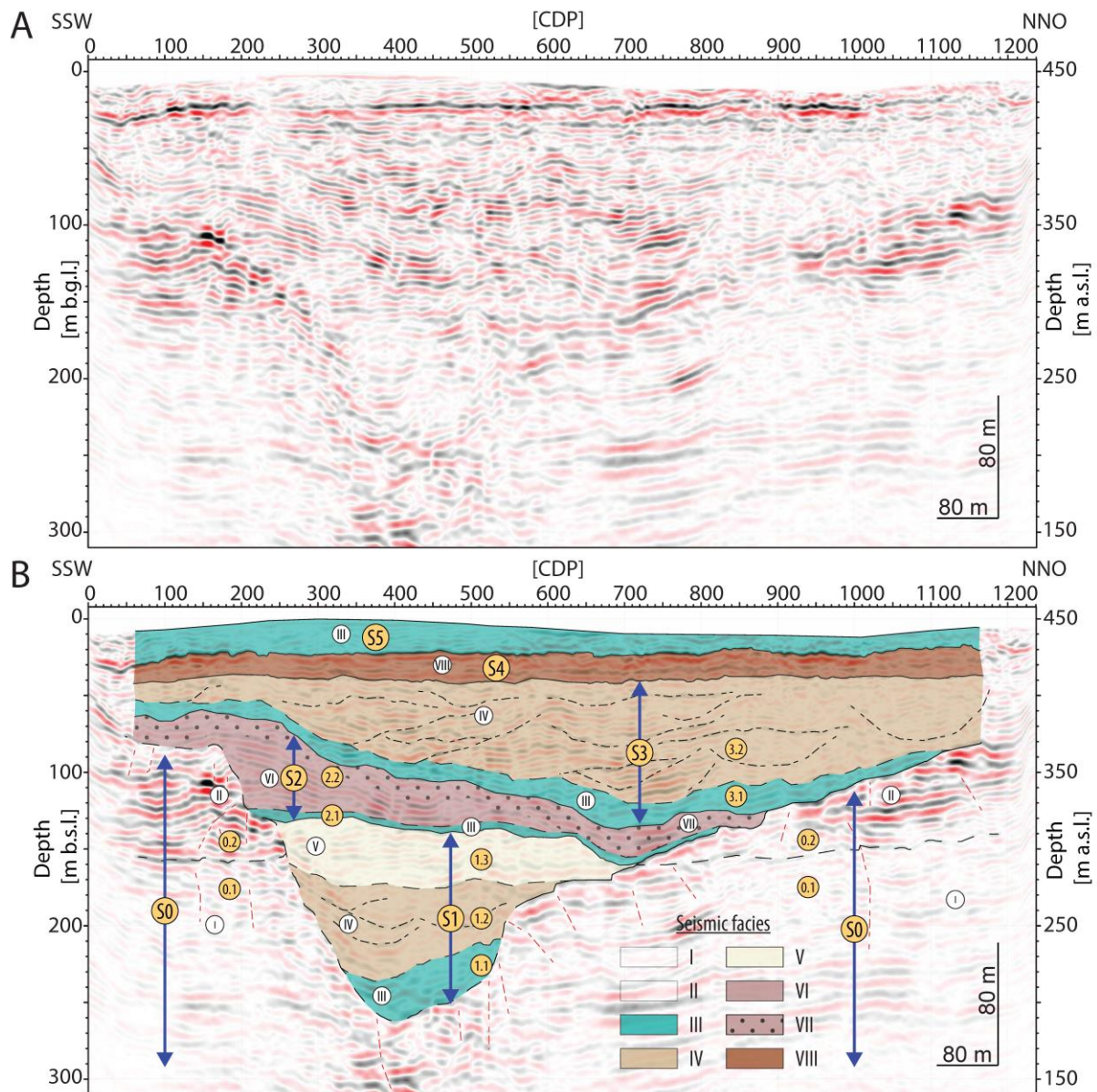


Figure 5: Depth-converted reflection seismic line BA-1P, (A) uninterpreted, (B) interpreted with seismic facies analysis and sequence stratigraphy with labeled (I-VIII) and color-coded seismic facies (III-VIII). Seismic sequences are indicated by yellow circles (S0-5) and blue arrows; corresponding subsequences (S0.1-2, S1.1-3, S2.1-2, and S3.1-2) are labeled with smaller yellow circles. Solid black lines indicate sequence boundaries, whereas dashed black lines indicate subsequence boundaries. Possible faults are indicated by dashed thin red lines and smile/cut-and-fill structures by dashed thin black lines. The depth scale is given in m b.g.l. (left side) and m. a.s.l. (right side); exact locations and extends of the lines are shown in Fig. 1C.

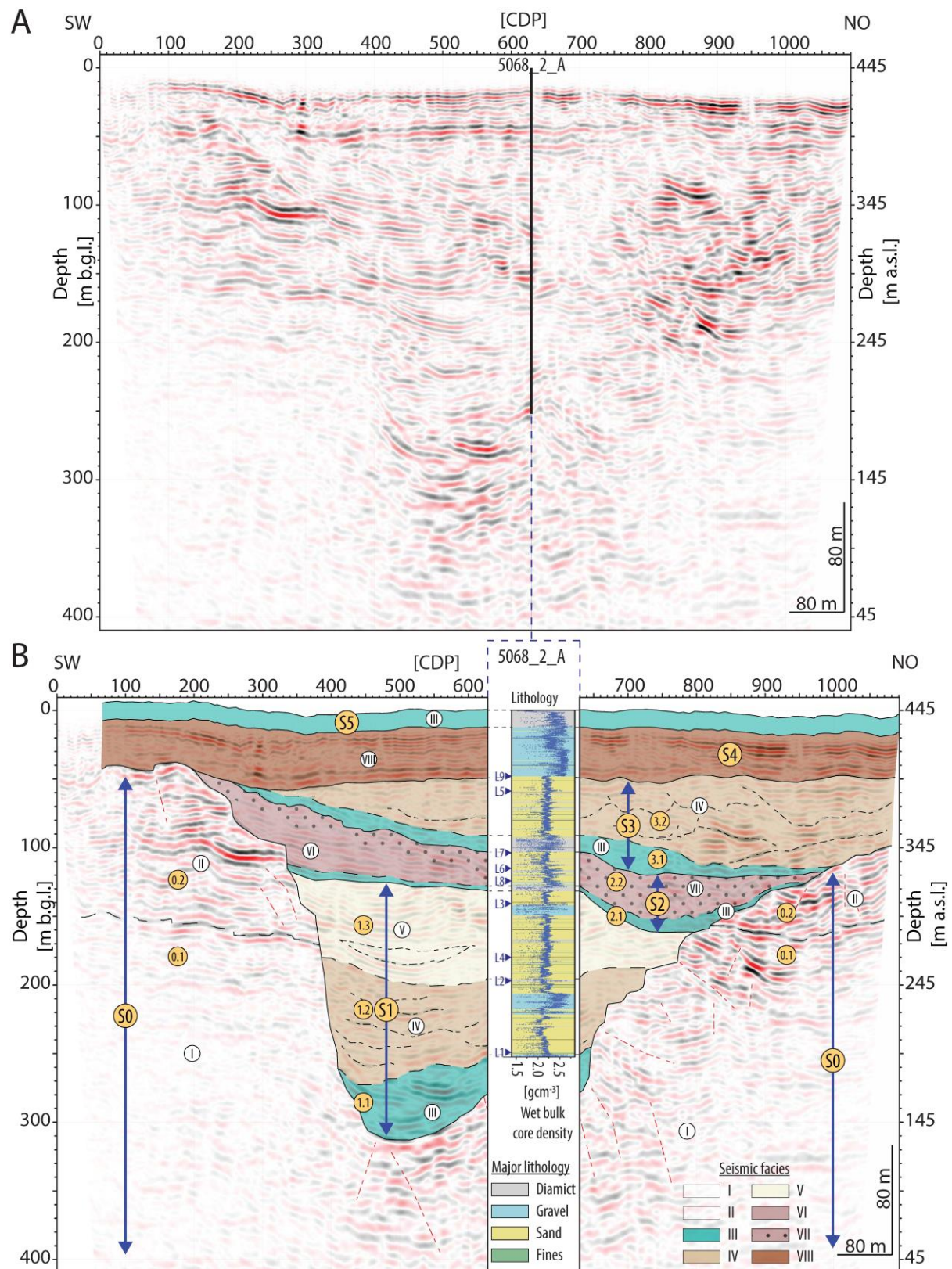


Figure 6: Depth-converted reflection seismic line BA-2P, (A) uninterpreted, (B) interpreted with seismic facies analysis and sequence stratigraphy with projected wet bulk density and lithologic log of Core 5068_2_A with the indicated position of the selected core examples of Figure 3 (L1-L9). (Information in the caption for Figure 5 also applies to Figure 6).

S3: The remaining part of the basin is filled by S3, shifting its axis to the northeastern sector where the overdeepening becomes shallower. The sediments of S3 are partly discordantly cut off by the overlaying sequence S4. This sequence is subdivided into subsequences S3.1 and 3.2: i) S3.1, at the base, consisting of a layer of more or less continuous thickness of Facies III, coinciding with clast-rich diamictic sediments of lithostratigraphic Unit A4, and ii) overlying S3.2 fills up the remaining space of the valley and is represented by Facies IV with its prominent cut-and-fill structures, showing a wavy lower boundary correlating with a sequence of sand-dominated sediments of lithostratigraphic Unit A5 (L5 and L9).

S4: The overdeepened basin fill (S2 and S3) is partly cut off by S4, showing sharp, planar, and wavy bottom and top boundaries. The sequence shows a constant thickness, is associated with Facies VIII, and is correlated with gravel-dominated sediments of lithostratigraphic Unit B (L9).

S5: Sequence S5 overlies S4 with a slightly wavy but planar boundary. It consists of Facies III and is correlated with the diamictic sediments of lithostratigraphic Unit C. This sequence only occurs in some areas of line BA-2P.

3.4.3 3D and 2D spatial visualization of overdeepened sequences

The reconstructed part of the Basadingen Trough and its stratified Quaternary filling, represented by the basal surfaces of the five seismic sequences (S1–S5), is visualized in 3D (Fig. 7). The reconstructed topography of the three major erosional surfaces associated with the basin infill (S1–S3; Fig. 8) reveals i) a shift in the trough's central axis and ii) a change of the trough shape from a narrow and deep incision (minimal elevation S1 = ~135 m a.s.l.) to a more shallow and broader one (minimal elevation S2 = ~275 m a.s.l.; minimal elevation S3 = ~310 m a.s.l.). The model yields a preserved maximum sediment thickness of ~183, ~64, and ~90 m for S1, S2, and S3, respectively. The data show a reconstruction of the modern situation, not a temporal succession, as eroded parts are not visualized.

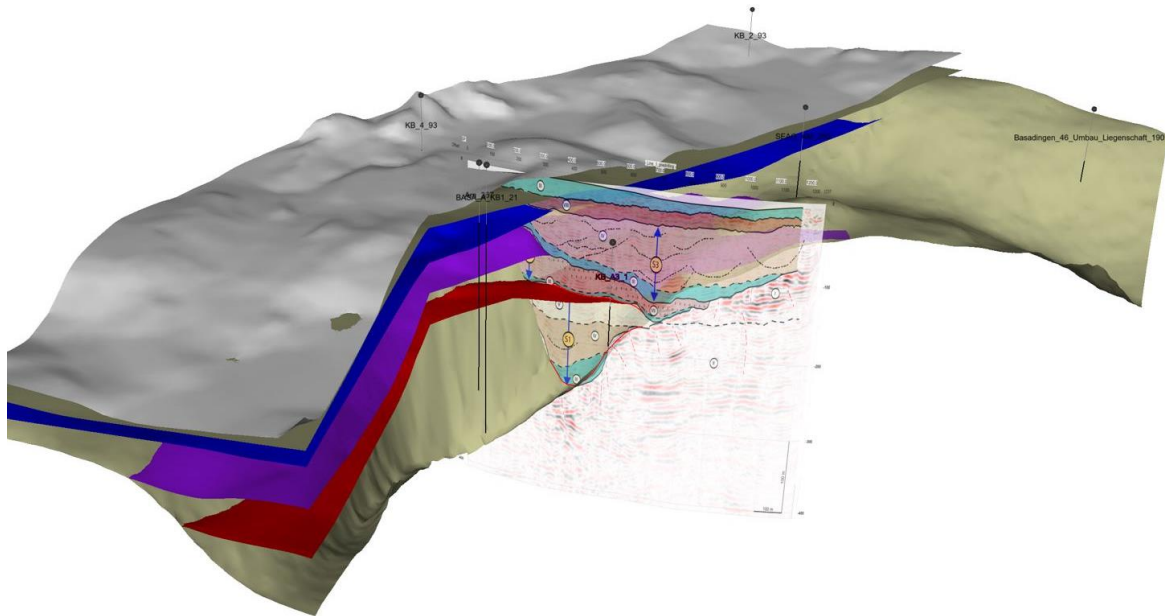


Figure 7: 3D section through the Basadingen Trough visualizing the BA-1P seismic profile, some projected wells (black pins), and the main horizons from the seismic sequence stratigraphy (S1: cumulative bedrock surface: beige; S2: red; S3: purple; S4: blue; S5: brown-beige; and the modern surface: light gray). The vertical exaggeration is 200%. (The model was created with MOVE V. 2019).

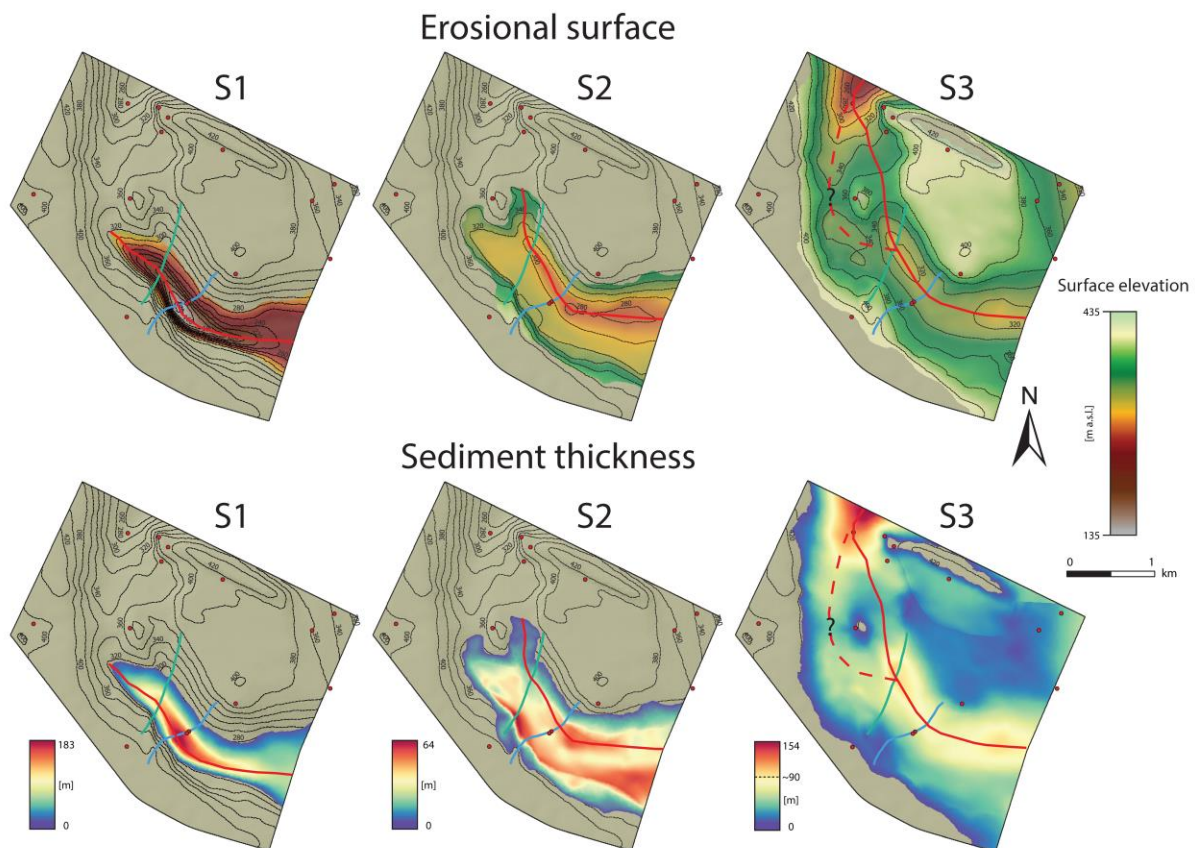


Figure 8: Basal erosional surface and preserved sedimentary infill of the overdeepened glacial seismic sequences S1–S3. The upper row shows the sequences' recorded and preserved basal erosion surfaces (colored). The bottom row shows the thickness of the preserved sedimentary infill of each sequence. The cumulative bedrock surface is displayed in grey in the background. The elevation of the erosional surfaces is indicated by color code and 20 m elevation lines, while the sediment thickness is only shown by color code. The proposed axis of each erosional surface is marked with a solid red line, which becomes dashed if speculative. For orientation, the extents of the two seismic lines (BA-1P and 2P) are marked with solid green and blue lines, respectively, and the drill points are marked with red dots (for a detailed overview of the input data, see Section Study site; Fig. 1C; and Tables A1 and A2).

3.5 Discussion

3.5.1 Depositional environment of the seismic sequences

The interpreted depositional environment of each seismic sequence (S0–S5) and corresponding subsequences (S0.1–2, S1.1–3, S2.1–2, and S3.1–2) is discussed from bottom to top in the following section and summarized in Table 2.

S0 (bedrock): Although not directly drilled, seismic sequence S0 correlates with the local Molasse bedrock (see Section Previous work). Subsequences S0.1 and S0.2 are associated with the Lower Freshwater Molasse (USM) and the Upper Marine Molasse (OMM), respectively. These lithologies are outcropping in the larger area surrounding the Basadingen Trough and were also encountered in nearby drillings (Fig. 1C, Table A1) and regional 2D seismic reflection data (e.g., Naef et al., 1995).

S1 (Overdeepened Basin Fill 1): Located at the base at the narrowest and deepest part of the basin, S1 represents the deepest and oldest overdeepened sequence of the basin fill. Its lowermost subsequence, S1.1, consists of various types of diamicts and is interpreted as subglacial deposits, including subglacial tills (e.g., Buechi et al., 2017; Fig. 3 L1). Overlying S1.2, with its prominent cut-and-fill structures and interbedded massive sand and gravel beds, is interpreted as an early stage of the glaciolacustrine basin phase (Fig. 3 L2). The sequence likely represents subaquatic-delta or basin-floor fan deposits in front of the glacier with a dynamic subaquatic channel-levee system resulting in the observed cut-and-fill structures (e.g., Bennett et al., 2002; Lønne, 1995). The uppermost subsequence S1.3, with its finer dominant grain size and its horizontal and partly lateral onlapping reflections, likely represents the shift from a glaciolacustrine depositional environment towards a more lacustrine setting. This shift is further supported by the presence of laminated and partly cross-bedded sand-dominated sediments, which indicates reduced depositional energy (Fig. 3 L4; i.e., T_b, T_c, or T_d elements of the Bouma-sequences; Bouma, 1962). This change in the depositional energy is likely related to the increasing distance to the retreating glacier front (e.g., Buechi et al. 2017, Kirkham et al. 2024, and Schaller et al. 2023).

S2 (Overdeepened Basin Fill 2): S2.1 at the base of S2 consists also of subglacial deposits. Its thickness is extrapolated from the cored and recovered sediment bed since it is below the vertical resolution of the seismic data of ~2 m (Brandt, 2020; Schaller et al., 2023). Overlying S2.2 represents possible delta deposits intercalated with hyperconcentrated density-flow deposits (Fig. 3 L6; Mulder & Alexander, 2001) originating from the southwest, building a

wedge that levels out the steep southwestern flank of the valley. Even though the top of S2.2 indicates traces of post-sedimentary deformation (Facies VII, lithostratigraphic Unit A3, and Fig. 3 L7 and L8), the continuous and parallel dipping reflections of Facies VI in the lower and southwestern part indicate original deposition.

S3 (Overdeepened Basin Fill 3): Representing the youngest recorded basin infill phase, S3 is very similar to S1, as subsequence S3.1 is interpreted as subglacial till and other glaciogenic diamicts, and S3.2 as glaciolacustrine to partly lacustrine deposits. The prominent cut-and-fill structures likely indicate a varying concentration of the depositional energy, similar to S1.2. The lack of gravel-dominated sediments indicates either i) lower depositional energy than in S1.2, pointing to an increased distance to the glacier, or ii) that the gravels were absent due to the shift of the trough axis and changing the depositional focus. The top of S3.2 indicates a shift towards a more lacustrine setting, which coincides with the partly laminated/crossbedded sections in the core, similar to the sediments of S1.3. Furthermore, a section rich in dropstones indicates deposition in a distal ice-contact lake (Fig. 3 L5).

S4 (Non-overdeepened Cover 1): The gravels of S4 are overlying the overdeepened strata of the valley fill with a laterally continuous but discordant basal contact. S4 is interpreted as a fluvial-to-glaciofluvial gravel deposit that erodes the top of the basin fill (Fig. 3 L9). Observations in many drillings and extensive gravel pit outcrops indicate that S4 can be correlated with the local "Buechberg Gravel" with a postulated Middle Pleistocene age (Frangi & Szepessy, 2003; Graf, 2009b, 2009a; Müller, 2013).

S5 (Non-overdeepened Cover 2): S5 correlates in the drill cores with the basal lodgment till that can also be found in local outcrops. The sequence correlates, at least in the upper part, to the last glaciation but likely comprises remains of previous Pleistocene glaciations at the base (Beringen Glaciation MIS6; Graf, 2009a; Müller, 2013). However, neither the seismic data nor the corresponding drill cores show signs of internal pedogenic or erosive unconformities. Therefore, either the youngest glacial advance eroded everything down to the underlying gravels of S4, or the unconformities are not visible due to i) the homogeneity of the sediments and ii) the potential planar shape of the unconformities. Both would make it hard to detect it in the cores as well as in the seismic data. Further, the chance to detect the unconformity in the seismic is hampered due to the relatively thin thickness of the sequence (~10 m) and the reduced data quality of the surface layer.

Table 2: Overview of the depositional environment of the seismic sequences and their role in the development of the Basadingen

Seismic Sequence	Sub-sequence	Seismic Facies	Lithostrat. Unit	Drilled Sediment	Depositional environment	Interpretation of Stratigraphic Elements	
S5	-	III	C	Diamict, matrix-supported, silty to sandy	Glacial till from the last glaciation (MIS2; Birrfeld Glaciation) and possibly older (MIS 6; Beringen Glaciation, e.g., Müller, 2013)	non-overdeepened cover	Subglacial erosion/deposition (Non-overdeepened erosion of underlying strata)
S4	-	VIII	B	Gravel, sandy to partly silty, dm-m-scaled bedded, with isolated sand beds	Fluvial- to glaciofluvial Middle Pleistocene gravel "Buechberg Gravel" (Graf, 2009b; Müller, 2013).		Fluvial- to glaciofluvial erosion/deposition (Non-overdeepened erosion of valley top, drop of fluvial baselevel)
S3	2	IV	A5	Sand, partly silty, massive dm-to-m-scale bedded, partly laminated to cross-bedded, isolated gravel layers	Clastic-dominated glaciolacustrine to lacustrine deposits with highly variable depositional energy, e.g., subaquatic delta or basin-floor fan deposits	Overdeepened basin fill	Reactivation phase II (partial erosion with a shift of focus/axis, final infilling)
	1	III	A4	Diamict, clast rich to clast-supported, silty to sandy	Glacigenic diamicts emplaced in submarginal to subglacial, possibly proximal glaciolacustrine position		
S2	2	VI+VII	A3	Sand, interlayered with gravel and partly diamictic beds, partly deformed	Subaquatic delta deposits, intercalated by mass-movement deposits, possibly from unstable slopes of the rapidly infilling basin		Reactivation phase I (partial erosion with a shift of focus/axis of overdeepening, infill from the southwest)
	1	III	A2	Diamict, clast rich to clast-supported, silty to sandy	Glacigenic diamicts emplaced in submarginal to subglacial, possibly proximal glaciolacustrine position		
S1	3	V	A2	Sand, partly silty, massive dm-to-m-scale bedded, partly laminated to cross-bedded, isolated gravel layers	Clastic-dominated glaciolacustrine to lacustrine deposits with highly variable depositional energy, e.g., subaquatic delta or basin-floor fan deposits with possibly decreased glacial proximity		Initial erosion/infill phase (Formation of major overdeepening and first infilling)
	2	IV	A2	Interbedded massive sand/gravel beds	Clastic-dominated glaciolacustrine to lacustrine deposits with highly variable depositional energy, e.g., subaquatic delta or basin-floor fan deposits		
S0	1	III	A1	Diamict, matrix to clast-supported, sandy to silty	Glacigenic diamicts emplaced in submarginal to subglacial, possibly proximal glaciolacustrine position		Basement
	2	II	-	Neogene siltstones and sandstones	Bedrock (OMM); originally marine/coastal		
	1	I	-		Bedrock (USM); originally fluvial		

Note: Based on the results displayed in Figures 2, 5, 6, and 8 and the observations from Schaller et al., 2023.

3.5.2 Formation of the Basadingen Trough: Three overdeepened glacial sequences

Based on the integration of all available data, the overdeepened Basadingen Trough and its fills formed during at least three major phases of glacial advance and retreat (Table 2), consisting of a major initial phase (S1) and at least two reactivation phases (S2–S3). Each sequence is characterized by a subglacial ice contact at the base that likely represents separate glacier advances across the overdeepening accompanied by changes in magnitude and focus of subglacial erosion (Buechi et al., 2018, 2024; Kirkham et al., 2024; Vegt et al., 2012). The bedrock incision is the cumulative product of these successive erosional phases. The morphology of the Basadingen Trough consists of at least two overlapping shapes, i.e., a combination of an older, deep, narrow incision and a younger, shallower one with broader erosional geometry. This pattern has been observed in other overdeepened valleys and is a clear sign of a multiphase formation (e.g., Bandou et al., 2023; Buechi et al., 2018, 2024; Kirkham et al., 2021).

Stratigraphically positioned in the deepest part of the valley, S1 thus represents the oldest preserved remains of the three overdeepened glacial sequences. It likely represents the remains of the initial trough-formation phase, during which the deep and narrow valley shape was formed. The deepest point of this initial valley lies at ~135 m a.s.l., resulting in an erosion of at least 263 m if the LPB of ~398 m a.s.l. is assumed (Fig. 2). Total erosion can be even greater since the fluvial base level during this phase was likely higher than the assumed LPB (Graf, 2009a, 2009b; Müller, 2013; Schaller et al., 2023). The base of S1.1 documents the maximal vertical erosion level reached. This coincides with the end of the initial erosion phase and the beginning of the initial infill of the basin under glacial to early deglacial conditions. Subsequences S1.2 (glaciolacustrine) and S1.3 (glaciolacustrine-lacustrine) indicate that a lacustrine depositional environment was already reached during the initial infill phase. This upsection development corresponds to decreasing glacial proximity, depositional energy, and sediment supply. Erosion during the following glacial advance-retreat cycle (S2) might have eroded parts of S1; it cannot be excluded that the valley was entirely filled.

Sequence S2 is the most complex of the three overdeepened glacial sequences and represents the following glacial advance-retreat cycle and the first preserved reactivation phase of the Basadingen Trough. This reactivation caused the trough axis to shift, leading to the transition from a deep and narrow incision to a shallow and wider one. The morphology of S2 (Figs. 5B, 6B, and 8) indicates that this renewed glaciation produced subglacial erosion again, but with a shift of the erosional focus and trough axis towards the northeastern flank. This shift initiated

a significant change in the valley morphology by widening the trough. Such shifts in the overdeepened trough axis and, thus, in the spatial focus of subglacial erosion have been observed in other overdeepened valley systems (Bandou et al., 2023; Buechi et al., 2018, 2024). The glacial erosional potential was probably limited due to changing subglacial conditions or due to limited time of active erosion. The morphology of the basal unconformity indicates that bedrock, rather than the older valley fill, was eroded. Thus, the shape of the active overdeepening is expanded mainly into the width rather than into depth. The older valley fill was only significantly eroded in the area of the shifted valley axis. This relatively limited erosion is supported by the partly horizontal basal erosional contact and the thin glacial deposits near the maximal resolution of the seismic data. S1 and S2 are also interpreted as individual overdeepened glacial sequences, with a seismic discontinuity and the diamictic bed at the base indicating ice contact. The deposition of the overlying sediments of S2.2 occurred in a clastic-dominated glaciolacustrine environment with, at least at the beginning, sediment influx from the southwest forming delta-like deposits. These clastic sediments are partly strongly overprinted and deformed by the following glacial advance of S3, especially in the center of the shifted valley axis. It is unclear to which level the valley was refilled at the end of the first reactivation phase.

Sequence S3 represents the third glacier advance-retreat cycle and the second reactivation phase of the Basadingen Trough. The fact that the erosional surface of this final glacial advance followed the underlying topography, especially that of the delta deposits (S2.2), and the occurrence of glacial deformation may indicate a limited basal erosion (Figs. 5 and 6). The morphology of S3 suggests an increase in lateral erosion, leading to a further widening of the valley and a shifting of the trough's axis. This evolution of the trough's morphology, initiated in S2, was possibly amplified by the wedge-like shape of the underlying sediments of subsequence S2.2, further compensating for the limited basal erosion and providing relevant accommodation space (Figs. 5B, 6B, and 8). Eventually, the valley became filled with sediments deposited in a subglacial to glaciolacustrine to lacustrine environment, similar to that observed in the remaining parts of the initial basin fill of S1.

After refilling during S2 and S3, the upper part of the infill in the Basadingen Trough was partly eroded by one or possibly multiple phases of (glacio)fluvial erosion, documented by the non-overdeepened gravel deposits of S4. This phase of fluvial erosion led to a locally strong topography (varying between ~370 and ~450 m a.s.l.; Müller, 2013) in the basal erosional surface with incisions into the former overdeepened valley fill (Figs. 5B, 6B, and 8), indicating

a clear drop in the fluvial base level between the end of S3 and the onset of S4. At the current stage, it is unclear if the deposition of the gravels of S4 occurred in one (e.g., Frangi & Szepessy, 2003; Müller, 2013) or several phases (e.g., Graf, 2009a, 2009b), as the internal stratigraphy of the corresponding gravel deposits is not well established. The deposits of S4 were then overridden by very likely more than one extensive foreland glaciation during the Middle to Late Pleistocene (e.g., Ellwanger et al., 2011; Müller, 2013; Preusser et al., 2011). It is remarkable that these latest glaciations with estimated ice thicknesses of 200–300 m at the study area (Bini et al., 2009) did not reactivate the Basadingen Trough but accumulated a basement lodgment till (S5) that lies conformably on the underlying strata.

3.5.3 The generic glacio-seismic sequence

Based on observations from the valley fill of the Basadingen Trough (i.e., seismic facies, associated sediments, and systematic subsequences), a generalized glacio-seismic sequence was defined (Fig. 9). This basic sequence includes the evolution from a subglacial (coarse-grained diamictic sediments; Facies III) over a glaciolacustrine (interlayered sand and gravel section with cut and fill structures; Facies IV) to a fully developed lacustrine depositional environment (interlayered to laminated sands and fines; Facies V) and represents a complete glacial advance-and-retreat cycle (Fig. 9 Sii; Facies III-V). A comparison between this defined glacio-seismic sequence and other observed architectural and sedimentary characteristics of overdeepened valley fills reveals consistent patterns in both geometry and facies distribution for clastic-dominated infill types (Buechi et al., 2024). However, Facies F was included to represent the more fine-grained dominated infill type (Fig. 9 Sⁱ). These deposits, not encountered in the Basadingen Trough, are often rich in dropstones and interpreted as proglacial lake sediments with typical ice-rafted debris (e.g., Dehnert et al., 2012; Schuster et al., 2024) and appear directly above the subglacial deposits (Facies III). Additionally, secondary features included are: i) lateral deltaic sediments (Facies VI), ii) deformation structures at contact zones with overlying glacial sequences (Facies VII), and iii) potential subaquatic mass-movement deposits are indicated as transparent lateral wedges (Facies M). Since this model is based on limited data, it does not cover all possible elements or variations that could occur in the infill of glacially overdeepened basins. This catalogue of glacio-seismic patterns should be further expanded to include major elements not encountered in the studied data by analyzing new data (e.g., combining Burschil et al., 2018 and Schuster et al., 2024) and integrating existing data (e.g., Nitsche et al., 2001; Spitzer et al., 2003). This would enable a

more comprehensive and systematic application of glacio-seismic sequence stratigraphy on glacially overdeepened structures and their sedimentary infill.

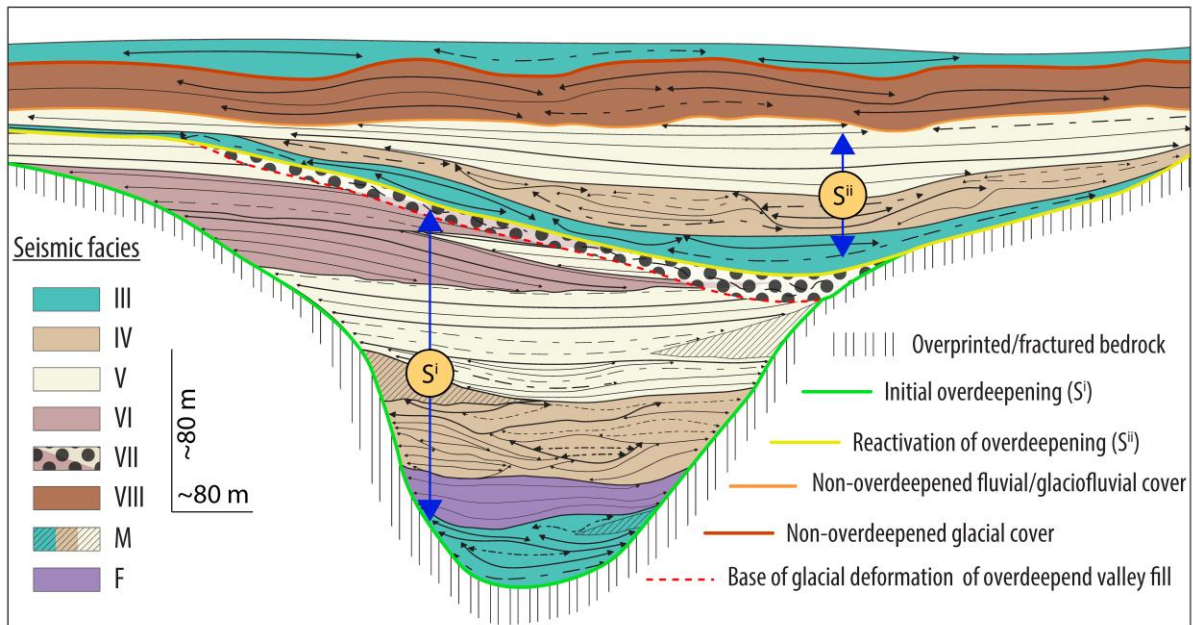


Figure 9: Generic model of a glacio-seismic sequence as a line drawing of an overdeepened valley fill with two preserved glacial sequences: Sⁱ with significant fine-grained deposits and Sⁱⁱ without.

Moreover, our glacial sequence model can be ground-truthed in modern proglacial lake systems in the pan-Alpine area, representing the underfilled remains of major overdeepenings from the last glacial cycle. These lakes can provide high-resolution insights into the sedimentary infill deposited since the last glacial cycle and partly even older ones (e.g., Fabbri et al., 2018; Schaller et al., 2022). Furthermore, studying young proglacial lakes in immediate glacial proximity (i.e., close to a calving glacier front) allows the direct observation of subglacial and proglacial processes with their depositional environments in an actualistic approach (e.g., Hosmann et al., 2024).

3.6 Conclusion

Based on seismic reflection and drill-core data, a seismic sequence stratigraphic approach was successfully applied to a Quaternary overdeepened glacial valley fill. The resulting glacial stratigraphy discerns unconformity-bounded seismic sequences, where each one is correlated through a robust core-to-seismic correlation with characteristic successions of glacial to proglacial valley-fill sediments. In the Basadingen Trough, three overdeepened glacial sequences (S1–S3) have been identified across both seismic profiles. They represent three glacial advance and retreat phases characterized by erosional-to-aggradational processes, which left characteristic geometric and lithologic imprints. Interestingly, the youngest glacier

advances during the last glacial cycle covered the Basadingen Trough but did not produce an overdeepening at this site, reflecting variations in subglacial processes over time.

Furthermore, based on the available seismic and drill-core data, a 3D model of the Basadingen Trough was established, enabling spatial analyses of its geometry and sedimentary filling. Specific patterns in the trough infill were observed, which may help to understand better the depositional architecture of overdeepened valleys (often only explored by individual drillings) that are increasingly relevant to applied geological challenges (e.g., geothermal, deep subsurface infrastructure, etc.). Additionally, systematic patterns of subglacial erosion in overdeepenings were identified, such as the initial deep erosion that is later widened during the succeeding glacial advances. These patterns provide crucial data to ground-truth numerical models. The study underlines the benefits of combining complementary geological and geophysical data in complex depositional settings. The presented approach of defining a detailed glacio-seismic sequence stratigraphy requires high-resolution seismic data, which in this case could be ground-truthed with high-quality core and borehole data for the calibration between sedimentary and seismic properties and facies. This systematic analysis of the correlated seismic facies patterns with the corresponding sediments allowed the definition of a generic ideal glacial sequence model, including lithologic content. This model lays the basis for defining glacial sequences, their lithologies, and their glacial history based on seismic data alone without relying on well/core control.

3.7 Appendix

Table A1: Metadata of the used drillings for the 3D model

Nr.	X	Y	Elevation [m a.s.l.]	Drilled length [m]	Drilling type	Accessibility/ Source
1	2698775	1278321	445	252	Scientific core-drilling	ThurGIS
2	2698751	1278300	442	201	Exploratory flush-drilling	Confidential
3	2699309	1278637	435	43	Exploratory core-drilling	ThurGIS
4	2698064	1278147	439	37	Exploratory core-drilling	ThurGIS
5	2698101	1279500	423	60	Exploratory flush-drilling	Confidential
6	2696998	1279549	435	42	Exploratory core-drilling	ThurGIS
7	2700390	1278810	416	65	Exploratory core-drilling	ThurGIS
8	2700183	1279473	414	56	Exploratory core-drilling	ThurGIS
9	2700438	1279664	415	8	Exploratory core-drilling	ThurGIS
10	2699161	1280055	455	180	Flush drilling for geothermal heating	ThurGIS
11	2698460	1280260	430	210	Flush drilling for geothermal heating	ThurGIS
12	2698536	1280425	423	88	Flush drilling for geothermal heating	ThurGIS
13	2698431	1280540	415	160	Flush drilling for geothermal heating	ThurGIS
14	2698076	1280585	413	28	Flush drilling for geothermal heating	ThurGIS

Notes: Nr. Represents the Label in Figure 1C, x- and y-coordinates are in CH1903+LV95 (EPSG:2056) reference system; except for drilling 2 and 5, all drilling profiles are publicly available on the official site of the Canton of Thurgau (<https://map.geo.tg.ch/apps/mf-geoadmin3/?lang=de&topic=ech>), and drilling Nr. 1 is also described in Schaller et al. (2023).

Table A2: Used spatial input data for 3D model

File name and Version	Resolution [m]	Reference system	Source	Accessibility
Bedrock elevation model - Digitales Höhenmodell Basis Quartär der Nordschweiz – Version 2014 ¹	25 x 25	CH1903+ LV03	NAGRA	upon request
DHM25 - Basismodell (V.2014)	25 x 25	CH1903+ LV03	Bundesamt für Landestopografie swisstopo	publicly available ²

1: Pietsch & Jordan, 2014

2: <https://www.swisstopo.admin.ch/de/hoeihenmodell-dhm25>

3.8 Further statements

3.8.1 Data availability

All data used and displayed in this study are publicly available according to the FAIR principle. The DOVE operational dataset (DOVE-Phase 1 Scientific Team et al., 2023b), containing all data concerning the drill core, is either available on the ICDP DOVE project website: <https://www.icdp-online.org/projects/by-continent/europe/dove-switzerland> or can be accessed on the GFZ-library (<https://doi.org/10.5880/ICDP.5068.001>) together with the operational report (DOVE-Phase 1 Scientific Team et al., 2023a) and the explanatory remarks

(DOVE-Phase 1 Scientific Team et al., 2023c). All other data used in this study (e.g., seismic data, 3D model horizons, in-hole check shot data; Schaller et al., 2024) are published on the BORIS-Portal, the University of Bern data repository (<https://doi.org/10.48620/398>).

3.8.2 Competing interests

The authors declare that they have no competing interests.

3.8.3 Funding

This research has been supported by the ICDP, the Deutsche Forschungsgemeinschaft (DFG, grant nos. KR2073/3-1, BU 2467/1-2, GA749/5-1, BU 2467/3-1, BU 3894/2-1, BU 3894/3-1, and PR 957/6-1), Nagra, ENSI, LGRB, LFU, LIAG, BOKU Vienna, and University of Bern.

3.8.4 Author's contribution

SS interpreted the seismic data, established the seismic sequence stratigraphy, did the core-to-seismic-correlation, created and analyzed the 3D model, developed the generic glacio-seismic sequence model, and was the paper's main author with the support of all co-authors. HB processed and interpreted the in-hole VSP data and reprocessed the seismic data with the help of SB and SS. Further, HB and SB wrote section 2.1. BS contributed to the initial analyses of the drill core and provided scientific input. MWB and FSA provided significant scientific input to all aspects of the study. All authors approved the text and the figures.

3.9 Acknowledgments

We are grateful for the continuing support of the International Scientific Continental Drilling Program (ICDP) and the DOVE science team for their efforts to keep this project thriving. A special thanks go to the technical staff of LIAG, who assisted with the seismic site surveys, the downhole logging, and the VSP. We acknowledge the strong support during the seismic survey and the drilling campaign by the members of the Bürgergemeinde Basadingen-Schlattingen, the members of the Jagdgesellschaft Hegi Belzhalden, the local inhabitants, the involved services of the political community Basadingen-Schlattingen, and the Canton of Thurgau. We would also like to thank the SEAG for providing us with some of their drill hole and core logs. Additionally, we would like to thank Ferdinando Musso Piantelli for his advice and support in creating the 3D model, Stefano Fabbri for his help with the seismic interpretation, and David Mair for his support using the QGIS software.

3.10 References

- Alley, R. B., Cuffey, K. M., & Zoet, L. K. (2019). Glacial erosion: Status and outlook. *Annals of Glaciology*, 60(80), 1–13. <https://doi.org/10.1017/aog.2019.38>
- Anselmetti, F. S., Bavec, M., Crouzet, C., Fiebig, M., Gabriel, G., Preusser, F., Ravazzi, C., & DOVE scientific team. (2022). Drilling Overdeepened Alpine Valleys (ICDP-DOVE): Quantifying the age, extent, and environmental impact of Alpine glaciations. *Scientific Drilling*, 31, 51–70. <https://doi.org/10.5194/sd-31-51-2022>
- Bandou, D., Schlunegger, F., Kissling, E., Marti, U., Reber, R., & Pfander, J. (2023). Overdeepenings in the Swiss plateau: U-shaped geometries underlain by inner gorges. *Swiss Journal of Geosciences*, 116(1), 19. <https://doi.org/10.1186/s00015-023-00447-y>
- Bennett, M. R., Huddart, D., & Thomas, G. S. P. (2002). Facies architecture within a regional glaciolacustrine basin: Copper River, Alaska. *Quaternary Science Reviews*, 21(20), 2237–2279. [https://doi.org/10.1016/S0277-3791\(02\)00027-6](https://doi.org/10.1016/S0277-3791(02)00027-6)
- Berger, A., Li, X. S., & Loutre, M. F. (1999). Modelling northern hemisphere ice volume over the last 3 Ma. *Quaternary Science Reviews*, 18(1), 1–11. [https://doi.org/10.1016/S0277-3791\(98\)00033-X](https://doi.org/10.1016/S0277-3791(98)00033-X)
- Bini, A., Buoncristiani, J.-F., Couterrand, S., Ellwanger, D., Felber, M., Florineth, D., Graf, H. R., Keller, O., Kelly, M., Schlüchter, C., & Schoeneich, p. (2009). *Die Schweiz während des letzteiszeitlichen Maximums (LGM)* [Map]. Bundesamt für Landestopografie Swisstopo.
- Bouma, A. H. (1962). *Sedimentology of some Flysch deposits: A graphic approach to facies interpretation*. Elsevier. <http://lib.ugent.be/catalog/rug01:000978747>
- Brandt, A. C. (2020). *Erkundung des alpinen, glazial-übertieften Basadingen-Beckens mithilfe von P-Wellen-Seismik* [BSc thesis]. Leibniz Universität Hannover.
- Buechi, M. W., Frank, S. M., Graf, H. R., Menzies, J., & Anselmetti, F. S. (2017). Subglacial emplacement of tills and meltwater deposits at the base of overdeepened bedrock troughs. *Sedimentology*, 64(3), 658–685. <https://doi.org/10.1111/sed.12319>
- Buechi, M. W., Graf, H. R., Haldimann, P., Lowick, S. E., & Anselmetti, F. S. (2018). Multiple Quaternary erosion and infill cycles in overdeepened basins of the northern Alpine foreland. *Swiss Journal of Geosciences*, 111(1–2), 133–167. <https://doi.org/10.1007/s00015-017-0289-9>
- Buechi, M. W., Landgraf, A., Madritsch, H., Mueller, D., Knipping, M., Nyffenegger, F., Preusser, F., Schaller, S., Schnellmann, M., & Deplazes, G. (2024). Terminal glacial overdeepenings: Patterns of erosion, infilling and new constraints on the glaciation history of Northern Switzerland. *Quaternary Science Reviews*, 344, 108970. <https://doi.org/10.1016/j.quascirev.2024.108970>
- Burschil, T., Buness, H., Tanner, D. C., Wielandt-Schuster, U., Ellwanger, D., & Gabriel, G. (2018). High-resolution reflection seismics reveal the structure and the evolution of the Quaternary glacial Tannwald Basin. *Near Surface Geophysics*, 16(6), 593–610. <https://doi.org/10.1002/nsg.12011>
- Clark, P. U., Archer, D., Pollard, D., Blum, J. D., Rial, J. A., Brovkin, V., Mix, A. C., Pisias, N. G., & Roy, M. (2006). The middle Pleistocene transition: Characteristics, mechanisms, and implications for long-term changes in atmospheric pCO₂. *Quaternary Science Reviews*, 25(23–24), 3150–3184. <https://doi.org/10.1016/j.quascirev.2006.07.008>
- Cohen, D., Gillet-Chaulet, F., Haeblerli, W., Machguth, H., & Fischer, U. H. (2018). Numerical reconstructions of the flow and basal conditions of the Rhine glacier, European Central Alps, at the Last Glacial Maximum. *The Cryosphere*, 12(8), 2515–2544. <https://doi.org/10.5194/tc-12-2515-2018>
- Cook, S. J., & Swift, D. A. (2012). Subglacial basins: Their origin and importance in glacial systems and landscapes. *Earth-Science Reviews*, 115(4), 332–372. <https://doi.org/10.1016/j.earscirev.2012.09.009>
- Dehnert, A., Lowick, S. E., Preusser, F., Anselmetti, F. S., Drescher-Schneider, R., Graf, H. R., Heller, F., Horstmeyer, H., Kemna, H. A., Nowaczyk, N. R., Züger, A., & Furrer, H. (2012). Evolution of an overdeepened trough in the northern Alpine Foreland at Niederweningen, Switzerland. *Quaternary Science Reviews*, 34, 127–145. <https://doi.org/10.1016/j.quascirev.2011.12.015>
- DOVE-Phase 1 Scientific Team, Anselmetti, F. S., Beraus, S., Buechi, M. W., Buness, H., Burschil, T., Fiebig, M., Firla, G., Gabriel, G., Gegg, L., Grelle, T., Heeschen, K., Kroe-mer, E., Lehne, C., Lüthgens, C., Neuhuber, S., Preusser, F., Schaller, S., Schmalfuss, C., Schuster, B., Tanner, D. C., Thomas, C., Tomonaga, Y., Wieland-Schuster, U., and Wonik, T. (2023a). Drilling Overdeepened Alpine Valleys (DOVE) – Operational Report of Phase 1, (ICDP Operational Report), GFZ German Research Centre for Geosciences, Potsdam, 70 pp., <https://doi.org/10.48440/ICDP.5068.001>
- DOVE-Phase 1 Scientific Team, Anselmetti, F. S., Beraus, S., Buechi, M. W., Buness, H., Burschil, T., Fiebig, M., Firla, G., Gabriel, G., Gegg, L., Grelle, T., Heeschen, K., Kroe-mer, E., Lehne, C., Lüthgens, C., Neuhuber, S., Preusser, F., Schaller, S., Schmalfuss, C., Schuster, B., Tanner, D. C., Thomas, C., Tomonaga, Y., Wieland-Schuster, U., and Wonik, T. (2023b). Drilling Overdeepened Alpine Valleys (DOVE) – Operational Dataset of DOVE Phase 1, GFZ Data Services [data set], <https://doi.org/10.5880/ICDP.5068.001>

- DOVE-Phase 1 Scientific Team, Anselmetti, F. S., Beraus, S., Buechi, M. W., Bunes, H., Burschil, T., Fiebig, M., Firla, G., Gabriel, G., Gegg, L., Grelle, T., Heeschen, K., Kroe-mer, E., Lehne, C., Lüthgens, C., Neuhuber, S., Preusser, F., Schaller, S., Schmalfuss, C., Schuster, B., Tanner, D. C., Thomas, C., Tomonaga, Y., Wieland-Schuster, U., and Wonik, T. (2023c). Drilling Overdeepened Alpine Valleys (DOVE) – Explanatory remarks on the operational dataset, ICDP Operational Dataset – Explanatory Remarks, GFZ German Research Centre for Geosciences, Potsdam, 34 pp., <https://doi.org/10.48440/ICDP.5068.002>
- Ellwanger, D., Wieland-Schuster, U., Franz, M., & Simon, T. (2011). The Quaternary of the southwest German Alpine Foreland (Bodensee-Oberschwaben, Baden-Württemberg, Southwest Germany). *E&G Quaternary Science Journal*, 60(2/3), 306–328. <https://doi.org/10.3285/eg.60.2-3.07>
- Fabbri, S. C., Affentranger, C., Krastel, S., Lindhorst, K., Wessels, M., Madritsch, H., Allenbach, R., Herwegh, M., Heuberger, S., Wieland-Schuster, U., Pomella, H., Schwestermann, T., & Anselmetti, F. S. (2021). Active Faulting in Lake Constance (Austria, Germany, Switzerland) Unraveled by Multi-Vintage Reflection Seismic Data. *Frontiers in Earth Science*, 9. <https://www.frontiersin.org/articles/10.3389/feart.2021.670532>
- Fabbri, S. C., Buechi, M. W., Horstmeyer, H., Hilbe, M., Hübscher, C., Schmelzbach, C., Weiss, B., & Anselmetti, F. S. (2018). A subaquatic moraine complex in overdeepened Lake Thun (Switzerland) unravelling the deglaciation history of the Aare Glacier. *Quaternary Science Reviews*, 187, 62–79. <https://doi.org/10.1016/j.quascirev.2018.03.010>
- Fiebig, M. (2011). Editorial. *E&G Quaternary Science Journal*, 60(2/3), 278–281. <https://doi.org/10.3285/eg.60.2-3.05>
- Fiebig, M., Herbst, P., Drescher-Schneider, R., Lüthgens, C., Lomax, J., & Doppler, G. (2014). Some remarks about a new Last Glacial record from the western Salzach foreland glacier basin (Southern Germany). *Quaternary International*, 328–329, 107–119. <https://doi.org/10.1016/j.quaint.2013.12.048>
- Frangi, T., & Szepešy, D. (2003). Spezielle Schottervorkommen zwischen Thur und Rhein. *Mitteilungen der Thurgauischen Naturforschenden Gesellschaft*, 59, 189–197. <https://doi.org/10.5169/SEALS-594086>
- Graf, H. R. (2009a). Stratigraphie und Morphogenese von frühpleistozänen Ablagerungen zwischen Bodensee und Klettgau. *E&G Quaternary Science Journal*, 58(1), 12–54. <https://doi.org/10.3285/eg.58.1.02>
- Graf, H. R. (2009b). *Stratigraphie von Mittel- und Spätpleistozän in der Nordschweiz. Beiträge zur Geologischen Karte der Schweiz (N.F.)* (Vol. 168). Landesgeologie.
- Gribenski, N., Valla, P. G., Preusser, F., Roattino, T., Crouzet, C., & Buoncristiani, J.-F. (2021). Out-of-phase Late Pleistocene glacial maxima in the Western Alps reflect past changes in North Atlantic atmospheric circulation. *Geology*, 49(9), 1096–1101. <https://doi.org/10.1130/G48688.1>
- Haeuselmann, P., Granger, D. E., Jeannin, P.-Y., & Lauritzen, S.-E. (2007). Abrupt glacial valley incision at 0.8 Ma dated from cave deposits in Switzerland. *Geology*, 35(2), 143. <https://doi.org/10.1130/G23094A>
- Hofmann, F. (1967). *Erläuterungen zu: Geologischer Atlas der Schweiz—1052 Andelfingen [Atlasblatt 52]*. Schweiz. Geol. Komm.
- Hofmann, F., & Hantke, R. (1964). *Erläuterungen zu Blatt 1032 Diessenhofen des geologischen Atlas der Schweiz*. Schweiz. Geol. Komm.
- Hosmann, S. L., Fabbri, S. C., Buechi, M. W., Hilbe, M., Bauder, A., & Anselmetti, F. S. (2024). Exploring beneath the retreating ice: Swath bathymetry reveals sub- to proglacial processes and longevity of future alpine glacial lakes. *Annals of Glaciology*, 1–6. <https://doi.org/10.1017/aog.2024.18>
- Ivy-Ochs, S., Kerschner, H., Reuther, A., Preusser, F., Heine, K., Maisch, M., Kubik, P. W., & Schlüchter, C. (2008). Chronology of the last glacial cycle in the European Alps. *Journal of Quaternary Science*, 23(6–7), 559–573. <https://doi.org/10.1002/jqs.1202>
- Kehew, A. E., Piotrowski, J. A., & Jørgensen, F. (2012). Tunnel valleys: Concepts and controversies — A review. *Earth-Science Reviews*, 113(1), 33–58. <https://doi.org/10.1016/j.earscirev.2012.02.002>
- Keller, O., & Krayss, E. (1993). The rhine-linth glacier in the upper wurm: A model of the last alpine glaciation. *Quaternary International*, 18, 15–27. [https://doi.org/10.1016/1040-6182\(93\)90049-L](https://doi.org/10.1016/1040-6182(93)90049-L)
- Kirkham, J. D., Hogan, K. A., Larter, R. D., Arnold, N. S., Ely, J. C., Clark, C. D., Self, E., Games, K., Huuse, M., Stewart, M. A., Ottesen, D., & Dowdeswell, J. A. (2024). Tunnel valley formation beneath deglaciating mid-latitude ice sheets: Observations and modelling. *Quaternary Science Reviews*, 323, 107680. <https://doi.org/10.1016/j.quascirev.2022.107680>
- Kirkham, J. D., Hogan, K. A., Larter, R. D., Self, E., Games, K., Huuse, M., Stewart, M. A., Ottesen, D., Arnold, N. S., & Dowdeswell, J. A. (2021). Tunnel valley infill and genesis revealed by high-resolution 3-D seismic data. *Geology*, 49(12), 1516–1520. <https://doi.org/10.1130/G49048.1>
- Knudsen, M. F., Nørgaard, J., Grischott, R., Kober, F., Egholm, D. L., Hansen, T. M., & Jansen, J. D. (2020). New cosmogenic nuclide burial-dating model indicates onset of major glaciations in the Alps during Middle Pleistocene Transition. *Earth and Planetary Science Letters*, 549, 116491. <https://doi.org/10.1016/j.epsl.2020.116491>

- Lisiecki, L. E., & Raymo, M. E. (2005). A Pliocene-Pleistocene stack of 57 globally distributed benthic $\delta^{18}\text{O}$ records: PLIOCENE-PLEISTOCENE BENTHIC STACK. *Paleoceanography*, 20(1). <https://doi.org/10.1029/2004PA001071>
- Lønne, I. (1995). Sedimentary facies and depositional architecture of ice-contact glaciomarine systems. *Sedimentary Geology*, 98(1), 13–43. [https://doi.org/10.1016/0037-0738\(95\)00025-4](https://doi.org/10.1016/0037-0738(95)00025-4)
- Mitchum, R. M., Jr., Vail, P. R., & Sangree, J. B. (1977). Seismic Stratigraphy and Global Changes of Sea Level, Part 6: Stratigraphic Interpretation of Seismic Reflection Patterns in Depositional Sequences1. In C. E. Payton (Ed.), *Seismic Stratigraphy—Applications to Hydrocarbon Exploration* (Vol. 26). American Association of Petroleum Geologists. <https://doi.org/10.1306/M26490C8>
- Monegato, G., Scardia, G., Hajdas, I., Rizzini, F., & Piccin, A. (2017). The Alpine LGM in the boreal ice-sheets game. *Scientific Reports*, 7(1), 2078. <https://doi.org/10.1038/s41598-017-02148-7>
- Mulder, T., & Alexander, J. (2001). The physical character of subaqueous sedimentary density flows and their deposits. *Sedimentology*, 48(2), 269–299. <https://doi.org/10.1046/j.1365-3091.2001.00360.x>
- Müller, E. R. (2013). Mittelpleistozäne Schottervorkommen zwischen dem Thurtal und Schaffhausen. *Swiss Bulletin für angewante Geologie*, 18(1), 3–27. <https://doi.org/10.5169/SEALS-391135>
- Muttoni, G., Carcano, C., Garzanti, E., Ghielmi, M., Piccin, A., Pini, R., Rogledi, S., & Sciunnach, D. (2003). Onset of major Pleistocene glaciations in the Alps. *Geology*, 31(11), 989–992. <https://doi.org/10.1130/G19445.1>
- Naef, H., Birkhäuser, P., & Roth, P. (1995). Interpretation der Reflexionsseismik im Gebiet nördlich Lägeren—Zürcher Weinland. *Nagra Technischer Bericht NTB 94-14*.
- Nitsche, F. O., Monin, G., & Marillier, F. (2001). Reflection seismic study of cenozoic sediments in an overdeepened valley of northern Switzerland: The Birrfeld area. *Eclogae Geologicae Helveticae = Swiss Journal of Geosciences*, 94(3), 363. <https://doi.org/10.5169/seals-168901>
- Pietsch, J., & Jordan, P. (2014). *Digitales Höhenmodell Basis Quartär der Nordschweiz – Version 2014 und ausgewählte Auswertungen* (Technical report 14–02; Nagra Arbeitsbericht NAB). <https://nagra.ch/downloads/arbeitsbericht-nab-14-02/>
- Pol, K., Masson-Delmotte, V., Johnsen, S., Bigler, M., Cattani, O., Durand, G., Falourd, S., Jouzel, J., Minster, B., Parrenin, F., Ritz, C., Steen-Larsen, H. C., & Stenni, B. (2010). New MIS 19 EPICA Dome C high resolution deuterium data: Hints for a problematic preservation of climate variability at sub-millennial scale in the “oldest ice.” *Earth and Planetary Science Letters*, 298(1), 95–103. <https://doi.org/10.1016/j.epsl.2010.07.030>
- Pomper, J., Salcher, B. C., Eichkitz, C., Prasicek, G., Lang, A., Lindner, M., & Götz, J. (2017). The glacially overdeepened trough of the Salzach Valley, Austria: Bedrock geometry and sedimentary fill of a major Alpine subglacial basin. *Geomorphology*, 295, 147–158. <https://doi.org/10.1016/j.geomorph.2017.07.009>
- Preusser, F., Graf, H. R., Keller, O., Krayss, E., & Schlüchter, C. (2011). Quaternary glaciation history of northern Switzerland. *E&G Quaternary Science Journal*, 60(2/3), 282–305. <https://doi.org/10.3285/eg.60.2-3.06>
- Preusser, F., Reitner, J. M., & Schlüchter, C. (2010). Distribution, geometry, age and origin of overdeepened valleys and basins in the Alps and their foreland. *Swiss Journal of Geosciences*, 103(3), 407–426. <https://doi.org/10.1007/s00015-010-0044-y>
- Ruddiman, W. F., Raymo, M., & McIntyre, A. (1986). Matuyama 41,000-year cycles: North Atlantic Ocean and northern hemisphere ice sheets. *Earth and Planetary Science Letters*, 80(1), 117–129. [https://doi.org/10.1016/0012-821X\(86\)90024-5](https://doi.org/10.1016/0012-821X(86)90024-5)
- Scardia, G., Donegana, M., Muttoni, G., Ravazzi, C., & Vezzoli, G. (2010). Late Matuyama climate forcing on sedimentation at the margin of the southern Alps (Italy). *Quaternary Science Reviews*, 29(7), 832–846. <https://doi.org/10.1016/j.quascirev.2009.12.002>
- Schaller, S., Böttcher, M. E., Buechi, M. W., Epp, L. S., Fabbri, S. C., Gribenski, N., Harms, U., Krastel, S., Liebezeit, A., Lindhorst, K., Marxen, H., Raschke, U., Schleheck, D., Schmiedinger, I., Schwalb, A., Vogel, H., Wessels, M., & Anselmetti, F. S. (2022). Postglacial evolution of Lake Constance: Sedimentological and geochemical evidence from a deep-basin sediment core. *Swiss Journal of Geosciences*, 115(1), 7. <https://doi.org/10.1186/s00015-022-00412-1>
- Schaller, S., Buechi, M. W., Schuster, B., & Anselmetti, F. S. (2023). Drilling into a deep buried valley (ICDP DOVE): A 252\,m long sediment succession from a glacial overdeepening in northwestern Switzerland. *Scientific Drilling*, 32, 27–42. <https://doi.org/10.5194/sd-32-27-2023>
- Schaller, S., Schuster, B., Beraus, S., Buechi, M. W., Buness, H., & Anselmetti, F. S. (2024). *Supplementary data set for seismic sequence stratigraphy of DOVE-site 5068_1* [Dataset]. Bern Open Repository and Information System. <https://doi.org/10.48620/398>
- Schlüchter, C. (2004). The Swiss glacial record – a schematic summary. In *Developments in Quaternary Sciences* (Vol. 2, pp. 413–418). Elsevier. [https://doi.org/10.1016/S1571-0866\(04\)80092-7](https://doi.org/10.1016/S1571-0866(04)80092-7)
- Schuster, B., Gegg, L., Schaller, S., Buechi, M. W., Tanner, D. C., Wielandt-Schuster, U., Anselmetti, F. S., & Preusser, F. (2024). Shaped and filled by the Rhine Glacier: The overdeepened Tannwald Basin in southwestern Germany. *Scientific Drilling*, 33(2), 191–206. <https://doi.org/10.5194/sd-33-191-2024>

- Schwenk, M. A., Schläfli, P., Bandou, D., Gribenski, N., Douillet, G. A., & Schlunegger, F. (2022). From glacial erosion to basin overfill: A 240 m-thick overdeepening–fill sequence in Bern, Switzerland. *Scientific Drilling*, 30, 17–42. <https://doi.org/10.5194/sd-30-17-2022>
- Spitzer, R., Nitsche, F. O., Green, A. G., & Horstmeyer, H. (2003). Efficient acquisition, processing, and interpretation strategy for shallow 3D seismic surveying: A Case Study. *Geophysics*, 68(6), 1792–1806. <https://doi.org/10.1190/1.1635032>
- Spötl, C., Koltai, G., Jarosch, A. H., & Cheng, H. (2021). Increased autumn and winter precipitation during the Last Glacial Maximum in the European Alps. *Nature Communications*, 12(1), Article 1. <https://doi.org/10.1038/s41467-021-22090-7>
- Vegt, P. van der, Janszen, A., & Moscariello, A. (2012). Tunnel valleys: Current knowledge and future perspectives. In M. Huuse, J. Redfern, D. P. L. Heron, R. J. Dixon, A. Moscariello, & J. Craig (Eds.), *Glaciogenic Reservoirs and Hydrocarbon Systems* (Vol. 368, p. 0). Geological Society of London. <https://doi.org/10.1144/SP368.13>

4

Wireline logging data-driven lithoprediction of unconsolidated sediments

Sebastian Schaller^{1,2}

Patrico Becerra³

Sarah Beraus⁴

MariusW. Buechi^{1,2}

David Mair¹

Mehrdad Sardar Abadi⁴

Bennet Schuster^{5,1,2}

Flavio S. Anselmetti^{1,2}

¹Institute of Geological Sciences, Universität Bern,

²Oeschger Centre for Climate Change Research, Universität Bern

³Space Research and Planetary Sciences, Physics Institute, Universität Bern

⁴LIAG Institute for Applied Geophysics

⁵Institute of Earth and Environmental Sciences, University of Freiburg

This manuscript was submitted to *Sedimentologica* in late January 2025

4. Wireline logging data-driven lithoprediction of unconsolidated sediments

4.1 Abstract

Detailed knowledge about the lithostratigraphy of unconsolidated Quaternary sediments is essential for many scientific and industrial applications. In most cases, only drill cores provide sufficient detail to extract crucial lithological and petrophysical information (e.g., lithofacies, permeability, consolidation). In contrast, flush-drilling methods provide only minimal lithological data in unconsolidated sediments but are faster and less expensive. Therefore, an approach that possesses the rapid, low-cost advantages of flush drillings but provides the data quality of core drillings could significantly improve subsurface investigations.

This study explores how advanced data analysis techniques can be used to create data-driven stratigraphic models with standard wireline logging data that may reduce the need for cored drillings by identifying complex relationships between multiple logs, surpassing the limitations of conventional cross plots and depth plots. In particular, hierarchical clustering of petrophysical and geochemical wireline logging data in combination with UMAP (Uniform Manifold Approximation and Projection) visualization for dimensionality reduction has successfully predicted distinct types of lithofacies. The purely data-driven approach finds clusters that can be directly correlated with geological data from drill cores. In this study, the method was developed and tested on one core and two wireline datasets acquired in the context of the International Continental Scientific Drilling Program (ICDP), which investigates multiple drill sites around the Alps (Drilling Overdeepened Alpine Valleys - DOVE). The drill site studied here is located in the former Rhine Glacier area in Germany and consists of a core-controlled well and an additional flush-drilling well. The reconstructed stratigraphic succession from the core-controlled well captured the major stratigraphic elements and even finer internal details, directly linking it with the geology identified at the drilled site. This direct link serves as a translation key, allowing a successful correlation between the reconstructed lithology of the core controlled and the flush drilling well. The study shows that developing sensitive and accurate wireline-log-based stratigraphy for unconsolidated Quaternary sediments has the potential to significantly improve the quality, the vertical, and the lateral resolution of stratigraphic models by integrating petrophysical and sedimentary properties of relatively fast acquired flush drilling profiles with high precision core drillings.

4.2 Introduction

4.2.1 Background and Motivation

Understanding the stratigraphy of the terrestrial subsurface is essential for a myriad of scientific and industrial applications. These include climate-change mitigation and paleoclimate studies (e.g., Drilling Overdeepened Alpine Valley Project; Anselmetti et al., 2022), subsurface exploration and classification (e.g., potential and use of geothermal energy; Giardini et al., 2021), natural hazard and risk assessments (e.g., earthquake vulnerability; Bergamo et al., 2023), or infrastructure projects (e.g., railroad-tunnels; Guntli et al., 2016). However, investigating subsurface formations is a major challenge in geoscience due to their natural inaccessibility. This challenge can be addressed by either i) geophysical methods such as seismic or gravimetric surveys or ii) direct methods. The two primary examples of the latter are destructive flush drillings – where the sediments/rocks are cut in tiny pieces ("cuttings") and flushed out by a drilling fluid (typically air or a mixture of water and additives termed "mud") – or core drillings, in which the rock/sediment sequence is maintained. Only core drillings provide direct, high-resolution access to in-situ geological information. In contrast, geophysical surveys generally return only indirect low-resolution models, and flush drillings give only incomplete "snapshots" of the subsurface.

Despite its advantages, high-quality core drillings are resource-intensive, with substantial financial and temporal commitments. This has a critical impact on project planning and makes the acquisition of funding difficult, often leading to the downsizing or canceling of projects; consequently, potentially critical scientific data is never acquired. Even if recent advances in the automated classification of sediment cores (e.g., Di Martino et al., 2023; Lauper et al., 2021) may reduce some of these costs in the future, core drilling will remain a significant investment.

Given these constraints, an approach that uses fast and low-cost flush drillings but provides the data quality of core drillings would significantly improve subsurface investigations. One promising solution is coupling destructive flush drilling with wireline logging surveys, partly compensating for expensive core drillings. This approach, relatively uncommon for applications in Quaternary sediments, is standard in energy exploration (e.g., hydrocarbon, geothermal), leading to advanced techniques such as "Logging While Drilling" (Selley & Sonnenberg, 2023). Wireline logs, traditionally used to evaluate carbonate host rocks and reservoirs with well-known and studied petrophysical properties (i.e., electrofacies: Serra &

Abbott, 1982; or acoustic properties: Anselmetti & Eberli, 1999), are a valuable source of geologic data, making them crucial for/when establishing data-based subsurface stratigraphy.

Processing and interpreting wireline logs is a well-established subdiscipline of geoscience with an extensive literature catalogue (e.g., Ghosh, 2022; Lai et al., 2024). Therefore, combining high-resolution core-drilling data with petrophysical data from wireline logging would increase subsurface stratigraphic models' reliability and level of detail. Though recent developments have explored supervised machine-learning techniques to correlate sediment and rock types with wireline data (e.g., Carrasquilla, 2023), such approaches are inherently limited in their ability to work on data that differs from their original training data. Furthermore, they require substantial amounts of training data, which is often unavailable. Hence, combining wireline and drill-core data would allow for obtaining crucial or currently missing subsurface data in cases and regions where this has not been possible due to logistical constraints.

Here, we present a new approach using unsupervised clustering methods that focus on the internal structures of wireline logging data to link them with core lithology. Employing dimensionality reduction and clustering allows for generalization in higher-dimensional datasets with few computational resources and no need for training a model. This uncovers complex relationships among multiple wireline logs beyond conventional cross or depth plots. Additionally, the study aims to evaluate a catalogue of useful petrophysical and chemical logs for meaningful wireline log-based classification and characterization of unconsolidated terrestrial Quaternary sediments. The proposed methodology is applied and tested in a case study that focuses on a glacially overdeepened trough in the former Rhine Glacier area. The case study contains wireline datasets from two adjacent wells, ~30 m apart, one from a core drilling and one from a destructive flush drilling. Integrating the wireline datasets with the high-resolution drill core data allows for establishing a wireline log data-based stratigraphy in a "cross-hole" approach.

4.2.2 Drill Site and Data Selection

The Tannwald area in southern Germany is located in the northern part of the former Rhine Glacier lobe and was heavily affected by past glaciations during the Quaternary, which formed several generations of overlain glacially overdeepened troughs (Fig. 1; e.g., Ellwanger et al., 2011; Preusser et al., 2011). These structures were eventually refilled by unconsolidated Quaternary sediments, i.e., sand, gravel, silt/clay, and diamicts, building up valuable sedimentary archives. These archives are targets of the "Drilling Overdeepened Alpine

Valleys" (DOVE) project (for a summary, see Anselmetti et al., 2022). All the data we present here were acquired on DOVE site 5068_1, which consists of a flush drilling (A; 588 m a.s.l.; WSG84: 47.9998°, 9.74864°) and a core drilling (C; 588 m a.s.l.; WSG84: 47.9995°, 9.74901°), with ~30 m between the two wells.

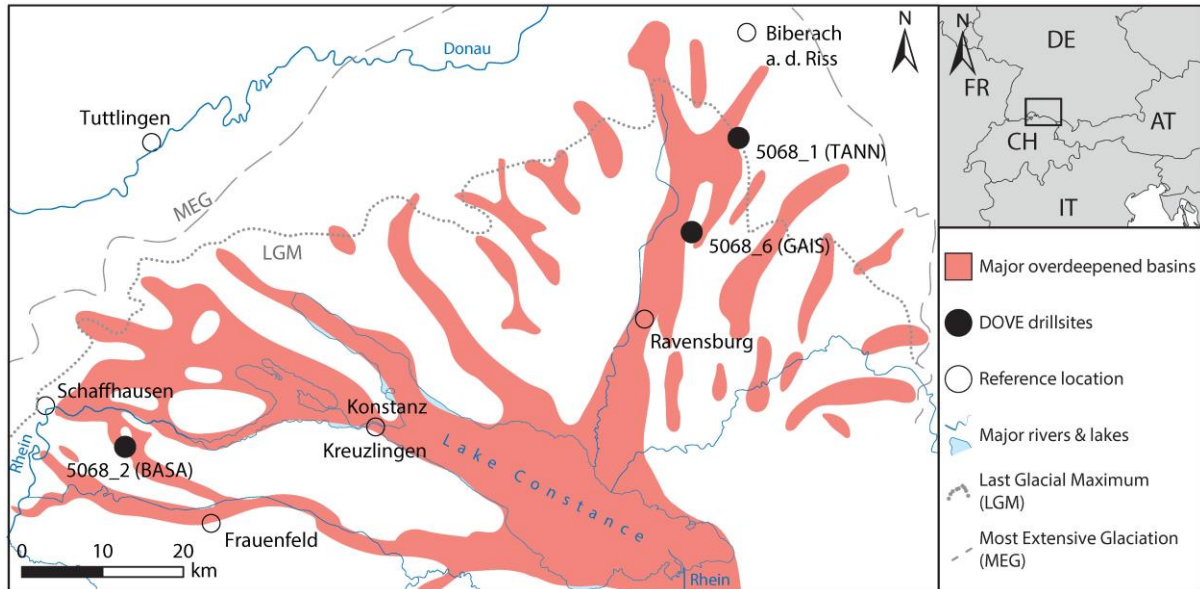


Figure 1: Overview of the glacially overdeepened systems within the former Rhine Glacier lobe (modified from Ellwanger et al., 2011) with the location of three DOVE Phase I sites: 5068_1 (TANN), 5068_2 (BASA), and 5068_6 (GAIS).

The used data consist of a high-quality drill core with an accompanying wireline log survey (5068_1_C) and an additional wireline log survey from a flush drilling (5068_1_A) with low-resolution cutting descriptions (1 m interval). The recovered drill core consists of ~156m unconsolidated Quaternary sediments and ~ 10 m Neogene sand- and siltstones (for examples, see Fig. 2 and Table A1). The high-resolution core-based lithological profile allows a direct correlation and linkage between the wireline logging data, visually described sedimentary properties, and proxy data (e.g., age-model). A brief overview of the systematic and hierarchical order behind the used lithotypes is provided in Table A2. The drill core and all related core data are described in detail by Schuster et al. (2024).

The measured wireline logs focus on petrophysical and chemical parameters that provide information about the lithological composition (e.g., magnetic susceptibility, photoelectric absorption, U-, Th-, and K-content), the depositional environment (e.g., clay/silt content: natural gamma radiation) or sedimentary properties (e.g., water content and permeability: electric resistivity, formation porosity and compaction: porosity and bulk density). Table A3 provides an overview of the wireline logs relevant to this study, including the abbreviations used. The wireline data were acquired with a depth spacing of 10 cm but could not be taken in the upper ~45 m (5068_1_A) and ~85 m (5068_1_C) due to the installation of a steel casing to

stabilize the boreholes. All used wireline data were measured below the deepest local groundwater table of ~ 43 m, documented during the drilling and measuring campaign in well A (Beraus et al., 2024). All further relevant information about the wireline surveys, including the data quality, coverage, and preprocessing, is provided in the DOVE Operational Report (DOVE-Phase 1 Scientific Team et al., 2023a) and in the Data Report (DOVE-Phase 1 Scientific Team et al., 2023b).

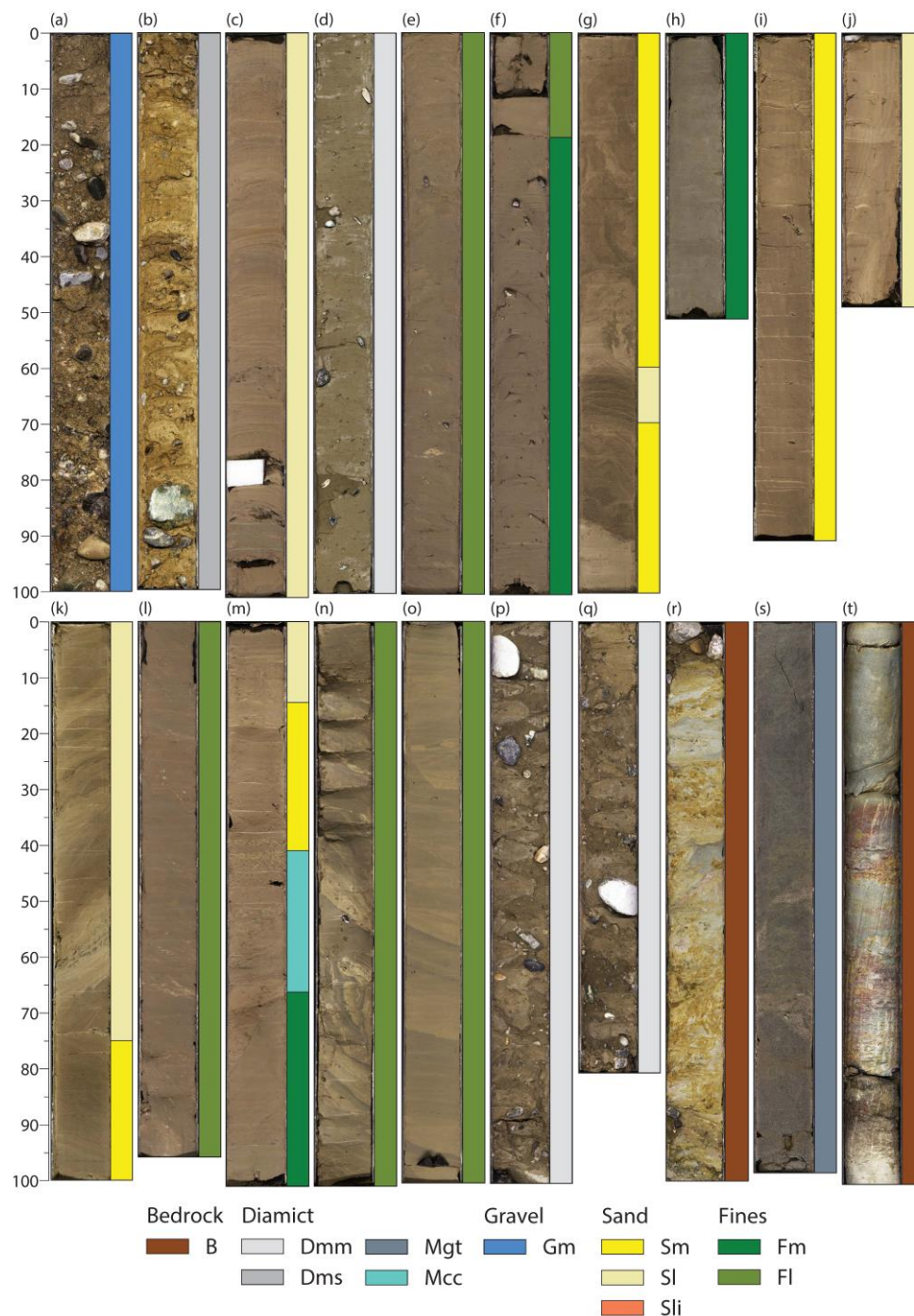


Figure 2: Representative core examples of 5068_1_C with assigned lithotypes. An overview of the used lithotypes is provided in Table A2. The corresponding core section ID and composite depth of the used examples are given in Table A1. The vertical scale is in cm.

4.3 Methods

Figure 3 summarizes the workflow developed for our study, which directly links data clusters defined by shared petrophysical and chemical properties of the measured sediments with the corresponding drill core-based lithology. These data clusters are extracted from the measured wireline logs through dimensionality reduction and hierarchical clustering. The direct link between the extracted data clusters and the actual lithology can be used as a translation key for cross-correlation with similar wireline datasets without a direct lithological link. All data manipulation, processing, analysis, and visualization were done using Python (V. 3.9.18) and Jupyter Notebooks (V.6.4.5). The code of the workflow is built around the following Python libraries: i) Pandas (V 1.3.4; The pandas development team, 2024), ii) NumPy (V 1.24.3; Harris et al., 2020), iii) SciPy (V 1.11.3; Virtanen et al., 2020) iv) Scikit-learn (V 1.3.0; Pedregosa et al., 2011), v) UMAP (V 0.5.5; McInnes et al., 2018), vi) Seaborn (V 0.13.2; Waskom, 2021), vii) Matplotlib (V 3.8.0; Hunter, 2007), and viii) Plotly (V 5.9.0; Plotly Technologies Inc., 2015).

4.3.1 Data Acquisition, Processing, and Analysis

All details regarding the data acquisition are provided in DOVE-Phase 1 Scientific Team et al. (2023a, 2023b) and Schuster et al. (2024).

In the first step, the averaged borehole geometry was derived from caliper logs and corrected for shifts that led to unrealistic values, such as values too small or too large for cased sections with known diameters. This corrected geometry was then used to apply a caving correction (i.e., Krammer & Pohl, 1987; Schlumberger, 1972, and internal documents from the ICDP OSG) on wireline logs measured without borehole-wall contact, including magnetic susceptibility (Susz), the combined spectral gamma log (SGR), and its three components (U, Th, and K). Sections measured in the cased hole and zones of intense outbreak/caving (>15% of the nominal borehole diameter) indicating poor data quality were removed. Additional optional filters were applied to individual logs to exclude implausible values (e.g., density <1.5 g/cm³). The original litholog, based on the initially defined "DOVE" lithotypes, was condensed into 13 lithotypes (for the "Full Lithology" see Table A2). The condensed lithotypes, primarily based on petrophysical and chemical properties rather than structural criteria, are further grouped into the following five "Major Lithologies": B: Bedrock; D: Diamict; G: Gravel; S: Sand; F: Fines. Based on this new litholog, a "major" and "full lithology" label was assigned to each measurement point in the core-controlled wireline dataset, directly linking lithology with wireline logging data.

Before applying dimensionality reduction and cluster analysis on the wireline data, classic qualitative and quantitative statistical methods (e.g., cross or depth plots, density distributions) were used for an initial investigation of several data properties. Further, principal component analysis (PCA) and covariance matrix analysis were applied to the wireline data to better understand its structure (e.g., degree of data variance, lithological distribution, and the relationship between individual logs) and identify valuable input logs for cluster analysis.

4.3.2 Clustering

In preparation for dimension reduction and clustering, each log was normalized into a distribution with a mean of 0 and a standard deviation of 1. Then, the original ten dimensions of the normalized input data (the selected wireline logs for clustering) were reduced to three dimensions using the "Uniform Manifold Approximation and Projection" method (UMAP; McInnes et al., 2018). The optimal UMAP hyperparameters ($n_neighbors$ and min_dist) were qualitatively determined to balance global and local structures and information loss. After the dimension reduction, hierarchical (agglomerative) clustering (Nielsen, 2016) was applied. The optimal number of clusters was determined empirically by calculating and comparing three cluster-quality metrics that reflect how well the clusters are defined and separated: Silhouette-Score (Rousseeuw, 1987), Calinski-Harabasz-Score (Caliński & Harabasz, 1974), and Davies-Bouldin-Score (Davies & Bouldin, 1979) for cases with $n_{clusters} = 2-49$. Ideally, the Silhouette and Calinski-Harabasz scores should be at a local maximum, and the Davies-Bouldin score should be at a local minimum for the same number of clusters. The quality of the clustering was further evaluated by interpreting/comparing i) 3D-scatter plots of the clusters and the assigned lithology, ii) hierarchical dendrograms, iii) depth plots of clusters and the litholog, and iv) by cross-checking with geological background knowledge such as the depth of bedrock contact.

4.3.3 Classification, Evaluation, and Depth Correlation

Each cluster was characterized using PCA, covariance matrices, wireline-log-data distributions, and interpretation of dendrogram similarities between individual clusters. Further, a dominant lithology was assigned to each cluster based on comparison with visually classified lithologies, establishing a direct link between the data-based clusters and the core-based litholog. This dominant lithology and the clusters were plotted against depth, compared, and correlated.

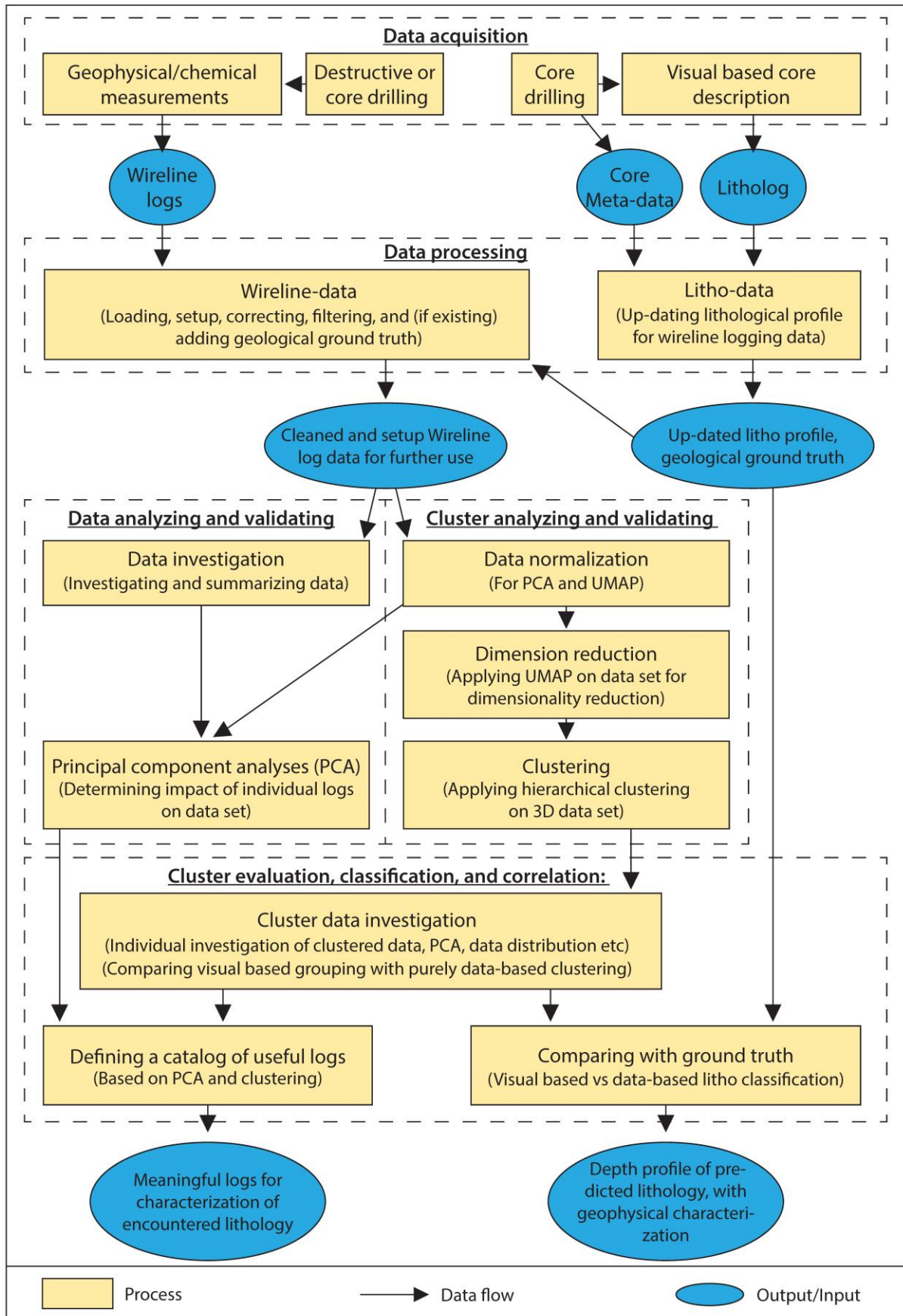


Figure 3: Schematic diagram of the applied data/workflow.

The simplest way to extend the workflow to additional wireline logging datasets without lithological ground truth (i.e., flush drilling) is to add placeholder data for lithology using the same preprocessing routine as for core drilling and then concatenate the selected datasets to be clustered (this technique was applied on 5068_1_A). The combined clustering allows for extrapolation of the dominant lithology from the core-controlled parts onto the uncontrolled parts of the combined wireline dataset and for cross-correlation between the individual cluster-based depth profiles. It is also advisable to compare and examine the wireline datasets individually before combining them, as there may be shifts in the calibration of the logging tools between different surveys. In such a case, where the data are from the same geological system and likely to represent identical lithological spectra, it is advisable to normalize the individual datasets before concatenation. This was done at the 5068_1 drill site (Figs. A1 and A2). UMAP was then run with a fixed random state (0 for the individual and 42 for the combined case) to maintain the exact reproducibility of the results.

4.4 Results

4.4.1 Data trends and impact of dimensionality reduction

The covariance data (Figs. 4A and B) and the PCA results (Figs. 4C and D; Tables 1 and 2; Tables A4 and A5) show strong similarities between the two wireline datasets (5068_1_A and C). First, both show a strong positive correlation between the deep and shallow resistivity (covariance ~ 1 , very narrow-angle between the corresponding loading vectors) and between the SGR, Th-, U-, and K-logs (covariance > 0.5 , loading vectors angles: $\sim 20-30^\circ$) and a negative correlation between the resistivity logs and the porosity-, SGR-, Th-, U-, and K-logs (covariance: < -0.25 , loading vector angles: $90-180^\circ$). Further, neither the loading plots nor the absolute values of the loading vectors show a strongly dominant log (Table 1). The two datasets differ mainly in the absolute value of the correlation, length, and direction of the loading vectors by preserving the primary trend. The range of variance ratio per principal component is narrow between the two datasets (e.g., var PC1: $\sim 45-47.5\%$; var PC2: $\sim 18-19.5\%$; Table 2). The projection of the first two principal components (PC1 and PC2, Figs. 4C and D) contains $\sim 63.5-67.5\%$ of the data variance, and the 3-dimensional projection contains $\sim 75-77\%$ (Table 2).

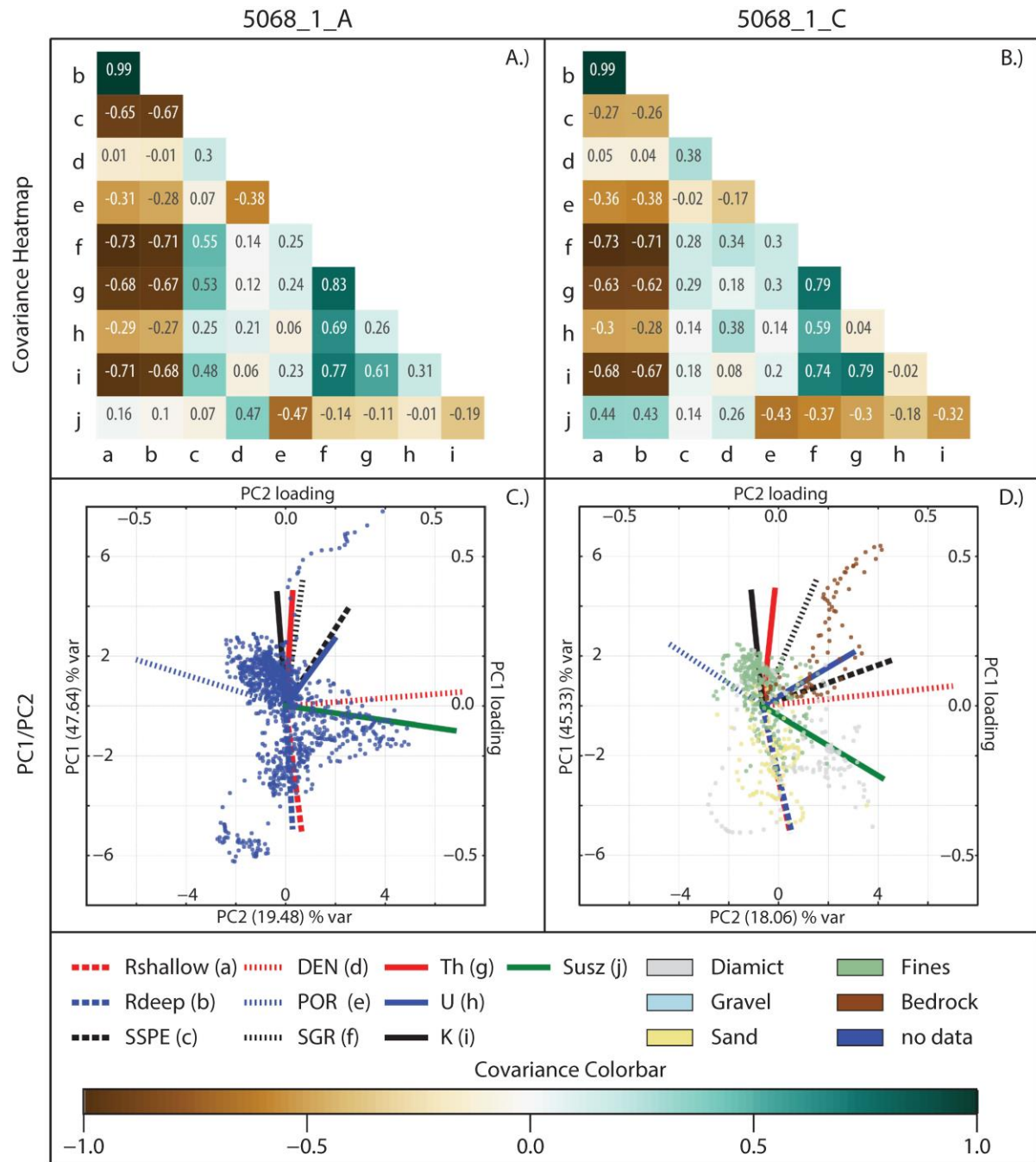


Figure 4: Compilation and comparison of the two cleaned wireline datasets (from 5068_1_A and 5068_1_C) used for clustering. A. and B.): Heatmaps showing the variance between each log combination (a-j); 1.0-0.5: Strong positive correlation; 0.50-0.25 medium to weak positive correlation; 0.25- -0.25: weak to no correlation; -0.25 - -0.5: medium to weak negative correlation; -0.5 - -1: medium to strong negative correlation. C. and D.): Biplot of the first two principal components (primary x and y axis). D shows the visually-assigned major lithology from 5068_1_C. The integrated loading plots (secondary x and y axes scaled between ~ 0.7 and -0.7) indicate the relationship between individual logs (angle) and their contribution to the principal components (length).

Table 1: Loading of the individual logs in the space spanned by PC1 and PC2 for each dataset.

Dataset	Rshallow [Ohmm]	Rdeep [Ohmm]	SSPE [b/e]	DEN [g/ccm]	POR [%]	SGR [gAPI]	Th [ppm]	U [ppm]	K [%wt]	Susz [1E-4SI]
5068_1_A	0.42	0.41	0.39	0.60	0.52	0.43	0.38	0.28	0.38	0.57
5068_1_C	0.44	0.43	0.46	0.64	0.38	0.47	0.39	0.35	0.38	0.47

Table 2: Explained variance in % of the principal component of each wireline dataset.

Dataset	PC01	PC02	PC03	PC04	PC05	PC06	PC07	PC08	PC09	PC10
5068_1_A	47.64	19.48	10.04	5.65	5.39	4.95	3.86	2.94	0.05	0.02
5068_1_C	45.33	18.06	12.21	7.67	6.97	4.98	2.87	1.85	0.06	0.00

The PCA biplots of PC1 and PC2 (Figs. 4C and D) and the two-dimensional UMAP projection (Figs. 5A-C) show a structured data distribution, both in general and within the assigned lithological data of 5068_1_C (Figs. 4D and 5B). The distribution of the cleaned lithological ground truth data of 5068_1_C shows a distribution dominated by fines (~50%) with a recognizable component of diamictic sediments (~19%) and bedrock (~11%; Table 3). A more detailed visualization of the three-dimensional UMAP and PCA projection of the two individual wireline datasets of 5068_1_A and C is shown in Supplementary Figures S1 and S2

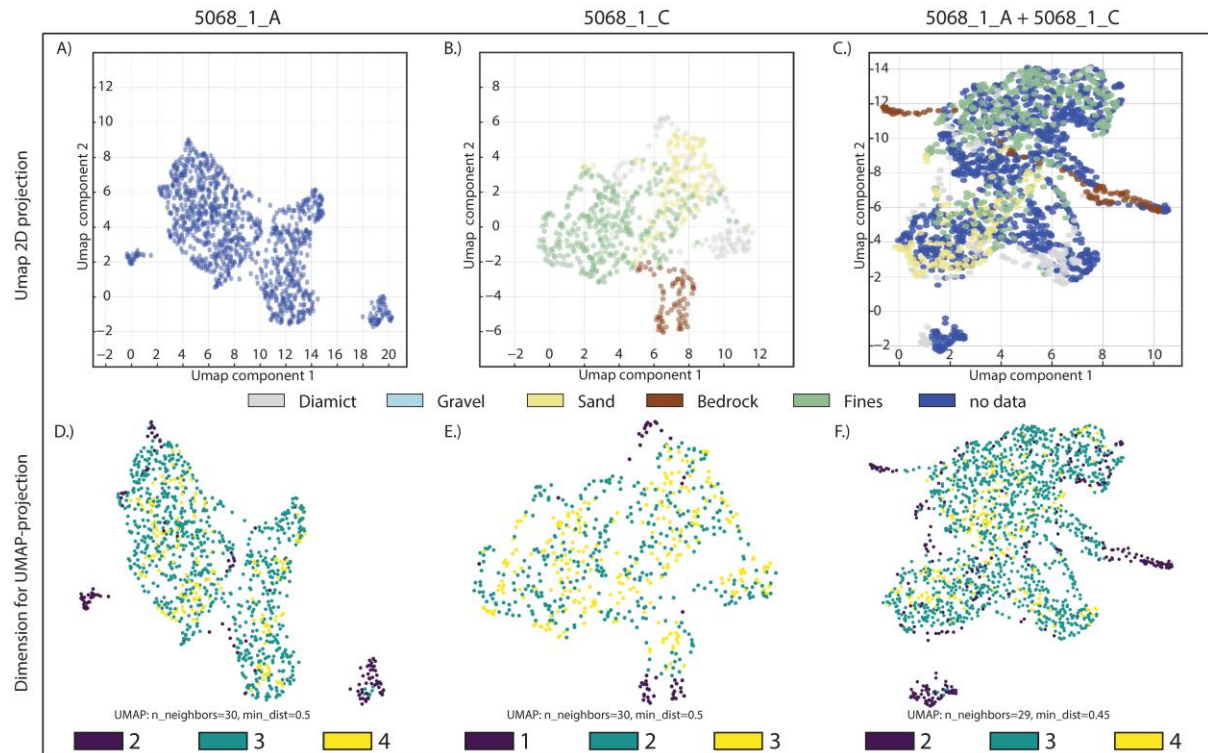


Figure 5: UMAP results of the two individual and the combined wireline datasets. A-C): UMAP-projection from 10 to 2 dimensions. (B-C) points are color-coded with the visually assigned major lithology. (D-F): The minimal number (color code is provided in the corresponding legend) of required dimensions (logs) to project each data point into a lower dimensional space while preserving as much individual variance between neighboring data points as possible. From left to right: 5068_1_A (A and D), 5068_1_C (B and E), and combined dataset of 5068_1_A and C (C and F).

Table 3: Distribution of geological ground-truth data (major and full lithologies) of the cleaned dataset of 5068_1_C

Major Lithologies			Full Lithologies		
Lithotypes	%	Data Points (n)	Lithotypes	%	Data Points (n)
Bedrock (B)	10.7	74	B	10.7	74
Diamict (D)	18.8	130	Dmm	7.4	51
			Dms	2.4	17
			Dcm	0	0
			Mgt	7.8	54
Gravel (G)	0	0	Mcc	1.1	8
			Gm	0	0
Sand (S)	20.3	141	Sm	14.6	101
			Sl	5.8	40
			Sli	0	0
Fines (F)	50.2	348	Fm	13.1	91
			Fl	37.1	257

Note: Data in %, with numbers of corresponding data points (n; total = 693), color coding represents the used colors in the figures, for more information about the lithotypes see Table A2.

4.4.2 Clustering Results

The optimal number of clusters for the three-dimensional UMAP projection of the combined wireline datasets of 5068_1_A and 5068_1_C was determined to be 6 (CC0-CC5; Fig. A3). The connection between individual clusters is illustrated in the dendrogram of the clustered combined dataset (5068_1_A and C), indicated by the vertical observation distance between connected clusters (Fig. 6). After re-separating, the distribution between the individual clusters of the two datasets (5068_1_A and 5068_1_C) shows some variance in relative size but preserves the general trend in cluster size of the combined one (Table 4). Further, the wireline-log-data distribution of the two re-separated datasets matches (Figs. A4 and A5), with slight variations in detailed distribution patterns visualized in the covariance and the PCA results (see Tables S1 and S2; Figs. S3 and S4). A lithological characterization and classification of the clusters can be made by comparing the composition and distribution of the assigned core-based lithological data, if available (Table 3), with the individual data-based clusters (Table 4). A detailed lithological composition of each cluster is shown in Figure 7 for the core-controlled case of 5068_1_C. Integrating the litho-classification of the clusters with the dendrogram structure and the individual wireline log data distributions, provides a more detailed characterization and understanding of the individual clustering and a direct link of log values with the sedimentological properties of stratigraphic units. The classification of value levels, such as high or low, is relative for each log and dataset due to the lack of cross-calibration between the datasets and lithological reference values.

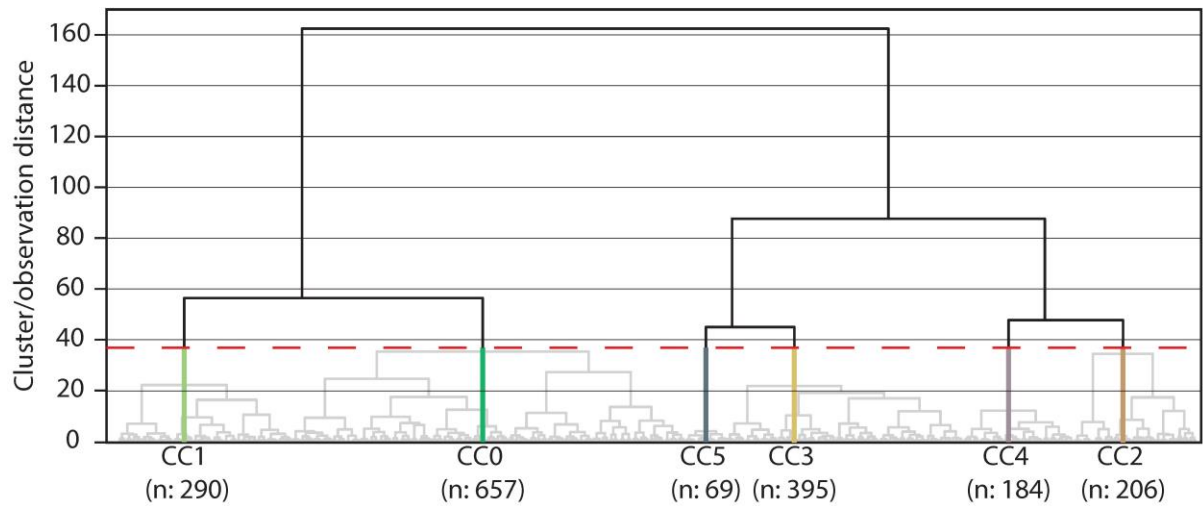


Figure 6: Hierarchical cluster dendrograms of the combined clustering of 5068_1_A and C with 6 clusters (CC0-CC5). The y-axis displays the cluster/observation distance, a measure of the similarity between two neighboring clusters; the red dashed line indicates the approximate minimal cluster distance for the suggested number of clusters; the path of the merged clusters below the threshold is indicated by semitransparent lines. The x-axis displays the individual clusters and includes the total counts of data points belonging to each cluster. The colors of the cluster branches indicate the hereafter used cluster colors.

Table 4: Data distribution of the individual clusters combined and after re-separation

Clusters	5068_1_A + C (n = 1801)		5068_1_A (n = 1108)		5068_1_C (n = 693)	
	%	Data points [n]	%	Data points [n]	%	Data points [n]
CC0	36.5	657	40.0	443	30.9	214
CC1	16.1	290	15.2	169	17.4	121
CC2	11.4	206	9.5	105	14.6	101
CC3	21.9	395	19.5	216	25.8	179
CC4	10.2	184	10.7	119	9.4	65
CC5	3.8	69	5.1	56	1.9	13

Note: Data distribution of the individual clusters of the combined data set (5068_1_A + C) and the two individual datasets (5068_1_A and 5068_1_C) after re-separation in % with the corresponding numbers of data points.

The dendrogram reveals two principal branches converging at an observation distance of over 160. The first main branch consists of clusters CC0 and CC1, which converge at an observation distance of ~60. Both clusters display low resistivity (R_{deep} and R_{shallow}), decreased density (DEN), and reduced S_{usz} , elevated SGR, Th, and K-values. The two clusters display slight differences in porosity, Th, and K values. CC0 shows a binomial distribution pattern in the resistivity logs. These clusters (CC0 and CC1), representing nearly 45-50% of the data, coincide with fine-dominated lithologies in the litholog of 5068_1_C.

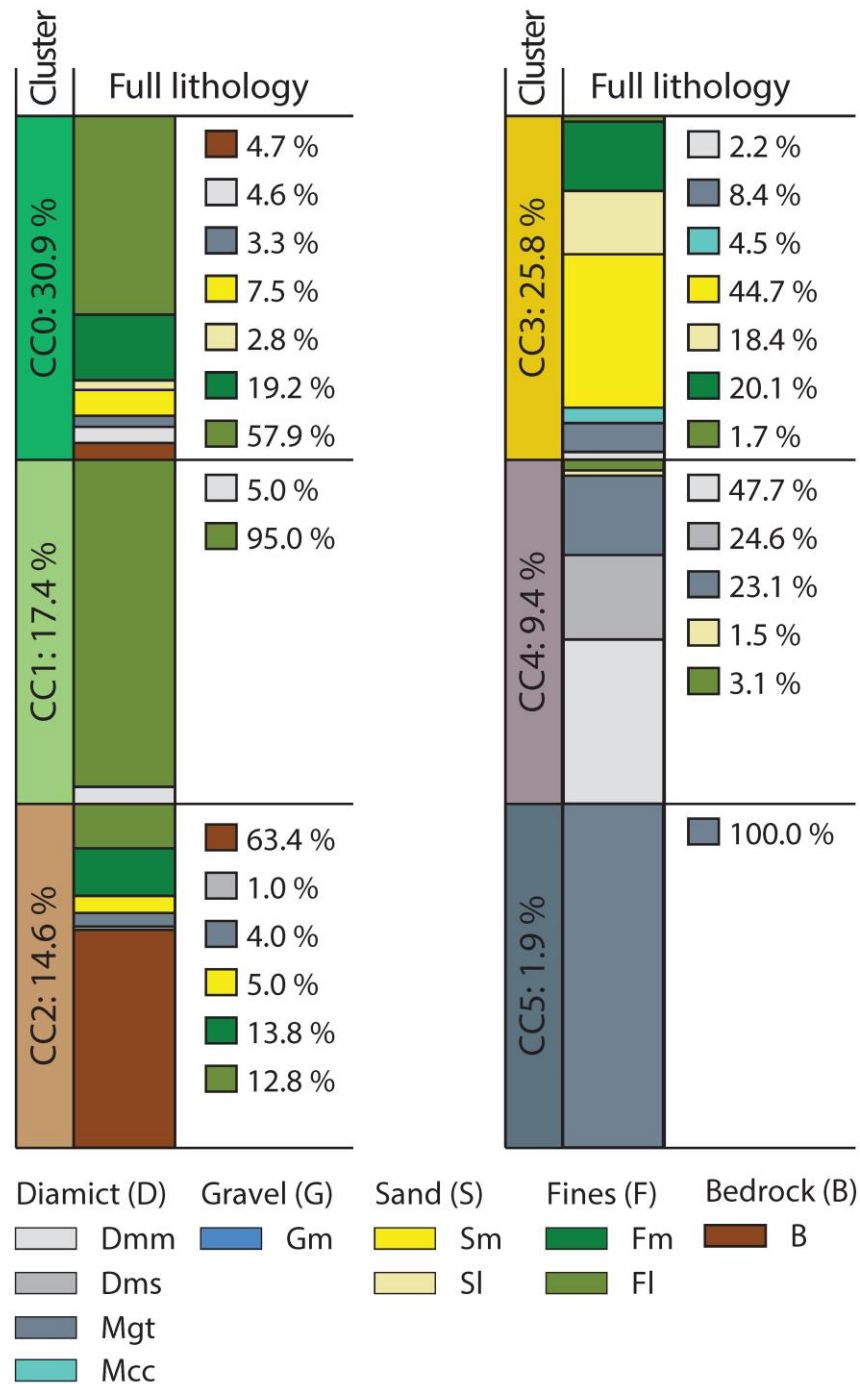


Figure 7: Lithological cluster composition of the re-separated data of 5068_1_C after combined clustering with 5068_1_A. The relative size of the clusters (CC0–CC5) of 5068_1_C and the internal contribution of the individual full lithologies to each cluster is given in %.

The second principal branch is formed in two steps: i) the merging of four individual clusters, CC2–CC5, into pairs, CC5/CC3 and CC4/CC2, at observation distances of 45 and 50, respectively, and ii) the further merging these two pairs into one at an observation distance of ~90. There are notable divergences between CC2/CC4 and CC3/CC5, particularly in the distributions of density and (partially) in the resistivity logs. The other logs show overlapping distributions or varying patterns between these four clusters. Cluster CC3 shows a more widely

distributed pattern than CC5, resulting in overlapping distributions with regard to density, porosity (POR), U-, and K-values. Further, CC3 shows elevated values for SGR, Th, Susz, and the short spectra photoelectric absorption (SSPE), as well as a reduction in resistivity compared to CC5. Cluster CC3 correlates with fine-rich sands, whereas CC5 consists entirely of lithotype Mgt (mostly sand; Fig. 2s and Table A2). Cluster CC2, dominantly consisting of Molasse bedrock, displays a broader distribution, particularly in the resistivity, density, SGR, Th-, U-, and K-logs, with some indications of several binomial distributions. This results in partial overlap with the distributions observed in CC4. Cluster CC4, linked to diamictic lithologies, also displays a broader distribution pattern, as evidenced by Susz, density, and resistivity logs, and exhibits elevated Susz and slightly diminished porosity, SGR, and Th-values relative to CC2.

4.4.3 Lithological ground truth versus cluster-based prediction

Applying the workflow to the drilled stratigraphic section of 5068_1_C results in an excellent match between the real core-based drilled stratigraphy and its wireline-log data-driven automated "cluster stratigraphy" (Fig. 8). The predicted cluster-based stratigraphy reveals major stratigraphic elements, including bedrock (CC2), (basal) diamict (CC4), sand-dominated (CC3), and the major fine-dominated sections (CC0 and CC1). In addition, more detailed structures in the m to sub-m scales are also visible inside the major stratigraphic elements, such as the intercalated sand and fine-dominated beds. In addition, some details are not present in the lithological profiles, i.e., suggesting a further split at the bedrock/basal diamictic contact (CC5) and some internal structures of the fine-dominated sections. The quality and reliability of the lithological profile are provided by comparing the core-quality profile, highlighting sections with disturbed or missing data, and interpolated sections of the profile.

4.4.4 Cross-hole correlation

The combined clustering allows a correlation between the core-based lithological profile of 5068_1_C and the cluster-based stratigraphy of 5068_1_A by using the predicted cluster-based profile of 5068_1_C as a translation key between geological ground truth and data-based prediction (Fig. 8). The correlation between the predicted profiles of 1C and 1A shows: i) decreasing thickness of the central sand-dominated section in 5068_1_A, located at ~73-116 m depth in 5068_1_C, ii) more or less horizontal correlation of the upper diamictic bed, situated at ~55-62 m depth in 5068_1_C, iii) increasing thickness of the basal diamictic bed in 5068_1_A, and iv) a more than three times increased thickness of the upper fine-rich section in 5068_1_A (~10 m vs. ~30 m).

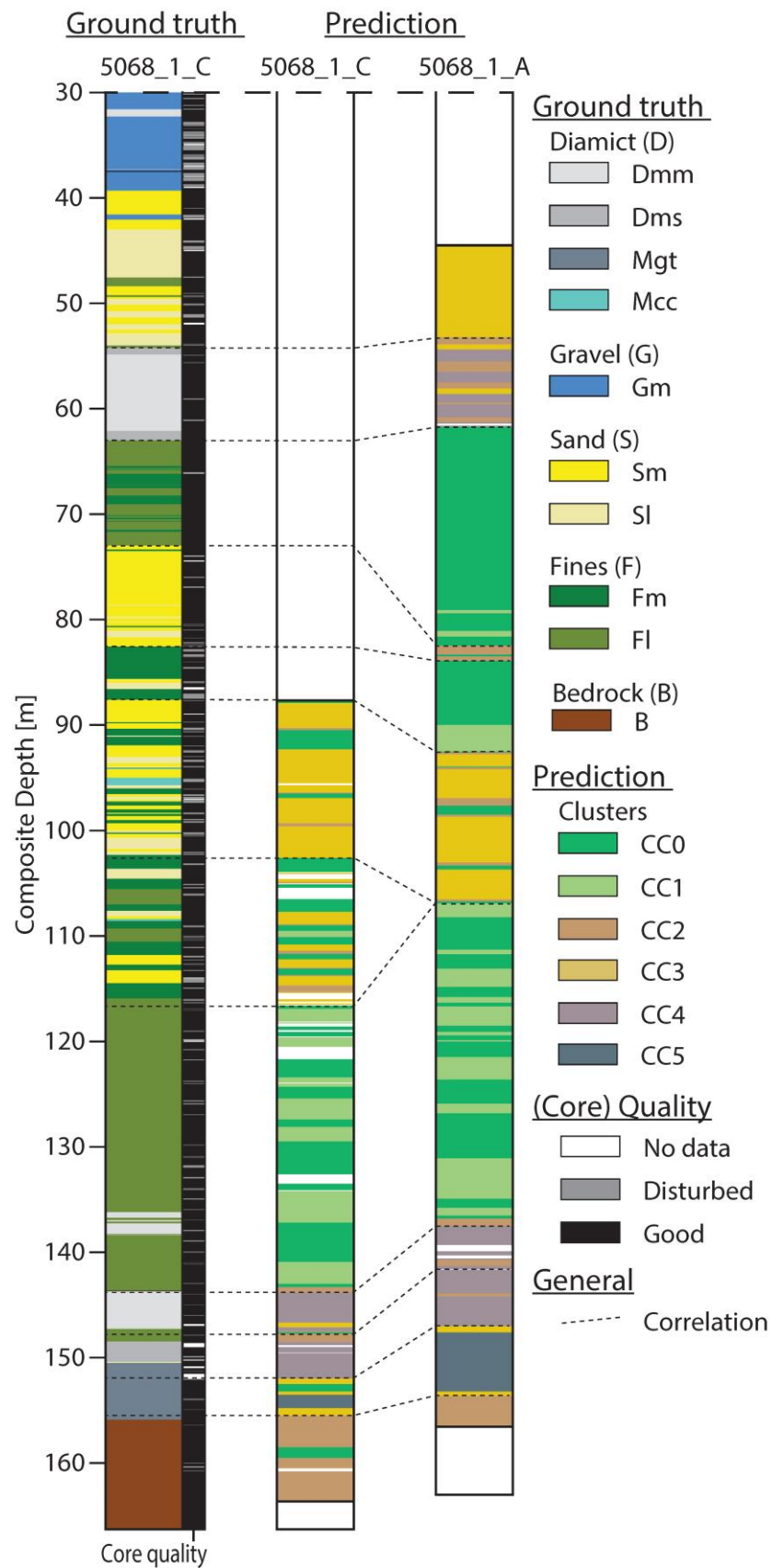


Figure 8: Wireline-logging-data-based prediction vs. lithological ground truth. Displays from left to right: i) full lithology-based ground truth and core quality of 5068_1_C, together with the data-based predicted profiles of ii) 5068_1_C and iii) 5068_1_A. The black dashed lines mark the proposed correlation between lithology and cluster profile; the required color codes for the different lithologies and clusters are provided by the accompanying legend.

4.5 Discussion

4.5.1 Importance of investigating the dataset structure

The importance of investigating and understanding the intrinsic data structures of the used datasets before confidentially combining them for dimensionality reduction and clustering is visualized by the rather surprising differences between the absolute values of the two individual wireline datasets (5068_1_A and 5068_1_C; Fig. A1). These absolute differences are surprising since the two drill holes are only ~30 m apart, and a similar sedimentological composition can be assumed for both. Which can be considered as a typical heterogenic sedimentary composition for a glacially overdeepened setting (Fig. 2 and Table 3; e.g., Buechi et al., 2018; 2024; Dehnert et al., 2012; Pomper et al., 2017). Both points, the individual internal heterogeneity and the common sedimentary composition of both boreholes, are supported by the matching patterns of the individual PCA and covariance analysis of the two separate datasets (Fig. 4). Therefore, it is very likely that the reasons for the absolute wireline log values are due to shifts in the calibration of the logging tool before each measurement campaign. Further, based on the points mentioned above, the two datasets were individually normalized before being combined for clustering. This solution is further justified by the high similarity between the normalized wireline log values (Fig. A2).

4.5.2 The case for dimensionality reduction

The combination of UMAP and hierarchical clustering provides a straightforward workflow for cluster analysis of time series data, relying on well-established and accepted methods in the data science community with a wide range of applications (UMAP: e.g., Becht et al., 2019; Cao et al., 2019; Hierarchical clustering: e.g., Belyadi & Haghighat, 2021). In the three wireline logging datasets examined, the two individual ones (A, C) and the combined one (A+C), UMAP introduces only a limited loss of information by reducing the 10-dimensional datasets to a 3-dimensional space (Figs. 5 D-F). This projection into a human-interpretable space allows an initial visual inspection and qualitative evaluation of the data distribution when combined with the corresponding lithological ground truth, visualized in two dimensions in Figures 5A-C. However, UMAP plots should be interpreted with caution. The distance between groups of data points and their shape and size may have no real meaning and highly depends on the selected hyperparameters, which should be chosen carefully (e.g., `n_neighbors` and `min_dist`; McInnes et al., 2018). Furthermore, these selected hyperparameters directly impact the suggested numbers of optimal clusters since the metrics use the UMAP projection as direct input. When comparing the explained/preserved variance of the UMAP reduction to that of

PCA, UMAP outperforms PCA. For the three datasets, PCA explains between 75% and 77% of the variance (Table 2).

In contrast, UMAP preserves 100% of the variance for 5068_1_C and leads to some information loss in ~15% of the data points in the case of 5068_1_A and 13% of the data points in the combined dataset (5068_1_A and C). In all three cases, UMAP would maintain the complete variance if a reduction to four dimensions were applied (Figs. 5D-F). However, reducing the data to four dimensions would hamper direct inspection of the visual data distribution. The superior performance of UMAP is likely due to its ability to detect nonlinear relationships in the datasets, unlike PCA, which is limited to linear combinations. Nevertheless, PCA and covariance analysis remain valuable tools for inspecting and understanding the data's internal structure since UMAP has no equivalent function to the PCA loading plots that would allow direct interpretations of the data.

4.5.3 Cluster characterization and classification

Since there is no straightforward way to tell which of the input features were used for the UMAP dimension reduction, the proposed way is to compare the dendrogram (Fig. 6) with the log-wise violin/probability-density distributions-plots of the individual clusters to assume which logs were likely used for the projection (Figs. A4 and A5). Some of these distributions indicate a more apparent separation of the data than others (Fig. 9). For example, the SGR separates three groups of clusters (Fig. 9A). In contrast, the U-log shows overlapping between all six clusters (Fig. 9B). However, as UMAP indicates (Figs. 5F), no individual log leads to a clear separation of all clusters.

Furthermore, combining the information of the dendrogram (Fig. 6) and the corresponding lithological composition (Fig. 7) helps to narrow down the dominant logs for cluster characterizing. This combination enables a direct link between the petrophysical and chemical measurements and actual geology. Even without having a reference catalogue for typical wireline log values and uncertainties in the calibration, the plausibility of the individual cluster values can be evaluated for the assigned lithology. Additionally, individual PCA and covariance data analyses for each cluster may help define dominant features and similarities between clusters. They may help to visualize differences in the internal data distribution between separated clusters originating from combined datasets (see Digital supplement). In cases of small cluster sizes ($n \leq 30$; e.g., Fischer, 2011), the results should be treated with caution since they are most likely not statistically relevant anymore.

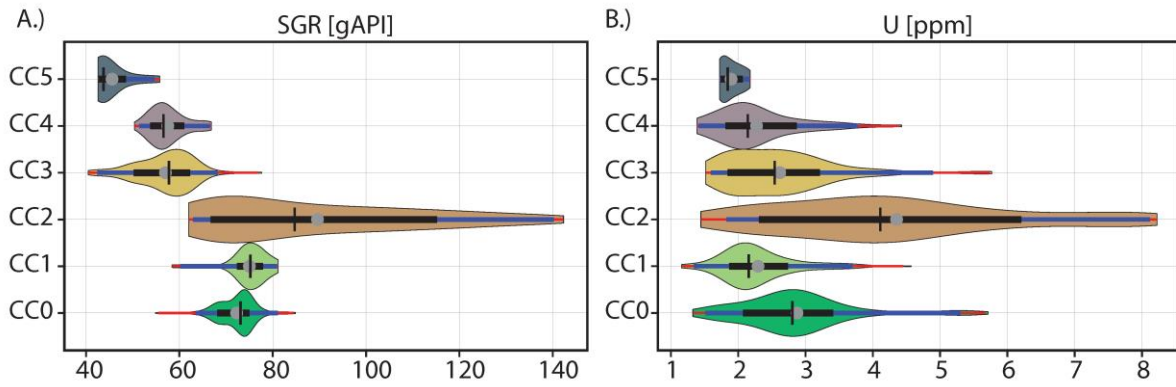


Figure 9: Violin plot example of cluster data distribution of 5068_1_C. A) Visualizing a relatively clear separation in the SGR and B) a rather unclear separation in the U-log. Clusters are labeled on the y-axis and color-coded according to Table 4. Each violin plot includes the position of the mean (grey dot), the median (centered vertical black line), and the 1-, 2-, and 3- σ -ranges are displayed on the horizontal (1 σ : black, 2 σ : black + red; 3 σ : black + red + blue).

The re-divided clusters of both datasets show substantial similarity, as indicated by the cluster data distribution, PCA, and covariance data. This similarity justifies the correlation of cluster-based profiles between the two boreholes. Consequently, the characterization and classification are primarily based on the 5068_1_C dataset to directly link the data-based clusters with the core-based geological ground truth. The assigned lithologies and the distributed logging data patterns support the proposed data-based linkage between the clusters. The two closely related clusters, CC0 and CC1, show reasonable log values for the assigned fine-dominated lithology, especially the high SGR log values. Their low resistivity and density suggest connected porosity, which aligns with the expected properties of these lithologies. Minor variations in sand or gravel content likely cause the small-scale log differences between the two clusters. While no clear multi-log trend explains the lower-level linkage between the remaining clusters, the assigned lithologies share some features supporting the clustering. CC3 and CC5, which are sand-dominated, have lower density and higher resistivity than CC2/CC4, indicating compaction and lower water content or permeability.

Further, the significant difference in the (SS)PE log of CC5 indicates a different lithological composition and likely a different origin. Although the lithological connection between the silt and sandstones of CC2 and the diamictic sediments of CC4 is surprising, it can be explained since both lithologies are mixtures of compacted or cemented sand and silt with some denser clasts or sections with lower porosity, yielding similar density logs. Additionally, the similar (SS)PE logs indicate a common sediment source, i.e., mostly reworked local bedrock, and the increased Susz-log of CC4 likely reflects the presence of crystalline clasts. Further, the moderate porosity with the wide range of the Gamma (SGR, U, Th, and K) logs matches the expected properties of a sand-siltstone mix with variable permeability, representing the local Molasses bedrock. UMAP likely projected CC0 and CC1 using a combination of resistivity,

SGR, and density logs. However, due to the lack of a consistent trend among CC2-CC5 and some induced data blur by the projection into the three-dimensional space, identifying the key logs for UMAP projection is more challenging.

4.5.4 Quality of cluster-based stratigraphy

Applying the clustering to the drilled stratigraphic section of 5068_1_C results in an excellent match with its wireline-log data-driven automated "cluster stratigraphy" (Fig. 8). The cluster-based stratigraphy reveals major stratigraphic packages: i) bedrock, ii) basal diamict, iii) a major fines-dominated section, iv) interlayered sand and fines-dominated layers, and v) a sand-dominated section. Furthermore, additional internal structures within these major packages are detected, such as: i) a fines-rich bed within the bedrock (e.g., claystone), ii) internal variations within the basal diamict bed, indicating a different lithology between the bedrock and the lower part of the basal diamictic bed description (not reworked bedrock, represented by cluster CC5), a feature undocumented in the visual core description, iii) internal variations within the major fines-dominated section, and iv) the detection of interlayered sand and fines at a dm-scale. Detecting the major stratigraphic packages and their internal structure underlines the high potential and quality of the developed workflow for establishing a wireline-logging data-based stratigraphy. Generally, the accuracy and quality of the predicted cluster-based stratigraphy strongly depend on i) the data quality of the wireline logs, ii) the quality of the lithological ground truth, and iii) the depth correlation between the core and the wireline logging. The core quality is essential for detecting small-scale features, determining the resolution of the prediction, and the accuracy of the lithological composition of the individual clusters.

4.5.5 Cross-hole correlation of cluster-based and core-based stratigraphies

The observed high-quality match between the core-based and complementary cluster-based stratigraphy of 5068_1_C justifies a cross-hole correlation between the two cluster-based stratigraphies of 5068_1_A and 5068_1_C. This successful correlation between the two cluster-based stratigraphies enables, by using the core-controlled case as a translation key between clusters and lithology (Fig. 7), the expansion of the detailed core-based lithologic interpretation of 5068_1_C to a borehole for which only wireline logs were available, resulting in a prediction of the detailed lithology in 5068_1_A. In addition, it is possible to directly correlate layers in the "cluster stratigraphy" of 5068_1_A with the core-based stratigraphy of 5068_1_C, even in areas with gaps in the "cluster stratigraphy" of 5068_1_C. For example, the upper diamictic bed or a significant sand bed below are both in the lithological profile of 5068_1_C. However, due to the installed steel casing, the corresponding wireline logging data

does not cover them. However, the diamictic bed appears clearly in the prediction of 5068_1_A, whereas the sand bed does not. The absence of this sand bed in the prediction of 5068_1_A is very likely real, as the lower sand bed is reproduced in both profiles. Detecting the relatively small-scale stratigraphic changes highlights the local system's highly complex "patchwork" stratigraphy and the potential of the presented workflow for detecting such small-scale changes in lithological features.

4.5.6 Log catalogue

The presented case study highlights the usefulness of the selected wireline logs, especially the SGR and partly its individual components, which proved to be of great value for detecting major trends in the encountered setting. However, redundancy exists between the deep and shallow resistivity logs. Therefore, the deep resistivity log appears to be the better of the two as it is less affected by borehole-wall conditions and infiltration of drill mud. If integration with seismic survey data is planned, such as in core-to-seismic correlations, including the sonic log would be recommended. The sonic log allows a robust connection between geological predictions, seismic data, synthetic seismograms, and vertical seismic profiles. Overall, log selection should be adjusted to the specific geological system and the primary focus of the study.

4.6 Conclusion

This study presents a linear and data-driven workflow for lithoprediction based on clustering and dimensionality reduction applied to a heterogeneous geological dataset. Its current format is specifically designed to analyse core and borehole data and aims at minimizing the subjectivity and operator bias of classical core descriptions. However, the proposed core workflow is flexible and can be adjusted to any time-series data as input. It can, for instance, easily be adapted to other types of core data, such as XRF or Multi-Sensor Core Logger (MSCL) data. Due to the data-driven nature of the workflow, the quality of the output is highly dependent on the quality of the input. The issue of missing absolute calibration in the used measured data values was addressed by specific assumptions, which justified using the data as a proof of concept for the developed workflow.

The presented case study demonstrates the potential of the workflow for a data-driven litho-reconstruction, which may help to quality check and improve classical lithological core descriptions. Further, the workflow enables correlation between different cores as well as cored and uncored wells by linking characteristic patterns in cluster-based predictions to geological

ground truth. This approach allows the construction of detailed generic lithologies even in areas where direct correlations between wireline logs and lithology are unavailable. The catalogue of selected wireline logs proved to be useful for the sediments encountered but should be individually adapted to the drilled geologic system.

Successful workflow applications require careful planning and coordination of drilling, coring, and logging campaigns and cross-hole calibration of wireline logs to absolute values based on common standards. This calibration enables the establishment of stratigraphic units' reliable petrophysical and chemical properties and improves lithological correlation across multiple wells. When integrated with seismic data, this correlated stratigraphy and associated properties could substantially enhance the development of sophisticated numerical and three-dimensional geological models. Future workflow development could include more advanced feature engineering and data processing tools to improve input data quality. The presented workflow could be significantly enhanced by i) combining with automated core description for the lithological classification and the establishment of the geological ground truth, ii) using advanced logging techniques such as "Logging While Drilling", and iii) establishing a catalogue of typical log values for the expected lithologies, enabling automated lithology-cluster correlation and characterization.

4.7 Appendix

4.7.1 Appendix Tables

Table A1: ID and composite depth of the core sections from Figure 2

Label	Core section id	Composite depth [m]	Label	Core section id	Composite depth [m]
a	5068_1_C_009_1	10-11	k	5068_1_C_125_1	101-102
b	5068_1_C_029_1	23-24	l	5068_1_C_130_1	106-107
c	5068_1_C_072_1	53-54	m	5068_1_C_132_1	108-109
d	5068_1_C_076_1	57-58	n	5068_1_C_142_1	118-119
e	5068_1_C_083_1	64-65	o	5068_1_C_150_1	126-127
f	5068_1_C_085_1	66-67	p	5068_1_C_168_1	144-145
g	5068_1_C_099_1	78-79	q	5068_1_C_170_1	146-146.8
h	5068_1_C_109_1	84.5-85	r	5068_1_C_176_1	152-153
i	5068_1_C_113_1	88-88.9	s	5068_1_C_177_1	153-154
j	5068_1_C_117_2	93-93.5	t	5068_1_C_187_1	163-164

Table A2: Brief overview of the systematic and hierarchical order of the used lithotypes.

Major lithologies	Full lithologies	DOVE-lithologies	description
B (Bedrock)	B	B	Bedrock (Upper freshwater Molasse)
D (Diamict)	Dmm	Dmm	Diamict, matrix-supported, massive
	Dms	Dms	Diamict, matrix-supported, stratified
	Dcm	Dcm	Diamict, clast-supported, massive
	Mgt	Mgt	Melange, shear zone with mixed Q/T units, dominantly sand
	Mcc	Mcc	Mud-clast conglomerate
G (Gravel)	Gm	Gm	Gravel, clast-supported, massive
		Gms	Gravel, clast-supported, massive, sandy
		Gmf	Gravel, clast-supported, massive, sandy with silt/clay
S (Sand)	Sm	Sm	Sand, massive
		SGm	Sand/Gravel-mix, massive
		Sh	Sand, horizontally bedded
	Sl	Sc	Sand, cross-bedded
		Sl	Sand, laminated
	Sli	Sli	Sand, laminated, with fines, irregular bedding
		Sd	Sand, synsedimentary deformed
F (Fines)	Fm	Fm	Silt/clay, massive
		Fm(d)	Silt/clay, massive, with dropstones
	Fl	Fl	Silt/clay, laminated
		Fl(d)	Silt/clay, laminated, with dropstones
		Flr	Silt/clay, laminated, rhythmites
		Flr(d)	Silt/clay, laminated, rhythmites, with dropstones

Note: Further information is provided by Schaller et al. (2023) and Schuster et al. (2024).

Table A3: Brief overview of the used wireline logs

Full name	Used abbreviation in data	Unit	Measured parameter	Application
Dual laterolog resistivity (Shallow)	Rshallow	Ohm m	electric resistivity of the shallow formation	Water saturation; formation correlation
Dual laterolog resistivity (Deep)	Rdeep	Ohm m	electric resistivity of deep formation	Water saturation; formation correlation
(Shortspectra) Photoelectric factor log	SSPE	b/e	photoelectric absorbtion	Lithological discrimination
Density log	DEN	g/ccm	gamma ray absorption	Bulk density, lithological discrimination
Neutron Porosity log	POR	%	neutron absorption by hydrogen atoms	Formation water content (if water-saturated, porosity can be determined)
(Combined spectral) gamma ray log	SGR	gAPI	total natural gamma radiation	Internal log calibration; lithology discrimination
Thorium-component of the SGR log	Th	ppm	amount of gamma radiation emitted from Th	Lithology discrimination; analysis of facies and depositional environment
Uranium-component of the SGR log	U	ppm	amount of gamma radiation emitted from U	Lithology discrimination; analysis of facies and depositional environment
Potassium-component of the SGR log	K	%wt	amount of gamma radiation emitted from K	Lithology discrimination; analysis of facies and depositional environment
Magnetic susceptibility log	Susz	1E-4SI	Natural magnetic susceptibility	Lithological discrimination; internal log integration; formation correlation
Caliper log	Cal (13/24; 1/2)	mm	multi-axis borehole diameter (2 or more)	Borehole geometry/caving

Note: Brief overview of the used wireline logs, measured parameters, and typical applications after Mondol (2015).

Table A4: PCA overview table of whole datasets

	PC	Rs [Ohm m]	Rd [Ohm m]	SSPE [b/e]	DEN [g/ccm]	POR [%]	SGR [gAPI]	Th [ppm]	U [ppm]	K [%wt]	Susz [1E-4SI]	EV.	EVR
5068_1_A	01	-0.420	-0.413	0.328	0.047	0.155	0.423	0.379	0.223	0.375	-0.082	4.768	0.476
	02	0.054	0.023	0.211	0.594	-0.501	0.057	0.023	0.164	-0.029	0.563	1.950	0.195
	03	0.247	0.288	-0.287	0.055	0.064	0.324	-0.061	0.789	-0.003	-0.188	1.005	0.100
	04	-0.023	-0.006	-0.332	-0.297	-0.758	0.120	0.115	-0.115	0.383	-0.199	0.565	0.056
	05	-0.276	-0.305	0.084	-0.550	-0.144	-0.074	-0.429	0.362	-0.208	0.369	0.539	0.054
	06	-0.049	-0.026	0.523	0.194	-0.271	-0.170	-0.402	0.110	-0.061	-0.637	0.496	0.050
	07	0.100	0.075	0.254	-0.258	-0.221	0.131	0.570	0.031	-0.670	-0.112	0.386	0.039
	08	0.392	0.407	0.557	-0.382	0.057	0.105	-0.026	-0.040	0.404	0.213	0.294	0.029
	09	-0.631	0.599	0.015	-0.019	-0.006	-0.400	0.208	0.174	0.089	0.030	0.005	0.000
	10	0.345	-0.349	0.013	-0.032	0.005	-0.690	0.354	0.333	0.212	-0.015	0.002	0.000
5068_1_C	01	-0.426	-0.422	0.154	0.067	0.211	0.430	0.387	0.178	0.380	-0.240	4.539	0.453
	02	0.092	0.097	0.434	0.637	-0.317	0.183	0.041	0.302	-0.038	0.399	1.809	0.181
	03	0.026	0.025	-0.220	0.100	0.292	0.124	-0.317	0.714	-0.373	-0.299	1.223	0.122
	04	0.205	0.212	-0.720	0.235	-0.344	0.253	0.222	0.042	0.308	-0.107	0.768	0.077
	05	0.352	0.330	0.060	0.315	0.725	0.029	0.298	-0.218	0.028	-0.030	0.698	0.070
	06	0.184	0.204	0.394	0.076	-0.318	-0.043	0.028	-0.095	-0.008	-0.807	0.499	0.050
	07	0.269	0.354	0.216	-0.646	-0.061	0.337	0.293	0.322	0.035	0.173	0.288	0.029
	08	-0.120	-0.128	-0.126	0.032	-0.140	-0.027	0.624	-0.086	-0.731	-0.022	0.185	0.019
	09	-0.723	0.688	-0.017	0.040	0.021	-0.044	-0.002	-0.010	0.000	0.000	0.006	0.001
	10	0.023	-0.018	-0.002	0.003	-0.002	-0.764	0.366	0.445	0.289	-0.002	0.000	0.000
Note: Each row represents a principal component vector (eigenvector; PC01-10) with the corresponding coordinates in the original data space, defined by the used logs. The last two colons contain the corresponding explained variance (eigenvalue; EV) and its ratio for each principal component vector (EVR).													

Table A5: Principal component analysis

	Space	Rshallow [Ohm m]	Rdeep [Ohm m]	SSPE [b/e]	DEN [g/ccm]	POR [%]	SGR [gAPI]	Th [ppm]	U [ppm]	K [%wt]	Susz [1E-4SI]
5068_1_A	PC1/PC2	0.423	0.414	0.390	0.595	0.525	0.427	0.379	0.277	0.376	0.569
	PC1/PC3	0.487	0.503	0.436	0.072	0.168	0.533	0.383	0.820	0.375	0.205
	PC2/PC3	0.253	0.289	0.356	0.596	0.505	0.329	0.065	0.806	0.029	0.594
5068_1_C	PC1/PC2	0.436	0.434	0.460	0.641	0.381	0.467	0.389	0.351	0.382	0.465
	PC1/PC3	0.427	0.423	0.269	0.120	0.361	0.447	0.500	0.735	0.533	0.384
	PC2/PC3	0.096	0.101	0.487	0.645	0.432	0.221	0.320	0.775	0.375	0.499
Note: Corresponding feature loading values (vector length in space given by the selected PC, see Appendix Table 4) of the biplot projections of the first three principal components.											

4.7.2 Appendix Figure

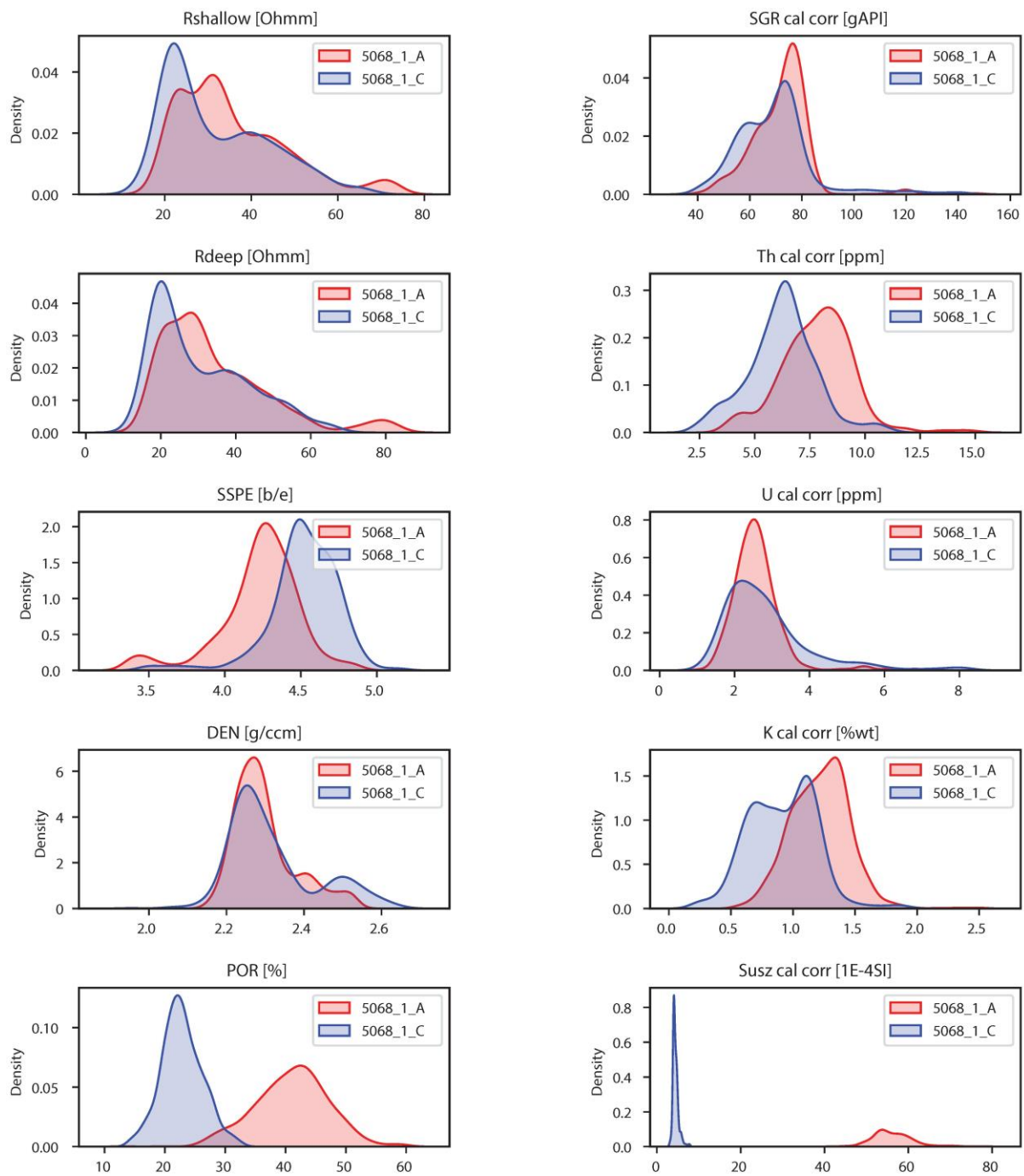


Figure A1: Comparison of the probability density distribution of the non-normalized wireline logging data of 5068_1_A and 5068_1_C.

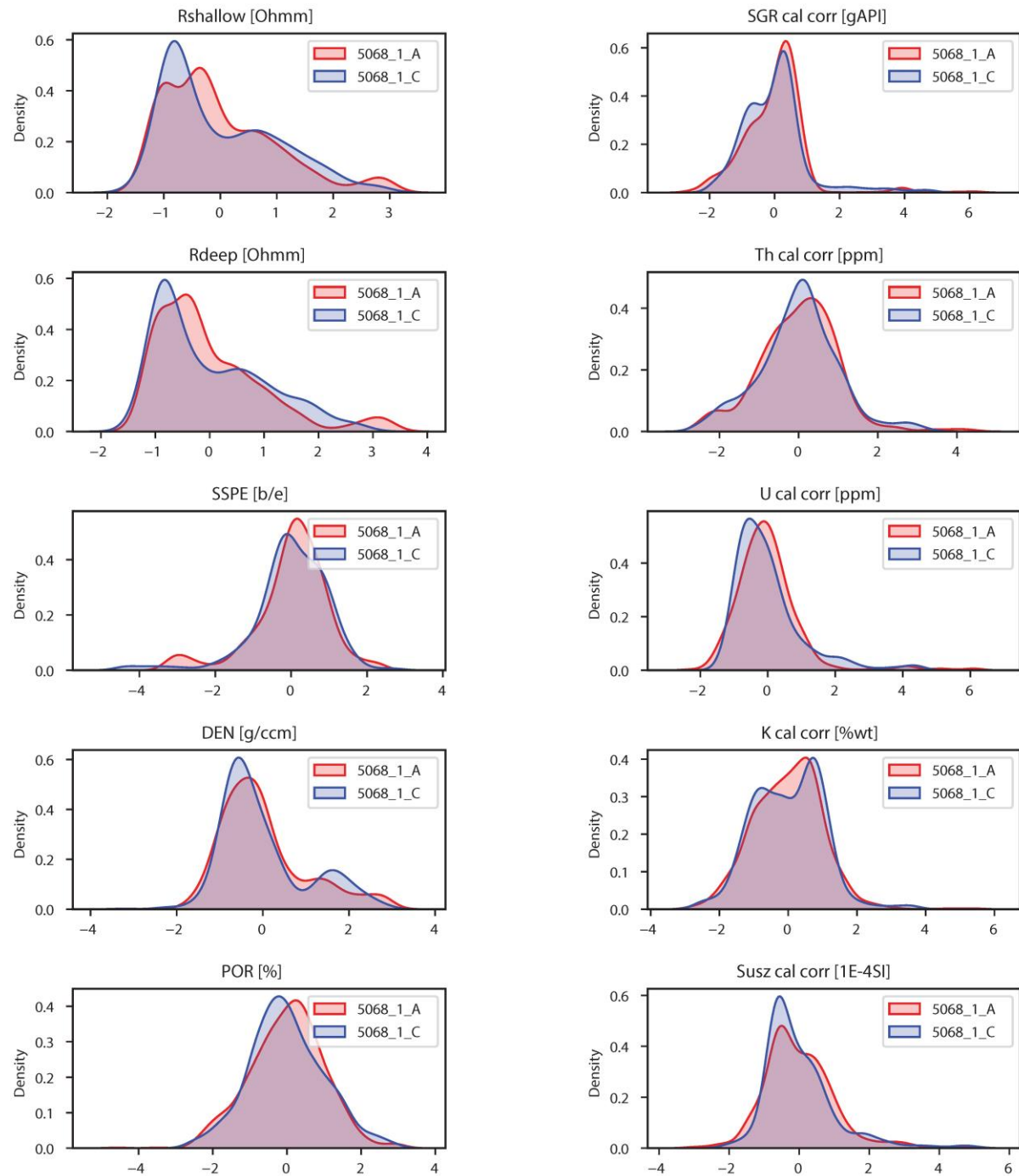


Figure A2: Comparison of the probability density distribution of the normalized (normal distribution around mean = 0 and std = 1) wireline logging data of 5068_1_A and 5068_1_C, used for combined clustering.

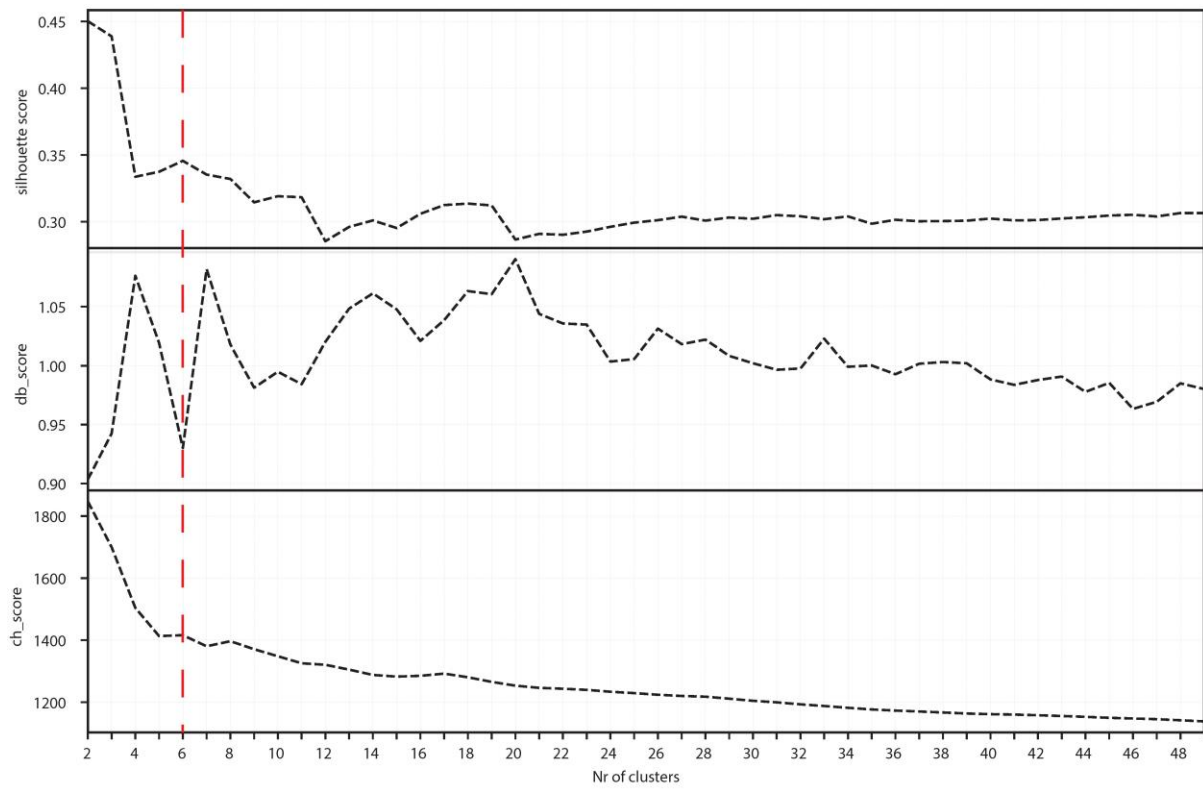


Figure A3: Cluster metrics for the combined dataset of 5068_1_A and C, displaying on the y-axis the calculated Silhouette-, Davies-Bouldin- (db), and Calinski-Harabasz (ch) Scores for (x-axis) a series of numbers of clusters ($n=2-49$). The red vertical line marks the selected numbers of clusters, leading to an acceptable solution.

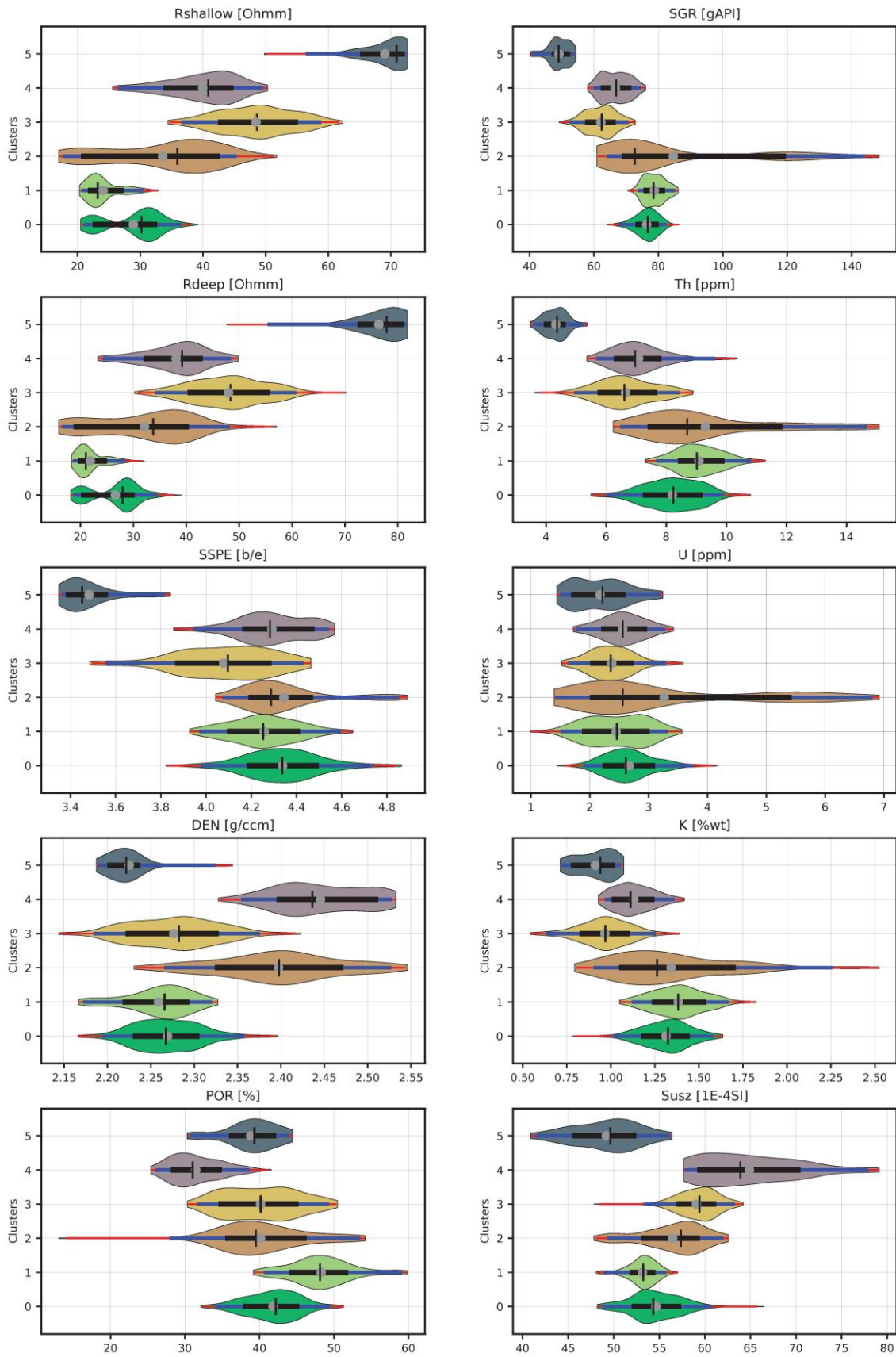


Figure A4: Violin plot of the individual log data distribution of the clusters of 5068_1_A, log with the corresponding unit is displayed as the title of each subplot, clusters are labeled on the y-axis form 0-5, and color-coded. Each violin plot includes the position of the mean (grey dot), the median (centered vertical black line), and the 1-, 2-, and 3- σ -ranges are displayed on the horizontal (1 σ : black, 2 σ : black + red; 3 σ : black + red + blue).

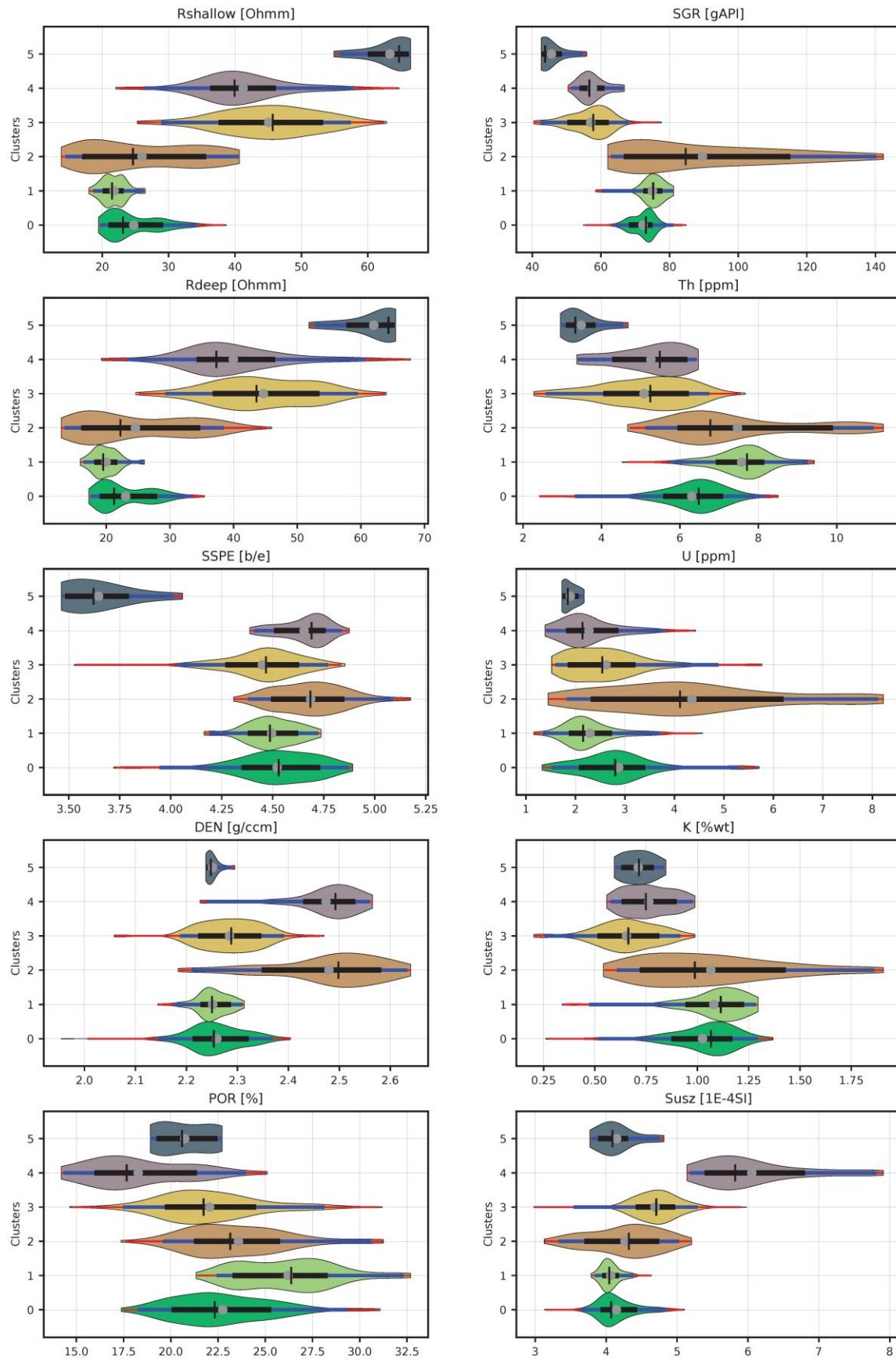


Figure A5: Violin plot of the individual log data distribution of the clusters of 5068_1_C, log with the corresponding unit is displayed as the title of each subplot, clusters are labeled on the y-axis form 0-5, and color-coded. Each violin plot includes the position of the mean (grey dot), the median (centered vertical black line), and the 1-, 2-, and 3- σ -ranges are displayed on the horizontal (1 σ : black, 2 σ : black + red; 3 σ : black + red + blue).

4.8 Further statements

4.8.1 Data availability

All data used and displayed in this study are publicly available according to the FAIR principle. The DOVE operational dataset (DOVE-Phase 1 Scientific Team et al, 2023b), containing all data concerning the drill core, is available on the ICDP DOVE project website: <https://www.icdp-online.org/projects/by-continent/europe/dove-switzerland> or can be accessed on the GFZ-library (<https://doi.org/10.5880/ICDP.5068.001>) together with the operational report (DOVE-Phase 1 Scientific Team et al., 2023a) and the explanatory remarks (DOVE-Phase 1 Scientific Team et al., 2023c). Other data and code are accessible under the following link: <https://github.com/schallersebastian/Lithoprediction-with-UMAP>.

4.8.2 Authors contribution

SS developed and implemented the presented workflow, processed and analyzed the data, and was the paper's main author with the support of all co-authors. DM and PB provided support during the development and implementation of the workflow. BS contributed to the initial analyses of the drill core and provided scientific input. MSA contributed to the (field) acquisition and initial pre-processing of the wireline logging data and provided, together with SB, scientific input regarding the wireline logging data. MWB and FSA provided significant scientific input to the paper as part of their role as PhD supervisors of SS. All authors approved the text and the figures.

4.9 Acknowledgments

We are grateful for the continued support by the International Scientific Continental Drilling Program (ICDP) and the DOVE science team. A special thanks goes to the technical staff of LIAG, who executed the downhole logging surveys and preprocessed the data. We want to thank the ICDP Operational Support Group, especially Simona Pierdominici and Jochem Kück, for providing support with the logging data corrections and handling, and the team of the Data Science Lab from the University of Bern for their technical and methodological support while developing the presented workflow. We acknowledge the strong support from the local inhabitants and the local authorities of the municipality of Ingoldingen in the district of Biberach during the drilling and logging campaigns. This research has been supported by the ICDP, the Deutsche Forschungsgemeinschaft (DFG, grant nos. KR2073/3-1, BU 2467/1-2, GA749/5-1, BU 2467/3-1, BU 3894/2-1, BU 3894/3-1, and PR 957/6-1), Nagra, ENSI, LGRB, LFU, LIAG, BOKU Vienna, and University of Bern.

4.10 References

- Anselmetti, F., & Eberli, G. (1999). The Velocity-Deviation Log: A Tool to Predict Pore Type and Permeability Trends in Carbonate Drill Holes from Sonic and Porosity or Density Logs. *Aapg Bulletin - AAPG BULL.*, 83, 450–466.
- Anselmetti, F. S., Bavec, M., Crouzet, C., Fiebig, M., Gabriel, G., Preusser, F., Ravazzi, C., & DOVE scientific team. (2022). Drilling Overdeepened Alpine Valleys (ICDP-DOVE): Quantifying the age, extent, and environmental impact of Alpine glaciations. *Scientific Drilling*, 31, 51–70. <https://doi.org/10.5194/sd-31-51-2022>
- Becht, E., McInnes, L., Healy, J., Dutertre, C.-A., Kwok, I. W. H., Ng, L. G., Ginhoux, F., & Newell, E. W. (2019). Dimensionality reduction for visualizing single-cell data using UMAP. *Nature Biotechnology*, 37(1), 38–44. <https://doi.org/10.1038/nbt.4314>
- Belyadi, H., & Haghighat, A. (2021). Chapter 4 - Unsupervised machine learning: Clustering algorithms. In H. Belyadi & A. Haghighat (Eds.), *Machine Learning Guide for Oil and Gas Using Python* (pp. 125–168). Gulf Professional Publishing. <https://doi.org/10.1016/B978-0-12-821929-4.00002-0>
- Beraus, S., Burschil, T., Buness, H., Köhn, D., Bohlen, T., & Gabriel, G. (2024). A comprehensive crosshole seismic experiment in glacial sediments at the ICDP DOVE site in the Tannwald Basin. *Scientific Drilling*, 33(2), 237–248. <https://doi.org/10.5194/sd-33-237-2024>
- Bergamo, P., Fäh, D., Panzera, F., Cauzzi, C., Glueer, F., Perron, V., & Wiemer, S. (2023). A site amplification model for Switzerland based on site-condition indicators and incorporating local response as measured at seismic stations. *Bulletin of Earthquake Engineering*, 21(13), 5831–5865. <https://doi.org/10.1007/s10518-023-01766-z>
- Buechi, M. W., Graf, H. R., Haldimann, P., Lowick, S. E., & Anselmetti, F. S. (2018). Multiple Quaternary erosion and infill cycles in overdeepened basins of the northern Alpine foreland. *Swiss Journal of Geosciences*, 111(1–2), 133–167. <https://doi.org/10.1007/s00015-017-0289-9>
- Caliński, T., & Harabasz, J. (1974). A dendrite method for cluster analysis. *Communications in Statistics*, 3(1), 1–27. <https://doi.org/10.1080/03610927408827101>
- Cao, J., Spielmann, M., Qiu, X., Huang, X., Ibrahim, D. M., Hill, A. J., Zhang, F., Mundlos, S., Christiansen, L., Steemers, F. J., Trapnell, C., & Shendure, J. (2019). The single-cell transcriptional landscape of mammalian organogenesis. *Nature*, 566(7745), 496–502. <https://doi.org/10.1038/s41586-019-0969-x>
- Carrasquilla, A. (2023). Lithofacies prediction from conventional well logs using geological information, wavelet transform, and decision tree approach in a carbonate reservoir in southeastern Brazil. *Journal of South American Earth Sciences*, 128, 104431. <https://doi.org/10.1016/j.jsames.2023.104431>
- Davies, D. L., & Bouldin, D. W. (1979). A Cluster Separation Measure. *IEEE Transactions on Pattern Analysis and Machine Intelligence*, PAMI-1(2), 224–227. *IEEE Transactions on Pattern Analysis and Machine Intelligence*. <https://doi.org/10.1109/TPAMI.1979.4766909>
- Dehnert, A., Lowick, S. E., Preusser, F., Anselmetti, F. S., Drescher-Schneider, R., Graf, H. R., Heller, F., Horstmeyer, H., Kemna, H. A., Nowaczyk, N. R., Züger, A., & Furrer, H. (2012). Evolution of an overdeepened trough in the northern Alpine Foreland at Niederweningen, Switzerland. *Quaternary Science Reviews*, 34, 127–145. <https://doi.org/10.1016/j.quascirev.2011.12.015>
- Di Martino, A., Carlini, G., Castellani, G., Remondini, D., & Amorosi, A. (2023). Sediment core analysis using artificial intelligence. *Scientific Reports*, 13(1), 20409. <https://doi.org/10.1038/s41598-023-47546-2>
- DOVE-Phase 1 Scientific Team, Anselmetti, F. S., Beraus, S., Buechi, M. W., Buness, H., Burschil, T., Fiebig, M., Firla, G., Gabriel, G., Gegg, L., Grelle, T., Heeschen, K., Kroe-mer, E., Lehne, C., Lüthgens, C., Neuhuber, S., Preusser, F., Schaller, S., Schmalfuss, C., Schuster, B., Tanner, D. C., Thomas, C., Tomonaga, Y., Wieland-Schuster, U., and Wonik, T. (2023a). Drilling Overdeepened Alpine Valleys (DOVE) – Operational Report of Phase 1, (ICDP Operational Report), GFZ German Research Centre for Geosciences, Potsdam, 70 pp., <https://doi.org/10.48440/ICDP.5068.001>
- DOVE-Phase 1 Scientific Team, Anselmetti, F. S., Beraus, S., Buechi, M. W., Buness, H., Burschil, T., Fiebig, M., Firla, G., Gabriel, G., Gegg, L., Grelle, T., Heeschen, K., Kroe-mer, E., Lehne, C., Lüthgens, C., Neuhuber, S., Preusser, F., Schaller, S., Schmalfuss, C., Schuster, B., Tanner, D. C., Thomas, C., Tomonaga, Y., Wieland-Schuster, U., and Wonik, T. (2023b). Drilling Overdeepened Alpine Valleys (DOVE) – Operational Dataset of DOVE Phase 1, GFZ Data Services [data set], <https://doi.org/10.5880/ICDP.5068.001>
- DOVE-Phase 1 Scientific Team, Anselmetti, F. S., Beraus, S., Buechi, M. W., Buness, H., Burschil, T., Fiebig, M., Firla, G., Gabriel, G., Gegg, L., Grelle, T., Heeschen, K., Kroe-mer, E., Lehne, C., Lüthgens, C., Neuhuber, S., Preusser, F., Schaller, S., Schmalfuss, C., Schuster, B., Tanner, D. C., Thomas, C., Tomonaga, Y., Wieland-Schuster, U., and Wonik, T. (2023c). Drilling Overdeepened Alpine Valleys (DOVE) – Explanatory remarks on the operational dataset, ICDP Operational Dataset – Explanatory Remarks, GFZ German Research Centre for Geosciences, Potsdam, 34 pp., <https://doi.org/10.48440/ICDP.5068.002>

- Ellwanger, D., Wielandt-Schuster, U., Franz, M., & Simon, T. (2011). The Quaternary of the southwest German Alpine Foreland (Bodensee-Oberschwaben, Baden-Württemberg, Southwest Germany). *E&G Quaternary Science Journal*, 60(2/3), 306–328. <https://doi.org/10.3285/eg.60.2-3.07>
- Fischer, H. (2011). *A History of the Central Limit Theorem: From Classical to Modern Probability Theory*. Springer. <https://doi.org/10.1007/978-0-387-87857-7>
- Ghosh, S. (2022). A review of basic well log interpretation techniques in highly deviated wells. *Journal of Petroleum Exploration and Production Technology*, 12(7), 1889–1906. <https://doi.org/10.1007/s13202-021-01437-2>
- Giardini, D., Guidati, G. (eds.), Amann, F., Driesner, T., Gischig, V., Guglielmetti, L., Hertrich, M., Holliger, K., Krause, R., Laloui, L., Lateltin, O., Lecampion, L., Löw, S., Maurer, H., Mazzotti, M., Meier, P., Moscariello, A., Saar, M.O., Spada, M., ... Zappone, A. (2021). *Swiss Potential for Geothermal Energy and CO2 Storage, Synthesis Report*. ETH Zurich.
- Guntli, P., Keller, F., Lucchini, R., & Rust, S. (2016). *Gotthard-Basistunnel: Geologie, Geotechnik, Hydrogeologie – zusammenfassender Schlussbericht* (Vol. 7). Schweizerische Eidgenossenschaft, Bundesamt für Landestopografie (swisstopo).
- Harris, C. R., Millman, K. J., van der Walt, S. J., Gommers, R., Virtanen, P., Cournapeau, D., Wieser, E., Taylor, J., Berg, S., Smith, N. J., Kern, R., Picus, M., Hoyer, S., van Kerkwijk, M. H., Brett, M., Haldane, A., del Río, J. F., Wiebe, M., Peterson, P., ... Oliphant, T. E. (2020). Array programming with NumPy. *Nature*, 585(7825), Article 7825. <https://doi.org/10.1038/s41586-020-2649-2>
- Hunter, J. D. (2007). Matplotlib: A 2D graphics environment. *Computing in Science & Engineering*, 9(3), 90–95. <https://doi.org/10.1109/MCSE.2007.55>
- Krammer, K., & Pohl, J. (1987). The susceptibility probe suslog 403-1. In *KTB Report 87-2: Grundlagenforschung und Bohrlochgeophysik; Beiträge zur Tagung der Deutschen Geophysikalischen Gesellschaft in Clausthal-Zellerfeld (31.3. - 4.4.1987)* (pp. 399–409). Projektleitung Kontinentales Tiefbohrprogramm der Bundesrepublik Deutschland im Niedersächsischen Landesamt für Bodenforschung. https://doi.org/10.48440/KTB.87-2_24
- Lai, J., Su, Y., Xiao, L., Zhao, F., Bai, T., Li, Y., Li, H., Huang, Y., Wang, G., & Qin, Z. (2024). Application of geophysical well logs in solving geologic issues: Past, present and future prospect. *Geoscience Frontiers*, 15(3), 101779. <https://doi.org/10.1016/j.gsf.2024.101779>
- Lauper, B., Zimmerli, G. N., Jaeggi, D., Deplazes, G., Wohlwend, S., Rempfer, J., & Foubert, A. (2021). Quantification of Lithological Heterogeneity Within Opalinus Clay: Toward a Uniform Subfacies Classification Scheme Using a Novel Automated Core Image Recognition Tool. *Frontiers in Earth Science*, 9. <https://doi.org/10.3389/feart.2021.645596>
- McInnes, L., Healy, J., Saul, N., & Großberger, L. (2018). UMAP: Uniform Manifold Approximation and Projection. *Journal of Open Source Software*, 3(29), 861. <https://doi.org/10.21105/joss.00861>
- Mondol, N. H. (2015). Well Logging: Principles, Applications and Uncertainties. In K. Bjørlykke (Ed.), *Petroleum Geoscience: From Sedimentary Environments to Rock Physics* (pp. 385–425). Springer Berlin Heidelberg. https://doi.org/10.1007/978-3-642-34132-8_16
- Nielsen, F. (2016). *Hierarchical Clustering* (pp. 195–211). https://doi.org/10.1007/978-3-319-21903-5_8
- Pedregosa, F., Varoquaux, G., Gramfort, A., Michel, V., Thirion, B., Grisel, O., Blondel, M., Prettenhofer, P., Weiss, R., Dubourg, V., & others. (2011). Scikit-learn: Machine learning in Python. *Journal of Machine Learning Research*, 12(Oct), 2825–2830.
- Plotly Technologies Inc. (2015). *Collaborative data science*. <https://plot.ly>
- Pomper, J., Salcher, B. C., Eichkitz, C., Prasicek, G., Lang, A., Lindner, M., & Götz, J. (2017). The glacially overdeepened trough of the Salzach Valley, Austria: Bedrock geometry and sedimentary fill of a major Alpine subglacial basin. *Geomorphology*, 295, 147–158. <https://doi.org/10.1016/j.geomorph.2017.07.009>
- Preusser, F., Graf, H. R., Keller, O., Krayss, E., & Schlüchter, C. (2011). Quaternary glaciation history of northern Switzerland. *E&G Quaternary Science Journal*, 60(2/3), 282–305. <https://doi.org/10.3285/eg.60.2-3.06>
- Rousseeuw, P. J. (1987). Silhouettes: A graphical aid to the interpretation and validation of cluster analysis. *Journal of Computational and Applied Mathematics*, 20, 53–65. [https://doi.org/10.1016/0377-0427\(87\)90125-7](https://doi.org/10.1016/0377-0427(87)90125-7)
- Schaller, S., Buechi, M. W., Schuster, B., & Anselmetti, F. S. (2023). Drilling into a deep buried valley (ICDP DOVE): A 252\,m long sediment succession from a glacial overdeepening in northwestern Switzerland. *Scientific Drilling*, 32, 27–42. <https://doi.org/10.5194/sd-32-27-2023>
- Schlumberger. (1972). *Log interpretation charts*. Schlumberger-Doll Research Center: Schlumberger Technology Coporation.
- Schuster, B., Gegg, L., Schaller, S., Buechi, M. W., Tanner, D. C., Wielandt-Schuster, U., Anselmetti, F. S., & Preusser, F. (2024). Shaped and filled by the Rhine Glacier: The overdeepened Tannwald Basin in southwestern Germany. *Scientific Drilling*, 33(2), 191–206. <https://doi.org/10.5194/sd-33-191-2024>
- Selley, R. C., & Sonnenberg, S. A. (2023). 3—Methods of Exploration. In R. C. Selley & S. A. Sonnenberg (Eds.), *Elements of Petroleum Geology (Fourth Edition)* (Fourth Edition, pp. 43–166). Academic Press. <https://doi.org/10.1016/B978-0-12-822316-1.00003-3>

- Serra, O., & Abbott, H. T. (1982). The Contribution of Logging Data to Sedimentology and Stratigraphy. *Society of Petroleum Engineers Journal*, 22(01), 117–131. <https://doi.org/10.2118/9270-PA>
- The pandas development team. (2024). *pandas-dev/pandas: Pandas (Version v2.2.2)* [Computer software]. Zenodo. <https://doi.org/10.5281/zenodo.10957263>
- Virtanen, P., Gommers, R., Oliphant, T. E., Haberland, M., Reddy, T., Cournapeau, D., Burovski, E., Peterson, P., Weckesser, W., Bright, J., van der Walt, S. J., Brett, M., Wilson, J., Millman, K. J., Mayorov, N., Nelson, A. R. J., Jones, E., Kern, R., Larson, E., ... SciPy 1.0 Contributors. (2020). SciPy 1.0: Fundamental Algorithms for Scientific Computing in Python. *Nature Methods*, 17, 261–272. <https://doi.org/10.1038/s41592-019-0686-2>
- Waskom, M. L. (2021). seaborn: Statistical data visualization. *Journal of Open Source Software*, 6(60), 3021. <https://doi.org/10.21105/joss.03021>

4.11 Digital Supplement

4.11.1 Tables Digital Supplement

	Rshallow [Ohm m]	Rdeep [Ohm m]	SSPE [b/e]	DEN [g/ccm]	POR [%]	SGR [g/API]	Th [ppm]	U [ppm]	K [%wt]	Susz [1E-4SI]	explained variance	explained variance ratio
CC0	PC01	0.552	0.550	-0.141	0.355	-0.348	0.014	-0.236	-0.184	0.135	2.851	0.284
	PC02	0.161	0.150	-0.508	-0.211	0.314	-0.070	0.295	0.118	0.576	1.666	0.166
	PC03	0.028	0.033	0.048	-0.140	-0.326	-0.705	0.527	-0.282	-0.116	1.603	0.160
	PC04	-0.009	-0.018	0.214	0.369	0.427	0.221	0.435	-0.401	0.233	1.131	0.113
	PC05	-0.042	-0.047	-0.169	-0.118	-0.079	0.349	0.015	-0.728	-0.230	0.999	0.100
	PC06	-0.191	-0.190	-0.638	-0.241	-0.170	0.076	-0.131	-0.162	0.016	0.733	0.073
	PC07	-0.125	-0.129	-0.479	0.697	-0.171	-0.143	0.140	0.173	-0.377	0.560	0.056
	PC08	-0.324	-0.358	0.093	0.339	-0.170	-0.095	-0.176	-0.120	0.621	0.471	0.047
	PC09	-0.713	0.700	-0.002	0.011	-0.007	0.017	0.015	0.004	0.019	0.004	0.000
	PC10	0.033	-0.007	0.001	-0.016	0.002	0.541	0.568	0.333	-0.020	0.004	0.000
CC1	PC01	0.512	0.514	-0.179	0.236	-0.039	0.156	-0.442	0.118	-0.062	2.857	0.284
	PC02	-0.182	-0.187	0.566	0.306	0.266	-0.271	-0.227	0.481	0.024	1.819	0.181
	PC03	0.198	0.177	-0.122	0.191	0.460	-0.545	0.393	-0.342	0.247	1.701	0.169
	PC04	-0.166	-0.182	-0.146	0.532	-0.275	0.220	-0.062	-0.107	0.704	1.320	0.131
	PC05	-0.273	-0.284	-0.082	0.005	-0.212	-0.081	-0.161	-0.502	-0.332	0.790	0.079
	PC06	0.101	0.108	-0.002	0.135	-0.735	-0.542	0.237	0.237	-0.111	0.654	0.065
	PC07	0.160	0.135	0.558	0.469	-0.073	0.269	0.219	-0.397	-0.310	0.468	0.046
	PC08	-0.180	-0.150	-0.540	0.540	0.222	-0.004	0.047	0.217	-0.468	0.434	0.043
	PC09	-0.060	0.080	-0.029	-0.040	-0.014	0.427	0.678	0.333	-0.018	0.013	0.001
	PC10	-0.701	0.705	0.023	0.010	0.002	-0.043	-0.062	-0.054	0.016	0.004	0.000
CC2	PC01	-0.366	-0.349	0.329	0.266	-0.014	0.376	0.359	0.374	-0.013	5.791	0.574
	PC02	0.045	-0.018	0.193	0.000	-0.686	0.041	-0.232	0.116	0.644	1.608	0.159
	PC03	-0.025	0.036	-0.387	-0.526	0.366	0.141	0.172	0.250	0.539	0.860	0.085
	PC04	0.523	0.597	-0.120	0.396	-0.043	0.258	0.180	0.213	0.008	0.777	0.077
	PC05	-0.146	-0.180	-0.294	0.668	0.375	-0.057	-0.322	0.084	0.342	0.525	0.052
	PC06	-0.147	-0.152	-0.693	0.083	-0.473	-0.289	0.230	0.232	-0.223	0.250	0.025
	PC07	-0.058	-0.077	-0.297	-0.134	-0.128	0.736	-0.503	-0.026	-0.270	0.167	0.017
	PC08	0.020	0.115	0.191	-0.157	0.096	-0.242	-0.381	0.802	-0.234	0.112	0.011
	PC09	-0.730	0.663	0.002	0.022	-0.047	0.040	0.040	-0.050	0.024	0.005	0.000
	PC10	-0.105	0.082	-0.007	0.019	0.012	-0.287	-0.446	-0.178	0.011	0.000	0.000

Table S1A: PCA overview table of individual clusters of dataset 5068_1_A, each row represents a principal component vector (eigenvector; PC01-10) with the corresponding coordinates in the original data space, defined by the used logs. The last two columns contain the corresponding explained variance (eigenvalue) and its ratio for each principal component vector.

		Rshallow [Ohm m]	Rdeep [Ohm m]	SSPE [b/e]	DEN [g/ccm]	POR [%]	SGR [g/API]	Th [ppm]	U [ppm]	K [%wt]	Susz [IE- 4SJ]	explained variance	explained variance ratio
CC3	PC01	0.523	0.487	-0.095	-0.262	0.135	-0.404	-0.118	-0.122	-0.427	0.137	2.542	0.253
	PC02	0.301	0.380	0.334	0.463	0.356	0.282	-0.032	0.365	0.098	-0.297	1.991	0.198
	PC03	-0.105	-0.116	-0.297	-0.092	0.101	-0.189	-0.757	0.491	0.121	-0.064	1.401	0.139
	PC04	0.134	0.115	-0.501	-0.401	0.164	0.530	0.309	0.329	0.085	0.195	1.268	0.126
	PC05	-0.005	-0.012	-0.452	-0.028	0.183	-0.114	0.129	-0.282	0.050	-0.805	0.958	0.095
	PC06	-0.206	-0.175	0.124	-0.103	0.875	-0.100	0.002	-0.238	0.099	0.241	0.801	0.080
	PC07	0.259	0.250	-0.079	-0.002	-0.117	-0.011	-0.183	-0.374	0.806	0.166	0.732	0.073
	PC08	-0.035	0.021	-0.560	0.729	0.053	-0.090	0.068	-0.069	-0.129	0.341	0.336	0.033
	PC09	-0.697	0.697	-0.010	-0.068	-0.033	-0.110	0.070	0.060	0.043	0.003	0.016	0.002
	PC10	0.100	-0.111	0.024	-0.006	0.010	-0.630	0.506	0.467	0.326	0.017	0.002	0.000
CC4	PC01	-0.482	-0.475	0.086	0.393	-0.116	-0.311	-0.336	-0.025	0.211	0.334	2.820	0.280
	PC02	-0.349	-0.368	-0.134	-0.199	0.464	0.520	0.171	0.403	0.084	0.036	2.022	0.201
	PC03	-0.121	-0.097	0.420	-0.164	-0.107	0.154	0.580	-0.524	0.191	0.301	1.471	0.146
	PC04	0.067	0.071	-0.541	-0.277	0.267	-0.147	-0.146	-0.380	0.599	0.063	1.234	0.122
	PC05	0.016	0.081	0.443	0.237	0.031	0.181	-0.125	0.061	0.598	-0.574	0.839	0.083
	PC06	-0.255	-0.239	-0.356	-0.228	-0.715	0.098	0.132	-0.003	0.045	-0.399	0.642	0.064
	PC07	-0.198	-0.211	-0.121	0.250	0.406	-0.268	0.252	-0.395	-0.327	-0.526	0.585	0.058
	PC08	0.161	0.119	-0.408	0.729	-0.106	0.330	0.318	-0.006	0.122	0.163	0.457	0.045
	PC09	-0.490	0.541	-0.037	-0.008	0.026	-0.409	0.383	0.354	0.157	0.021	0.012	0.001
	PC10	0.506	-0.457	0.015	-0.029	0.005	-0.444	0.395	0.365	0.215	-0.013	0.001	0.000
CC5	PC01	-0.425	-0.416	-0.294	0.312	0.370	-0.031	-0.345	0.254	-0.348	-0.144	3.141	0.309
	PC02	-0.355	-0.388	0.188	-0.070	-0.060	-0.403	0.239	-0.512	0.200	-0.396	2.538	0.249
	PC03	0.152	-0.010	0.088	0.124	-0.278	-0.609	-0.350	-0.220	-0.375	0.440	1.431	0.141
	PC04	-0.056	0.051	0.470	0.616	-0.327	0.158	0.318	0.162	-0.321	-0.175	1.218	0.120
	PC05	-0.244	-0.200	0.696	-0.114	0.312	0.144	-0.161	0.091	0.201	0.459	0.700	0.069
	PC06	0.284	0.294	0.031	0.524	0.627	-0.194	0.023	-0.270	0.225	-0.041	0.507	0.050
	PC07	-0.039	0.007	0.005	0.312	-0.400	0.086	-0.604	0.038	0.580	-0.175	0.410	0.040
	PC08	-0.187	-0.247	-0.401	0.341	-0.154	0.134	0.380	-0.140	0.268	0.592	0.230	0.023
	PC09	0.700	-0.697	0.059	0.033	0.019	0.069	0.026	0.087	0.040	-0.073	0.006	0.001
	PC10	0.026	-0.029	0.003	0.005	0.000	0.593	-0.253	-0.699	-0.307	-0.003	0.000	0.000

Table S1B: PCA overview table of individual clusters of dataset 5068_1_A, each row represents a principal component vector (eigenvector; PC01-10) with the corresponding coordinates in the original data space, defined by the used logs. The last two columns contain the corresponding explained variance (eigenvalue) and its ratio for each principal component vector.

	Rshallow [Ohm m]	Rdeep [Ohm m]	SSPE [b/e]	DEN [g/ccm]	POR [%]	SGR [g/API]	Th [ppm]	U [ppm]	K [%wt]	Suz [1E-4SI]	Expl. variance	Expl. variance ratio
CC0	PC01	-0.251	-0.243	-0.015	-0.321	0.169	-0.273	0.453	-0.448	0.203	3.154	0.314
	PC02	0.552	0.549	-0.127	0.093	0.353	-0.427	-0.070	-0.193	0.013	2.382	0.237
	PC03	0.135	0.118	-0.308	0.301	-0.202	0.359	0.485	-0.111	-0.541	1.254	0.125
	PC04	0.022	0.073	-0.807	-0.424	-0.002	0.170	-0.044	0.249	0.267	1.175	0.117
	PC05	0.172	0.174	0.056	0.231	-0.689	-0.008	0.125	-0.121	0.609	0.789	0.079
	PC06	0.072	0.169	0.124	-0.617	-0.533	-0.264	-0.125	-0.080	-0.440	0.630	0.063
	PC07	0.090	0.133	0.327	-0.137	0.056	0.082	0.082	0.682	0.057	0.361	0.036
	PC08	0.251	0.241	0.336	-0.401	0.206	0.574	0.289	-0.204	0.164	0.279	0.028
	PC09	-0.713	0.696	0.009	0.064	0.035	0.022	0.008	-0.027	0.012	0.022	0.002
	PC10	-0.001	-0.012	0.006	-0.012	-0.002	0.422	-0.657	-0.399	0.000	0.000	0.000
CC1	PC01	-0.063	-0.060	-0.133	-0.206	0.372	-0.341	0.412	-0.392	0.410	3.485	0.346
	PC02	0.648	0.640	0.208	0.204	0.114	-0.090	0.082	-0.226	-0.081	2.230	0.221
	PC03	0.052	0.102	0.254	-0.530	-0.206	-0.544	-0.453	0.145	-0.105	1.323	0.131
	PC04	-0.078	-0.057	0.699	-0.252	0.516	0.273	-0.015	0.135	0.196	0.976	0.097
	PC05	0.222	0.263	-0.547	-0.497	0.265	0.314	-0.025	0.401	0.071	0.851	0.084
	PC06	0.076	0.075	0.076	0.423	-0.118	-0.008	-0.159	0.495	0.637	0.495	0.049
	PC07	0.017	0.018	-0.204	-0.049	-0.014	-0.169	-0.416	-0.333	0.524	0.469	0.046
	PC08	0.065	0.097	0.195	-0.377	-0.675	0.308	0.386	-0.126	0.300	0.249	0.025
	PC09	-0.712	0.699	-0.007	0.047	0.007	0.013	-0.005	-0.028	-0.009	0.006	0.001
	PC10	-0.017	0.019	0.003	0.008	-0.012	-0.532	0.520	0.472	-0.002	0.000	0.000
CC2	PC01	-0.390	-0.383	0.146	0.324	0.164	0.422	0.296	0.362	0.045	5.000	0.495
	PC02	0.183	0.173	-0.222	0.318	0.393	0.113	0.393	-0.305	-0.606	1.910	0.189
	PC03	0.138	0.091	0.912	0.195	0.191	-0.093	-0.016	-0.005	-0.041	0.931	0.092
	PC04	0.246	0.287	-0.095	-0.271	0.731	0.102	-0.024	0.215	0.402	0.763	0.076
	PC05	0.357	0.433	0.164	-0.113	-0.470	0.351	0.404	-0.038	0.118	0.609	0.060
	PC06	-0.233	-0.206	0.023	-0.244	0.064	0.050	0.565	-0.437	0.412	0.537	0.053
	PC07	0.146	0.126	-0.193	0.779	-0.064	-0.099	-0.064	-0.127	0.529	0.262	0.026
	PC08	0.131	0.088	-0.154	0.037	-0.138	0.123	0.230	0.677	-0.053	0.074	0.007
	PC09	-0.717	0.692	0.014	0.038	0.006	-0.039	-0.017	0.023	-0.026	0.014	0.001
	PC10	0.014	-0.011	0.000	0.002	-0.003	-0.799	0.467	0.250	-0.001	0.000	0.000

Table S1C: PCA overview table of individual clusters of dataset 5068_1_C, each row represents a principal component vector (eigenvector; PC01-10) with the corresponding coordinates in the original data space, defined by the used logs. The last two columns contain the corresponding explained variance (eigenvalue) and its ratio for each principal component vector.

5068_1_C													
		Rshallow [Oh mm]	Rdeep [Ohm m]	SSPE [b/e]	DEN [g/ccm]	POR [%]	SGR [g-API]	Th [ppm]	U [ppm]	K [%wt]	Susz [1E-4SI]	Expl. variance	Expl. variance ratio
CC3	PC01	0.449	0.442	0.091	0.080	-0.044	-0.502	-0.379	0.040	-0.434	-0.017	3.432	0.341
	PC02	-0.339	-0.324	-0.139	0.085	-0.138	0.081	-0.439	0.647	-0.327	-0.098	2.217	0.220
	PC03	0.064	0.070	0.157	0.677	0.189	0.128	0.048	0.027	0.114	-0.663	1.494	0.149
	PC04	0.056	-0.015	-0.709	-0.275	0.528	-0.129	-0.109	-0.069	0.040	-0.323	1.118	0.111
	PC05	-0.087	-0.177	0.524	-0.081	0.780	-0.057	-0.078	0.079	-0.121	0.203	0.943	0.094
	PC06	-0.120	0.083	0.406	-0.632	-0.174	-0.041	-0.110	0.009	0.114	-0.598	0.460	0.046
	PC07	0.336	0.478	-0.024	-0.172	0.133	0.579	0.090	0.503	0.077	0.092	0.230	0.023
	PC08	0.044	0.038	0.033	0.095	-0.001	-0.092	-0.616	0.037	0.751	0.181	0.143	0.014
	PC09	-0.734	0.652	-0.059	0.088	0.090	-0.086	0.012	-0.040	-0.017	0.080	0.019	0.002
	PC10	0.021	-0.023	-0.006	0.005	-0.001	-0.593	0.493	0.558	0.304	-0.001	0.000	0.000
CC4	PC01	-0.119	-0.129	-0.379	0.091	0.181	-0.296	-0.480	0.450	-0.477	-0.192	3.268	0.322
	PC02	0.568	0.555	-0.172	-0.057	-0.170	-0.371	-0.162	-0.117	-0.089	0.351	2.867	0.282
	PC03	0.005	0.090	-0.188	-0.493	-0.609	0.302	-0.207	0.327	0.221	-0.230	1.629	0.160
	PC04	-0.157	-0.139	-0.094	-0.753	0.381	-0.011	0.048	-0.007	-0.087	0.475	0.822	0.081
	PC05	-0.087	-0.031	-0.553	0.395	-0.050	0.416	0.113	0.186	0.114	0.542	0.708	0.070
	PC06	0.099	0.225	0.600	0.097	0.231	0.289	-0.328	0.509	0.074	0.247	0.427	0.042
	PC07	0.038	0.027	-0.251	0.013	0.415	-0.106	-0.389	-0.130	0.744	-0.170	0.263	0.026
	PC08	0.281	0.393	-0.230	-0.109	0.441	0.394	0.358	0.103	-0.185	-0.423	0.170	0.017
	PC09	0.735	-0.664	0.007	-0.024	0.019	0.088	0.011	0.093	0.014	0.002	0.003	0.000
	PC10	-0.016	0.014	-0.001	0.000	-0.001	-0.503	0.546	0.589	0.318	0.000	0.000	0.000
CC5	PC01	-0.344	-0.367	-0.338	-0.148	0.332	0.370	0.381	-0.026	0.385	-0.265	7.023	0.648
	PC02	-0.285	-0.209	0.298	0.510	0.161	0.172	0.088	0.555	-0.087	0.384	3.065	0.283
	PC03	-0.031	-0.048	0.095	-0.449	-0.647	0.226	0.243	0.477	-0.117	-0.128	0.542	0.050
	PC04	-0.076	-0.049	0.002	0.338	0.036	-0.144	-0.190	0.236	-0.248	-0.838	0.184	0.017
	PC05	0.153	0.164	0.559	0.340	-0.213	0.246	0.392	-0.353	0.302	-0.215	0.017	0.002
	PC06	-0.496	-0.400	-0.098	0.196	-0.454	-0.208	0.064	-0.458	-0.270	0.099	0.001	0.000
	PC07	0.162	0.172	-0.130	0.000	0.263	0.046	0.618	-0.089	-0.683	0.016	0.001	0.000
	PC08	0.256	0.196	-0.669	0.497	-0.351	0.150	0.079	0.117	0.170	0.088	0.000	0.000
	PC09	0.658	-0.749	0.046	0.037	-0.004	-0.025	0.003	-0.009	-0.040	0.012	0.000	0.000
	PC10	-0.003	0.005	-0.002	-0.001	0.002	-0.796	0.455	0.228	0.329	0.000	0.000	0.000

Table S1D: PCA overview table of individual clusters of dataset 5068_1_C, each row represents a principal component vector (eigenvector; PC01-10) with the corresponding coordinates in the original data space, defined by the used logs. The last two columns contain the corresponding explained variance (eigenvalue) and its ratio for each principal component vector.

			Rshallow [Ohm m]	Rdeep [Ohm m]	SSPE [b/e]	DEN [g/ccm]	POR [%]	SGR [g/API]	Th [ppm]	U [ppm]	K [%wt]	Susz [1E-4SI]	Expl. variance
5068_1_A	CC0	5D	0.6	0.6	0.6	0.58	0.8	0.7	0.82	0.78	0.9	0.69	0.82
		4D	0.6	0.6	0.57	0.57	0.6	0.7	0.74	0.78	0.54	0.65	0.72
		3D	0.6	0.6	0.53	0.44	0.4	0.6	0.71	0.65	0.36	0.6	0.61
		2D	0.6	0.6	0.53	0.41	0.4	0.5	0.07	0.38	0.22	0.59	0.45
	CC1	5D	0.7	0.7	0.63	0.68	0.6	0.8	0.67	0.66	0.79	0.82	0.84
		4D	0.6	0.6	0.62	0.68	0.6	0.5	0.67	0.64	0.61	0.75	0.77
		3D	0.6	0.6	0.61	0.43	0.5	0.5	0.63	0.63	0.6	0.26	0.63
		2D	0.5	0.6	0.59	0.39	0.3	0.5	0.31	0.5	0.5	0.07	0.46
	CC2	5D	0.7	0.7	0.63	0.97	0.9	0.5	0.48	0.59	0.52	0.91	0.95
		4D	0.6	0.7	0.56	0.71	0.8	0.5	0.48	0.49	0.51	0.84	0.9
		3D	0.4	0.4	0.54	0.59	0.8	0.4	0.4	0.46	0.46	0.84	0.82
		2D	0.4	0.4	0.38	0.27	0.7	0.4	0.38	0.43	0.39	0.64	0.73
	CC3	5D	0.6	0.6	0.81	0.67	0.5	0.8	0.84	0.76	0.47	0.89	0.81
		4D	0.6	0.6	0.68	0.67	0.4	0.8	0.83	0.71	0.46	0.39	0.72
		3D	0.6	0.6	0.46	0.54	0.4	0.5	0.77	0.62	0.46	0.33	0.59
		2D	0.6	0.6	0.35	0.53	0.4	0.5	0.12	0.38	0.44	0.33	0.45
	CC4	5D	0.6	0.6	0.83	0.59	0.6	0.7	0.72	0.77	0.9	0.73	0.83
		4D	0.6	0.6	0.7	0.55	0.6	0.6	0.71	0.76	0.67	0.46	0.75
		3D	0.6	0.6	0.45	0.47	0.5	0.6	0.69	0.66	0.3	0.45	0.63
		2D	0.6	0.6	0.16	0.44	0.5	0.6	0.38	0.4	0.23	0.34	0.48
	CC5	5D	0.6	0.6	0.91	0.71	0.7	0.8	0.65	0.64	0.67	0.78	0.89
		4D	0.6	0.6	0.59	0.71	0.6	0.8	0.63	0.63	0.64	0.63	0.82
		3D	0.6	0.6	0.36	0.34	0.5	0.7	0.55	0.61	0.55	0.61	0.7
		2D	0.6	0.6	0.35	0.32	0.4	0.4	0.42	0.57	0.4	0.42	0.56
5068_1_C	CC0	5D	0.6	0.6	0.87	0.66	0.8	0.6	0.57	0.68	0.57	0.88	0.87
		4D	0.6	0.6	0.87	0.62	0.4	0.6	0.56	0.67	0.56	0.64	0.79
		3D	0.6	0.6	0.33	0.45	0.4	0.6	0.56	0.67	0.5	0.58	0.68
		2D	0.6	0.6	0.13	0.33	0.4	0.5	0.49	0.46	0.49	0.2	0.55
	CC1	5D	0.7	0.7	0.96	0.82	0.7	0.8	0.54	0.62	0.64	0.48	0.88
		4D	0.7	0.7	0.78	0.65	0.7	0.7	0.54	0.62	0.49	0.47	0.79
		3D	0.7	0.7	0.35	0.6	0.4	0.7	0.5	0.62	0.47	0.43	0.7
		2D	0.7	0.6	0.25	0.29	0.4	0.4	0.43	0.42	0.45	0.42	0.57
	CC2	5D	0.6	0.7	0.97	0.58	1	0.6	0.59	0.64	0.52	0.74	0.91
		4D	0.5	0.5	0.95	0.56	0.9	0.5	0.48	0.49	0.52	0.73	0.85
		3D	0.5	0.4	0.95	0.49	0.5	0.5	0.46	0.49	0.47	0.61	0.78
		2D	0.4	0.4	0.27	0.45	0.4	0.4	0.39	0.49	0.47	0.61	0.68
	CC3	5D	0.6	0.6	0.91	0.74	1	0.5	0.6	0.66	0.57	0.77	0.92
		4D	0.6	0.6	0.75	0.74	0.6	0.5	0.59	0.65	0.56	0.74	0.82
		3D	0.6	0.6	0.23	0.69	0.2	0.5	0.58	0.65	0.55	0.67	0.71
		2D	0.6	0.6	0.17	0.12	0.2	0.5	0.58	0.65	0.54	0.1	0.56
	CC4	5D	0.6	0.6	0.72	0.99	0.8	0.7	0.56	0.6	0.55	0.86	0.92
		4D	0.6	0.6	0.47	0.91	0.8	0.6	0.55	0.57	0.54	0.66	0.85
		3D	0.6	0.6	0.46	0.5	0.7	0.6	0.55	0.57	0.53	0.46	0.76
		2D	0.6	0.6	0.42	0.11	0.3	0.5	0.51	0.46	0.49	0.4	0.6
	CC5	5D	0.5	0.5	0.72	0.84	0.8	0.6	0.63	0.85	0.57	0.99	1
		4D	0.5	0.4	0.46	0.77	0.8	0.5	0.5	0.77	0.48	0.97	1
		3D	0.5	0.4	0.46	0.7	0.7	0.5	0.46	0.73	0.41	0.48	0.98
		2D	0.5	0.4	0.45	0.53	0.4	0.4	0.39	0.56	0.39	0.47	0.93

Table S2: Summary table of PCA loading values for 2-5d with the combined total explained variance ratio of the corresponding dimensional space of the individual clusters of the datasets for 5068_1_A and 5068_1_C.

4.11.2 Figures Digital Supplement

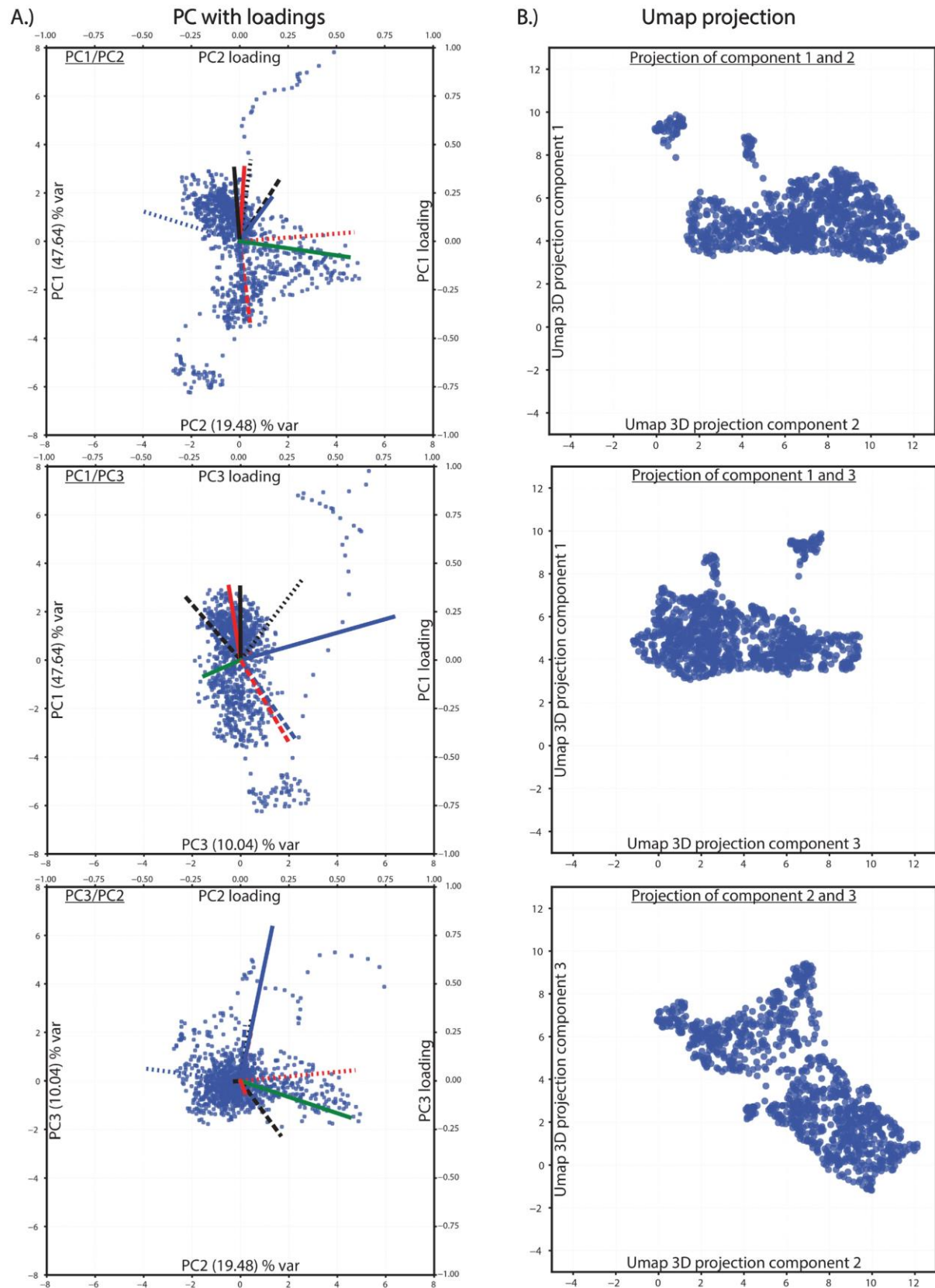


Figure S1: Biplot projections of the dimension reduction to 3d by PCA (A) and Umap (B) of 5068_1_A. The corresponding loading plots (secondary x and y-axis between 1 and -1), indicating the impact of each log, accompany the PCA biplots. Color codes for scatter data (assigned major lithology) of biplots and loading plots are included in Figure 1. The data for the loading plots are provided in Appendix Tables 4 (vector coordinates = direction starting from 0/0) and 5 (vector value = length).

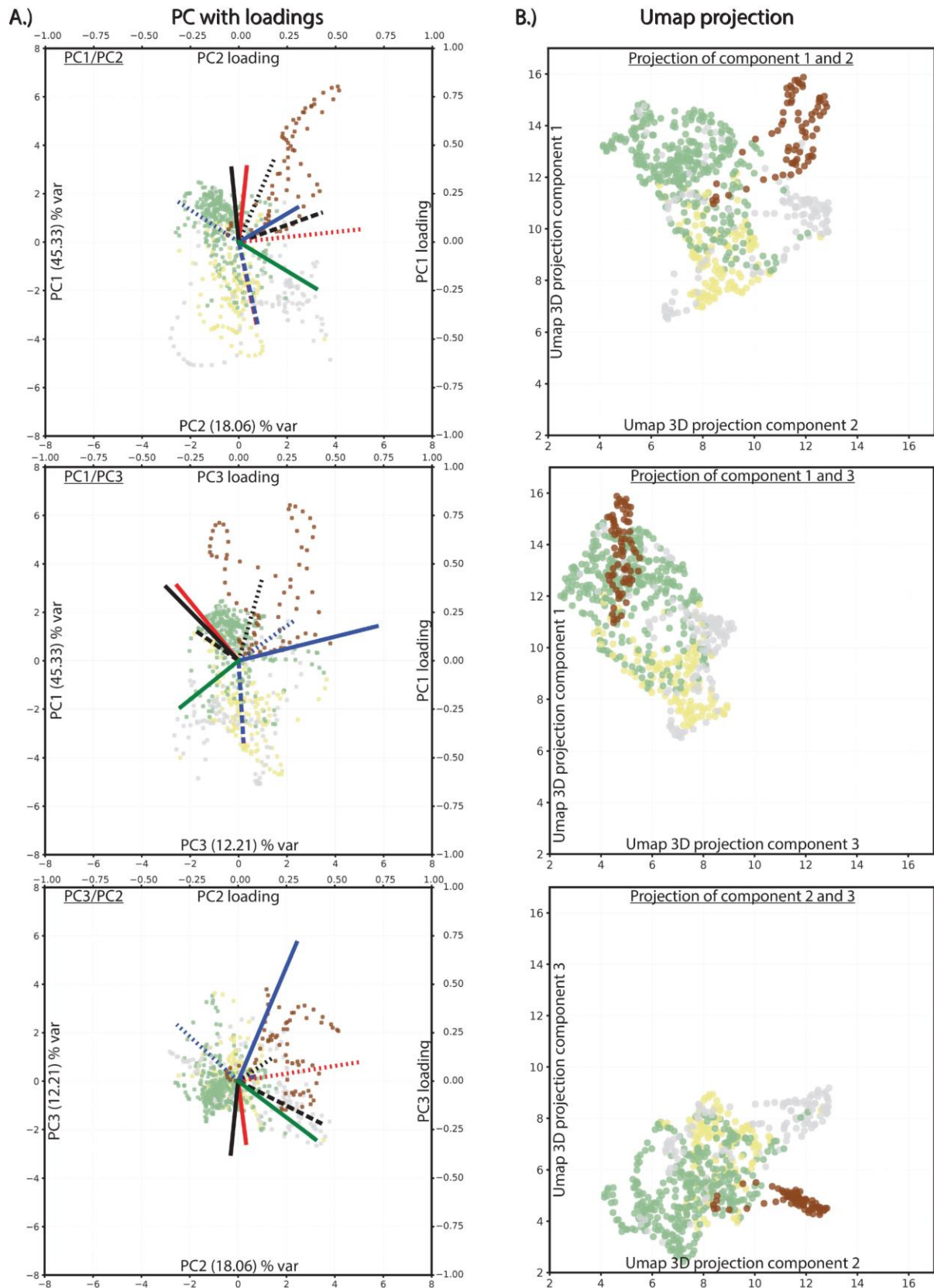


Figure S2: Biplot projections of the dimension reduction to 3d by PCA (A) and Umap (B) of 5068_1_C. The corresponding loading plots (secondary x and y-axis between 1 and -1), indicating the impact of each log, accompany the PCA biplots. Color codes for scatter data (assigned major lithology) of biplots and loading plots are included in Figure 1. The data for the loading plots are provided in Appendix Tables 4 (vector coordinates = direction starting from 0/0) and 5 (vector value = length).

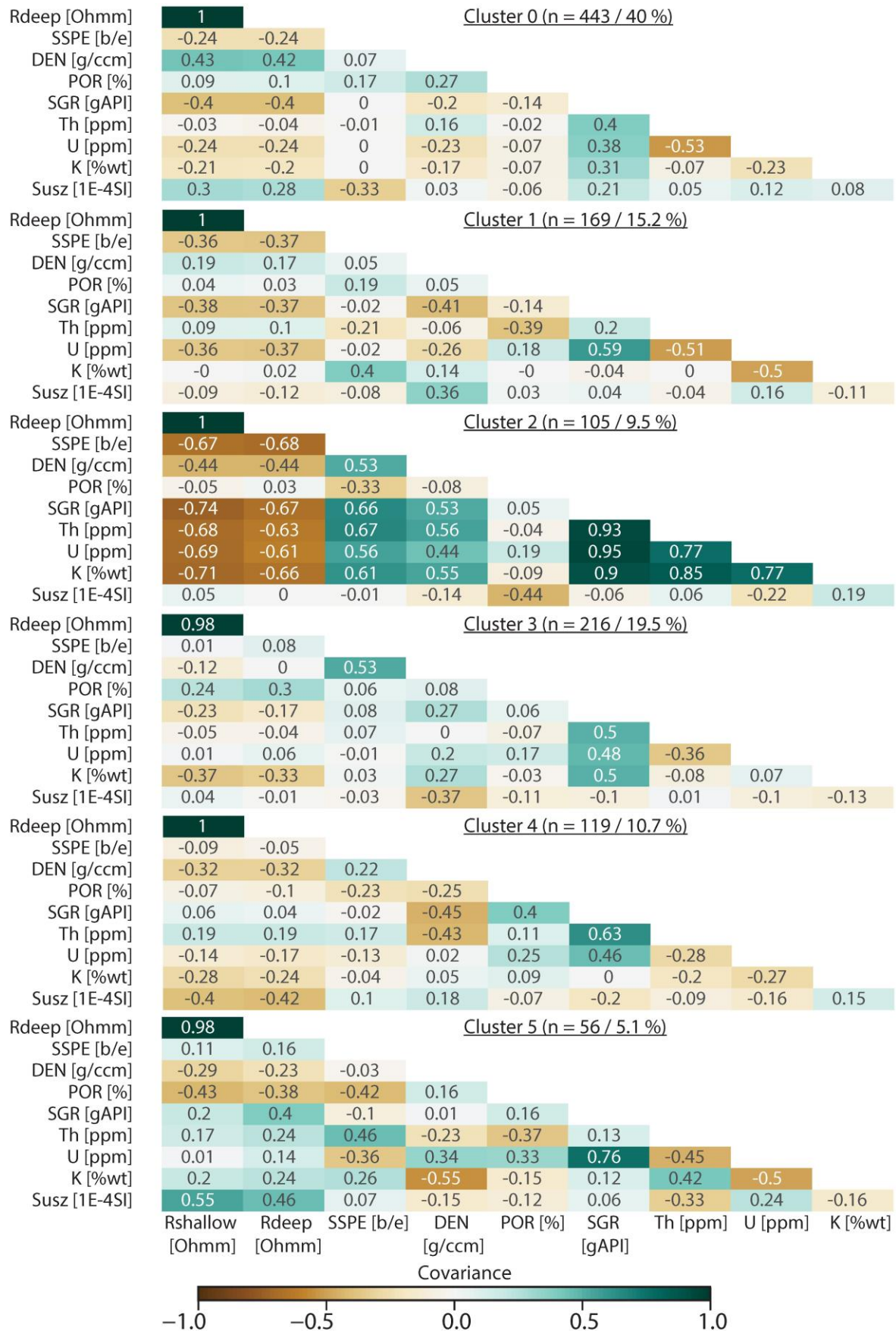


Figure S3: Triangular covariance matrix without self-correlation heatmap of the clusters (CC0-CC5) of 5068_1_A from the combined clustering of 5068_1_A and C, indicating the variance between each log (1-05 Strong positive correlation; 0.5-0.25 medium to weak positive correlation; 0.25- -0.25 -> weak to no positive or negative correlation; -0.25 - -0.5 medium to weak negative correlation; -0.5 - -1 -> medium to strong negative correlation).

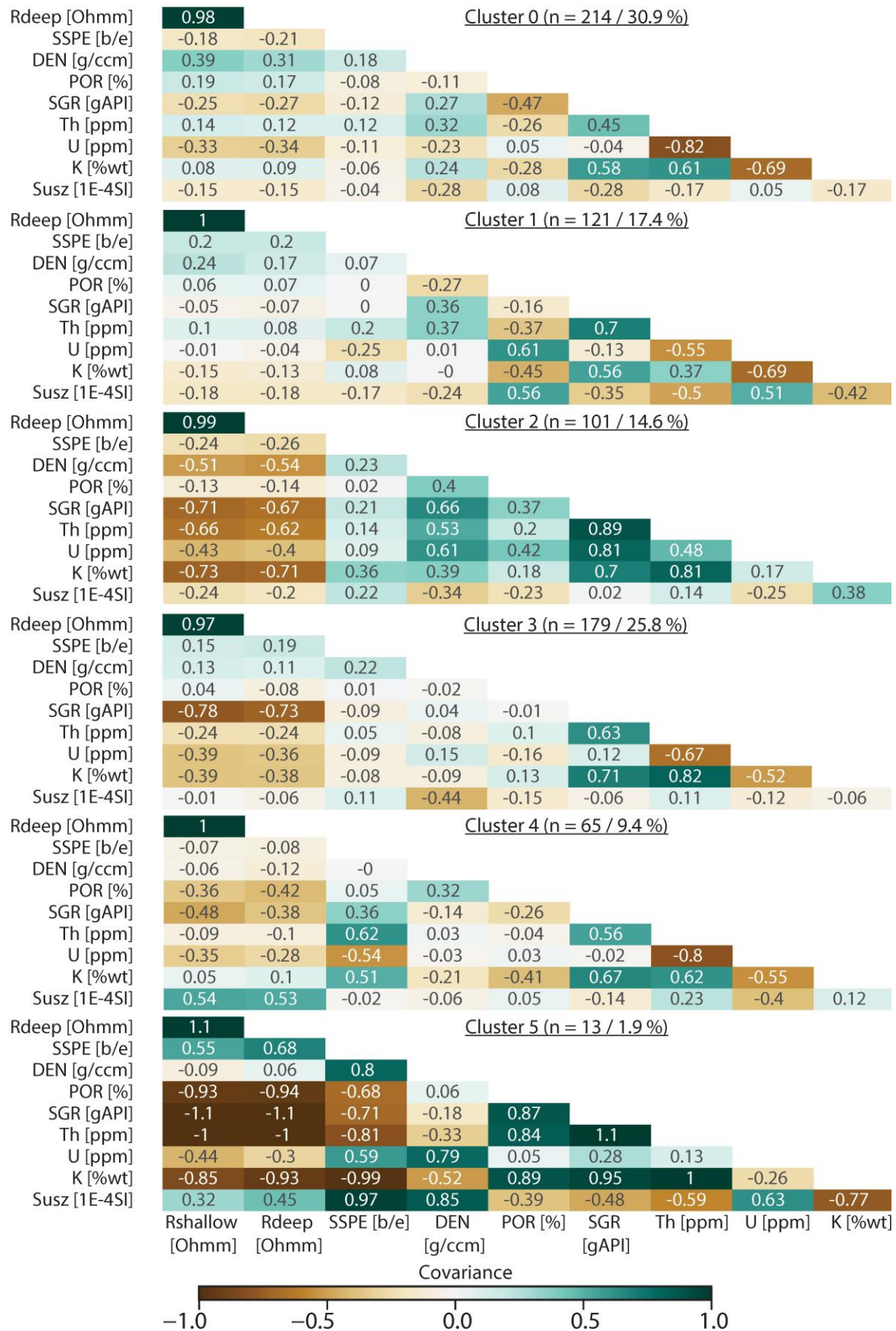


Figure S4: Triangular covariance matrix without self-correlation heatmap of the clusters (CC0-CC5) of 5068_1_C from the combined clustering of 5068_1_A and C indicating the variance between each log; (1-0.5 Strong positive correlation; 0.5-0.25 medium to weak positive correlation; 0.25- -0.25 weak to no positive or negative correlation; -0.25 - -0.5 medium to weak negative correlation; -0.5 - -1 medium to strong negative correlation).

5

Conclusion and outlook

5. Conclusion and outlook

The results of this thesis illustrate the potential of combining high-quality core drillings with borehole measurements and high-resolution 2D reflection seismic data for the systematic investigation of glacially overdeepened valleys and unconsolidated (Quaternary) sediments in general. More specifically, in the context of the DOVE project (Anselmetti et al., 2022), the key contributions of the thesis are:

- I) Improving the understanding of the local to regional landscape evolution with the detailed investigation of the glacially overdeepened Basadingen Trough with its multi-phase infill (Chapters 2 and 3)
- II) Enabling systematic over-regional comparability of glacially overdeepened valleys with the establishment of the conceptual glacio-seismic sequence model (Chapter 3) and the characterization of unconsolidated (Quaternary) sediments with petrophysical and chemical in-situ borehole data (Chapters 4)
- III) The development of project-internal protocols for core handling, sampling, and describing, as well as for data handling, managing, and processing (Chapter 2, Appendix A and B)

5.1 The implications for the regional landscape evolution

The detailed study of the recovered sediment succession and seismic data in Chapters 2 and 3 reveals a multi-phase infill of the Basadingen Trough. By combining the sediment succession with seismic data (core-to-seismic correlation), evidence of two glacial advance and retreat cycles, with a potential third cycle, was identified in the overdeepened valley fill. This valley fill is overlain by glaciofluvial gravel deposits capped with basal lodgment till. These stratigraphic and sedimentary elements are in good agreement with the existing pre-DOVE landscape evolution model (Chapter 1.6) and the postulated formation of the Basadingen Trough in more than one glacial cycle (Müller 2013).

However, luminescence dating results from the DOVE project (Frila et al., 2025, in prep) indicate that the entire overdeepened valley fill at drill site 5068_2 was deposited during MIS 6 (Beringen Glacial), while the overlying glaciofluvial gravel dates to late MIS 5 (Early Birrfeld, pre-LGM). These findings challenge the pre-DOVE hypothesis and, consequently, require the formulation of an updated working hypothesis for the formation of the Basadingen Trough:

- I) Erosion and deposition in the Basadingen Trough occurred during MIS 6, and no sediments dating back to MIS 12–10 were encountered, suggesting that there was either no trough formed at this earlier time or that MIS 6 glaciation fully re-excavated any existing trough fill.

- II) The discovered glacial sequences represent individual glacial advances during the penultimate MIS 6 glacial (Beringen Glacial)
- III) The late MIS 5 (substage b/a) age of the recovered gravels suggests an additional phase of (glacio)fluvial erosion and deposition
- IV) The basement lodgment till at the topmost section represents, with high certainty, the LGM advance

This updated working hypothesis has some direct implications for the model of the local landscape evolution (Fig. 1):

- I) The Basadingen Trough was likely active simultaneously with the Andelfingen Trough, rather than the older Marthalen Trough (Buechi et al., 2024), during MIS 6
- II) An intense phase of local glacial overdeepening occurred during MIS 6, during which the Basadingen Trough was re-excavated and refilled through multiple glacial advance-retreat cycles
- III) The younger age of the overlying gravel deposits suggests a complex internal stratigraphy, consistent with Graf's (2009) hypothesis, but includes an even younger depositional phase
- IV) No evidence was found for reactivation of the Basadingen Trough during the last (Birrfeld) Glacial (This is notable since the overdeepening forming the modern basin of Lake Constance was (re)excavated during this period (Ellwanger et al., 2011), and there are also traces of reactivation in the Thur valley (e.g., Buechi et al., 2024))

Following the DOVE approach, these local findings provide broader insights into the former Rhine Glacier area:

- I) MIS 6 was characterized by intense glaciation, with at least two to three glacial advances separated by phases of lake formation
- II) Even if older structures were reactivated, maximum erosion at the drilled, rather external, positions occurred during MIS 6
- II) Rapid sedimentation during MIS 6 resulted in the complete infilling of overdeepenings with (glacio)lacustrine sediments.
- IV) In contrast, the MIS 2 overdeepenings (e.g., Lake Constance) remain underfilled and will likely remain so for several 10 ka years.

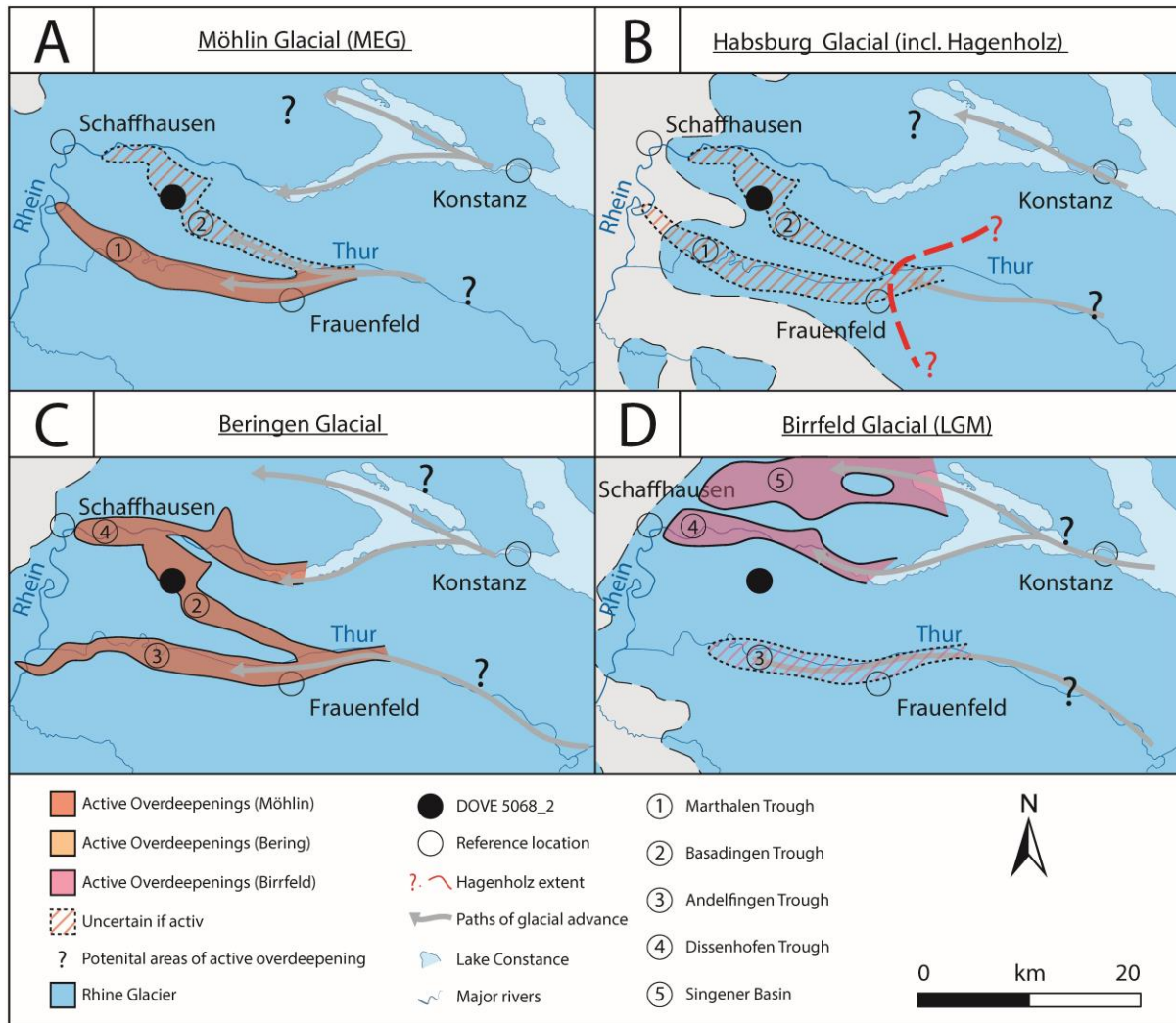


Figure 1: Updated overview sketches of the Middle to Late Pleistocene glaciations at the Dove site 5068_2. Showing the extent of the Rhine Glacier (Graf, 2009 and Preusser et al., 2011) and (active) overdeepenings (Buechi et al., 2024; Graf, 2009; Müller, 2013) during the A) Möhlin Glacial (MEG), B) Habsburg Glacial (including the extent of the debated Hagenholz Glacial), C) Beringen Glacial, and D) Birrfeld Glacial (LGM).

In conclusion and in the context of the overall DOVE goals (Chapter 1; Anselmetti et al., 2022), MIS 6 played an essential role in the development of the Rhine Glacier area. The period saw significantly more material eroded than previously assumed, highlighting underestimated surface-process rates and reduced land-surface stability, indicating different paleoclimatic conditions compared to MIS 2.

5.2 Methodological developments

Using data from the DOVE sites 5068_1 and 5068_2, this thesis successfully demonstrates the potential of adapting and integrating established techniques from the (energy) exploration industry to systematically investigate unconsolidated Quaternary sediments. The successful linking of geophysical and sedimentary properties allows a data-driven and comparable approach to analyzing complex geological structures such as glacially overdeepened valleys. This is of great value to the DOVE project, as it adds a powerful tool for the DOVE toolbox.

Chapter 3 presents the development of an adaptive model for a seismic sequence stratigraphy for glacially overdeepened valleys and their sedimentary infill. The model integrates depositional environments and sedimentary properties from cores with architectural elements identified in seismic data by combining core-to-seismic correlation and seismic sequence stratigraphy to define a basic glacio-seismic sequence. Such a sequence represents a full glacial advance and retreat cycle, with an ice-contact surface at the base, overlain by a subglacial unit followed by several units representing the development to a fully lacustrine environment. However, only the lower part of these sequences is often preserved due to the basal erosion during the next glacial advance. Therefore, the basal subglacial units are the key markers for identifying and separating the individual infill phases. Extending this glacio-seismic sequence stratigraphy into three dimensions by incorporating multiple seismic lines allows for spatial visualization and structural analysis. This is particularly valuable as the morphology of these structures provides insight into their formation, evolution, and internal architecture. Such information is critical for both scientific (e.g., understanding subglacial erosion patterns to provide ground truth for numerical models) and applied purposes (e.g., geothermal, groundwater, deep subsurface infrastructure).

Chapter 4 highlights the potential of wireline logging data to investigate and characterize the sedimentary infill of glacially overdeepened valleys. The workflow combines sophisticated data-analysis techniques with petrophysical and chemical properties from borehole data to predict lithological profiles derived from wells from flush and core drillings. This approach enables cross-hole correlation between cored and uncored wells using the core-controlled well as a translation key, linking wireline and core-based lithological data and profiles. This technique maximizes the information gained from destructive flush drilling, together with an increase in the number of wells drilled by replacing some core drillings with faster and cheaper flush drillings. This will allow to obtain additional lithological well-control for seismic data. Further, the increasing amount of data and the direct link between the different data types will provide critical information for developing and ground-truthing sophisticated numerical and three-dimensional geological subsurface models.

Both methods have individual technical and scientific aspects that can be further developed and improved. In particular, both methods are still highly dependent on high-resolution drill cores to calibrate between seismic data, borehole measurements, and sedimentary properties, which is crucial to ensure comparability between different sites. Therefore, making their application less resource-intensive by reducing this dependency would be of great value.

Therefore, making their application less resource-intensive by reducing this dependency would be of great value. For example, this could be achieved by systematically collecting the sedimentary characteristics and depositional environments of the glacial sequence elements and the typical petrophysical and chemical properties of the sediments encountered in databases. These data collections would eventually allow the methods to be applied similarly to their role models from the exploration industries (e.g., electro facies: Serra & Abbott, 1982 and (marine) seismic sequence stratigraphy: e.g., Mitchum et al., 1977). Further, a significant improvement would be to combine the two techniques to form a powerful tool for data-based, systematic, and comparable investigations of glacially overdeepened valleys and the geological subsurface in general. However, the aim is not to completely replace core drillings but to maximize the geological information that can be obtained from them to set the recovered sediments into a solid geological frame.

Therefore, these methods have great potential for the DOVE project by providing a strong geological framework to establish absolute chronologies for the investigated glacial overdeepened valleys and their infill. In the case of Basadingen Trough, the absolute chronology helped to overcome the limitations of the initial relative chronology, in which each glacial sequence was interpreted as the remains of an individual glacial cycle. Additionally, establishing such over-regional absolute chronology would help to unify or at least enable a practical translation between the different local Quaternary stratigraphic systems (e.g., Ellwanger et al., 2011; Graf & Burkhalter, 2016).

5.3 Practical Lessons Learned for DOVE Phase II

DOVE Phase I (Northern Alpine Transect, see Introduction) was, besides or because of the many challenges encountered and solved, a scientific, operative, and technical success. It demonstrated the immense potential of the DOVE approach for systematically studying glacial overdeepened valleys and troughs in the Northern Alps and beyond. Advancing to this next level would not have been possible without the commitment of the entire DOVE Phase I team. However, critical reflection on Phase I is essential to address and learn from the challenges encountered. The (practical) key lessons from DOVE Phase I include:

Allocating enough time and resources for initial data acquisition: It is essential to reserve sufficient time and resources for drilling and data acquisition activities, including personnel and logistical support, ensuring high-quality data. Drilling and borehole measurements are particularly

sensitive to unpredictable technical challenges and represent a potential "point of single failure" for the project.

Standardizing metadata and data documentation: Complete and systematic metadata and scientific data documentation is crucial for ensuring site comparability. Without standardized documentation of (meta)data, the integration and comparative analysis of datasets from different locations become significantly limited, reducing the effectiveness of the DOVE approach.

Integrating technical requirements across phases: Building on the methods established in Phase I, Phase II must account for technical requirements to improve a data-based integration between sites and across project phases. This includes ensuring compatibility in high-resolution reflection seismic data, vertical seismic profiles, wireline logging surveys, luminescence dating, and 3D CT core analyses, surpassing only qualitative comparison.

Coordinating multi-disciplinary activities: Effective coordination between geophysical surveys, drilling operations, and borehole measurements is crucial to limit potential hampering between different analyses.

Establishing absolute chronologies: Establishing absolute chronologies has been crucial for comparing the individual overdeepenings effectively. Even though some methods did not work in Phase I, they may work in Phase II or can be improved or substituted by different approaches.

Addressing and integrating these lessons from Phase I will not only help to secure the definitive funding for Phase II but also be crucial for the future scientific success of the project. Even though, Helmuth von Moltke once stated (Hughes, 1995): "No plan survives contact with the enemy.", effective and adaptive planning and coordination during the operational phases of the different sides are crucial for the successful application of the DOVE approach and for making the most out of the unique scientific opportunity of the project. This demonstrated the scientific potential of DOVE Phase I, which is the best recommendation for Phase II.

5.4 References

- Anselmetti, F. S., Bavec, M., Crouzet, C., Fiebig, M., Gabriel, G., Preusser, F., Ravazzi, C., & DOVE scientific team. (2022). Drilling Overdeepened Alpine Valleys (ICDP-DOVE): Quantifying the age, extent, and environmental impact of Alpine glaciations. *Scientific Drilling*, 31, 51–70. <https://doi.org/10.5194/sd-31-51-2022>
- Buechi, M. W., Landgraf, A., Madritsch, H., Mueller, D., Knipping, M., Nyffenegger, F., Preusser, F., Schaller, S., Schnellmann, M., & Deplazes, G. (2024). Terminal glacial overdeepenings: Patterns of erosion, infilling and new constraints on the glaciation history of Northern Switzerland. *Quaternary Science Reviews*, 344, 108970. <https://doi.org/10.1016/j.quascirev.2024.108970>
- Ellwanger, D., Wielandt-Schuster, U., Franz, M., & Simon, T. (2011). The Quaternary of the southwest German Alpine Foreland (Bodensee-Oberschwaben, Baden-Württemberg, Southwest Germany). *E&G Quaternary Science Journal*, 60(2/3), 306–328. <https://doi.org/10.3285/eg.60.2-3.07>
- Firla, G., Lüthgens, C., Gegg, L., Preusser, F., & Fiebig, M. (in prep). Not all glaciations are the same - Divergent sedimentation patterns during Late and Middle Pleistocene glaciations in the northern Alpine foreland.
- Graf, H. R. (2009). *Stratigraphie von Mittel- und Spätpleistozän in der Nordschweiz. Beiträge zur Geologischen Karte der Schweiz (N.F.)* (Vol. 168). Landesgeologie.
- Graf, H. R., & Burkhalter, R. (2016). Quaternary deposits: Concept for a stratigraphic classification and nomenclature—an example from northern Switzerland. *Swiss Journal of Geosciences*, 109(2), 137–147. <https://doi.org/10.1007/s00015-016-0222-7>
- Hughes, D. (1995). *Moltke on the Art of War: Selected Writings*. Random House Publishing Group. https://books.google.ch/books?id=_FSPEAAQBAJ
- Mitchum, R. M., Jr., Vail, P. R., & Sangree, J. B. (1977). Seismic Stratigraphy and Global Changes of Sea Level, Part 6: Stratigraphic Interpretation of Seismic Reflection Patterns in Depositional Sequences1. In C. E. Payton (Ed.), *Seismic Stratigraphy—Applications to Hydrocarbon Exploration* (Vol. 26). American Association of Petroleum Geologists. <https://doi.org/10.1306/M26490C8>
- Müller, E. R. (2013). Mittelpleistozäne Schottervorkommen zwischen dem Thurtal und Schaffhausen. *Swiss Bulletin für angewante Geologie*, 18(1), 3–27. <https://doi.org/10.5169/SEALS-391135>
- Preusser, F., Graf, H. R., Keller, O., Krayss, E., & Schlüchter, C. (2011). Quaternary glaciation history of northern Switzerland. *E&G Quaternary Science Journal*, 60(2/3), 282–305. <https://doi.org/10.3285/eg.60.2-3.06>
- Serra, O., & Abbott, H. T. (1982). The Contribution of Logging Data to Sedimentology and Stratigraphy. *Society of Petroleum Engineers Journal*, 22(01), 117–131. <https://doi.org/10.2118/9270-PA>

Appendix A: Drilling Overdeepened Alpine Valleys (DOVE) – Operational Report of Phase I

Comment:

This report documents the drilling operations and initial core description of the ICDP Project "Drilling Overdeepened Alpine Valleys" (DOVE). In my role as drill site geologist of DOVE site 5068_2 and the lead geologist for the initial core description of core 5068_2_A, the documentation of it was a core task in my first year of the PhD studies. The chapter about site 5068_2, providing the technical background for Chapter 3 of this thesis, was written by Marius W. Buechi and myself.

ICDP Operational Report

<https://doi.org/10.48440/ICDP.5068.001>

Drilling Overdeepened Alpine Valleys (DOVE) – Operational Report of Phase 1

DOVE-Phase 1 Scientific Team, Anselmetti, F. S., Beraus, S., Buechi, M. W., Bunes, H., Burschil, T., Fiebig, M., Firla, G., Gabriel, G., Gegg, L., Grelle, T., Heeschen, K., Kroemer, E., Lehne, C., Lüthgens, C., Neuhuber, S., Preusser, F., Schaller, S., Schmalfuss, C., Schuster, B., Tanner, D. C., Thomas, C., Tomonaga, Y., Wieland-Schuster, U., and Wonik, T.

Citation of this report:

DOVE-Phase 1 Scientific Team, Anselmetti, F. S., Beraus, S., Buechi, M. W., Buness, H., Burschil, T., Fiebig, M., Firla, G., Gabriel, G., Gegg, L., Grelle, T., Heeschen, K., Kroemer, E., Lehne, C., Lüthgens, C., Neuhuber, S., Preusser, F., Schaller, S., Schmalfuss, C., Schuster, B., Tanner, D. C., Thomas, C., Tomonaga, Y., Wieland-Schuster, U., and Wonik, T. (2023) Drilling Overdeepened Alpine Valleys (DOVE) – Operational Report of Phase 1. ICDP Operational Reports. GFZ German Research Centre for Geosciences. <https://doi.org/10.48440/ICDP.5068.001>

Referencing Article:

Schaller, S., Buechi, M. W., Schuster, B. and Anselmetti, F. S. (2023). Drilling into a deep buried valley: A 252 m long sediment succession from a glacial overdeepening in northwestern Switzerland, Scientific Drilling, 32, <https://doi.org/10.5194/sd-32-27-2023>

Supplementary Data:

DOVE - Phase 1 Scientific Team; Beraus, S., Buechi, M. W., Buness, H., Burschil, T., Fiebig, M., Firla, G., Gabriel, G., Gegg, L., Grelle, T., Heeschen, K., Kroemer, E., Lehne, C., Lüthgens, C., Neuhuber, S., Preusser, F., Schaller, S., Schmalfuss, C., Schuster, B., Tanner, D. C., Thomas, C., Tomonaga, Y., Wieland-Schuster, U., and Wonik, T. (2023): Drilling Overdeepened Alpine Valleys (DOVE) - Operational Dataset of DOVE Phase 1. GFZ Data Services. <https://doi.org/10.5880/ICDP.5068.001>

Imprint

International Continental Scientific Drilling Program

Helmholtz Centre Potsdam

GFZ German Research Centre for Geosciences

Telegrafenberg

D-14473 Potsdam

Published in Potsdam, Germany

2023

DOI: <https://doi.org/10.48440/ICDP.5068.001>



This work is licensed under a Creative Commons Attribution 4.0 International License. (CC BY 4.0)
<https://creativecommons.org/licenses/by/4.0/>

Drilling Overdeepened Alpine Valleys (DOVE)

- Operational Report of Phase 1

DOVE-Phase 1 Scientific Team, Anselmetti, F. S.*, Beraus, S., Buechi, M. W., Buness, H., Burschil, T., Fiebig, M., Firla, G., Gabriel, G., Gegg, L., Grelle, T., Heeschen, K. U., Kroemer, E., Lehne, C., Lüthgens, C., Neuhuber, S., Preusser, F., Schaller, S., Schmalfuss, C., Schuster, B., Tanner, D. C., Thomas, C., Tomonaga, Y., Wieland-Schuster, U., and Wonik, T.

* corresponding author

1. Introduction & site overview

1.1. Introduction

This report documents the drilling operations of the ICDP Project "Drilling Overdeepened Alpine Valleys" (DOVE) and includes information on the six different sites investigated during Phase 1 of the DOVE project. Two sites, site 5068_1 (Tannwald) and site 5068_2 (Basadingen) have been drilled in 2021 with the support of ICDP funding. The drilling operations at both sites are published in this operational report. In addition, the report includes summarized information on the four legacy sites, all drilled in the framework of earlier projects and cited before. The remnants of these legacy cores have been curated, described and re-sampled in the framework of the DOVE project.

All sites are investigating overdeepened troughs along the northern Alps and their foreland. The sedimentary infill of glacially overdeepened valleys (i.e. excavated structures below the fluvial base level) are, together with glacial geomorphology, the best-preserved direct archives of extents and ages of past glaciations in and around mountain ranges. The cores are investigated with regard to several aspects of environmental dynamics during the Quaternary, with focus on the glaciation, vegetation, and landscape history. Besides the scientific goals, DOVE also addresses a number of applied objectives such as groundwater resources, geothermal energy production, and seismic hazard assessment. Details on the scientific objectives and approach of the DOVE project are explained in Anselmetti et al. (2022).

The initial core description and interpretation of the cores from the Tannwald Area (5068_1_A, 5068_1_B, 5068_1_C; Schuster et al., in prep) and the Basadingen Trough (5068_2_A, Schaller et al., subm.) are presented in the scientific reports, which are intended to be published in Scientific Drilling in 2023. Table 1 lists all the sites of the Phase 1, their coordinates, IGSN and the first scientific report/publication on the respective site if applicable.

1.2. Objectives

For Details on the objectives of the project please see Anselmetti et al. (2022)

1) What was the timing and extent of past Alpine glaciations?

Hypothesis: Glacier advances and related erosion and infilling of overdeepened troughs varied in timing and extent around the Alps during the Quaternary.

2) How did atmospheric circulation patterns control ice flow across the Alps?

Hypothesis: Atmospheric circulation over the Alps varied during past glaciations so that moisture distribution became the pivotal control of ice build-up.

3) How were mountain ranges and their foreland shaped by repetitive glaciations?

Hypothesis: The timing and amount of erosion and infill varied not only around the Alps, but also within one system.

Add-ons:

- Geophysical investigations
- Potential of overdeepened structures as groundwater resources
- Potential of the Quaternary valley fills for shallow geothermal applications
- Alpine vegetation history
- Microbial activity in the sediments,
- later: Modelling landscape response, glacial erosion, and climate.

1.3. Referencing articles

Schaller, S., Buechi, M. W., Schuster, B. and Anselmetti, F. S. (in press). Drilling into a deep buried valley: A 252 m long sediment succession from a glacial overdeepening in northwestern Switzerland, *Scientific Drilling*, 32, (2023) <https://doi.org/10.5194/sd-32-27-2023>.

1.4. Supplementary data

DOVE-Phase 1 Scientific Team et al. (2023c) Drilling Overdeepened Alpine Valleys (DOVE) – Explanatory Remarks, <https://doi.org/10.48440/ICDP.5068.002>

DOVE-Phase 1 Scientific Team et al. (2023b) Drilling Overdeepened Alpine Valleys (DOVE) - Operational Dataset of Phase 1, <https://doi.org/10.5880/ICDP.5068.001>

1.5. The locations of the drill sites DOVE Phase 1

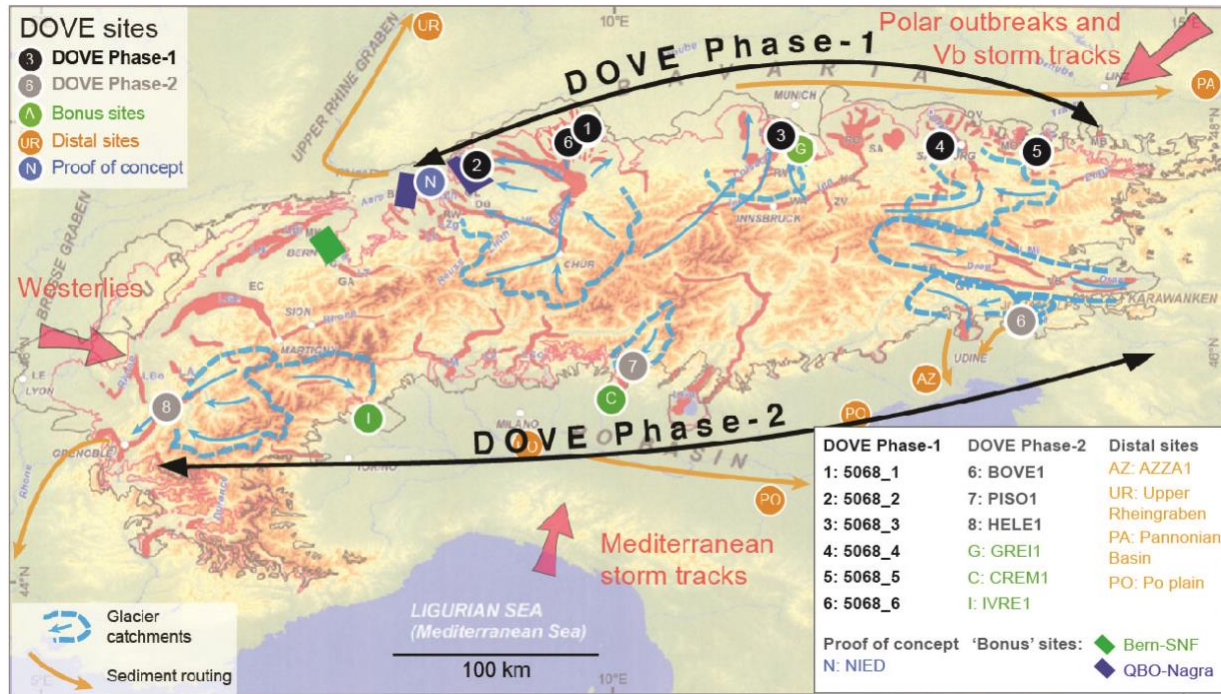


Figure 1 Map of the Alps and their forelands including the locations of the drill sites of the DOVE project (Anselmetti et al. 2022, updated). The sites of DOVE Phase-1 5086_1 to 5086_6 are covered by this report.

Table 1 Location and Identifiers of boreholes from DOVE Phase 1

Borehole Combined-ID	Borehole IGSN https://doi.org/10.60510/..	Latitude decimal WGS84	Longitude decimal WGS 84	Operational Phase in	First Scientific Reports
5068_1_A	ICDP5068EH50001	47.9998028	9.7486417	2021	Schuster et al., in prep
5068_1_B	ICDP5068EH60001	47.9995528	9.7486111	2021	Schuster et al., in prep
5068_1_C	ICDP5068EH70001	47.9995500	9.7490139	2021	Schuster et al., in prep
5068_2_A	ICDP5068EH40001	47.6480956	8.7532566	2021	Schaller et al., 2023
5068_3_A	ICDP5068EHC0001	47.9710190	11.460135	2017	Firla et al. in prep
5068_4_A	ICDP5068EHD0001	47.8628920	12.909791	2009	Fiebig et al. (2014)
5068_5_A	ICDP5068EHE0001	47.6069711	13.7741043	1998	Husen van & Mayr (2007)
5068_6_A	ICDP5068EHG0001	47.8880460	9.7112920	2016	Ellwanger, 2015; Schaaf, 2017; Rolf, 2021

1.6. DOVE-Phase 1 Scientific Team Members

(alphabetic order, see site reports for detailed responsibilities, **bold: PI**)

Anselmetti	Flavio S.	Institute of Geological Sciences and Oeschger Centre for Climate Change Research, University of Bern, 3012 Bern, Switzerland
Beraus	Sarah	Leibniz Institute for Applied Geophysics, 30655 Hanover, Germany
Buechi	Marius W.	Institute of Geological Sciences and Oeschger Centre for Climate Change Research, University of Bern, 3012 Bern, Switzerland
Buness	Hermann	Leibniz Institute for Applied Geophysics, 30655 Hanover, Germany
Burschil	Thomas	Federal Institute for Geosciences and Natural Resources, 30655 Hannover, Germany
Fiebig	Markus	Department of Civil Engineering and Natural Hazards, Institute of Applied Geology, University of Natural Resources and Life Sciences, Vienna (BOKU), 1190 Vienna, Austria
Firla	Gustav	Department of Civil Engineering and Natural Hazards, Institute of Applied Geology, University of Natural Resources and Life Sciences, Vienna (BOKU), 1190 Vienna, Austria
Gabriel	Gerald	Leibniz Institute for Applied Geophysics, 30655 Hanover, Germany and Institute of Geology, Leibniz University Hanover, 30167 Hanover, Germany
Gegg	Lukas	Institute of Earth and Environmental Sciences, University of Freiburg, 79104 Freiburg, Germany
Grelle	Thomas	Leibniz Institute for Applied Geophysics, 30655 Hanover, Germany
Heeschen	Katja	Department 4.2 Geomechanics and Scientific Drilling, Helmholtz-Centre Potsdam, German Research Centre for Geosciences, 14473 Potsdam, Germany
Kroemer	Ernst	Ref. 102 Landesaufnahme Geologie, Geogefahren, Bayerisches Landesamt für Umwelt, 95030 Hof, Germany
Lehne	Carlos	Leibniz Institute for Applied Geophysics, 30655 Hanover, Germany
Lüthgens	Christopher	Department of Civil Engineering and Natural Hazards, Institute of Applied Geology, University of Natural Resources and Life Sciences, Vienna (BOKU), 1190 Vienna, Austria
Neuhuber	Stephanie	Department of Civil Engineering and Natural Hazards, Institute of Applied Geology, University of Natural Resources and Life Sciences, Vienna (BOKU), 1190 Vienna, Austria
Preusser	Frank	Institute of Earth and Environmental Sciences, University of Freiburg, 79104 Freiburg, Germany
Schaller	Sebastian	Institute of Geological Sciences and Oeschger Centre for Climate Change Research, University of Bern, 3012 Bern, Switzerland

Schmalfuss	Clemens	Department of Civil Engineering and Natural Hazards, Institute of Applied Geology, University of Natural Resources and Life Sciences, Vienna (BOKU), 1190 Vienna, Austria
Schuster	Bennet	Institute of Earth and Environmental Sciences, University of Freiburg, 79104 Freiburg, Germany
Tanner	David C.	Leibniz Institute for Applied Geophysics, 30655 Hanover, Germany
Thomas	Camille	Institute of Geological Sciences and Oeschger Centre for Climate Change Research, University of Bern, 3012 Bern, Switzerland
Tomonaga	Yama	Eawag, Department of Water Resources and Drinking Water, 8600 Dübendorf, Switzerland
Wieland-Schuster	Ulrike	Regierungspräsidium Freiburg, Landesamt für Geologie, Rohstoffe und Bergbau, Referat 92 Landesgeologie, 79104 Freiburg i.Br., Germany
Wonik	Thomas	Leibniz Institute for Applied Geophysics, 30655 Hanover, Germany

Table of Contents

1. Introduction & site overview.....	1
1.1. Introduction.....	1
1.2. Objectives.....	2
1.3. Referencing articles.....	2
1.4. Supplementary data	2
1.5. The locations of the drill sites DOVE Phase 1.....	3
1.6. DOVE-Phase 1 Scientific Team Members.....	4
2. Site 5086_1.....	8
2.1. Site Introduction.....	8
2.2. Personnel in the Operational Phase.....	9
2.3. Site Selection and Permits.....	9
2.4. Site Preparation and Infrastructure	11
2.5. Technical Operations.....	13
2.5.1. Summary of drilling, coring and logging operations.....	13
2.5.2. Detailed report of operations	16
2.5.3. Borehole deviation	20
2.5.4. Refilling and post-drilling finishing procedure	21
2.5.5. Borehole geometry and preliminary lithology assessment.....	22
2.6. Scientific operations on-site.....	26
2.6.1. Workflow flush drilling.....	26
2.6.2. Workflow drill-core handling.....	27
2.6.3. On-site sampling	28
2.6.4. Downhole geophysical measurements.....	29
2.7. Storage, initial core description and 1 st sampling party.....	31
2.7.1. Sites 5068_1 and 5068_2.....	31
2.7.2. Legacy sites 5068_3 through 5068_6	31
2.8. Site-specific preliminary scientific assessment	32
2.8.1. Geology	32
2.8.2. Borehole Geophysics	32
3. Site 5086_2.....	34
3.1. Site Introduction.....	34
3.2. Personnel in the Operational Phase.....	34
3.3. Site selection and permits.....	35
3.4. Site preparation and infrastructure	36
3.5. Technical operations	38
3.5.1. Summary of drilling, coring and logging operations.....	38
3.5.2. Detailed report of operations	42
3.5.3. Borehole deviation	45
3.5.4. Refilling and Post-Drilling Finishing Procedure.....	46
3.5.5. Borehole geometry and preliminary lithology assessment.....	47
3.6. Scientific operations on-site.....	48
3.6.1. Workflow drill-core handling.....	48
3.6.2. On-site sampling	49

3.6.3.	Downhole geophysical measurements.....	49
3.7.	Storage, initial core description and 1 st sampling party.....	51
3.8.	Site-specific preliminary scientific assessment.....	51
3.8.1.	Geology	51
3.8.2.	Geophysics.....	51
4.	Site 5068_3.....	53
4.1.	Site Introduction.....	53
5.	Site 5068_4.....	55
5.1.	Site Introduction.....	55
6.	Site 5068_5.....	56
6.1.	Site Introduction.....	56
7.	Site 5068_6.....	57
7.1.	Site Introduction.....	57
8.	DOVE Operational Dataset.....	59
8.1.	Data und Metadata from mDIS.....	59
8.2.	Image Reports and Primary Images exported from mDIS	61
9.	Summary of Preliminary Scientific Assessment.....	62
10.	Conclusions	63
11.	Acknowledgements	63
12.	References.....	64
13.	Appendices.....	65
Appendix A – 5086_2 Hydrogeological report by Dr. von Moos AG		66
Appendix B –		70

2. Site 5086_1

2.1. Site Introduction

The Tannwald Basin is located approximately 45 km northeast of Lake Constance in the central part of the Alpine foreland. Its overdeepened structure was incised into Tertiary Molasse sediments by subglacial erosion under the Rhine Glacier. Later it was filled by glacial, fluvial, and lacustrine deposits of up to 250 m thickness. As shown by Ellwanger et al. (2011), the Tannwald Basin site is characterised by two superimposed unconformities (Fig. 1; D2 and D3). The site therefore has the potential to characterize sedimentary sequences above both of these unconformities. The earlier interpretations are based, amongst other things, on the sediment succession found in a previously-drilled borehole (Schneidermartin research borehole; LGRB-ID: 8024-925; Burschil et al., 2018), about 1200 m southeast of the newly-drilled Tannwald site, ICDP 5068_1 (Figs. 2 and 3). The whole sequence apparently comprises the deposits of three glacial cycles. However, neither the sedimentary record nor the results of pollen analysis have been documented in detail. Furthermore, no geochronological data are available for the Schneidermartin borehole.

Three individual boreholes were drilled (ICDP 5068_1_A; 5068_1_B; 5068_1_C): The first two are flush drillings (ICDP 5068_1_A & 5068_1_B), with the main purpose of enabling post-drilling cross-borehole geophysical measurements, and the third one was a core drilling (ICDP 5068_1_C).

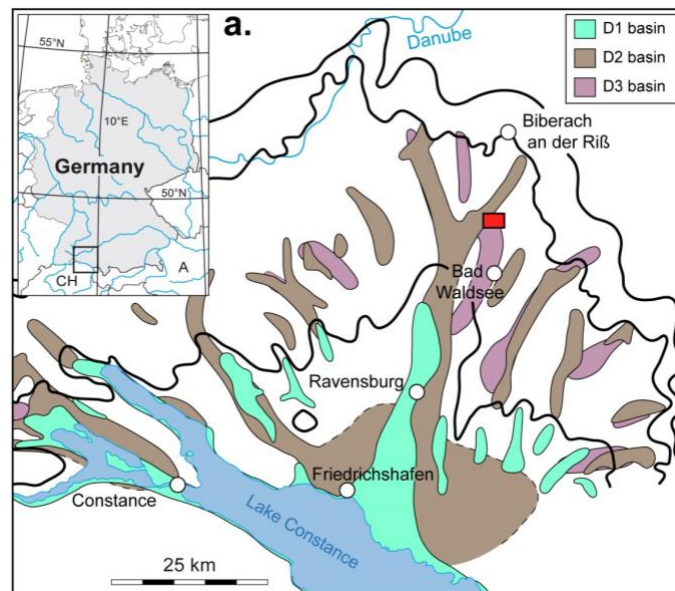


Figure 1: Map of basins of the Rhine Glacier, modified after Ellwanger et al. (2011). Three different generations of unconformities can be identified, known as D1–D3. These correspond to the advances of the Rhine glacier in the Würmian, Rissian and Hosskirchian glacial periods. The red box marks the area shown in Figure 3 including the current drilling location in the Tannwald Basin.

2.2. Personnel in the Operational Phase

Technical project management and supervision

David C. Tanner, Leibniz Institute for Applied Geophysics, Germany (responsible)

Project and on-site science coordination

David C. Tanner, Leibniz Institute for Applied Geophysics, Germany

Bennet Schuster, (Ph.D. student) University of Freiburg, Germany

Volunteers

Julia Silov-Tepic (1-month practical experience), University of Potsdam, Germany

Drilling advisors

Ulrike Wielandt-Schuster, Landesamt für Geologie, Rohstoffe und Bergbau, Germany

Marius W. Buechi, University of Bern, Switzerland

Downhole geophysical measurements (LIAG, Hanover)

Hermann Buness, Leibniz Institute for Applied Geophysics, Germany

Thomas Grelle, Leibniz Institute for Applied Geophysics, Germany

Carlos Lehne, Leibniz Institute for Applied Geophysics, Germany

Thomas Wonik, Leibniz Institute for Applied Geophysics, Germany

Drilling team (H. Anger's Söhne, Bohr- und Brunnenbaugesellschaft mbH)

Mirko Huber (company liaison)

Jürgen Pröhl (drilling manager, flush drilling)

Markus Schick (drilling manager, core drilling)

J. Achler, Mohammad Alhamad, Hsaan Alsasihl, Asabdi, Peter Goor, Frank Hapke, Zoltan

Mihalti, Zoltan Olah, Jens Täubert, Lutz Tonne, Peter Toth

Off-site assistance & Data management

Katja Heeschen, ICDP, GFZ German Research Centre for Geosciences, Potsdam, Germany

2.3. Site Selection and Permits

To determine the optimal location for the drillsite (ICDP 5068_1), LIAG carried out a high-resolution reflection P-wave seismic campaign over the basin structure at this location in 2014 and 2015 (Fig. 2). The profiles concentrated on the deepest part of the Tannwald Basin, as known from seismic refraction surveys (Behnke and Bram 1998). The seismic grid was connected to the Schneidermartin borehole (Fig. 2). Details can be found in Burschil et al. (2018).

In consideration of groundwater safety regulations and drilling suitability, a site was located on the western flank of the basin structure, so that drillholes would have to drill 150-160 m to reach the base of the Quaternary glacial fill (Fig. 4).

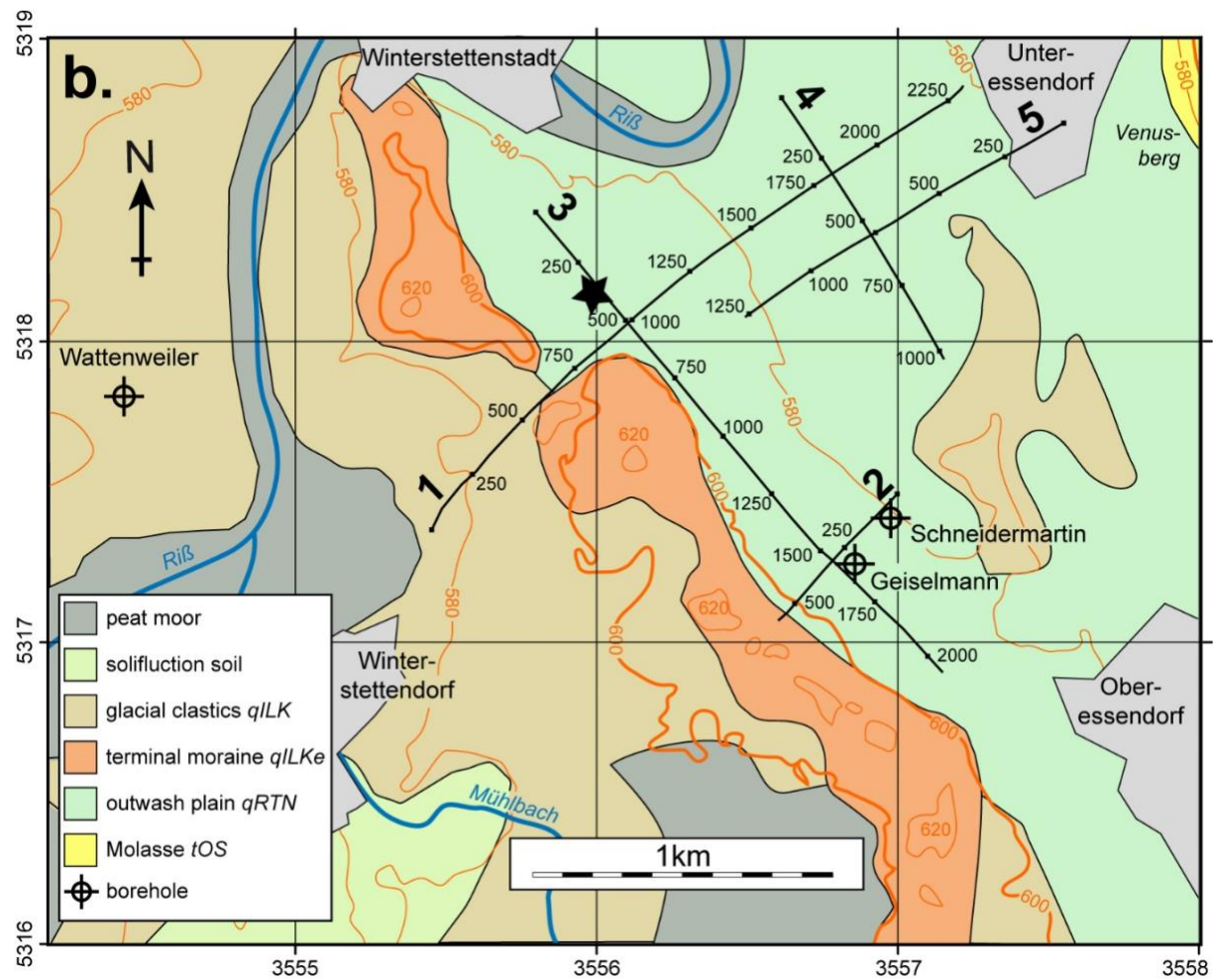


Figure 2: Geological map of the survey area of the Tannwald Basin, showing the location of seismic reflection profiles 1–5 and previous boreholes (from Burschil et al., 2018). The drillsite location is indicated by a star.

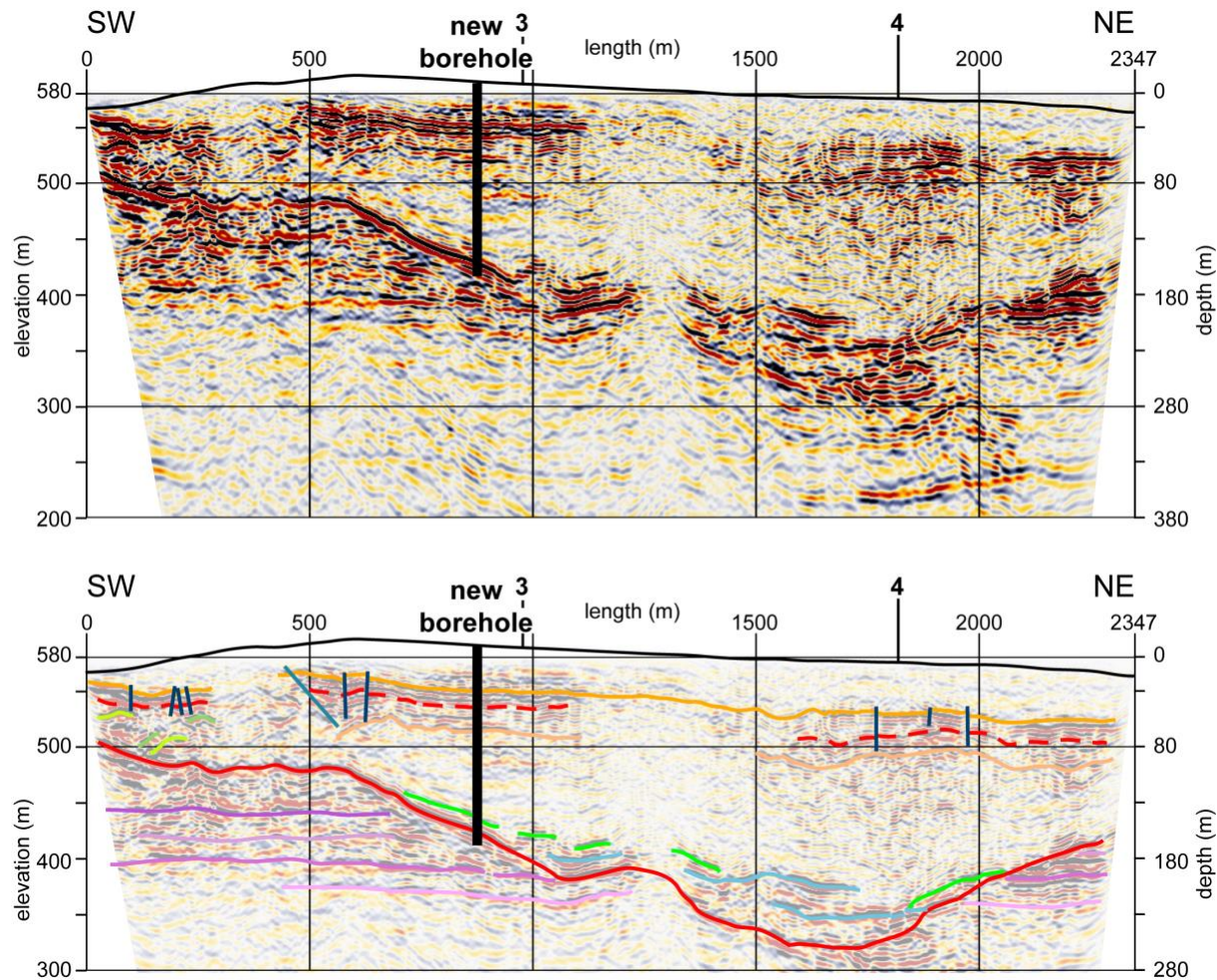


Figure 3: Seismic section 1, for location see Fig. 2. Above: seismic profile, below: interpreted structure and seismic facies. Vertical exaggeration, 2.5x. Profile intersections (black numbers), elevation (black line), faults with offsets >2 m (dark blue), and faults with unknown offsets (light blue). Dashed red line shows D2 unconformity, base of the overdeepened valley (D3) is solid red line. Green lines indicate top of a layer of waterlain till, blue lines show allochthonous blocks of Tertiary molasse. Purple lines represent bedding in the Tertiary molasse sediments (Burschil et al., 2018). The location of the three new boreholes is projected 100 m towards the south east.

2.4. Site Preparation and Infrastructure

1500 m² of land in the NE corner of an arable field (known from now on as the drillsite) was leased from a local farmer. It was agreed that the drillsite would be sown with clover, while the rest of the field was sown with sweet corn. The drillsite was directly next to an asphalted road. Therefore, no additional access road was required, at least to start with. Top soil was not removed, but large wooden plank mats were used to protect the ground around the drilling rig and containers.

On-site facilities included workshops for repairs to equipment, waste and drill-mud tanks around the drill rig, and containers for the drilling team and science crew (Figs. 4 and 5). LIAG set up an information tent to cater for casual tourists and arranged visits of schoolchildren and local geologists.

Electricity for the site was provided on-site by a generator. Water was obtained from the local authority and kept in a lorry-mounted, 9 m³ tank. Later, because of torrential rain, it became necessary to construct a small (ca. 25 m length) cambered road across the drillsite (27th-30th June 2021). The road was constructed by laying 25 cm of gravel and hogging on top of a geotextile sheet.

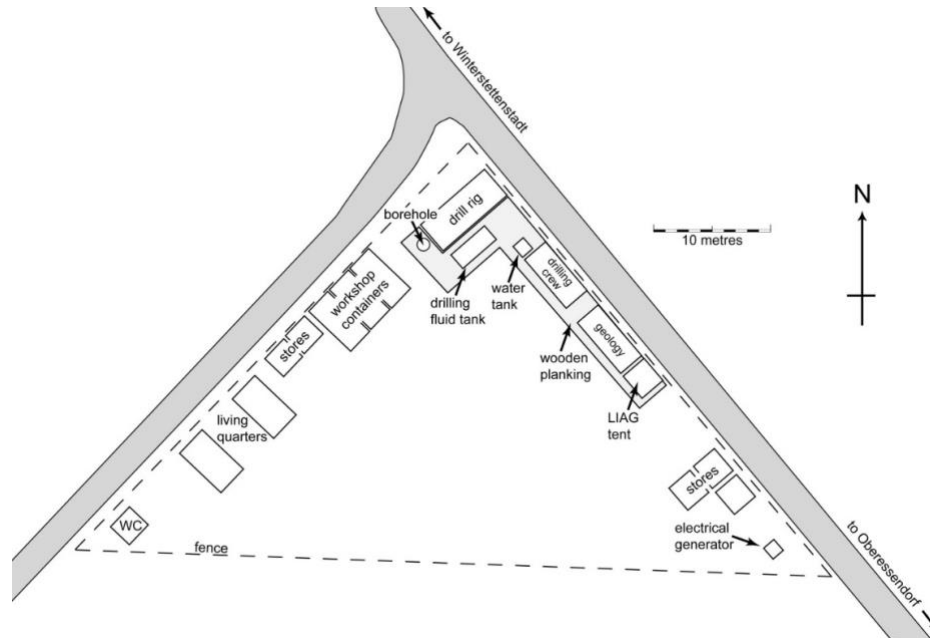


Figure 4: Layout of the drillsite (5068_1) for the borehole A. See Appendices for layouts of the other boreholes.



Figure 5: Aerial view of the drill site during the drilling of borehole 5068_1_C.

2.5. Technical Operations

2.5.1. Summary of drilling, coring and logging operations

The Leibniz Institute for Applied Geophysics (Hannover, Germany) coordinated technical operations. A German drilling company, H. Anger's Söhne, Bohr- und Brunnenbaugesellschaft mbH (known hereafter as Angers), was the drilling contractor. The drilling crew consisting of two/three persons (one drilling manager/controller, one to two drilling workers), nominally worked 12 hour shifts from Monday through Thursday. Occasionally, they worked Friday to complete various tasks.



Figure 2: The drill rig (MB Actros 3341A, UH2) used for all three boreholes, with the manual casing handling system.

Table 2: Technical details of the drill rig.

Hook nominal force/ max. force	240 kN / 360 kN
Hydraulic force (pull/push)	110 kN/50 kN
Drill winch ZHP 4.25-EG	120 kN
Cable coring winch ZHP 4.19-EG1	20 kN
Auxiliary winch ZHP 4.13	25 kN
Drill head Type UH2 -14000 torque	14 kNm
Roller block Type 240 kN	240 kN
Compressor Atlas Copoco XAHS 107 (pressure/flow rate)	12 bar/5.5 m ³ /min

Angers provided a lorry (MB Actros 3341A)-mounted drill rig, UH2, for the drilling (Fig. 6). It was last tested and found to be in working order on 7th May 2020. For details of the device, see Table 2. The timing of the drilling operations at DOVE Site 1 are summarised in Table 3.

Table 3. Site 5068_1 (Tannwald Basin) drilling operations by time

date (all 2021)	working days	task
6 th – 13 th April	6	Construction of site, mobilization
15 th April – 5 th May	15	Flush drilling 5068_1_A
10 th – 11 th May	1.5	Downhole geophysical logging (open hole) 5068_1_A
12 th – 20 th May	6	Completion of 5068_1_A
31 st May – 21 st June	13	Flush drilling 5068_1_B
28 th June – 30 th June	3	Construction of road across drillsite
28 th June – 1 st July	4	Completion of 5068_1_B
6 th July – 8 th July	3	VSP (zero-offset and walkaway) of 5068_1_A and B
12 th July – 3 rd Aug.	17	Changing drilling rig over
4 th Aug. – 5 th Aug.	2	Core drilling of 5068_1_C
9 th Aug. – 20 th Aug.	20	Holiday for the drilling team
23 rd Aug. – 11 th Nov.	48.5	Core drilling of 5068_1_C
11 th – 12 th Nov.	1.5	Downhole geophysical logging (open hole) of 5068_1_C
15 th – 18 th Nov.	3	Completion of 5068_1_C
22 nd Nov. – 2 nd Dec.	8	Demobilization
10 th – 12 th March 2022	3	Downhole geophysical logging (closed hole) of all boreholes 5068_1_A, B and C

Flush drilling procedure

ICDP 5068_1_A. The standpipe (318 mm inner diameter (ID)) was drilled dry using an auger down to 10 m. From then on, drilling mud was pumped through the drill stem. With a 273 mm rolling drill bit the borehole was advanced to a depth of 42 m, with casing. Because the borehole was stable and not leaking drilling mud, it was decided to continue drilling with a 241 mm rolling drill bit without casing. This was continued to a depth of 163 m, i.e. 10 metres in to the Tertiary Molasse sediments. Mud samples were taken and washed discontinuously after advancing 1 m.

ICDP 5068_1_B. The standpipe (318 mm ID) was drilled dry using an auger down to 11 m. From then on, drilling mud was pumped through the drill stem. With a 273 mm rolling drill bit the borehole was advanced to a depth of 47 m, with casing. Because the borehole was stable and not leaking drilling mud, it was decided to continue drilling with a 241 mm rolling drill bit, without casing. This was continued to a depth of 155 m, i.e. 1 m in to the Tertiary Molasse sediments. Mud samples were taken and washed discontinuously after advancing 1 m. The sediment material was accumulated on a sieve that was not cleaned after every metre. It became obvious that the sand fraction must have been completely removed during flush drilling. The flush fluid flux, fluid velocity and fluid pressure were not monitored and hence quite a large uncertainty also exists with regard to the sample depths.

Core drilling procedure

ICDP 5068_1_C. Two different coring systems were used for this borehole; 1/ a percussion drilling technique (Nordmeyer system) and 2/ a wireline rotational **SK6L** core system. The standpipe (318 mm ID) was drilled dry using an auger down to 14.6 m. Percussion coring with drilling mud began at the same time from a depth of 2 m, using 178 mm casing with a drill crown and a 101 mm coring tool. At a depth of 26.25 m, due to strong loss of drilling mud, a second casing (273 mm) was introduced and advanced to a depth of 25 m. Subsequently, this 273 mm casing was extended in line with the 178 mm casing down to a final depth of 47.7 m. On 20.10.2021, at a depth of 82.5 m, after drilling in to strongly-compacted sand, the decision was made to switch to a wireline rotational **SK6L** core system (146 mm) with 101 mm coring. Core drilling was carried out using the wireline rotational core system until the end of the borehole. Tertiary Molasse bedrock was reached at 155.35 m. We then drilled for another 10.85 m into the Molasse bedrock to exclude the possibility of drilling into an allochthonous block of Molasse, as the seismic survey and the Schneidermartin borehole (Fig. 2 & 3) had predicted such blocks. A total length of 164.25 m of core was recovered, with an overall recovery of 95% (Fig. 7). Core lengths were mostly of 1 m.

Core loss mainly occurred in the top 45 m, where core runs of 1 m could often not be completed due to technical problems with the percussion drilling technique. At 82.5 m, after the coring method was changed to a wireline rotational core system, recovery speed picked up. Recovery speed decreased again in the basal coarser units because of a significant sand component, which is prone to outwashing by the rotational technique.

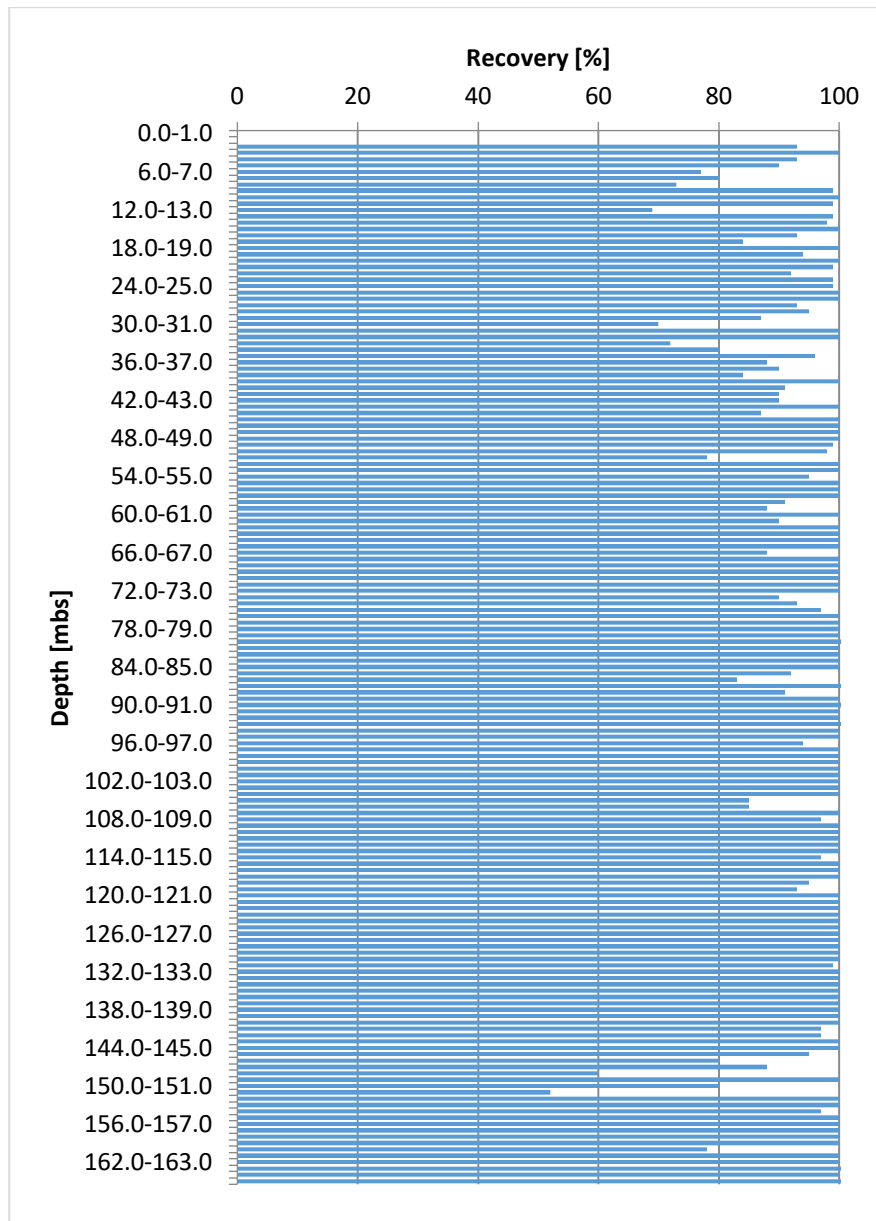


Figure 3: Recovery of the ICDP 5068_1_C drill core (total recovery 95%). Note that recovery was determined based on actual liner length. Therefore, expansion of the core due to pressure release could not be determined. Note also that possible unconsolidated re-core material falsifying the recovery could not be detected, because the cores were not opened and liners were opaque.

2.5.2. Detailed report of operations

For all boreholes, the drilling mud consisted of approximately 9 m³ of water, mixed with Antisol and bentonite (1 part to 6 parts, respectively). The ratio of additives to water was approximately 1-1.2 kg/l (Table 4).

Table 4: Drilling mud parameters over time, for the three boreholes.

Daily report No.	Day (all in 2021)	Mixing ratio (Y)	Drain time (AZ)	Remaining drain time (RAZ)	Temperature	Conductivity (LF)	Water release time (WAZ)	pH
	5068_1_A	kg/l	sec	sec	°C	mS/cm	min	
10	21 April		44.0	29.0	11.5	1.268	13.8	9.0
12	23 April		48.3	37.9	9.8	1.096	17.8	11.0
14	27 April	1.2	50.2	41.5	10.3	1.068	18.1	10.8
16	29 April	1.2	50.0	41.0	11.0	1.200	19.0	10.8
	5068_1_B							
33	02 June		50.3	40.1	10.8	1.140	18.8	11.0
36	09 June	1.2	50.3	40.1	10.8	1.140	18.8	11.0
48	15 June	1.2	50.3	40.1	12.5	1.350	18.8	11.1
	5068_1_C							
67	08 September		39.0	36.0				
68	09 September	1.0	36.0	35.0				
69	13 September	1.1	43.0	49.0				
70	14 September	1.1	46.0	43.0	14.5	0.716	13.0	7.7
72	16 September	1.1	47.0	46.0	15.9	0.728	10.0	7.7
73	20 September	1.1	43.0	39.0	13.5	0.789		7.8
74	21 September	1.1	40.0	37.0	14.7	0.755		7.9
75	22 September	1.1	45.0	43.0	13.9	0.782		7.8
76	23 September	1.1	55.0	53.0	13.9	0.756		7.9
78	28 September	1.1	38.0	36.0				
79	29 September	1.1	39.0	36.0			10.0	
91	21 October						17.0	
92	25 October						31.0	
93	26 October	1.1	32.0	27.0			34.0	
95	28 October	1.1	33.0	27.0			38.0	
96	01 November	1.1	34.0	28.0			36.0	
97	02 November	1.1	35.0	28.0			40.0	
98	03 November	1.1	33.0	26.0			41.0	
100	05 November	1.1	33.0	26.0			48.0	
106	15 November	1.0	34.0	28.0			35.0	

Problems that occurred during drilling

Flush drilling ICDP 5068_1_A

- 22nd April – Breakdown of electrical generator. The generator was replaced.
- 4th May – Breakdown of the next electrical generator. New generator rented and then replaced.
- 17th May – The drill rig could not pull out the casing out of the first borehole. A hydraulic press was used to raise a bar that was temporally welded to the casing. Finally, the casing was raised after 2 days delay.

Flush drilling ICDP 5068_1_B

- 9th June – Strong loss of drill mud. Remedied by sinking the casing deeper and raising the viscosity of the drill mud.
- 9th June – High-pressure hydraulic pipe bursts. This was replaced in a few hours.
- 15th June – Strong loss of drill mud. Remedied by sinking the casing deeper.

6.3.3 Core drilling ICDP 5068_1_C

- 25th August – A large (metamorphic and calcareous) rocks in the top 10 m of the borehole cause the crown of the coring body to be damaged (bent). The same crowns are used until 30th August, until the firm creates a stronger, reinforced crown with spikes on the top edge. This is used from 31st August onwards.
- 1st September – Pump on the drill rig breaks down due to a fault in a solenoid valve. Electrical engineers are called out to fix the problem. Problem fixed by 6th September.
- 7th September – Piston rod of drill rig broken. Problem fixed by 8th September.
- 8th September – Drill crown worn out due to attrition. Replaced by 9th September.
- 13th September – Loss of flush drilling fluid is too large. Driller decides to add additional casing (273 mm). Done by 14th September.
- 15th September – Drill crown worn out due to attrition again. Replaced by 20th September.
- 23th September – Drill rig is out-of-balance. Repaired by 28th September.
- 29th September – Chuck head of drill rig broke. Repaired by 4th October.
- 6th October – Supply difficulties with new crown. Crown arrives at the same day.
- 14th October – Supply difficulties with crown. Crown arrives at 19th October.

Summary of progress

Figure 8 shows the depth of the three boreholes over time. ICDP 5068_1_B was quicker than ICDP 5068_1_A because the geology and its physical properties were better known after the first borehole had been drilled. From Fig. 8 it is also clear that drilling became faster with depth in the flush boreholes; this is because the lower lithologies, being finer and more homogenous, were easier to drill. The obvious kink in the drilling progress at ca. 40 m in both wells is caused by the changing of the drill bit and casing at this level. By comparison, coring took twice as long. Ramming to depth of 82 m took over two months, coring then became easier using rotary core technique and also it was easier to core the lower lithologies. Thus, contrary to other drilling campaigns, we have the unusual situation that the drilling became faster with depth.

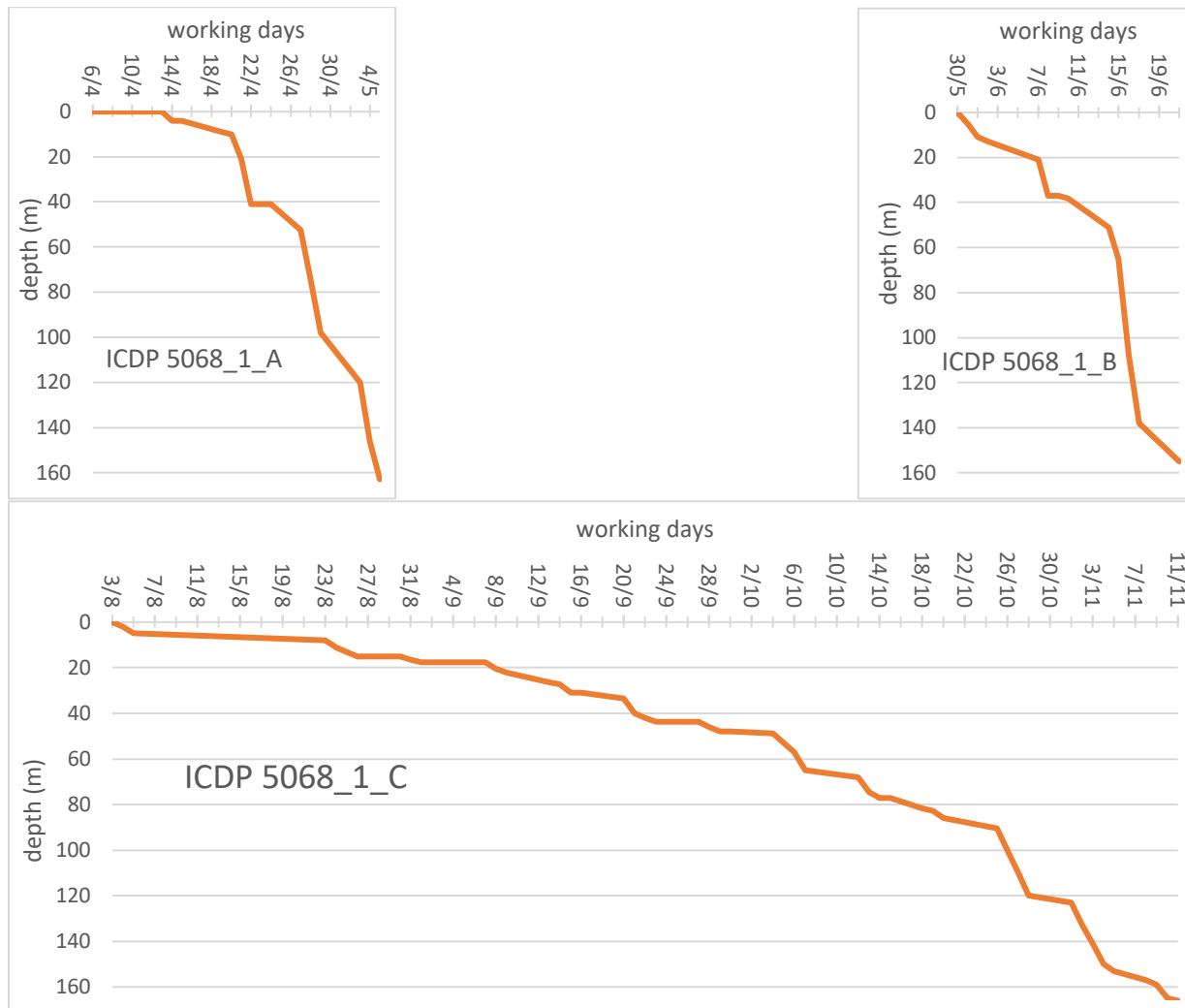


Figure 8: Depth/time plots for the three boreholes, at the same scale.

2.5.3. Borehole deviation

The borehole geophysics, run in ICDP 5068_1_A and ICDP 5068_1_C, also measured borehole deviation (Figs. 9 and 10). 5068_1_A first plunges south-eastwards for 0.5 m, before heading north and north-west to be 3.5 m due north of the origin. 5068_1_C is closer to vertical; it plunges near-straight north-westwards, northwards by 2 m and west by 1 m. This information is necessary to obtain true-vertical depth, especially for geophysical modelling.

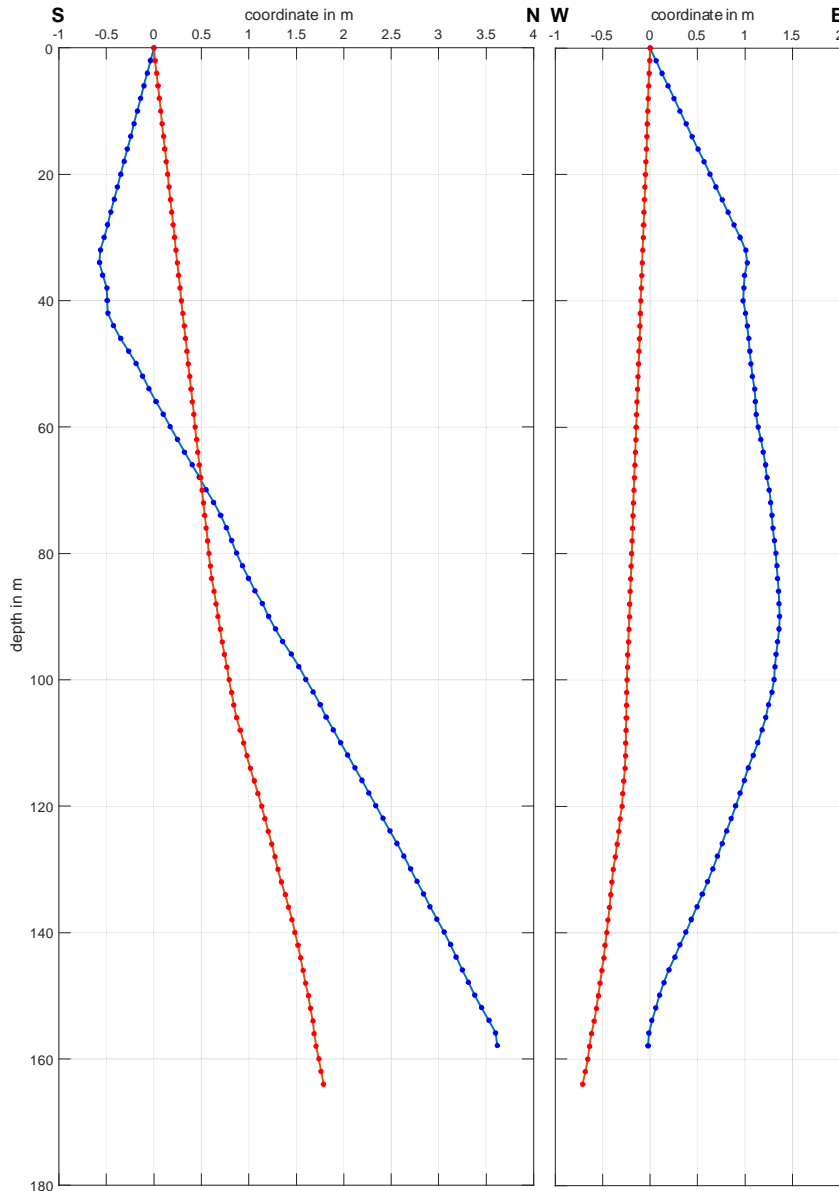


Figure 9: Deviation of ICDP 5068_1_A (blue) and ICDP 5068_1_C (red) in the S-N and E-W planes.

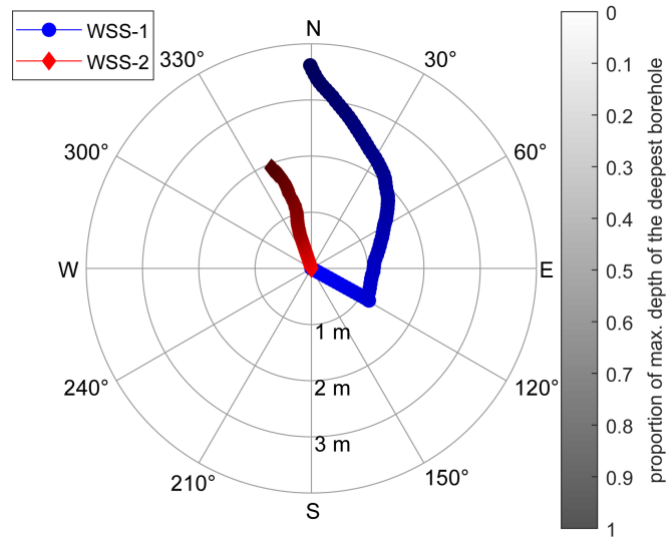


Figure 10: Deviation of ICDP 5068_1_A (blue) and ICDP 5068_1_C (red) in polar view.

2.5.4. Refilling and post-drilling finishing procedure

All three boreholes were finished by inserting a DN80mm plastic pipe, with a 1-metre filter (in ICDP 5068_1_C, 3 m) at a certain depth. In the first, second and third boreholes, filters were placed at depths of 153 m, 45 m, and 153 m, respectively. The annular spaces of the first and second drill holes were then backfilled with bentonite pellets, except for the depths of ca. 5 m around the filters, which were backfilled with fine gravel. Because the third drill hole was very narrow, it was decided to backfill its annular space to a depth of 82 m first with gravel, and from 82 m on to the surface with bentonite (Fig. 12).

At the surface, all three boreholes were closed using a lockable SEPA cap below the ground level (Fig. 11), and covered by a lockable manhole cover at ground level.



Figure 11: SEPA lockable borehole cap on top of a DN80 mm pipe.

2.5.5. Borehole geometry and preliminary lithology assessment

The final geometries of the boreholes 5068_1_A, B, C are shown in Figure 12A-C, respectively. A preliminary geological interpretation is shown on the left-hand side. Note the position of the filters, close to the base of the Quaternary basin at 153 m depth in 5086_1_A and C, and at the depth of 45 m in 5086_1_B.

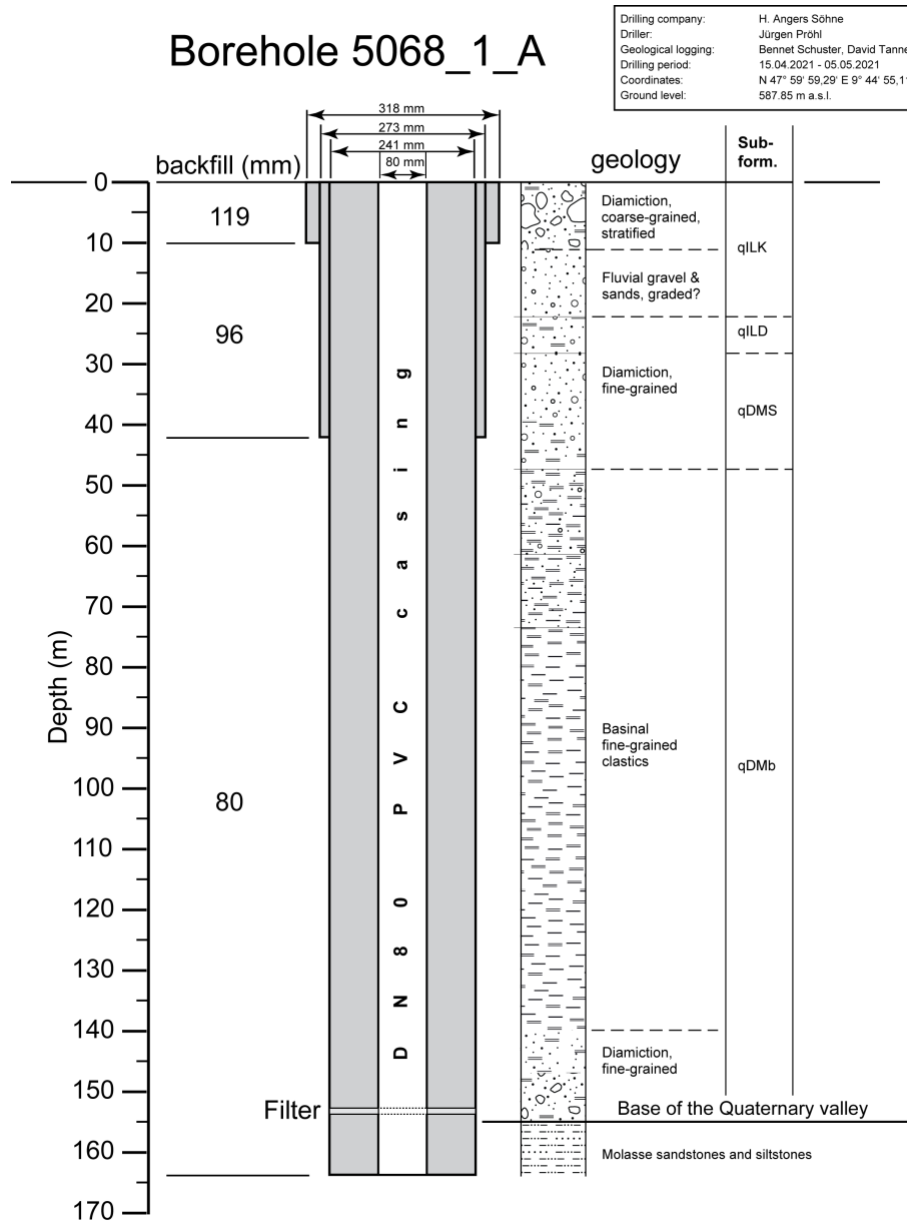


Figure 12A: Final geometry of the borehole 5068_1_A. Preliminary Quaternary subdivisions: qLK – Kisslegg Subformation (Wurmian); qLD – Illmensee basin sediment (Rissian – Wurmian), qDMS – Scholterhaus Subformation (Rissian), qDMb – Dietmanns basin sediments (Hosskirchian – Rissian). Molasse sandstones are Tertiary (Miocene) in age.

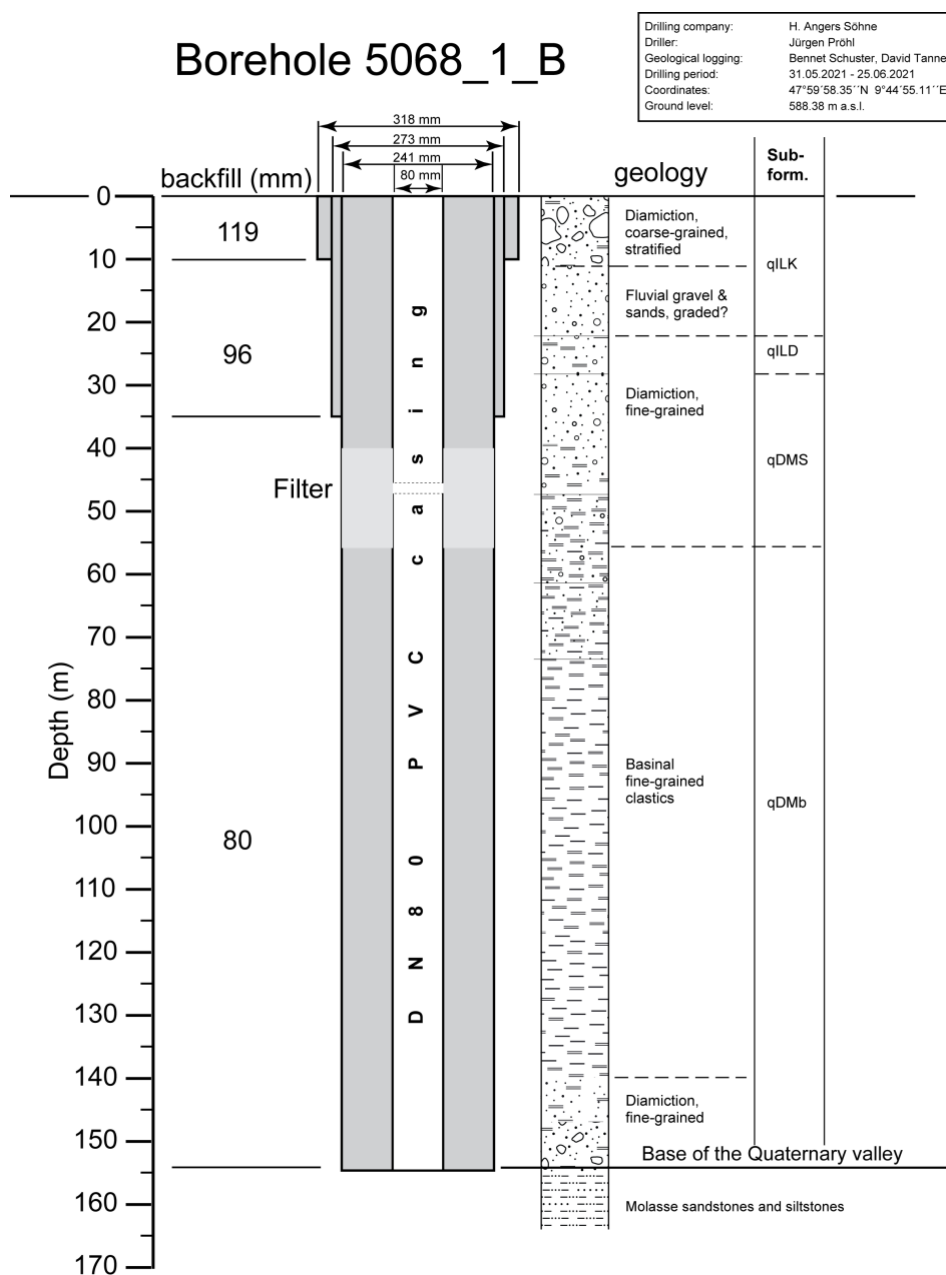


Figure 12B: Final geometry of the borehole 5068_1_B. Preliminary Quaternary subdivisions: gLK – Kisslegg Subformation (Wurmian); qLb – Illmensee basin sediment (Rissian – Wurmian), qDMS – Scholterhaus Subformation (Rissian), qDMb – Dietmanns basin sediments (Hosskirchian – Rissian). Molasse sandstones are Tertiary (Miocene) in age.

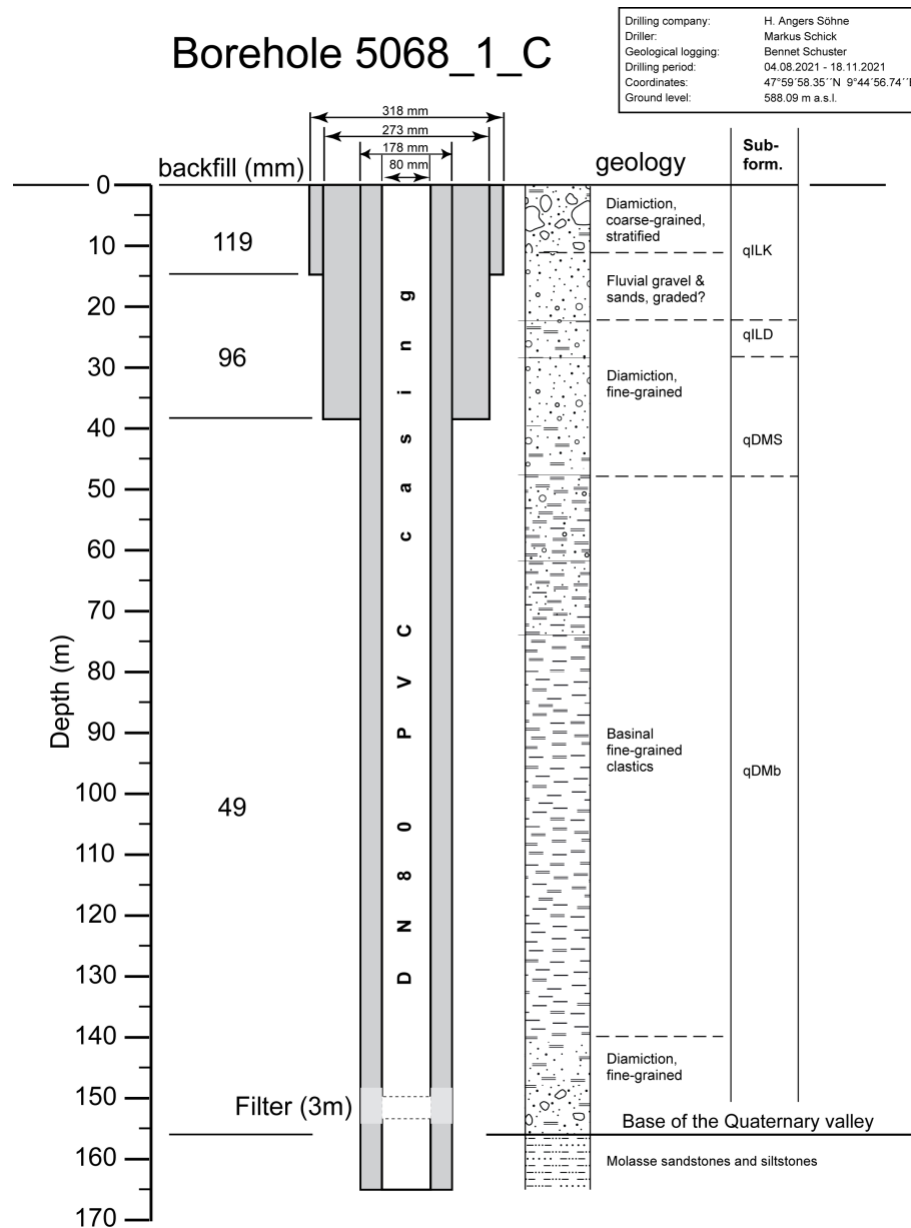


Figure 12C: Final geometry of the borehole 5068_1_C. Preliminary Quaternary subdivisions: gLK – Kisslegg Subformation (Wurmian); qLb – Illmensee basin sediment (Rissian – Wurmian), qDMS – Scholterhaus Subformation (Rissian), qDMb – Dietmanns basin sediments (Hösskirchian – Rissian). Molasse sandstones are Tertiary (Miocene) in age.

The ICDP 5068_1_C drill hole penetrated a succession of gravel-dominated, partly diamictic units (Fig. 12C). Below 38 m the sediments become finer, mostly silt dominated with varying clay content, occasionally interrupted by sand units (e.g., at 73–81 m and 99–104 m). In this section, rare outsized clasts were visible and indicate the presence of dropstones. At 136 m, the sediments become coarser and well-sorted sand units alternate with fine-grained diamicts, occasionally containing a significant amount of gravel. Sand becomes dominant at 149 m and the bedrock Tertiary Molasse deposits were

encountered at 155 m. The bedrock is marly in appearance at the top (including macroscopically-observable fossil fragments), occasionally transected by pure sandstone. The occurrence of sandstone increases towards the bottom and finally dominates from 164 m to the final depth of 166 m.

DOVE Quarternary Flush Drilling in Winterstettenstadt Tannwald Basin, Borehole ICDP 5068_1_A							DOVE Quarternary Flush Drilling in Winterstettenstadt Tannwald Basin, Borehole ICDP 5068_1_B							
Drilling company: Driller: Geological logging: Drilling period: Coordinates: Ground level:		H. Angers Söhne, Gutenbergstr. 33, 37235 Hess. Licht. Jürgen Prohl Bennet Schuster, David Tanner 15.04.2021 - 05.05.2021 N 47° 59' 59,29" E 9° 44' 55,11" 587.85 m a.s.l.					Drilling company: Driller: Geological logging: Drilling period: Coordinates: Ground level:		H. Angers Söhne, Gutenbergstr. 33, 37235 Hess. Licht. Jürgen Prohl Bennet Schuster, David Tanner, Julia Silov-Tepic 31.05.2021 - 21.06.2021 N 47° 59' 58,39" E 9° 44' 55,10" 588.38 m a.s.l.					
Coring tool	Preliminary interpretation	Sub-form.	Elev. [m a.s.l.]	Composite depth [m]	Sed. struct.	Lithological description	Coring tool	Preliminary interpretation	Sub-form.	Elev. [m a.s.l.]	Composite depth [m]	Sed. struct.	Lithological description	
Auger / Coring Bit (318 mm)	Diamiction, coarse-gained, stratified	qILK	586.85	1.0		Gr/Sa, osi/ocl, co/bo Gr/Sa, si, co/bo	Auger / Coring Bit (318 mm)	Diamiction, coarse-gained, stratified	qILK	587.38	1.0		Gr/Sa, osi/ocl, co/bo Gr/Sa, si, co/bo	
	Fluvial gravels & sands		576.85	11.0		Gr/Sa		577.38		11.0		Gr/Sa		
			571.85	16.0		Gr/Sa, si at top		567.38		21.0		Gr/Sa, si at top		
		568.85	19.0		qLD			561.38	27.0		Gr/Sa, locally si			
		565.85	22.0					546.38	38.0		Gr/Sa, si, cl			
	Fluvial gravels alternating with diamiction	qDMS	559.85	28.0		Gr/Sa, locally si		qDMS	533.38	55.0		Si, cl, sa, gr		
			548.85	39.0		Gr/Sa, si			516.38	72.0			Si, cl/Cl, si	
		Diamiction, fine-grained	qDMb	540.85	47.0			Si, sa/gr, cl at top	qDMb	Basinal fine-grained clastics	491.38	97.0		Si/Cl, sa, gr
				526.85	61.0			Si, sa/Si, cl			480.38	108.0		
	514.85			73.0		Si, cl/Cl, si		452.38			136.0			
	508.85			79.0				Upper Marine Molasse			436.38	152.0		
	503.85			84.0							Molasse sand- and siltstones			
	495.85			92.0										
	Diamiction		483.85	104.0		Sa, gr, si/Si, sa, gr								
			471.85	116.0		Gr/Sa, si								
			450.85	137.0		Si, f, sa								
			448.85	139.0										
			441.85	146.0										
			433.85	154.0										

Figure 13: Preliminary profiles of the two flush boreholes ICDP 5068_1_A (left) and 5068_1_B (right). Larger stratigraphic units are linked to subformations found in the Schneidermartin research borehole (Fig. 2). Note that the lithological description uses the following abbreviations (capital letters for main components): boulders (Bo/bo), cobbles (Co/co), gravel (Gr/gr), sand (Sa/sa), silt (Si/si), clay (Cl/cl), organic silt (Osi/osi), organic clay (Ocl/ocl).

The flush drilling samples observed on-site have little potential to represent the lithologies encountered at depth, if not compared with existing information on the regional geology. However, the local geological setting is well documented based on extensive seismic p-wave survey (Burschil et al., 2018), geological maps, and the detailed description of an archived drilling (Schneidermartin

borehole, see Figs. 2 and 3, and Buschil et al. 2018). Thus, with the help of this information, we were able to detect certain changes and connect them to units of the Dietmanns and Illmensee Formations. Two sedimentary profiles were constructed (see Fig. 13). Although these interpretations are preliminary and based on the flush boreholes, they still show the very local extent of known lithologies. Furthermore, they were useful for orientation during the core drilling, preparation for lithological changes while coring, and to enhance core quality.

Despite the limitations related to the interpretation of the cuttings from holes 5068_1_A and 5068_1_B, close monitoring of the lithologies during drilling in all three boreholes (by observing flush drilling samples, and surfaces at the top and the bottom of the drilled cores) allowed us to determine small-scale changes in the glacial-interglacial deposits between the three drilling locations. In only ca. 28 m distance between the two flush boreholes, the qDMS unit (Fig. 13) has a thickness difference of 9 m. Also surprising is the much thicker than expected uppermost qILK gravel layer (Fig. 13), despite its location on the western flank of the basin.

2.6. Scientific operations on-site

The scientific operations for the flush drillings were coordinated by the Leibniz Institute for Applied Geophysics, Germany, and the scientific operations for the core drilling were coordinated by the University of Freiburg, Germany. For the two flush drillings, two scientists were on-site all the time during the operational phase from the 12th April until the 1st July 2021. One scientist was on-site to accompany the core drilling from 4th August until the 11th November 2021 and was supported by a second scientist in the case of additional work, e.g. publicity.

2.6.1. Workflow flush drilling

At every metre of drilling, approx. 1 – 1.5 kg of drill cuttings from the drilling mud (known as cuttings in mDIS) was sampled using a large 0.5 mm mesh sieve. The sample was then carefully washed in water to remove most of the mud. At the geologist's table, a small portion (< 50 g) of the sample was placed on an aluminium tray. The rest of the sample was weighed and stored. The details, shown in Fig. 14, were noted, as applicable. For fine-grained material or grain characteristics, the sample was viewed with a hand lens or stereo, light-reflecting microscope. Finally, the sample in the aluminium tray was photographed for reference.

Each cuttings sample was stored in a clear plastic container with a lid. Each container was labelled with an ICDP label that contains a QR code and unique identifier of the sample. The details of each sample were then uploaded in to ICDP's database, the mDIS (mobile Drilling Information System).

Identifier and drillers information			
Project/Site		Curator	
Depth [m]		Day/Time	
Sieve [mm]		Comment by Driller	
Unwashed sample			
Sample weight [g]		Inferred Lithology	
Sorting		Colour	
Max grain size [mm]		Perc. Rock Clasts	
Perc. Mud clasts		Max diameter Mud clasts [mm]	
Comments			
Cuttings from rock clasts (> 2 mm)			
Petrography		Roundness	
Shape		Surface Texture	
Fossil		Plant remains	
Intact mud/matrix cuttings (> 2 mm)			
Internal Structures		Consistency	
Smear slide?			
Microscope analysis (< 0.2 mm)			
Petrography		Roundness	
Fossil		Plant remains	
Accessory Minerals			

Figure 14: The form used to document cutting samples from the flush drillholes.

2.6.2. Workflow drill-core handling

The on-site science team was present at the drill rig when each core was pulled on deck, noting timing and other details about the specific drilling procedure on the core run protocol. We inspected the bottom face of the core, conducted a first lithological assessment, and, when appropriate, sampled and/or photographed it. The drill team then pulled out the drill core in its plastic liner and transported it to a pipe handling rack, noting top and bottom depths. If the core was less than one metre long, the core liner was shortened accordingly to stop core material moving during transport. If excess material was present at the top of the core from drilling the casing after the last core run (re-core material), it was sampled in addition (cutting sample). If the quality of drilling was not satisfactory we discussed possibly reasons for core loss with the drilling team and were prepared to adjust drilling technology, bit type, or drilling fluid composition at any given time.

After the caps were taped on at each end of the liner, we received the closed liner from the drilling team and transported it to the geologist's core handling table. We then proceeded to label the liner, measure the total weight and length of the drill core/liner, and placed the drill core in a wooden box. The wooden

core boxes were transferred to a cool storage room in the community centre of Winterstettenstadt the next evening, where the local authorities were kind enough to let us store the cores temporarily. We packed the core boxes on to pallets and transported them to the long-term cool storage at the Emmi Group AG, Bern, on the 3rd December 2021.

We continuously uploaded drill core metadata (number of core run, length of core run, time of core on deck, sections, length of sections, weight of sections, information on core loss, coring technology, onsite lithological description of core bottom, samples) to mDIS. Hole, Core, and any kind of sample were automatically assigned an IGSN (International Generic Sample Number). All samples were labelled.

2.6.3. On-site sampling

Biosphere sampling

We took samples to investigate microbial activity within the sediments at intervals of 3 m throughout the whole core. For this, preferably fine-grained sediment was sampled at the bottom of the core or the top of the removable core-catcher (85 cm in-section depth). Wearing gloves, we performed the sampling directly after the core was recovered in order to preserve the biological material and minimize contamination. The biosphere samples consist of two parts: The first part is the DNA sample. We used a sterile plastic syringe to punch out about 2 cm³ of sediment and push it into a plastic tube (Fig. 15, left). The second part of the sample is the additional material sample. We used a conventional spatula that was sterilized with ethanol to fill about 20 cm³ of sediment in a second plastic tube. This sample is reserved for optional additional measurements or as backup for the DNA sample. We stored the samples temporarily in a cool box, before freezing them the following evening. We took fifty-three samples and, after the drilling was completed, we send them to the University of Geneva for further investigation, planned to start in February 2022.



Figure 15: Left, taking a bio sample from the core. Right, vessel used to store samples for noble gas.

Noble-gas pore water sampling

We took bulk sediment samples of preferably fine-grained clastic materials with trapped pore water. We took the samples, similar to the biosphere samples, as early as possible after the core was recovered, just so as little volatiles as possible could escape the pore water. If possible (depending on type of sediment), we took cohesive chunks of material to capture and preserve as much pore-water as possible. The samples were stored in special containers, from which noble-gas concentrations will be measured directly (Fig. 15, right). We developed a sampling strategy in advance, based on findings from the nearby boreholes, existing geological mapping and the results from the first two flush drillings. Due to geological uncertainties, we often had to adjust the sampling distance, which is why the aspired sampling interval of about 13 m could not always be kept. We took a total of 14 samples. After drilling, we sent the samples to the Swiss Federal Institute of Aquatic Science and Technology on the 3rd December 2021 for further analysis. The samples will be used to date the glacial sediment succession using the ⁴He/U-Th method on the pore water.

MSCL geophysical core logging

The following sensors were used: gamma attenuation, core diameter deviation, P-wave travel time and magnetic susceptibility. This resulted in processed data for: density (calculated from gamma attenuation and core diameter), P-wave velocity (calculated from an automatically picked P-wave travel time and core diameter), and corrected volume specific magnetic susceptibility (calculated from sensor loop and core diameter). The MSCL dataset provides valuable data on rock/sediment density and magnetic susceptibility. However, P-wave velocity values are constantly low and of poor quality, therefore, they were not published. For details please see Explanatory Remarks.

2.6.4. Downhole geophysical measurements

Downhole geophysical measurements were conducted upon completion of the drilling operations of Hole 5068_1_A from 10.-11.05.2021 and Hole 5068_1_C from 11.-12.11.2021. After equipping the boreholes with PVC pipes all three holes 5068_1_A, 5068_1_B and 5068_1_C were logged from 09.-10.03.2022. Thomas Grelle and Carlos Lehne from LIAG carried out all the downhole geophysical measurements in the three campaigns.

In the first two campaigns, the first measurement was made using spectral gamma ray SGR (i.e., the instrument measures gamma ray (GR) plus K (wt%), Th (ppm), and U (ppm)) along the entire length of the borehole through the drill string. The drill string was then removed by the drill crew to a depth that precluded collapse of the borehole. The remaining probes were deployed in the open hole interval:

- CAL; Caliper (in perpendicular directions, in mm),
- DEV and DAZ; Deviation and deviation direction (in degrees from the horizontal and from north, respectively),
- DIP; Dipmeter (including CAL, DEV, DAZ plus the dip of geological strata)
- DLL; Resistivity (in Ω m, both near- and far-field),
- NN: Porosity (%),
- PE: Photoelectric absorption (barns/electron; b/e) and density (g/cm³ in Fig. 16),
- SALTEMP: Salinity (mS/cm) Temperature (°C) of the borehole fluid,
- SONIC; Seismic velocity (in m per second),
- SUSZ; Magnetic susceptibility (10⁻⁴ SI in Fig. 16).

In the third measurement campaign, in which LIAG surveyed the boreholes that had in the meantime been equipped with PVC pipes, only a limited measurement program could be carried out. In addition to the SGR, SONIC and SUSZ probes, it also includes our Array Induction Tool (AIND), which measures the electrical conductivity of the rock. However, it can only measure up to a few hundred Ωm . With our BHTV probe we tried to be able to see behind the PVC piping; however, this was not successful. The only information that can be obtained from this data is the location of the filter section and the borehole lining with the PVC pipes.

On 6th-8th July 2021, Jan Bayerle and Thomas Burschil from LIAG also carried out Vertical Seismic Profiling (VSP) measurements on boreholes 5068_1_A and 5068_1_B. Two types of VSP were acquired, i.e., zero offset and walk-away VSP measurements, in both boreholes. These measurements are still being processed.

Table 5: Wire-line logging overview. Tool abbreviations: AIND: Array Induction (electric conductivity), BHTV: Borehole Televiwer, CAL: Caliper, DIP: Dipmeter, DLL: Dual laterolog resistivity, GR: Gamma Ray, NN: Neutron porosity, PE: Density/Photoelectric factor, SGR: Spectral Gamma Ray, SONIC: Sonic log (seismic velocity), SUSZ: Magnetic susceptibility, TEMPSAL: Temperature and salinity of mud. Other Abbreviations: OH: measurements in open hole, CH: measurements in cased hole, OD: outer diameter.

Date/Hole	Run	Parameter	From [m]	To [m]	Hole Condition
10./11.05.2021 5068_1_A	1	CAL	160	43	OH
	1	DLL	160	43	OH
	1	NN	160	43	OH
	1	PE	160	43	OH
	1	SGR	143	0	CH
	1	SGR	160	130	OH
	1	SONIC	160	43	OH
	1	SUSZ+GR	160	43	OH
	1	TEMPSAL+GR	0	160	OH+CH
Remarks: Casing 0-43 m: 273 mm OD					
11./12.11.2021 5068_1_C	2	BHTV	164	85	OH
	2	DIP+GR	164	85	OH
	2	DLL	164	85	OH
	2	NN	164	20	OH+CH
	2	PE	164	10	OH+CH
	2	SGR	164	0	CH
	2	SONIC	164	85	OH
	2	SUSZ+GR	164	85	OH
	2	TEMPSAL+GR	0	164	OH+CH
Remarks: Drill string retracted 85 m					
09./10.03.2022 5068_1_A_3	3	AIND+GR	97	0	CH
	3	AIND+GR	155	95	CH
	3	BHTV	155	45	CH
	3	SGR	155	0	CH
	3	SONIC+GR	155	45	CH
	3	SUSZ+GR	120	105	CH

Remarks: -					
10.03.2022 5068_1_B_3	3	AIND+GR	145	40	CH
	3	BHTV	145	40	CH
	3	SGR	145	0	CH
	3	SONIC+GR	145	40	CH
	3	SUSZ+GR	145	0	CH
Remarks: -					
09./10.03.2022 5068_1_C_3	3	AIND+GR	165	0	CH
	3	BHTV	165	30	CH
	3	PE	165	0	CH
	3	SGR	165	0	CH
	3	SONIC+GR	165	50	CH
	3	SUSZ+GR	165	50	CH
Remarks: -					

2.7. Storage, initial core description and 1st sampling party

2.7.1. Sites 5068 1 and 5068 2

Prior to opening and initial core description and 1st sampling, the drill cores were stored in the cold-storage (4 °C) facility at the Institute of Geological Sciences, University of Bern and at Eawag Dübendorf. The sampling party and initial core description took place from 09/2022 to 02/2023. Each core section was cut, opened, and split lengthwise into an archive half for non-destructive analyses and a working half for physical sampling. The following work was conducted on each archive half: A high-resolution line scan was obtained, and each section was sedimentologically described and documented on a log sheet. The focus of these descriptions was: i) the dominant grain size; ii) type and thickness of bedding; iii) color; iv) contacts between different beds; v) secondary sedimentary structure; vi) quality of the core section; and vii) an overview of clast lithology and morphology. Furthermore, undrained shear strength (c_u') and undrained uniaxial compressive strength (q_u') were measured at 25, 50, and 75 cm section depth where applicable with a pocket vane-shear tester and a pocket penetrometer. Sedimentary lithotypes were defined and described based on the combined findings, and the whole sediment succession was assigned to the best-fit lithotype. X-ray computed tomography (CT) images of selected core sections were taken. Each working half was sampled for: i) grain-size distribution; ii) total inorganic and organic carbon (TIC and TOC); and iii) water content. Smear slides have been taken from interesting silt/clay-rich sections. Based on the line scans, samples were taken for a first screening of pollen content, luminescence dating, cosmogenic nuclide burial dating, and geotechnical analyses). After completing the description and the sampling campaign, the core halves were sealed in lightproof black foil, stored in standard-sized wooden boxes, and labelled according to the ICDP guidelines. After processing, the cores were sent to a large cool storage facility of the Emmi AG (Milchstrasse 9, 3012 Ostermundigen, Switzerland), where they are stored currently at the date of this report (August 2023). Till the end of the official moratorium (December 2024), access to samples/core is only possible by contacting Flavio Anselmetti or Gerald Gabriel.

2.7.2. Legacy sites 5068 3 through 5068 6

2.8. Site-specific preliminary scientific assessment

2.8.1. Geology

See Chapter 2.5.5 for the preliminary lithological assessment and Figures 12 A- C and 13 for a graphical overview of the lithological units.

2.8.2. Borehole Geophysics

The Explanatory Notes describe in detail how the pre-processing of the data of the three measurement campaigns was carried out. This includes, among other things, the matching of the depths of the individual measurements, the elimination of false measurement data, the splicing of measurement curves etc. With this knowledge it can be understood how to get from the raw data to the respective composite dataset, which is e.g. the basis for the presentation of the measurements in 5068_1_A (Fig. 16). At this stage of the project, the temperature values and gradient are disregarded because the measurements were taken a few days after drilling, before the temperature in the borehole could re-equilibrate. The temperature profile will be remedied by later downhole logging.

Resistivity is high ($>50 \Omega\text{m}$) around 50 m depth, gradually sinking with depth down to 95-105 m, where, in unison with the Spectral Gamma Ray (SGR), it irregularly rises to higher values, before returning to the background (clay) values of $10\text{--}20 \Omega\text{m}$ until 137 m: Here similar to SGR, the basal units have a very high value (up to $100 \Omega\text{m}$) before returning to very low values in the Tertiary Molasse. Magnetic susceptibility shows very little change apart from a very large peak at 140 m (which must be considered an artefact, possibly caused by a piece of metal, perhaps from the drill bit) and slightly higher values in the Molasse. When this artefact is removed, the magnetic susceptibility may show more detail. Seismic velocity (V_p) is between 1700-1900 m/s at 50 m depth, peaking at 2200 m/s at the geophysical anomaly at 95-110 m depth. The sharp Quaternary base at 154 m is very clear in all measurements.

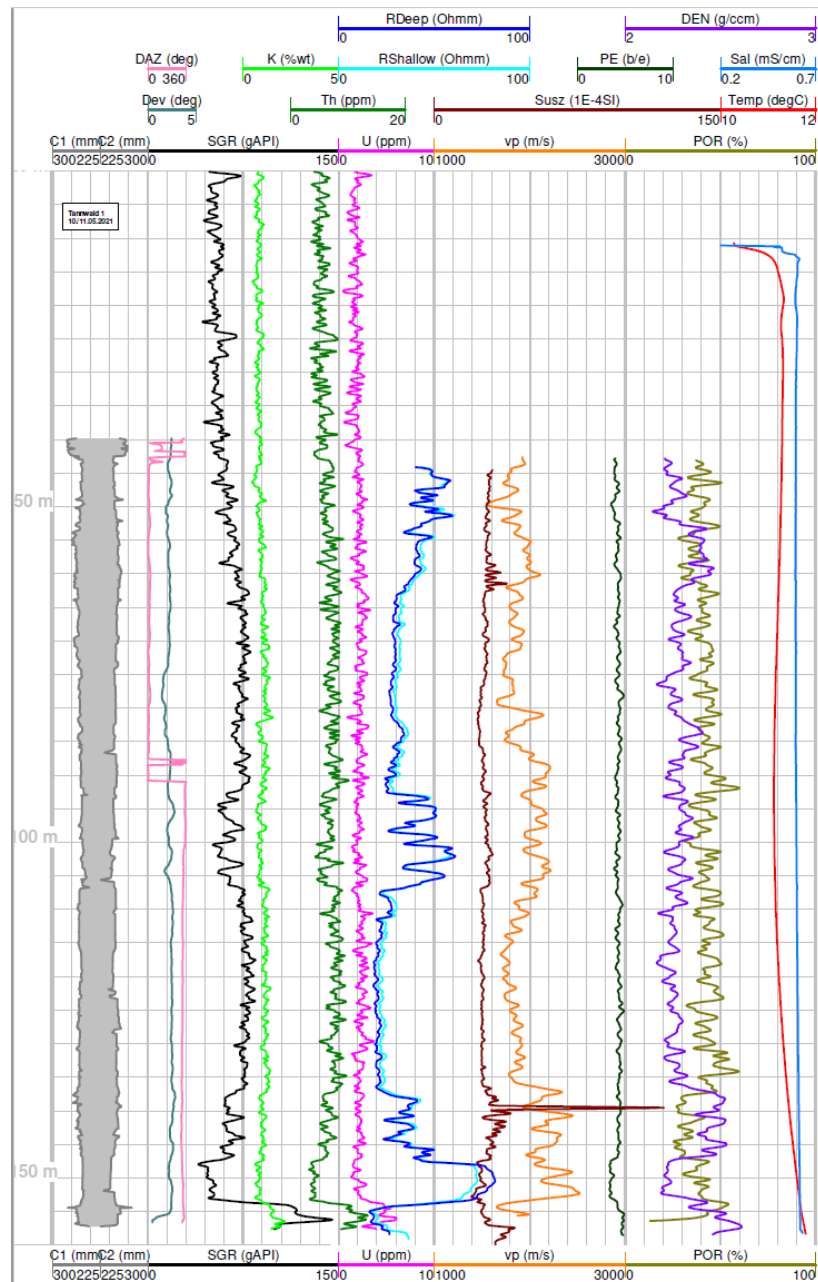


Figure 16: Results of the downhole geophysical measurements on the open hole of 5068_1_A.

3. Site 5086_2

3.1. Site Introduction

This section documents the drilling operations at ICDP Site 5086_2 that explored the sedimentary infill of the glacial overdeepening ‘Basadingen Trough’ located in the western Rhine-paleoglaciar area (Müller, 2010). The scientific objectives and approach of the DOVE project are explained in detail in Anselmetti et al. (2022). The initial core description and interpretation of the cores from the Basadingen Trough (ICDP 5068_2_A) are presented in Schaller et al. (2023). For more details on the operations at the drill site also see Büchi et al. (2023).

3.2. Personnel in the Operational Phase

Technical project management and supervision

Marius W. Buechi, University of Bern, Switzerland
Flavio Anselmetti, University of Bern, Switzerland

Project and on-site science coordination

Sebastian Schaller (Ph.D. student), University of Bern, Switzerland
Bennet Schuster (Ph.D. student), University Freiburg, Germany
Marius W. Buechi, University of Bern, Switzerland
Flavio Anselmetti, University of Bern, Switzerland

Downhole geophysical measurements (LIAG, Hanover)

Hermann Buness, Leibniz Institute for Applied Geophysics, Hanover, Germany
Thomas Grelle, Leibniz Institute for Applied Geophysics, Hanover, Germany
Thomas Wonik, Leibniz Institute for Applied Geophysics, Hanover, Germany

External drilling advisor

Luka Seslak, Nagra, Hardstrasse 73, 5430 Wettingen, Switzerland

Drilling company (Fretus AG, Bad Zurzach)

Alex Küng (company liaison)
Lukas Seiler (company liaison)
Juan Gonzalez (driller)
Marek Bajcura (driller assistant)
Joaquim Teixeira (driller assistant)

Hydrogeological supervision

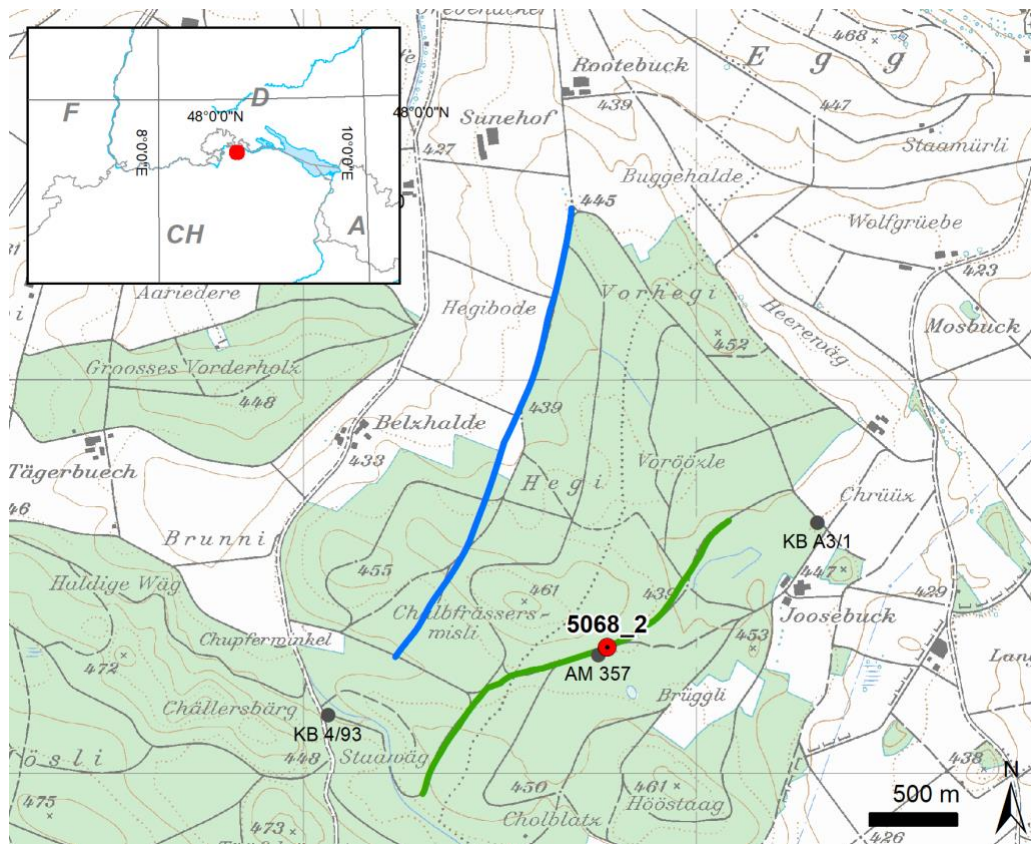
Lawrence Och, Dr. von Moos AG, Zurich, Switzerland

Off-site assistance & data management

Katja Heeschen, ICDP-OSG, GeoForschungsZentrum Potsdam, Germany

3.3. Site selection and permits

To determine the best location for the BASA drill site, LIAG (Leibniz Institute for Applied Geophysics, Hannover, Germany), in collaboration with ETH Zurich (Switzerland), acquired two high-resolution P-wave reflection seismic profiles across the Basadingen overdeepening in September 2019 (Fig. 17; Approval by Kanton Thurgau, Departement für Bau und Umwelt, 61.03). The resulting seismic sections revealed the general shape of the overdeepening as well as a potentially multiphase internal facies architecture, which was found in both profiles (Brandt, 2020). The central part of profile 2 (Fig. 18, ca. CDP 640-680) seemed most suited for drilling because all seismically mappable units could be cored by one vertical well.



At this site, located just N of the basin axis, the depth to bedrock was estimated to 240 m but considerable depth uncertainty was expected as only a simplified depth conversion had been applied (Brandt 2020). Minimal well control was provided from an archived description of a nearby flush drilling conducted in 1984 (AM-357, ca. 30 m WSW) with final depth of 201 m that did not reach bedrock (Müller, 2010).

The responsible authorities (mainly 'Politische Gemeinde Basadingen-Schlattingen' and 'Amt für Umwelt Kanton Thurgau') decided that the permission would be coordinated under the regular building permit procedure ('Baubewilligung'). The final building permit (No. 2021-0002 / 2021.01-122) was handed in on 11.01.2021, open for public consultation between 15.01. and 04.02.2021 and granted on 10.04.2021. The building permit included a permit for a temporary clearing of forest area around the drill site ('Rodungsbewilligung').

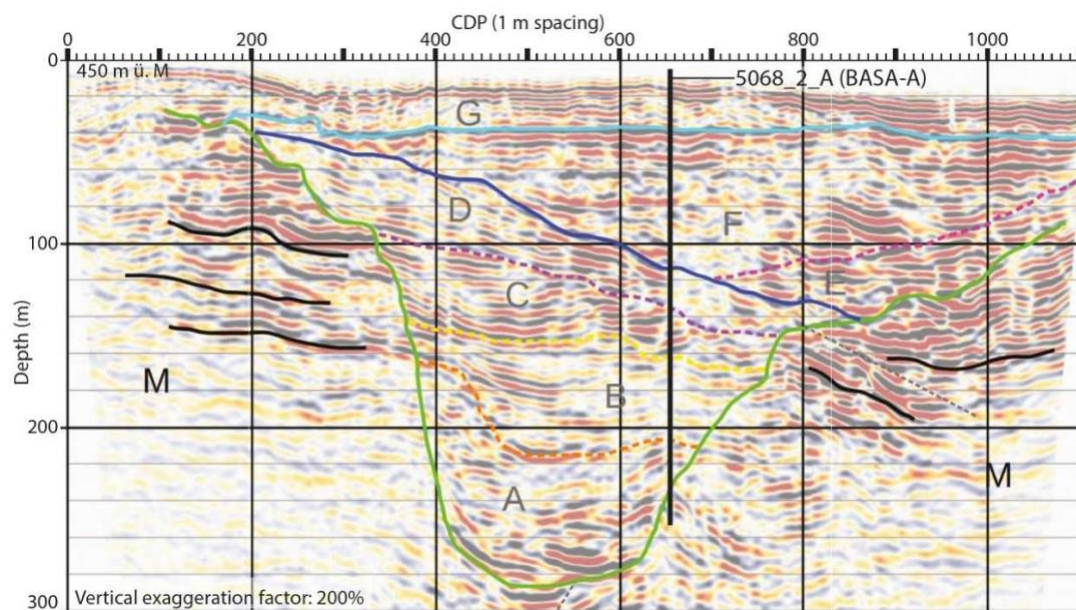


Figure 18: Pre-drilling interpretation of the seismic section 2 across the Basadingen Trough with the position of the final drill site (for location see Fig. 17, Brandt, 2020). M = bedrock (Molasse); green line = Base Quaternary; A-G = Seismic units; Black vertical line = drillhole 5068_2-A (BASA-A) with predicted bedrock at ~240 m depth. From Brandt 2020; see Schaller et al. (subm.).

3.4. Site preparation and infrastructure

After a joint visit of the drill site by representatives of the University of Bern, the drilling contractor (Fretus AG, Bad Zurzach) and the local authorities, landowner, forester and hunters on 21.4.2021, the final position of the drill point was marked (see Table 6) and the site was prepared for the operational phase. The forester moved wooden material to the backside of the open area and had to fell one tree close to the road. The remaining preparatory work was organized and installed by the drilling contractor (Fretus AG, Bad Zurzach) in accordance with the permit (Fig. 19).

Table 6: The coordinates of the final drill point at the surface.

Reference system	Coordinates	Ground elevation
CH1903+/LV95	2'698'774 / 1'278'321	445.1 m ü. M.
WGS84 *	47.648095564°N, 8.753256645°E	492.429 m

* Conversion according to NAVREF transformation service, www.swisstopo.admin.ch

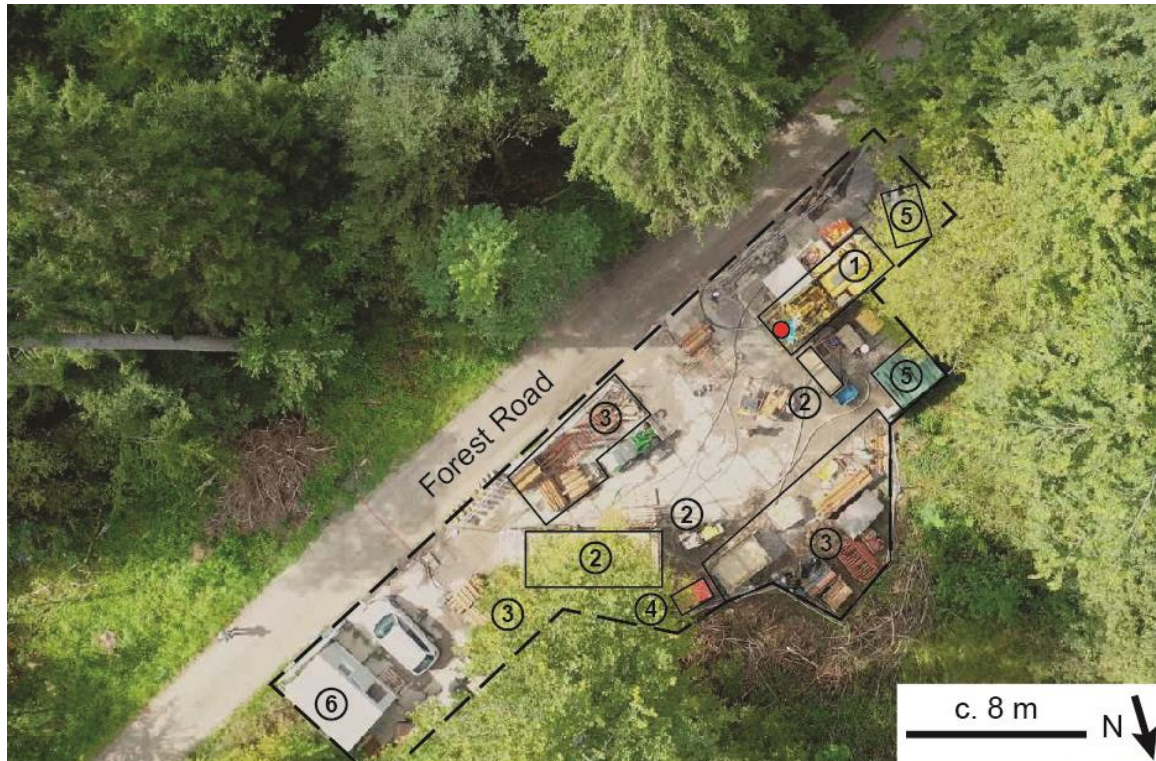


Figure 19: Aerial view of the installations at site 5068_2: 1) Drill rig, red dot marks the location of borehole 5068_2_A, 2) mud pump and tanks, 3) storage area of various components, 4) power generator, 5) tools and drill crew container, 6) science container.

The soil was protected by soil-protection mats extending from the existing forest road into the cleared areas. The drill rig was additionally supported by wooden planks. In addition, the ground beneath the drill rig was covered by a plastic tarp to protect the underground in the unlikely event of a leakage. Before the second drill rig (AGBO) was installed (see 5.2 detailed report of operations), a gravel bed was built to support the additional loads. Fretus AG installed a temporary water connection along the road from the next hydrant (Josenbuck) to the drill site. Electricity was supplied by a power generator on site.

For the scientific operations, a container was installed on the drill site for sampling and as a field office, while more space was available in a garage of a forestry repository at Josenbuck, where the cores were scanned for petrophysical properties using a Geotek MSCL scanner (owned by ICDP OSG) and temporarily stored before transport to the University of Bern.

3.5. Technical operations

3.5.1. Summary of drilling, coring and logging operations

After a public tender in late 2020, the University of Bern contracted the drilling company Fretus AG (Bad Zurzach, Switzerland) for the drilling operations, with the requirement to core in high-quality down to a depth of max. 300 m. The drilling crew consisted of two to three people (one drilling operator, one to two drilling workers). To achieve the scientific goals, the drilling company planned to work with different drill rigs depending on the depth and type of operations (Table 7).

Table 7: Drill rigs used during the operations.

Rig 1 - Nordmeyer DSB 1/6	0 - 228m depth drilling and coring
Rig 2 - AGBO G750	228 - 252 m depth, drilling and coring, (leased by Fretus from Groupe Grisoni)
Rig 3 - Comacchio MC15	Logging, refilling

Table 8 summarises the technical parameters of the drilling and coring operations in hole 5068_2_A. For coring of the first 58.0 m, a percussion coring system (Düsterloh-Hammer) was used. This system works without mud circulation ('dry coring') and was therefore very successful for the loose and, in parts, very permeable gravelly lithologies encountered in the upper part. Below 57.0 m the wireline triple tube core-barrel system CSK-146 was used. This method in combination with suited drill bits, core-catchers, and a fine-tuned mud-circulation yielded excellent core recovery and rapid progress in cohesive and sandy lithologies. In gravelly zones, repeated borehole collapses, and large drilling mud losses slowed down progress significantly (see 5.2 detailed report of operations). A total length of 252.0 m of core was recovered, with an overall recovery of 94 % (Fig. 20).

The time vs. depth plot shows the drilling processes for site 5068_2 (Fig. 21) and a weekly summary of the drilling operations (Table 8). Three longer periods without depth progress (marked with (1) to (3)) relate to technical challenges during the drilling process. (1) standstill was needed to deblock the casing (280 mm and 245 mm) and to stabilise the borehole walls, (2) is related to the change of the drill rig and unforeseen mechanical problems with drill rig 2, and (3) to deblocking the casing for before cementation.

At 252.0 m depth, drilling-mud losses and borehole collapses could not be managed (risk of blocking the drill string). It was therefore decided to stop the drilling even though the targeted bedrock had not been reached yet. After a return run down to 252 m, a successful geophysical downhole logging was performed by LIAG (see section 6.3). The lowest 2-3 m were blocked so that wire-line logging tools reached 249 m.

After completion of the coring and downhole geophysical logging, the borehole was refilled (see section 5.5) as there was no further use of the hole for further experiments. While retracting the casing after many months proved to be challenging, the refilling was conducted according to the plan and all casing was retracted. The drill site was fully cleaned up by the drilling contractor and returned to the landowner on 23.11.2021.

Table 8: Summary of the technical drilling and coring parameters for hole 5068_2_A.

	From [m]	To [m]	Diameter	Description
Drilling/Coring	0.0	57.0	133 mm	Düsterloh-Hammer (percussion drilling technique)
	57.0	252.0	146 mm	Wireline coring, CSK-146
	104.0	143.0	200 mm	Rolling cutter drill bit, for reopening & widening borehole
Casing (final state)	0.0	35.0	OD: 324 mm ID: 302 mm	Drill pipe, OD
	0.0	88.0	OD: 280 mm ID: 246 mm	Drill pipe
	0.0	105.0	OD: 245 mm ID: 224 mm	Drill pipe
Drilling mud	57.0	252.0	-	Polymer & bentonite
Liner	0.0	252.0	OD: 110 mm ID: 104 mm	PVC, dark orange, pre-cut to 1 m pieces

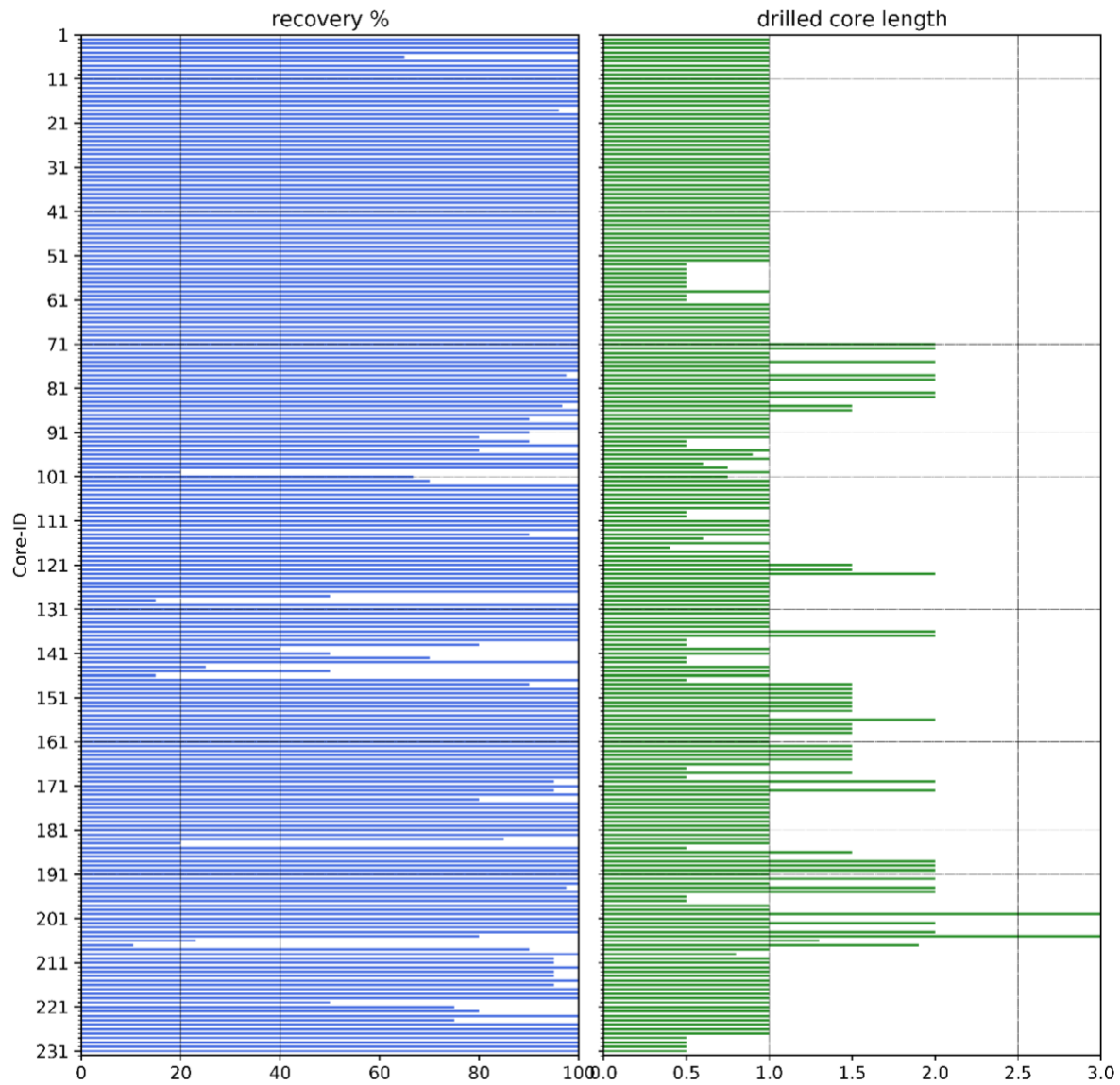
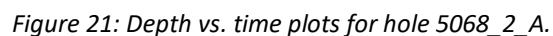


Figure 20: Recovery and core length for hole 5068_2_A. Recovery was determined based on the driller's information, which were transferred to mDIS.



3.5.2. Detailed report of operations

A detailed weekly summary of the drilling operations is given in Table 9.

Table 9: Detailed report of operations for site 5068_2.

Calendar week	Summary of technical operations and decisions
CW 20 (17.5.-21.5.2021)	<ul style="list-style-type: none"> • Transport and installation of drill rig (Nordmeyer DSB 1/6)
CW 21 (24.5.-28.5.2021)	<ul style="list-style-type: none"> • Inspection of drill site with external supervisor (L. Seslak), installations accepted • Drilling 0-15 m using Düsterloh Hammer (Ø 133 mm, core Ø 110 mm) • Continuous installation of casing (Ø 324 mm) down to 15 m • Ground water entering borehole 3-4 m and 10-11 m
CW 22 (31.5.-5.6.2021)	<ul style="list-style-type: none"> • Drilling down to 35 m using Düsterloh Hammer (Ø 133 mm, core Ø 110 mm) • Continuous installation of casing Ø 324 mm • Ground water entering borehole 28-29 m, disturbed water table at 28.5 m • Installation of casing Ø 280 mm down to 35 m • Drilling down to 42 m using Düsterloh Hammer (Ø 133 mm, core Ø 110 mm) • Continuous installation of casing Ø 280 mm down to 42 m
CW 23 (7.6.-11.6.2021)	<ul style="list-style-type: none"> • Drilling down to 57 m using Düsterloh Hammer (Ø 133 mm, core Ø 110 mm) • Continuous installation of casing Ø 280 mm down to 58 m • Switching to wire-line coring (CSK 146), • Drilling down to 58 m using CSK 146 (Ø 146 mm, core Ø 110 mm) • Changing drill bit • Drilling down to 61 m using CSK 146 (Ø 146 mm, core Ø 110 mm)
CW 24 (14.6.-18.6.2021)	<ul style="list-style-type: none"> • Drilling down to 95 m using CSK 146 (Ø 146 mm, core Ø 110 mm) • Core loss (see recovery plot) • Loss of drill mud at 93.9-95 m • Drilling down to 95 m using CSK 146 (Ø 146 mm, core Ø 110 mm) • Continued core losses (see recovery plot) • Continued loss of drill mud at 95-98.9 m • Attempt to seal borehole wall with bentonite
CW 25 (21.6.-25.6.2021)	<ul style="list-style-type: none"> • Re-open borehole, sealing borehole wall, and changing drill bit • Continued loss of drill mud at 95-98.9 m • Drilling down to 109 m using CSK 146 (Ø 146 mm, core Ø 110 mm) • Continued core losses down to c. 103 m (see recovery plot) • Continued loss of drill mud at 98.9-103 m
CW 26	<ul style="list-style-type: none"> • Re-open borehole down to 109 m • Drilling down to 126 m using CSK 146 (Ø 146 mm, core Ø 110 mm)

(28.6.-2.7.2021)	<ul style="list-style-type: none"> Installing casing Ø 245 mm down to 60 m
CW 27	<ul style="list-style-type: none"> Installing casing Ø 245 mm down to 95 m
(5.7.-9.7.2021)	<ul style="list-style-type: none"> 6.7.2021: casing Ø 245 mm blocked, no rotation possible To unblock casing Ø 245 mm: drill with casing Ø 280 mm over casing Ø 245 mm, down to 71 m
CW 28	<ul style="list-style-type: none"> Continue workaround to unblock casing 245 mm: drill with casing Ø 280 mm over casing Ø 245 mm, continued in steps down to 89 m
(12.7.-16.7.2021)	
CW 29	<ul style="list-style-type: none"> Casing 245 mm Ø finally deblocked
(19.7.-23.7.2021)	<ul style="list-style-type: none"> Complete retraction and reinstallation casing Ø 245 mm Re-opening borehole with CSK 146 down to 105 m Changing drill bit Re-opening borehole with CSK 146 down to 123 m Continued borehole instability. Installation of rolling cutter bit
CW 30	<ul style="list-style-type: none"> Re-opening borehole with rolling cutter drill bit (200 mm Ø) down to 126 m
(26.7.-30.7.2021)	<ul style="list-style-type: none"> Installation of CSK Drilling down to 143 m using CSK 146 (Ø 146 mm, core Ø 110 mm) Minor core and drilling mud losses
CW 31	<ul style="list-style-type: none"> Re-opening borehole with rolling-cutter drill bit (Ø 200 mm) from 126-143 m
(2.8.-6.8.2021)	<ul style="list-style-type: none"> Installation of CSK Drilling down to 154.5 m using CSK 146 (Ø 146 mm, core Ø 110 mm) Continued bore-hole instability, core losses and drilling-mud losses
CW 32	<ul style="list-style-type: none"> Drilling down to 194 m using CSK 146 (Ø 146 mm, core Ø 110 mm)
(9.8.-13.8.2021)	<ul style="list-style-type: none"> Minor drilling-mud losses
CW 33	<ul style="list-style-type: none"> Changing drill bit, maintenance, mud curation
(16.8.-20.8.2021)	<ul style="list-style-type: none"> Drilling down to 213 m using CSK 146 (Ø 146 mm, core Ø 110 mm) Minor drilling-mud losses
CW 34	<ul style="list-style-type: none"> Drilling down to 228.3 m using CSK 146 (Ø 146 mm, core Ø 110 mm)
(23.8.-20.8.2021)	<ul style="list-style-type: none"> Performance limit of drill rig reached; decision to switch drill rig Minor drilling mud losses
CW 35	<ul style="list-style-type: none"> Remove & transport drill rig (Nordmeyer DSB 1/6)
(30.8.-3.9.21)	<ul style="list-style-type: none"> No drilling
CW 36	<ul style="list-style-type: none"> Laying of a stable gravel bed for heavier truck-mounted drill rig
(6.9.-10.9.21)	<ul style="list-style-type: none"> Installation of new drill rig (AGBO G750) Repair work on hydraulic pump No drilling
CW 37	<ul style="list-style-type: none"> Continued repair work on hydraulic pump and other components
(13.9.-17.9.21)	<ul style="list-style-type: none"> No drilling

CW 38 (20.9.-24.9.21)	<ul style="list-style-type: none"> Continued repair work (various components), support by technician from manufacturer No drilling
CW 39 (27.9.-1.10.21)	<ul style="list-style-type: none"> Final preparatory work Re-opening borehole and widening borehole rolling-cutter drill bit (Ø 152 mm) down to 228.3 m, replace drilling mud Prepare installation of CSK
CW 40 (1.10.-8.10.2021)	<ul style="list-style-type: none"> Installation of CSK Flush and re-open borehole down to 228.3 m Drilling down to 250 m using CSK 146 (Ø 146 mm, core Ø 110 mm) Retract CSK 146 to changing drill bit
CW 41 (11.10.-15.10.2021)	<ul style="list-style-type: none"> Retract CSK 146, changing drill bit and re-install CSK 146 Drilling down to 252 m using CSK 146 (Ø 146 mm, core Ø 110 mm) Core losses Attempts to continue drilling but borehole cannot be sealed (drill mud is lost) and borehole collapses (with high risk of blocking the drill string). Joint decision to stop drilling Retract CSK 146
CW 42 (18.10.-22.10.2021)	<ul style="list-style-type: none"> Remove & transport drill rig (AGBO G750) Transport & installation of new drill rig (Comacchio MC15) for downhole logging and refilling
CW 43 (25.10.-29.10.2021)	<ul style="list-style-type: none"> Install CSK 146 Perform return run with CSK 146 down to 248 m and retract to 175.9 m to clean borehole in preparation to downhole logging of first stage Downhole logging of first stage (see logging report) Retract CSK 146 up to 118.9 m Downhole logging of second stage (see logging report) Fully retract CSK 146 Attempt to retract Ø 245 mm casing fails (same for Ø 280 mm casing) Downhole logging of third and final stage (see logging report) Clean up and preparatory work for borehole cementation and re-filling
CW 44 (1.11.-5.11.2021)	<ul style="list-style-type: none"> Continued attempts to deblock Ø 245 mm and Ø 280 mm casing Fully retract casing Ø 245 mm and Ø 280 mm casing Clean up and preparatory work for borehole cementation and re-filling Refilling borehole according to accepted refilling scheme Cementation of first stage (248-200 m, 400 kg cement Küchler INJEK THERM 110 HS) before weekend break
CW 45 (8.11.-12.11.2021)	<ul style="list-style-type: none"> Continued refilling borehole according to refilling scheme Cementation 200-80 m and 80-55 m in two stages (2000 and 1200 kg cement Küchler INJEK THERM 110 HS) Fill borehole with swelling clay 55-50 m (500 kg, Mikolit 300 M) Fill borehole with gravel 50-12 m (3 m³)

	<ul style="list-style-type: none"> • Fill borehole with swelling clay 12-5 m (1000 kg, Mikolit 300 M) • Fill borehole with earth/humus 5-0 m • Retracting Ø 323 mm casing parallel to refilling stages
CW 46 (15.11.- 19.11.2021)	<ul style="list-style-type: none"> • De-installation of drill site • Disposal of gravel bed and recultivation of drill site • 17.11.2021 Fretus AG finished work on site
CW 47 (22.11-26.11.2021)	<ul style="list-style-type: none"> • 23.11.2021: Inspection of site with forester/representative of landowner (S. Pachera); site acceptance and returned • 23.11.2021: Inspection of forest road with responsible (P. Eicher); no damages found

3.5.3. Borehole deviation

The borehole deviation of 5068_2_A was measured as part of the downhole geophysical logging after completion of the drilling operations. The results indicate only a minor deviation of max. 0.77 m to the SSE (Fig. 22). The borehole can be considered essentially vertical. Note that due to the still existing drill pipe for the top 105 m, only the inclination of the borehole could be determined with accelerometers. The direction of the deviation is determined with fluxgate magnetometers. Therefore, the borehole direction in the cased area was assumed.

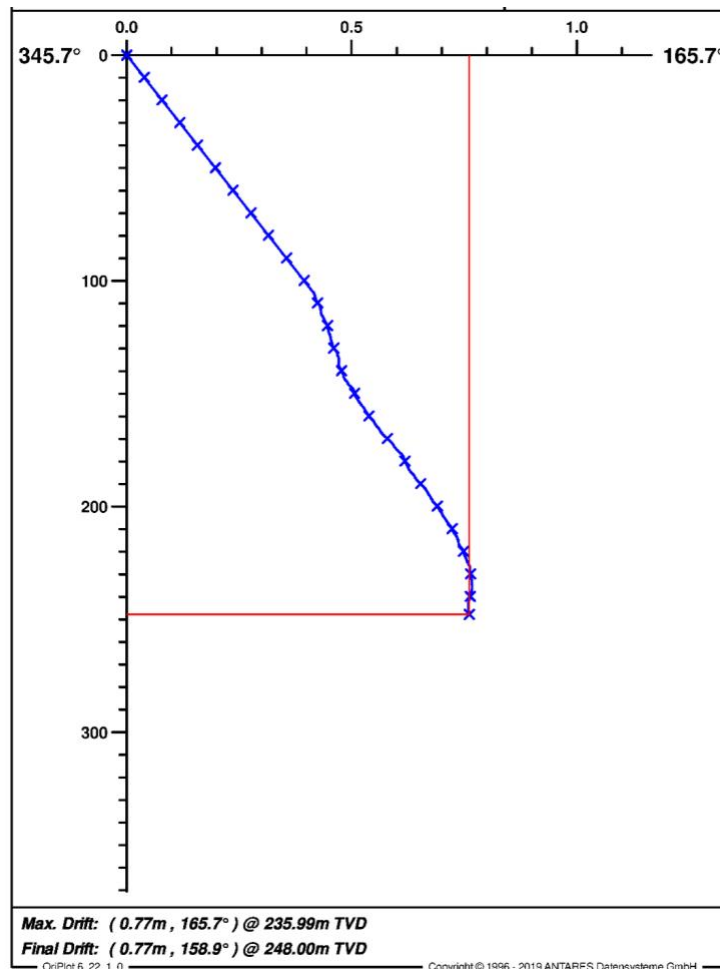


Figure 22: Borehole deviation of 5068_2A in vertical view (unit of both axes is meter).

3.5.4. Refilling and Post-Drilling Finishing Procedure

After completion of the coring and downhole geophysical logging, the borehole was refilled. Fig. 23 shows the preliminary lithological profile at that point (based on core ends, core catchers, and preliminary MSCL data) and the borehole geometry. The following refilling plan was then proposed by the hydrogeological consultants (Dr. von Moos AG, Appendix A) and accepted by environmental authorities (Amt für Umwelt, Kanton Thurgau), the drilling contractor (Fretus AG) and the University of Bern:

- 253-55 m: Cementation in 2-3 stages using sulphate-resistant cement (product used: Küchler INJEK THERM 110 HS)
- 55-50 m: Swelling clay (product used: Mikolit 300 M)
- 50-12 m: Clean gravel
- 12-5 m: Swelling clay (product used: Mikolit 300 M), water to be added to ensure fast swelling.

- 5-0 m: Clean cover material & humus/soil ("Deckschicht (Erde/Humus)")

3.5.5. Borehole geometry and preliminary lithology assessment

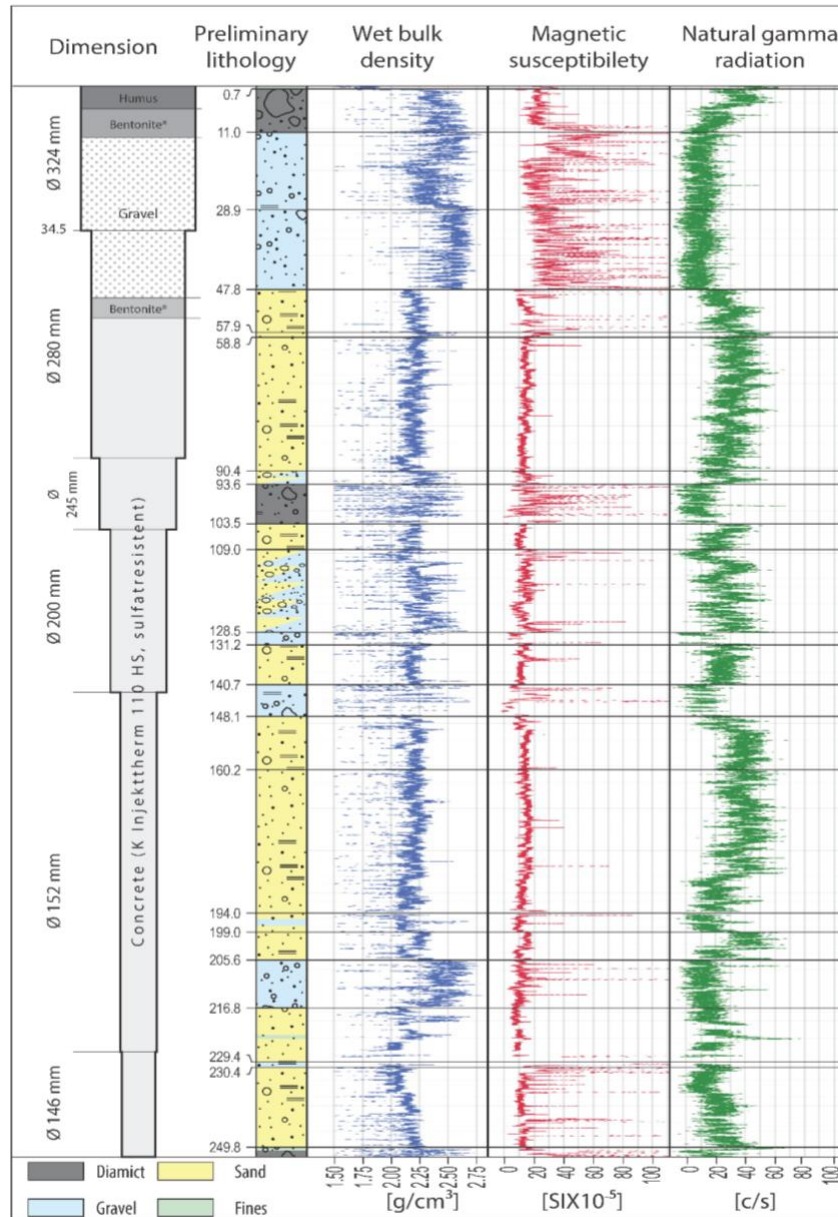


Figure 23: Borehole geometry and preliminary lithological profile (based on core end and MSCL data only) with final refilling scheme.

The drilled succession of the Basadingen overdeepening (Fig. 23) can be roughly divided into two parts: In the lower part between 252 and c. 48 m depth, the valley filling consists of sand with a highly variable silt/clay content, which is divided into larger packages by gravel and diamict layers. Between c. 90 and c. 148 m depth, the dominance of sands decreases, and alternating bedding with gravels on a meter to

decimeter scale is observed. The upper part of the succession, between c. 48 and c. 11 m depth, consists of mostly sandy gravels and is capped by a primarily diamictic succession above c. 11 m.

3.6. Scientific operations on-site

The scientific operations for the core drillings were coordinated by the University of Bern. At least one scientist (mainly S. Schaller) was on site to accompany the core drilling, take samples, and to MSCL scan the cores. The drill-site geologist/scientist was supported by a second scientist and the external drilling advisor (L. Seslak) if needed.

3.6.1. Workflow drill-core handling

The cores handling was divided between the drilling team and the scientist according to defined procedures. After recovery, the drill crew and the scientists would usually first inspect the lithology visible at the core end. The drill crew was then responsible for closing the plastic liner with caps, adding a preliminary label (with core run, driller's depth, and orientation) and cutting the core into 1 m-sections if needed (Fig. 20). The core catchers were usually not kept as separate sections but pushed back into the liner. The core would then be handed over to the drill-site scientist, who documented the drilling procedure per core in a detailed core-run protocol (Fig. 24) and completed labelling of the core and the core-box according the ICDP standards. As there was no stable network coverage on the drill site, the data upload to mDIS was usually done at the end of the working day.

Geologist:		Place:		Core run (CR):		Date:	
Core info for mDIS		Core ID:					
Core on Deck (CoD)	Top Depth [mblf]	Drilled Core Length [m]	Nr of Section	Core type		Core Ø [mm]	Oriented
				Hammer	Rotation		Yes No
Reason for core loss/ General core remarks:							
Barrel length [m]	Bit type	Drilling fluid type	Additional drillers info:				
Section info for mDIS		Section ID:					
Section length [m]	Exists extra Core catcher	CC pushed back	Weight [kg]	Nobel gas samples		Deep-Bio samples	
				Yes	No	Yes	No
CC-Section info for mDIS	Length [m]:	Weight [kg]:	Nobel gas samples: yes/no		Deep-Bio samples: yes/no		
Lithology:			Nobel gas Samples				
If light exposed:			Deep-Bio Samples				
General Remarks:							

Figure 24: Core-run protocol template filled out by the drill-site scientist. The paper-based version was then

transferred to mDIS.

The drill-site scientist also took the on-site samples according to the sample requests and instructions for noble-gas and deep-biosphere sampling (section 6.2). These samples were taken before closing of the liner if the core end suggested a suited lithology and high core quality. Samples were automatically assigned an IGSN (International Geo Sample Number) and labelled according to the ICDP-standard, automatically generated by mDIS.

The cores were stored in wooden core boxes and first transferred to the forestry repository at Josenbuck by car. There, the cores were scanned with the ICDP-OSG's Geotek MSCL and temporarily stored. The cores were then transported to the cool storages at the Institute of Geological Sciences, University of Bern, and once this was full, to the one at Eawag, Dübendorf (usually within 2-3 days after recovery).

3.6.2. On-site sampling

Biosphere sampling (method identical to site 5068_1; see 2.6.3)

According to sample request DOVE_2_2-A-MBIO, we took samples to search for microbial activity within the fine sediments at intervals of ca. 3 m and within the coarse sediments at intervals of ca. 10 m throughout the whole core. We stored the samples temporarily in a cool box, before freezing them in a freezer in the forestry repository at Josenbuck (usually within hours after sampling). We took 61 samples and, after the drilling was completed, we sent them to University of Geneva for further investigation in February 2022.

Noble-gas porewater sampling (method identical to site 5068_1; see 2.6.3)

According to sample request DOVE_1_2-A-NOBE, we took bulk-sediment samples of preferably fine-grained clastics with trapped pore water at intervals between ca. 10 - 20 m due to varying geology and the developed sampling strategy. We took a total of 16 samples, which were sent batch-wise during the drilling operation to Eawag, Dübendorf for further analysis. The samples will be used to date the glacial sediment succession using the $^4\text{He}/\text{U-Th}$ method on the pore water.

Bulk samples from borehole widening

When working with the Düsterloh-Hammer technique, the driller first pulled the core, then widened the bore hole to the diameter of the casing (\varnothing 324 mm and later to \varnothing 280 mm) and then remove the excess material using the Düsterloh (with varying core chambers attached). This excess material is a disturbed mix of the last core/casing interval, but the components are relatively original. We therefore sampled additional bulk samples of this material in 5l buckets as back-up material for upcoming analysis (e.g., clast analysis).

MSCL geophysical core logging (method identical to site 5068_1; see 2.6.3)

Same procedure and tools as at Site 5068_1, with the addition that at Site 2 (5068_2) natural gamma radiation including K, Th, and U-Log was also measured. For details please see Explanatory notes.

3.6.3. Downhole geophysical measurements

Downhole geophysical measurements and a vertical seismic profile (VSP) were conducted upon completion of the coring operations from 26. - 29.10.2021. Prior to logging the open hole section (105-250 m) a return run was ordered to have a clean borehole and stable borehole for logging. Thomas Grelle, Carlos Lehne and Hermann Bunness (all LIAG, Hanover) carried out the downhole geophysical measurements.

Table 10: Wire-line logging overview. Tool abbreviations: BHTV: Borehole Televiwer, CAL: Caliper, DLL: Dual laterolog resistivity, EBS: Elemental composition, GR: Gamma Ray, NN: Neutron porosity, PE: Photoelectric index, SGR: Spectral Gamma Ray, SONIC: Sonic log, SUSZ: Magnetic susceptibility Log, VSP: Vertical Seismic Profile. OH: measurements in open hole, CH: measurements in cased hole

Date	Run	Parameter	From [m]	To [m]	Hole Condition
26.10.2021	1	BHTV	250	175	OH
	1	CAL	250	175	OH
	1	DLL	250	175	OH
	1	EBS	250	175	OH
	1	NN	250	175	OH
	1	PE	250	175	OH
	1	SGR	250	175	OH
	1	SONIC	250	175	OH
	1	SUSZ + GR	250	175	OH
Remarks: CSK-164 drill string retracted to 175 m					
27.10.2021	2	BHTV	175	120	OH
	2	DLL	175	120	OH
	2	NN	175	120	OH
	2	SGR	175	120	OH
	2	SONIC	175	120	OH
	2	SUSZ+GR	175	120	OH
	2	VSP	246	120	OH+CH
Remarks: CSK-164 drill string retracted 120 m, EBS not working					
28.10.2021	3	BHTV	120	105	OH
	3	SUSZ + GR	120	105	OH
	3	VSP	208	82	OH+CH
Remarks: CSK-164 drill string retracted 105 m					
29.10.2021	4	CAL	175	105	OH
	4	NN	120	105	OH
	4	PE	175	105	OH
	4	SGR	120	0	OH+CH
	4	SONIC	120	105	OH
Remarks: -					

The first measurement was made using spectral gamma ray SGR (i.e., the instrument measures the sum of natural gamma ray (GR) plus K (wt%), Th (ppm), and U (ppm)) along the entire length of the borehole through the drill string. The drill string was then removed by the drill crew at intervals to depths that precluded collapse of the borehole (175 m, 120 m, and 105 m). The remaining probes were deployed in the area of the open hole:

- BHTV; Borehole Televiwer, ultrasonic image of the borehole wall
- CAL; Caliper (in perpendicular directions, in mm),
- DLL; Resistivity (in Ωm , both near- and far-field),
- EBS; pulsed neutron induced borehole n-/ γ -spectroscopy; element composition (in cps)
- NN: Porosity (%),
- PE: Photoelectric absorption (barns/electron; b/e) and density (g/cm^3 in Fig. 26),
- SONIC; Seismic velocity (in m per second),
- SUSZ; Magnetic susceptibility (10^{-4} SI in Fig. 26),
- VSP; Vertical seismic profile.

3.7. Storage, initial core description and 1st sampling party

Please see Chapter 2.7. For sample accessibility please contact: Falvio Anselmetti, University of Bern

3.8. Site-specific preliminary scientific assessment

3.8.1. Geology

See Chapter 3.5.5 for the preliminary lithological assessment and Figure 23 for a graphical overview of the lithological units.

3.8.2. Geophysics

The Explanatory Notes describe in detail how the pre-processing of the data of the measurement campaign at Site 5068_2 was done. This includes, among other things, the matching of the depths of the individual measurements, the elimination of false measurement data, and the splicing of measurement curves. The respective composite dataset for hole 5068_2_A is shown in Fig. 26.

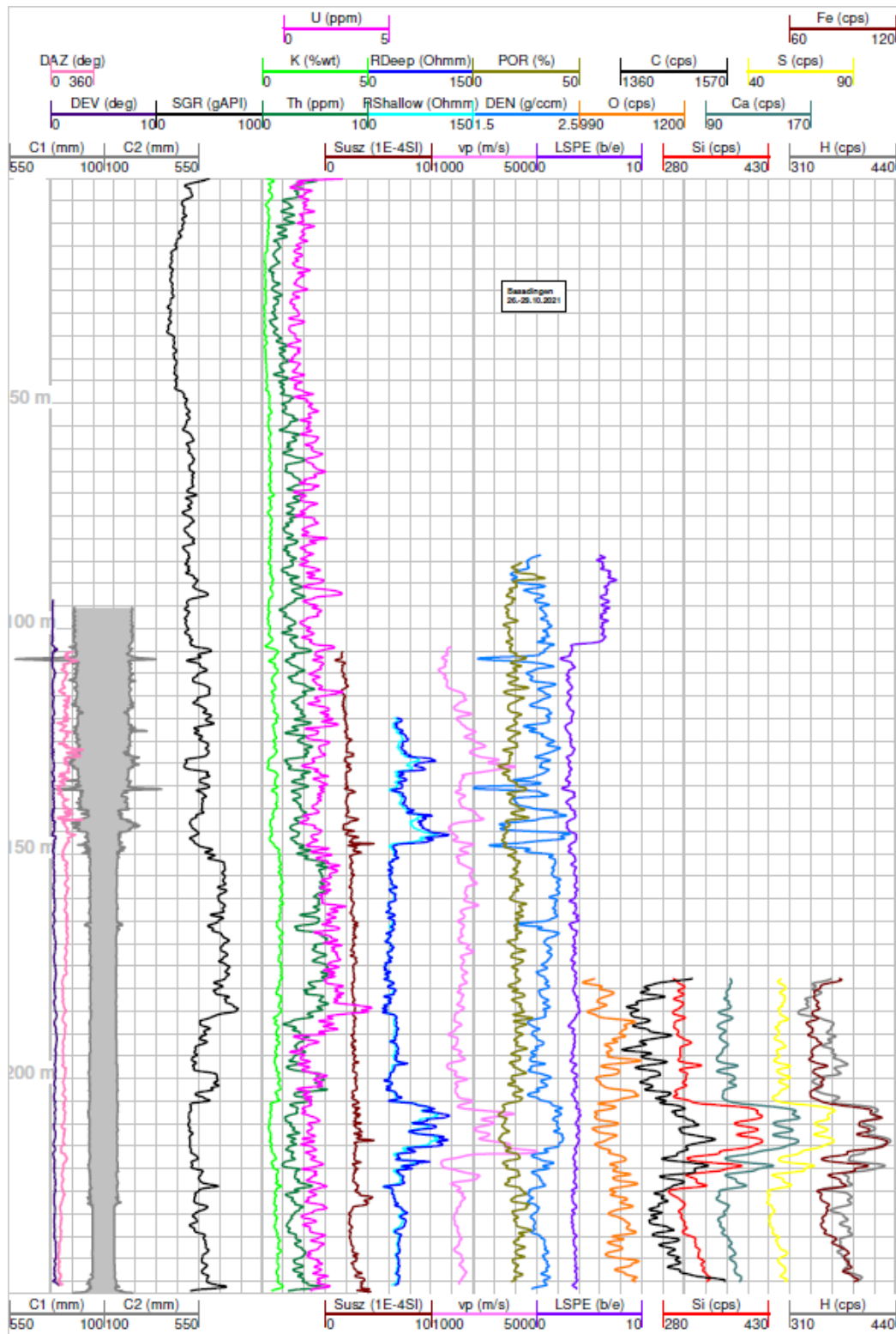


Figure 26: Results of the downhole geophysical measurements on the open hole of 5068_2_A.

4. Site 5068_3

4.1. Site Introduction

The drill-site is located south of Munich, Germany in the municipality of Schäftlarn. To the east lies the slope of the Isar valley and further to the west the Lake Starnberg. The investigated overdeepened structure was eroded by glacial activity of the Isar-Loisach glacier. It is located in a distal position in the foreland glacier-lobe, just south of the limits of the maximum ice extent of the last glaciation. It is suggested by Jerz (1979) that the Schäftlarn overdeepening is a northeast-directed branch basin of the Wolfratshausener basin. Drilling operations in 2017 conducted by the LfU (Bavarian Environment Agency – Bayerisches Landesamt für Umwelt) retrieved 198.8 m of Quaternary sediments. The core can be divided into diamicton remnants (198.8-198.5 m) at the base, overlain by silty sand with dropstone presence (198.5-184 m), again overlain by partly laminated silt (184-170 m), fine sand interlayered with silt and dropstones (170-158 m) and partly laminated silt with decreased presence of dropstones (158-115.5 m). The sequence is topped by sandy-silty gravel (115.5-6 m) and a clast supported diamicton (6-0 m) below the surface. 5068_3_A is stored in the drill-core storage facility (LfU reference number: 8034BG015807) of the LfU in Hof an der Saale, Germany.

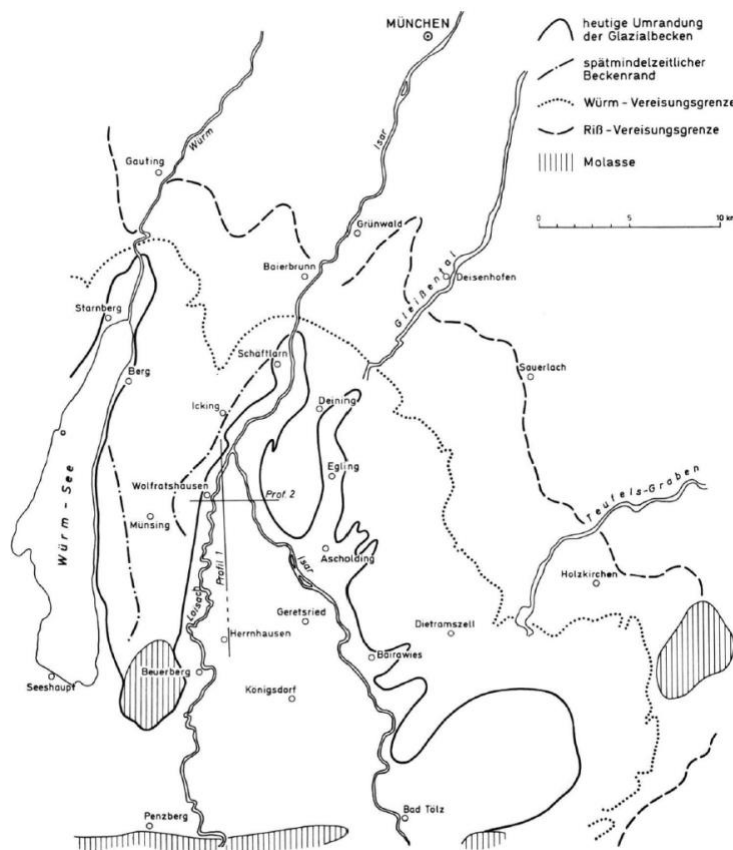


Figure 27: Map of the overdeepened structure of the Wolfratshausen basin and the drill-site Schäftlarn located in a north-east extending branch basin published in Jerz (1979). Context is provided by evidence of past glaciations on the surface.

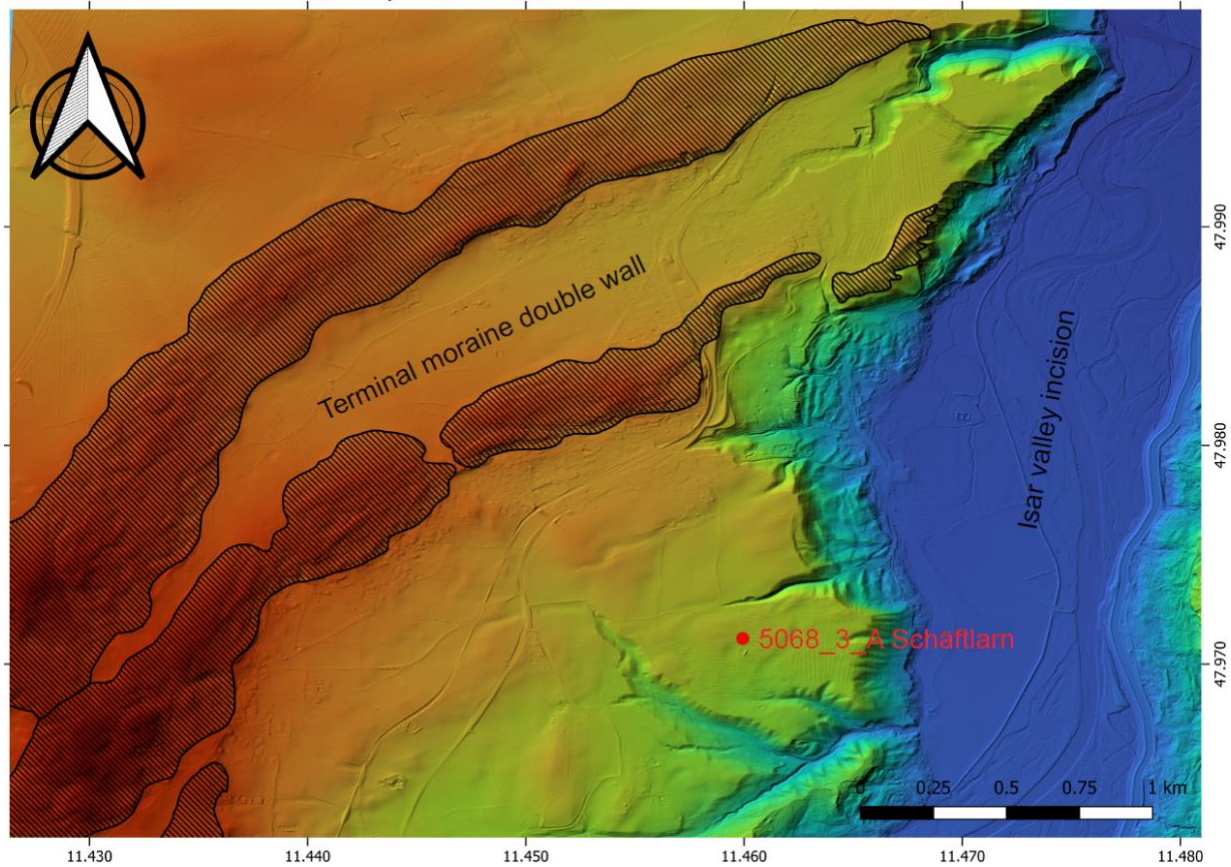


Figure 28: Map of the surrounding area of drill-site 5068_3. The site is located south of the limits of the maximum ice extent of the last glaciation. Digital Elevation Model (DGM 1m resolution) provided by the Bayerische Vermessungsverwaltung.

5. Site 5068_4

5.1. Site Introduction

Site 5068_4 Neusillersdorf is located west of Freilassing and Salzburg on the border between Germany and Austria. The site is positioned centrally under the foreland lobe of the Salzach paleoglacier. A distinct branch basin diverting northwest from the main glacier basin was detected by the LfU (Bavarian Environment Agency – Bayerisches Landesamt für Umwelt) during their update of the Quaternary base map. The 136 m long core 5068_4_A, drilled by the LfU in 2009 targeted this overdeepened branch basin and consists of 117 m of Quaternary sediments on top of 19 m of Flysch bedrock. The Quaternary sediments can be further divided into a base diamicton (117-115 m) overlain by fine-sand/silt sized laminated sediments (115-27 m) that are covered by sandy-gravel/diamicton sediments (27-0 m). 5068_4_A is stored in the drill-core storage facility (LfU reference number: 8143BG015394) of the LfU in Hof an der Saale, Germany. For first results and a more detailed drill-core description we refer to Fiebig et al. (2014).

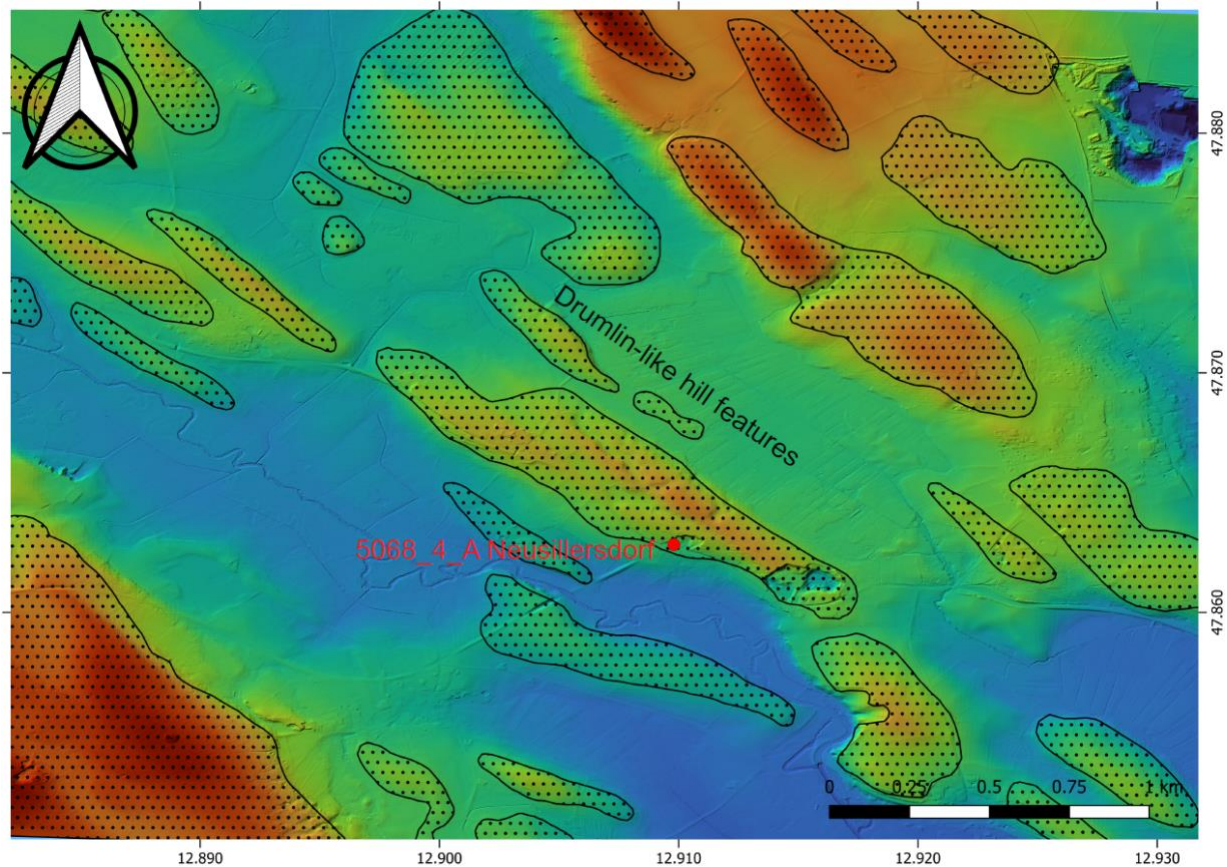


Figure 29: The drill-site 5068_4 is located in a landscape characterized by drumlin-like glacial hills. These hills are oriented parallel to the paleo ice flow direction. Digital Elevation Model (DEM 1m resolution) provided by the Bayerische Vermessungsverwaltung.

6. Site 5068_5

6.1. Site Introduction

Drill-site 5068_5 is located near Bad Aussee (Austria), in the central part of the Northern Calcareous Alps within the extent of the Pleistocene Traun Glacier. Geophysical data (Steinhauser et al., 1985) show a narrow, up to 1100 m deep structure with a highly unusual shape for an overdeepened basin ('Hole of Bad Aussee'). A possible explanation for this feature is the dissolution of a large salt body under subglacial conditions resulting in the formation and subsequent filling of a lake. Drilling operations by the Salinen Austria AG recovered 880 m of Quaternary sediments. They can be divided into ~ 700 m of fine sediments, interpreted as being of glaciolacustrine origin at the base and ~ 200 m of cover sediments. The cover deposits can be further divided into a coarse gravel sequence (~ 200 – 67 m), interpreted as glaciofluvial sediments ("Vorstoßschotter"), and a thick cover of subglacial till (~ 67 – 0 m). A first general description of 5068_5_A was published in Husen van & Mayr (2007).

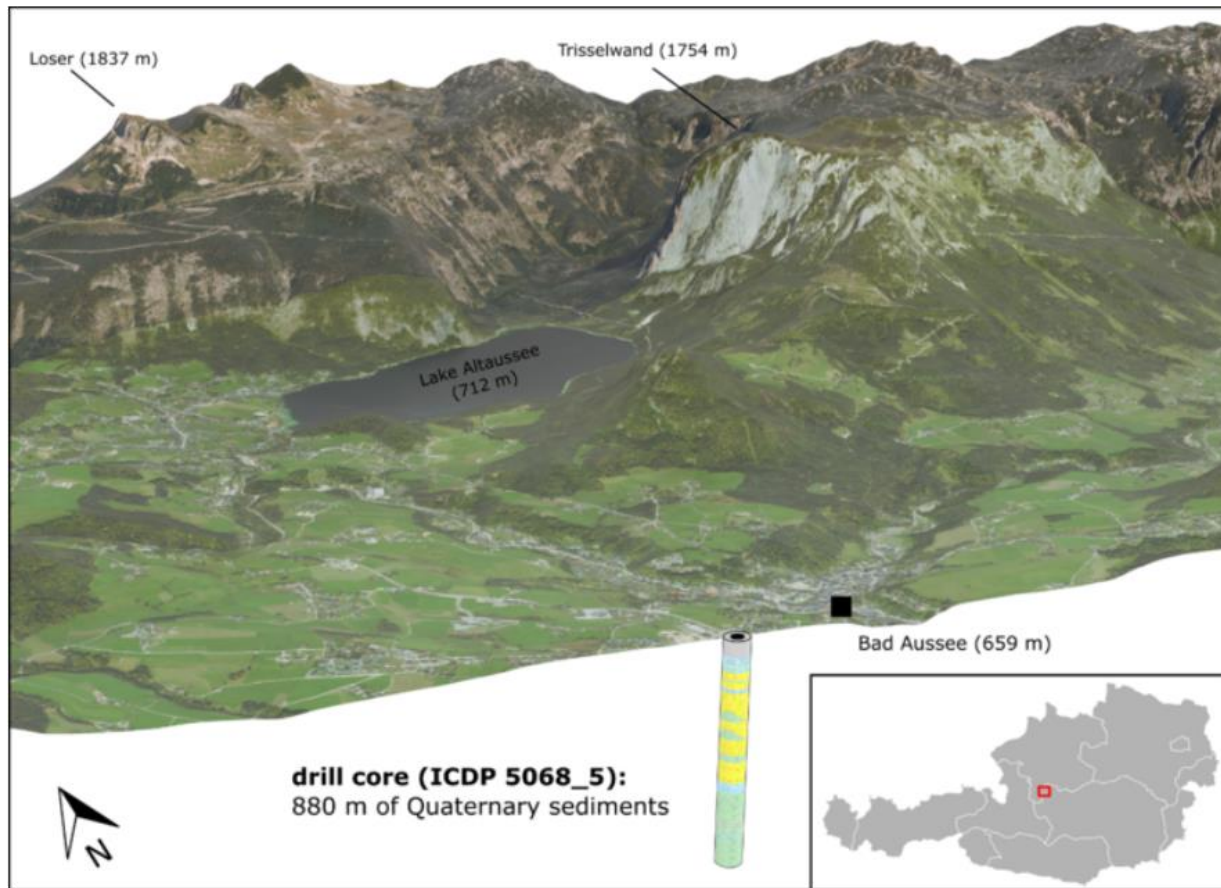


Figure 30: 3D-visualisation of the drill-site and the 5068_5_A drill-core. (Source of orthophoto: www.geoland.at, source of digital elevation model: gis.stmk.gv.at)

7. Site 5068_6

7.1. Site Introduction

The Site 5068_6 is a so-called legacy site. Drilling was undertaken by the State Office for Geology, Resources and Mining of Baden-Württemberg (LGRB) in 2016 where the core material is stored. The original identifier at the LGRB is: 8124-1291. The borehole was drilled to a depth of 144 m with a bedrock depth of 133 m.

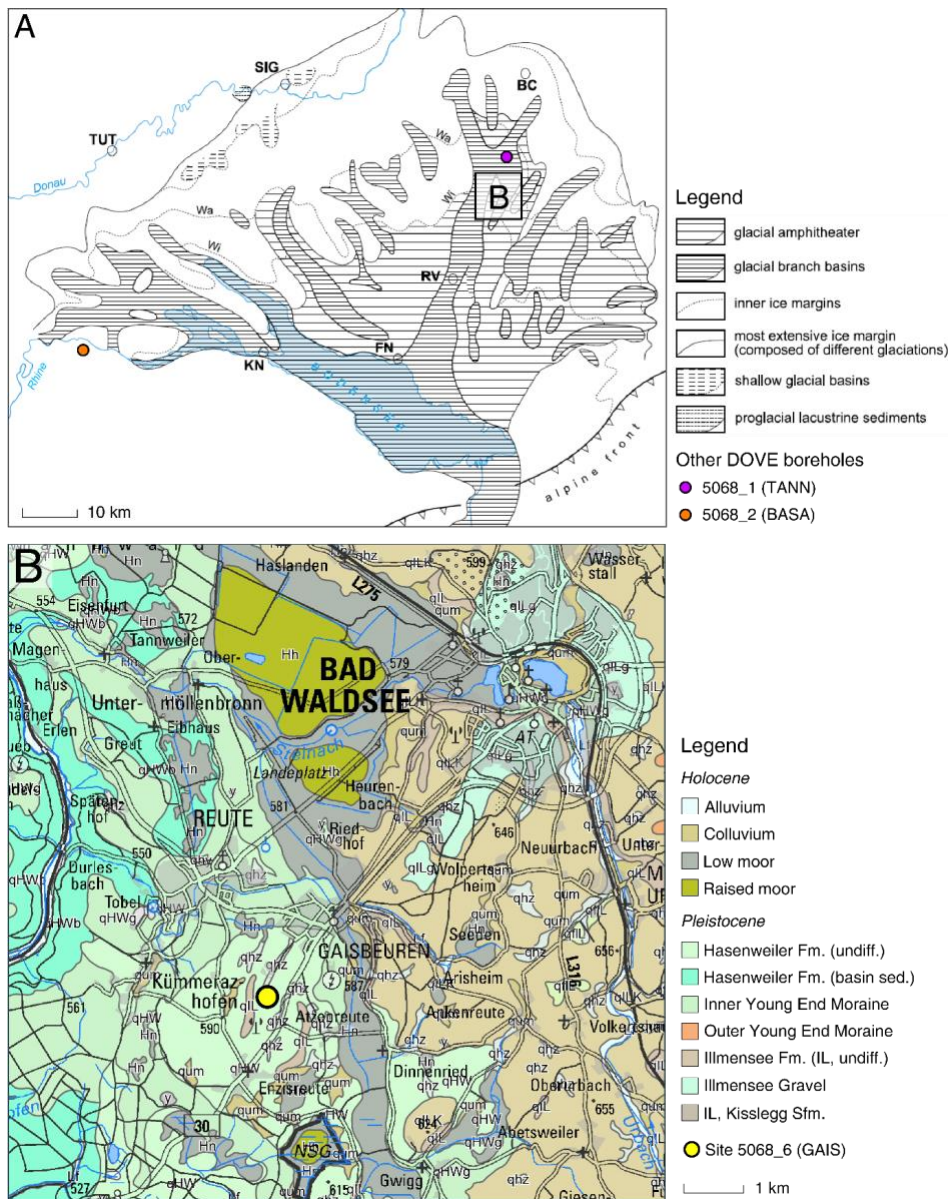


Figure 27: Overview map of the Lake Constance amphitheatre with boreholes 5068_1 and 5068_2 (A; from Ellwanger et al., 2011, altered) and the vicinity of the 5068_6 drill site (B; map data courtesy of the LGRB)

The site is located near the village of Gaisbeuren, which lies at the southern end of the Tannwald Basin, an overdeepening that has presumably been eroded during the third-to-last Hosskirch Glaciation (Ellwanger et al., 2011; Ellwanger, 2015) (Fig. 27). There, another isolated basin (Gaisbeuren Basin) underlying the Tannwald Basin is presumed based on results from a previous but not anymore existing drill core, which is not unlikely to represent an early Middle Pleistocene glaciation (Ellwanger, 2015). Due to the supposed exceptional stratigraphic position of the Gaisbeuren Basin, drilling was undertaken.

Previous investigations include:

- in-liner drilling and borehole geophysical survey
- whole-core scans for magnetic susceptibility and natural remanent magnetisation
- preliminary profile description based on core catcher pieces

8. DOVE Operational Dataset

The following tables list the data, metadata and images included in the DOVE phase 1 operational dataset (DOVE-Phase 1 Scientific Team et al., 2023b). The complete dataset is available on the GFZ data services repository using the following link <https://doi.org/10.5880/ICDP.5068.001> or through the ICDP DOVE project website <https://www.icdp-online.org/projects/by-continent/europe/dove-switzerland>. Explanatory remarks (DOVE-Phase 1 Scientific Team et al., 2023c) are available together with the dataset on the project website <https://www.icdp-online.org/projects/by-continent/europe/dove-switzerland> or using the following link: <https://doi.org/10.48440/ICDP.5068.002>. This includes descriptions on basic laboratory measurements.

NOTE: The operational dataset as well as this report are work in progress and will be updated at least two more time from now on (October, 2023) for the legacy drill sites.

8.1. Data und Metadata from mDIS

Table 11: Available archive file (zip) containing the following reports & data from the DOVE Project Phase 1. Light gray files are still to come.

DATA	Description or Related Lists (pdf files)	DOVE Locations (xlsx, csv, zip)
1 All Data		All Data
2 Expedition		Expedition
3 Site Locations		All Sites
4 Hole Locations		All Holes
5 Cuttings (5068_1) & Borehole Expansion samples (5068_2_A)		5068_1_A 5068_1_B 5068_1_C 5068_2_A
6 Cores	CoreSection- Report_5068_1_C CoreSection- Report_5068_2_A CoreSection- Report_5068_3_A CoreSection- Report_5068_4_A CoreSection- Report_5068_5_A CoreSection- Report_5068_6_A	5068_1_C 5068_2_A 5068_3_A 5068_4_A 5068_5_A 5068_6_A
7 Core Sections		5068_1_C

		5068_2_A
		5068_3_A
		5068_4_A
		5068_5_A
		5068_6_A
8	Section Splits	5068_1_C
		5068_2_A
		5068_3_A
		5068_4_A
		5068_5_A
		5068_6_A
9	Samples	List of all Samples taken from Site 1 – 5 until 17 Aug 2023
		5068_All Samples
10	Sample Request	All Requests for Samples taken in the field and during 1 st sampling party
		5068_Sample Requests
11	Lithological Description of Section Units (Visual Section Logs)	<p>this includes:</p> <ul style="list-style-type: none"> • mDIS records on lithology • Table on Lithological Units • Visual Core Description (VCD) Logs per Section (pdf)
		5068_1_C
		5068_2_A
		5068_3_A
		5068_4_A
		5068_5_A
		5068_6_A
		Lithological Units
		SectionLogs_VCD Hole 1C
		SectionLogs_VCD Hole 2A
		SectionLogs_VCD Hole 3A
		SectionLogs_VCD Hole 4A
		SectionLogs_VCD Hole 5A
		SectionLogs_VCD Hole 6A
12	Driller Reports	Daily Drillers reports exported from mDIS Data Tables & scans of written reports
		5068_1_A
		5068_1_B
		5068_1_C
		5068_2_A
13	Borehole Logging Data	Borehole Logging Data, Meta Data on Runs & Logs (csv) and Composite Logs (combined in 1 zip file for each hole); composite logs also as separate files
		5068_1_BL_All Data
		5068_2_BL_All Data
		5068_3_BL_All Data
		5068_4_BL_All Data
		5068_1_BL_CompositeLogs
		5068_2_A_BL_CompositeLog
		5068_3_A_BL_CompositeLog
		5068_4_A_BL_CompositeLog

			Summary of Tools
14	Vertical Seismic Profile	All VSP Data Site 1 (zip file incl Read me)	5068_1_VSP
15	Auxiliary Tables (incl.)	Sites 1 & 2	Borehole Diameter Casing Diameter
16	MSCL Data	Data Files Site 1 and 2 (zip) Calibration File (xlsx) (also see Explanatory Remarks)	5068_1_C 5068_2_A MSCL Calibration File
17	Additional Data	Carbon, Nitrogen, Sulfur, Water, Uniaxial Shear and Compressive Strength	5068_1_C 5068_2_A
18	READ ME	External Link	https://doi.org/10.48440/ICDP.5068.002

8.2. Image Reports and Primary Images exported from mDIS

NOTE: The images of the operational dataset are work in progress and will be updated at least two more time from now on (October, 2023) for the legacy drill sites. As of now they are available for Sites 1 and 2.

Available images include

- 1) **Section images** were taken from the archive half once the core was opened at the University of Bern (Sites 5068-1 & 2). Image file names begin with the abbreviation CS followed by the combined_id of the sections and are available in JPEG format.
- 2) **Cuttings images** taken at the drill site (Site 5068-1). The file names start with the abbreviation CU followed by the combined_id and are available in JPEG format
- 3) **Hole overview** reports showing images of all sections taken sorted after depths (exported from mDIS)
- 4) **Core overview** were taken from the archive half once the core was opened at the University of Bern (Sites 5068-1 & 2). Image file names begin with the abbreviation CS followed by the combined_id of the sections and are available in JPEG format.

Table 1: Available image files from the DOVE Project Phase 1 (as of October 2023)

	DATA	Description	Locations/Holes
1	Hole Overview Reports	Image Hole Overview (pdf files)	5068_1_C 5068_2_A
2	Section Images	Slabbed Section Overviews (zip)	5068_1_C 5068_2_A
3	Cutting Images	Images (zip file with .jpg)	5068_1_B 5068_1_C
4	Core Overview	Image Core Overviews (pdf files)	5068_1_C 5068_2_A

9. Summary of Preliminary Scientific Assessment

OVERALL

Preliminary data indicates that it will be possible at all the sites to better understand the local glaciation and landscape history and – by merging it with the other sites – in the entire alpine region.

SITE-SPECIFIC

Site 5068_1

In the Tannwald Basin at site 5068_1 glacial deposits were successfully drilled within an overdeeped valley with high-quality core recovery of with a core with 95% recovery. The ICDP 5068_1_C drill hole first penetrated a succession of gravel-dominated, partly diamictic units. Below 38 m the sediments become finer, mostly silt dominated with varying clay content, occasionally interrupted by sand units (e.g., at 73–81 m and 99–104 m). In this section, rare outsized clasts were visible and indicate the presence of dropstones. At 136 m, the sediments become coarser and well-sorted sand units alternate with fine-grained diamicts, occasionally containing a significant amount of gravel. Sand becomes dominant at 149 m and the bedrock Tertiary Molasse deposits were encountered at 155 m. The bedrock is marly in appearance at the top (including macroscopically-observable fossil fragments), occasionally transected by pure sandstone. The occurrence of sandstone increases towards the bottom and finally dominates from 164 m to the final depth of 166 m. In addition:

- Three boreholes were finished and kept open for future research (cross-hole seismic).
- We were able to conduct borehole geophysics in open-hole conditions, which is remarkable for this kind of sediment.
- The boreholes were sampled by the local state authority to test the water quality at the filtered points.
- Future work will refine the preliminary lithological succession and integrate it the various other datasets, especially age dating of the sediments, reflection seismic and borehole geophysics.

Site 5068_2

At site 5068_2 the infilling of the Basadingen overdeepening was successfully cored down to the basal part at a depth of 252 m in mostly excellent core quality. Only the transition to the bedrock could not be reached (by probably only a few meters) due to major drilling difficulties. Based on the preliminary core assessment (prior to opening), the recovered sequence can roughly be divided into two parts: In the lower part, between 252 and 48 m depth, the valley filling consists mainly of sands, which are divided into larger packages by gravel and diamictic interbeds. Between c. 90 and 148 m depth, the sands are interbed gravels (forming dm-m thick beds). In the upper part of the core between 48 and 11 m depth the valley fill is overlain by gravels and above 11 m by diamicts. Future work will refine this preliminary lithological succession and integrate it the various other datasets.

Site 5068_3: upcoming

Site 5068_4: upcoming

Site 5068_5: upcoming

Site 5068_6: upcoming

10. Conclusions

This operational report summarizes the relevant operational aspects of DOVE-Phase 1. For DOVE such a joint report is particularly important because the operations have been conducted under different operational conditions: Sites 5068_1 and 5068_2 were freshly drilled, sites 5068_3 and 5068_6 were drilled earlier but in anticipation of the DOVE project and temporarily stored, and sites 5068_4 and 5068_5 are legacy cores initially not anticipated for use in DOVE. Despite these differences, this report shows that the recovered cores and data are for most parts of equivalent quality across all sites. This common dataset is an excellent basis for the upcoming data analysis and integration steps towards the overarching, pan-Alpine goals of DOVE.

The coring operations at all sites show that drilling operations in overdeepenings are very challenging. This is mainly due to the highly variable, unconsolidated and difficult to predict lithological successions encountered in this overdeepened valley fills. However, with the chosen drilling strategies we have achieved very high recovery and excellent core quality. The emphasis on core quality has led to longer than expected drilling operations (but generally within budget constraints).

In conclusion, the operational procedures have proven very reliable and successful. The operations for DOVE-Phase 1 have set a new standard of how such valley fills can be explored successfully and can be adopted for a potential upcoming DOVE-Phase 2 (see Anselmetti et al. 2022).

11. Acknowledgements

DOVE is financially supported by ICDP, Deutsche Forschungsgemeinschaft (DFG, grant nos. KR2073/3-1, BU 2467/1-2, GA749/5-1, BU2467/3-1, BU3894/2-1, BU3894/3-1, and PR 957/6-1, DFG Project: 2100361301), Nagra, ENSI, LGRB, LFU, Leibniz Institute for Applied Geophysics (LIAG), BOKU Vienna, University of Bern, the Regierungspräsidium Freiburg, Landesgeologie.

Drilling at Site 5068_1 was carried out by H. Anger's Söhne, Bohr- und Brunnenbaugesellschaft mbH. Despite a number of technical problems and protracted drilling operation, they successfully completed the three drillholes and supplied good quality core with a recovery rate of 95%. We thank the firm's contact person, Mirko Huber, for constructive talks and helpful suggestions. The drillsite at Winterstettenstadt was leased from Herr and Frau Wiedmann and we are grateful for their support. A number of local groups and schools visited the site and we thank them for their interest. Greta Clasen at LIAG coordinated the media and press releases.

Site 5068_2 was drilled by Fretus AG, we are thankful for providing us with high-quality drill cores despite many technical challenges. We also acknowledge strong support by the communities of Basadingen-Schlattingen by the Bürgergemeinde Basadingen-Schlattingen, the members of the Jagdgesellschaft Hegi Belzhalden, the local residents, and the involved services of the political community Basadingen-Schlattingen and the Kanton of Thurgau. Technical staff of LIAG assisted with the seismic pre-site surveys and the downhole logging.

We acknowledge all ICDP workshop participants in Como, who contributed to realizing this larger DOVE initiative.

12. References

- Anselmetti, F., Bavec, M., Crouzet, C., Fiebig, M., Gabriel, G., Preusser, F., Ravazzi, C. and DOVE scientific team (2022): Drilling Overdeepened Alpine Valleys (ICDP-DOVE): Quantifying age, extent and environmental impact of Alpine glaciations. *Scientific Drilling* **31**, 51-70. <https://doi.org/10.5194/sd-31-51-2022>
- Behnke, C. and Bram, K. (1998): Erforschung der würmzeitlichen Tannwald-Becken-Struktu (Fallgewichtseismik II – 1996). Report, *NfB Archive* **116**, pp. 833.
- Brandt, A.-C. (2020): Erkundung des alpinen, glazial-übertieften Basadingen-Beckens mithilfe von P-Wellen-Seismik, BSc thesis, Leibniz Universität Hannover, unpublished.
- Buechi, M. W., Schaller, S and Anselmetti, F. (2023). Die DOVE-Forschungsbohrung in Basadingen-Schlattingen: Geologische Erkundung einer eiszeitlichen Übertiefung. *Mitteilungen der Thurgauischen Naturforschenden Gesellschaft*, **71**, 9-22.
- Burschil, T., Bunes, H., Tanner, D.C., Wielandt-Schuster, U., Ellwanger, D. and Gabriel, G. (2018). High-resolution reflection seismics reveal the structure and the evolution of the Quaternary glacial Tannwald Basin. *Near Surface Geophysics*, **16(6)**, p. 593–610, <https://doi.org/10.1002/nsg.12011>
- Ellwanger, D. (2015). Lithostratigraphische Entwicklung des baden-württembergischen Rheingletschergebiets: Übertiefte Becken- und Moränen-Landschaft: LGRB Fachbericht 2015/4.
- Ellwanger, D., 2015, Lithostratigraphische Entwicklung des baden-württembergischen Rheingletschergebiets: Übertiefte Becken- und Moränen-Landschaft: LGRB Fachbericht 2015/4. URL: https://produkte.lgrb-bw.de/docPool/c525_data.pdf
- Ellwanger, D., Wielandt-Schuster, U., Franz, M. and Simon, T. (2011): The Quaternary of the southwest German Alpine Foreland (Bodensee-Oberschwaben, Baden-Württemberg, Southwest Germany). *Quaternary Science Journal*, **60**, p. 306–328, <https://doi.org/10.3285/eg.60.2-3.07>.
- Fiebig, M., Herbst, P., Drescher-Schneider, R., Lüthgens, C., Lomax, J. and Doppler, G., 2014. Some remarks about a new Last Glacial record from the western Salzach foreland glacier basin (Southern Germany). *Quaternary International* 328-329, 107–119, <http://dx.doi.org/10.1016/j.quaint.2013.12.048>
- Husen van, D. and Mayr, M. (2007). The hole of Bad Aussee. An unexpected overdeepened area in NW Steiermark, Austria. *Aust. J. Earth Sci.*, **100**, 128–136.
- Huuse, M. and Lykke-Andersen, H. 2000. Overdeepened Quaternary valleys in the eastern Danish North Sea: morphology and origin. *Quat. Sci. Rev.* **19**, p. 1233–1253, [https://doi.org/10.1016/S0277-3791\(99\)00103-1](https://doi.org/10.1016/S0277-3791(99)00103-1).
- Jerz, H. (1979). Das Wolfratshausener Becken – seine glaziale Anlage und Übertiefung. *E&G Quaternary Sci. J.*, **29**, 63–69, <https://doi.org/10.23689/fidgeo-1646>.
- Müller, E. (2010): Schotterssysteme zwischen dem Thurtal und Schaffhausen. Geologischer Bericht. Technical Report for Swiss Federal Nuclear Safety Inspectorate (ENSI), Nr. **8600-3**.

- Pomper, J., Salcher, B.C., Eichkitz, C., Prasicek, G., Lang, A., Lindner, M. and Götz J. (2017): The glacially overdeepened trough of the Salzach Valley, Austria: Bedrock geometry and sedimentary fill of a major Alpine subglacial basin. *Geomorphology* **295**, p. 147–158, <https://doi.org/10.1016/j.geomorph.2017.07.009>
- Preusser, F., Reitner, J. and Schlüchter, C. (2010): Distribution, geometry, age and origin of overdeepened valleys and basins in the Alps and their foreland. *Swiss J. Geosci.* **103**, p. 407–426, <https://doi.org/10.1007/s00015-010-0044-y>.
- Rolf, C., Wonik, T., Blanke, J.T., Grelle, T., Lehne, C., Wallbrecht, L., and Worm, K. (2021). Die Forschungsbohrungen Lichtenegg und Gaisbeuren (Baden-Württemberg): Gesteinsmagnetik und Bohrlochgeophysik: Leibniz Institute for Applied Geophysics, Report.
- Schaaf, A. (2017). Geologische Aufnahme der Bohrung Gaisbeuren: Bachelor thesis, University of Freiburg
- Schaller, S., Buechi, M. W., Schuster, B. and Anselmetti, F. S. (in press). Drilling into a deep buried valley: A 252 m long sediment succession from a glacial overdeepening in northwestern Switzerland. *Scientific Drilling* **32**, (in press), <https://doi.org/10.5194/sd-32-27-2023>.
- Steinhauser, P., Meurers, B., Aric, K., Granser, H., Hösch, K., Klinger, G. and Lenhardt, W. (1985). Geophysikalische Detailuntersuchung der Schwereanomalie von Bad Aussee. – Geophysikal. Forschungsbericht Nr. 18. Institut f. Meteorologie und Geophysik Univ. Wien, 31 pp.

13. Appendices

A: Hydrogeological report by Dr. von Moos AG

B: Drill Site Layout during drilling boreholes 5068_1_B and 5068_1_C

Appendix A – 5086_2 Hydrogeological report by Dr. von Moos AG

	Dr. von Moos AG Geotechnisches Büro Bachofnerstrasse 5, CH - 8037 Zürich Zweigniederlassungen: Mäderstrasse 8, CH - 5400 Baden	Beratende Geologen und Ingenieure www.geovm.ch info@geovm.ch Telefon +41 44 363 31 55 Dorfstrasse 40, CH - 8214 Gächlingen
---	--	--

Auftrag: **13162 Tiefbohrung BASA 1, Muedihaa, Basadingen-Schlattigen**
 Aktennotiz: **Hydrogeologische Bohrbegleitung**
 Verfasser: **Lawrence Och**
 Datum: **03.02.2022** erg: Visum: **GH**

Verteiler:

- Amt für Umwelt des Kanton Thurgau (erika.tanner@tg.ch)
- Sebastian Schaller, Uni Bern (sebastian.schaller@geo.unibe.ch)
- Marius Büchi, Uni Bern (marius.buechi@geo.unibe.ch)

1. Einleitung / Auftrag

Im Rahmen des Forschungsprojekts "Drilling Overdeepened Alpine Valleys (DOVE)" wurde im Auftrag des Instituts für Geologie der Universität Bern für wissenschaftliche Zwecke auf der Parzelle Kat.-Nr. 2610 bei Muedihaa in Basadingen-Schlattigen über der glazial übertieften Waltalingen-Basadingen-Rinne eine Kernbohrung (BASA 1) abgeteuft (Landeskoordinaten: 2'698'774 / 1'278'321 / 445.1 m ü.M.). Da die Tiefbohrung in einem Grundwassergebiet ausgeführt wurde, mussten gemäss Bewilligung Nr. 2021.01-122 des Amtes für Umwelt des Kantons Thurgau die Bohrarbeiten sowie der Rückbau mit Verfüllung durch eine hydrogeologische Fachperson begleitet werden. Gemäss unserem Angebot vom 4. Mai 2021 und der Auftragsbestätigung mit Email vom 5. Mai 2021 haben wir die Bohr- und Verfüllarbeiten hydrogeologisch begleitet. Die Arbeiten werden in dieser Aktennotiz dokumentiert und beurteilt.

2. Ausgeführte Arbeiten

Die Kernbohrung dauerte vom 25. Mai bis zum 13. Oktober 2021 und erreichte eine Endtiefe von 253 m unter OK Terrain. Dabei kam es vom 1. bis 27. Juli 2021 in einer Tiefe von 126 m unter OKT aus bohrtechnischen Gründen (Probleme mit der Verrohrung, welche überbohrt werden musste) und vom 27. August bis 5. Oktober 2021 in einer Tiefe von 228.3 m unter OKT (Ersatz Bohrgerät) zu längeren Unterbrüchen.

Die Bohrung wurde von 0 bis 57 m unter OKT als Trockenbohrung im Rammbohrhammerverfahren (System Düsterloh) und zwischen 57 und 253 m unter OKT als Spülbohrung im Seilkernbohrverfahren ausgeführt. Zur Stabilisierung der Bohrlochwand wurde ein Spülungszusatz verwendet (GS 550), welcher bei der Trockenbohrung auch zur Schmierung der Verrohrung eingesetzt wurde. Die Bohrung wurde durchgehend und mit der Tiefe abnehmendem Durchmesser verbohrt (vgl. Anhang A1).

Tiefbohrung BASA 1, Muedihaa, Basadingen-Schlattingen

Auftrag: 13162

Hydrogeologische Bohrbegleitung

Zürich, 03.02.2022

Die Bohrkern wurden in opaken Linern extern gelagert und nicht geöffnet. Die geologische Aufnahme wurde vom Geologen Sebastian Schaller der Universität Bern (Auftraggeber) anhand des ca. meterweise sichtbaren Bohrguts vorgenommen (vgl. Anhang A1). Die Bohrung wurde vom 5. bis 10. November 2021 rückgebaut und verfüllt.

Die Dr. von Moos AG stand während der gesamten Bohrung regelmässig mit Sebastian Schaller und zeitweise mit dem Bauführer des Bohrunternehmens (Fretus AG) in Kontakt. Die Tagesrapporte des Bohrunternehmens sowie eine tabellarische Nachführung der Bohrtiefen, Wasserstände, Wassereintritte und Spülverluste wurden uns regelmässig durch Sebastian Schaller übermittelt. Baustellenbegehungen durch Mitarbeiter der Dr. von Moos AG fanden am 31. Mai, 23. Juni und 9. November 2021 statt.

3. Hydrogeologische Folgerungen

Gemäss Bohrprofil im Anhang A1 ist von folgender **geologischer Schichtabfolge** auszugehen:

- 0 – 22 m: Moräne (letzteiszeitlich)
- 22 – 48 m: Buchberg-Schotter
- 48 – 253 m: Moränenkomplex (ältere Eiszeiten) mit Seeablagerungen und Kieslager

Gemäss einer älteren Bohrung, welche in der näheren Umgebung bis auf 201 m u.T. abgeteuft wurde, sollte der obere Teil des älteren Moränenkomplexes (Möhlin- und Beringen-Eiszeiten) überwiegend aus Seeablagerungen und der untere Teil vor allem durch Moräne aufgebaut sein. Da die Kerne der aktuellen Bohrung nicht im Detail aufgenommen werden konnten (opake Liner), sind die Schichtgrenzen noch nicht eindeutig bestimmbar. Der **Fels wurde nicht erreicht**. Allerdings wurden unterhalb von ca. 250 m Tiefe Molassekomponenten (Fels) beobachtet. Die Flanken der Waltalingen-Basadingen-Rinne verlaufen gemäss heutigem Wissensstand von oben nach unten durch Obere Süsswasser-, Obere Meeres- und Untere Süsswassermolasse.

Anlässlich der Trockenbohrung bis in eine Tiefe von 57 m wurden **Wasserzutritte** in Tiefen von ca. 3 und 10 m unter OKT innerhalb der Moräne sowie bei 28 m unter OKT innerhalb des Buchberg-Schotters festgestellt. Bei den oberen Zutritten dürfte es sich um Schichtwasser handeln, wobei der Wasserstand nicht gehalten wurde. Die Wasserzutritte aus dem Buchberg-Schotter führten zu einem **Wasserstand**, welcher sich über die gesamte Bohrung grösstenteils zwischen 26 und 32 m unter OKT (ungefähre Koten 413 bis 419 m ü.M.) bewegte. Während der gespülten Bohrung wurden vollständige **Spülverluste** in Tiefen von ca. 90 – 110 m, 125 – 130 m, 140 – 145 m, 205 – 230 m sowie im Bereich der Endtiefe bei 250 m unter OKT festgestellt. Dabei dürfte es sich um Lagen von gut durchlässigem, überwiegend sandig-kiesigem Material handeln. Wesentliche Wasserzutritte aus dem Moränenkomplex unterhalb des Buchberg-Schotters konnten nicht festgestellt werden.

Tiefbohrung BASA 1, Muedihaa, Basadingen-Schlattigen
Hydrogeologische Bohrbegleitung

Auftrag: 13162
Zürich, 03.02.2022

4. Rückbau und Verfüllung der Bohrung

Die Verfüllung der Bohrung hatte so zu erfolgen, dass das im Buchberg-Schotter zirkulierende Grundwasser weder von Wasserzuflüssen von oben (Geländeoberfläche) noch von unten beeinträchtigt werden kann. Nach dem vollständigen Rückzug der Verrohrung wurde die Bohrung gemäss Anweisungen der Dr. von Moos AG und in Rücksprache mit Auftraggeber, Bohrunternehmer sowie AfU Thurgau folgendermassen verfüllt:

- 0 – 5 m: Deckschicht (Erde/Humus)
- 5 – 12 m: Tonabdichtung (Mikolit 300M)
- 12 – 50 m: Kies
- 50 – 55 m: Tonabdichtung (Mikolit 300M)
- 55 – 253 m: Zement, sulfatresistent (K Injektherm 110 HS)

5. Schlussbemerkungen

Die Kommunikation mit Auftraggeber und Bohrunternehmer verlief häufig und zufriedenstellend. Anlässlich der Begehungen konnten hinsichtlich gewässerschutzrechtlichen Auflagen keine Bedenken angemeldet werden. Durch die vorstehend erläuterte Verfüllung der Bohrung sind keine nachteiligen Auswirkungen auf das Grundwasservorkommen im Buchberg-Schotter zu erwarten.

Zürich, 3.2.2022
Dr. von Moos AG

Anhang:

- A1 Bohrprofil Forschungsbohrung BASA 1, nicht massstäblich (dat. 24.11.2021, Universität Bern)

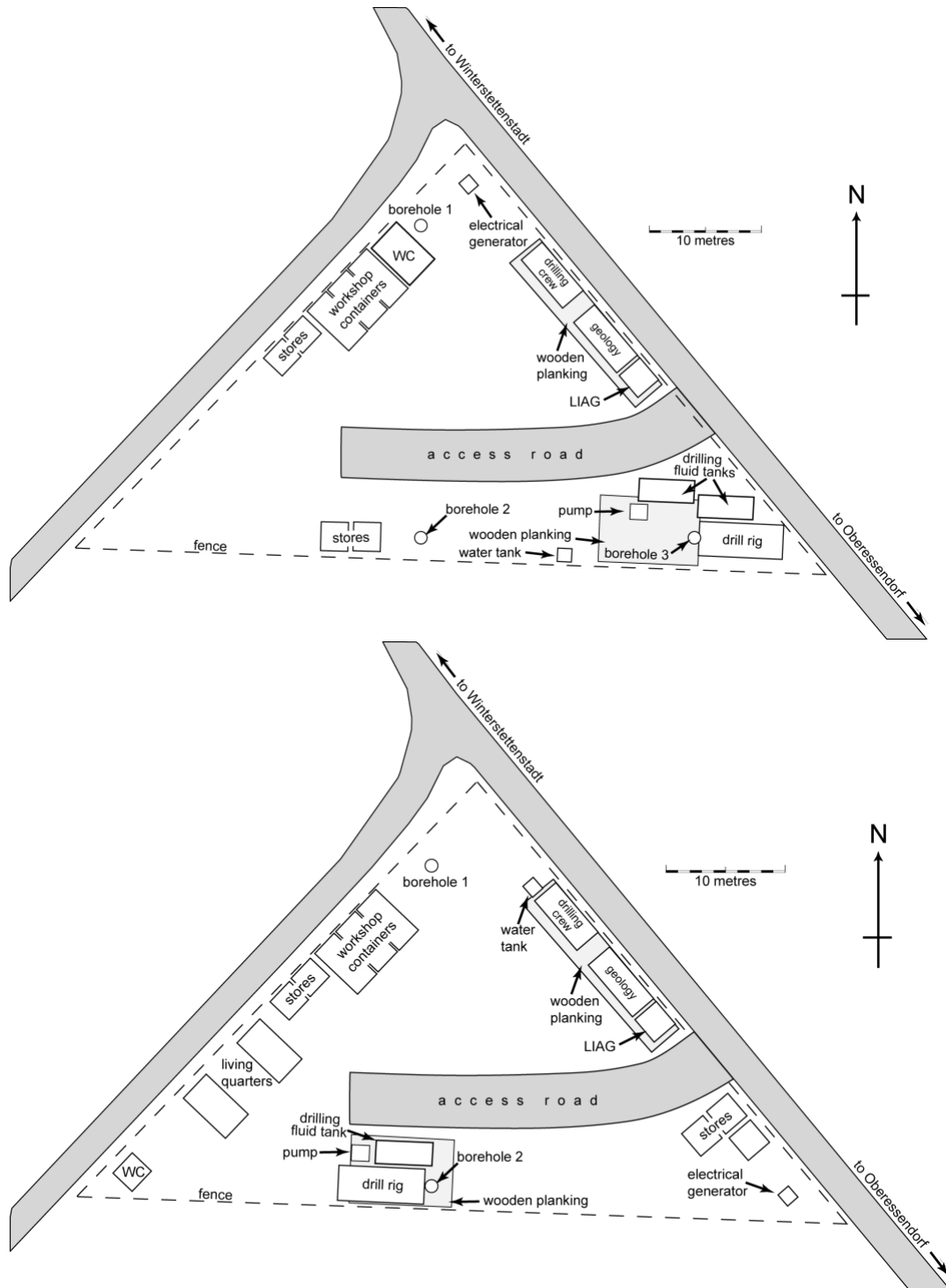
Tiefbohrung BASA 1, Muedihaa,
Basadingen-Schlattingen

Bericht Nr. 13162
Anhang A1

ICDP-DOVE Forschungsbohrung BASA1 / 5068-2, Basadingen-Schlattingen		
Bohrloch-Architektur, Verfüllung und vorläufige lithologische Aufnahme		
Koordinaten (LV95) 2'698'774 / 1'278'321 Oberkante Terrain (OKT) 445.1 m ü. M.		Bearbeiter: S. Schaller, M. Buechi, Universität Bern Datum: 24.11.2021
Bohrlochdurchmesser und Verfüllung Alle Tiefen ab OKT [m]	Litho- logie	Beschreibung erwartetes Bohrgut (basierend auf Beobachtungen an den Kernenden & Bohrmeisterangaben)
Ø 324 mm Humus 5 Dichtungston* 12 Kies 34.5	~2 ~12 ~22	Silt, sandig tonig, kiesig Mittelkies, stark bis schwach sandig, stark bis schwach siltig, teilweise tonig, vereinzelte Blöcke (>10 cm), diamiktisch Fein- bis Mittelkies, teils sandig, schwach siltig
Ø 280 mm Dichtungston* 50 55	~48 ~55	Fein- bis Mittelsand, schwach siltig, mit vereinzelten kies-reichen Lagen, diamiktisch
Ø 245 mm 88 245 mm	~90 ~94	Wechselagerung von Sand und Kies Fein- bis Mittelkies, teilweise siltig bis tonig, durchlässig, Kernverluste
Ø 200 mm 105	~103 ~111	Fein- bis Mittelsand, schwach siltig, mit vereinzelten kies-reichen Lagen, diamiktisch Wechselagerung von Sand und Kies
Ø 152 mm 143	~124 ~131 ~138 ~148	Fein- bis Mittelkies, teilweise siltig bis tonig, durchlässig, Kernverluste Fein- bis Mittelsand, schwach siltig, mit vereinzelten kies-reichen Lagen, diamiktisch Fein- bis Mittelkies, teilweise siltig bis tonig, durchlässig, Kernverluste Fein- bis Mittelsand, schwach siltig, mit vereinzelten kies-reichen Lagen, diamiktisch
Ø 146 mm 228 253	~205 ~218 ~250 253	Fein- bis Mittelkies, teilweise siltig bis tonig, durchlässig Fein bis Mittelsand, schwach siltig, mit vereinzelten kies-reichen Lagen, diamiktisch Fein- bis Mittelkies, vermutlich sandig, teilweise siltig-tonig, Kernverluste
* Dichtungston: Mikolit 300M		

Erstellt von: Sebastian Schaller, Universität Bern

Appendix B –



Layout of the drillsite (5068_1) for the borehole B (top) and C (bottom); supplement to chapter 2.4

Appendix B: Drilling Overdeepened Alpine Valleys (DOVE) – Explanatory remarks of Phase I

Comment:

The following documentation contains explanatory remarks for the required metadata to understand and use the DOVE Phase I operational data set. This data set includes all data acquired during the drilling operation and the initial core description of DOVE Phase I, including those used in Chapters 2, 3, and 4. Since DOVE site 5068_2 was used to define many of the project's internal documentation standards, Katja Heeschen from the ICDP and I mainly wrote this documentation.



ICDP Operational Dataset – Explanatory Remarks

<https://doi.org/10.48440/ICDP.5068.002>

Drilling Overdeepened Alpine Valleys (DOVE) - Explanatory remarks on the operational dataset

DOVE-Phase 1 Scientific Team, Anselmetti, F. S., Beraus, S., Buechi, M. W., Buness, H., Burschil, T., Fiebig, M., Firla, G., Gabriel, G., Gegg, L., Grelle, T., Heeschen, K., Kroemer, E., Lehne, C., Lüthgens, C., Neuhuber, S., Preusser, F., Schaller, S., Schmalfuss, C., Schuster, B., Tanner, D. C., Thomas, C., Tomonaga, Y., Wieland-Schuster, U., and Wonik, T.

Citation of this report:

DOVE-Phase 1 Scientific Team, Anselmetti, F. S., Beraus, S., Buechi, M. W., Bunness, H., Burschil, T., Fiebig, M., Firla, G., Gabriel, G., Gegg, L., Grelle, T., Heesch, K., Kroemer, E., Lehne, C., Lüthgens, C., Neuhuber, S., Preusser, F., Schaller, S., Schmalfuss, C., Schuster, B., Tanner, D. C., Thomas, C., Tomonaga, Y., Wieland-Schuster, U., and Wonik, T. (2023) Drilling Overdeepened Alpine Valleys (DOVE) - Explanatory remarks on the operational dataset. ICDP Operational Dataset – Explanatory Remarks. GFZ German Research Centre for Geosciences. <https://doi.org/10.48440/ICDP.5068.002>

Data described by this report:

DOVE - Phase 1 Scientific Team; Beraus, S., Buechi, M. W., Bunness, H., Burschil, T., Fiebig, M., Firla, G., Gabriel, G., Gegg, L., Grelle, T., Heesch, K., Kroemer, E., Lehne, C., Lüthgens, C., Neuhuber, S., Preusser, F., Schaller, S., Schmalfuss, C., Schuster, B., Tanner, D. C., Thomas, C., Tomonaga, Y., Wieland-Schuster, U., and Wonik, T. (2023): Drilling Overdeepened Alpine Valleys (DOVE) - Operational Dataset of DOVE Phase 1. GFZ Data Services. <https://doi.org/10.5880/ICDP.5068.001>

Referencing Article:

Schaller, S., Buechi, M. W., Schuster, B. and Anselmetti, F. S. (2023). Drilling into a deep buried valley: A 252 m long sediment succession from a glacial overdeepening in northwestern Switzerland, Scientific Drilling, 32, <https://doi.org/10.5194/sd-32-27-2023>

Operational Report

DOVE-Phase 1 Scientific Team, Anselmetti, F. S., Beraus, S., Buechi, M. W., Bunness, H., Burschil, T., Fiebig, M., Firla, G., Gabriel, G., Gegg, L., Grelle, T., Heesch, K., Kroemer, E., Lehne, C., Lüthgens, C., Neuhuber, S., Preusser, F., Schaller, S., Schmalfuss, C., Schuster, B., Tanner, D. C., Thomas, C., Tomonaga, Y., Wieland-Schuster, U., and Wonik, T. (2023) Drilling Overdeepened Alpine Valleys (DOVE) – Operational Report of Phase 1. ICDP Operational Reports. GFZ German Research Centre for Geosciences. <https://doi.org/10.48440/ICDP.5068.001>

Imprint

International Continental Scientific Drilling Program

Helmholtz Centre Potsdam

GFZ German Research Centre for Geosciences

Telegrafenberg

D-14473 Potsdam

Published in Potsdam, Germany

2023

DOI: <https://doi.org/10.48440/ICDP.5068.002>



This work is licensed under a Creative Commons Attribution 4.0 International License. (CC BY 4.0)

<https://creativecommons.org/licenses/by/4.0/>

ICDP Project DOVE – Explanatory remarks on the operational dataset

DOVE-Phase 1 Scientific Team, Anselmetti, F. S. *, Beraus, S., Buechi, M. W., Buness, H., Burschil, T., Fiebig, M., Firla, G., Gabriel, G., Gegg, L., Grelle, T., Heeschen, K. U., Kroemer, E., Lehne, C., Lüthgens, C., Neuhuber, S., Preusser, F., Schaller, S., Schmalfuss, C., Schuster, B., Tanner, D. C., Thomas, C., Tomonaga, Y., Wieland-Schuster, U., and Wonik, T.

* corresponding author

Abstract

All datasets provided in the operational dataset (DOVE-Phase 1 Scientific Team et al., 2023b) of the ICDP project DOVE phase 1 (ICDP 5068) consist of metadata, data and/or images. Here, we summarize explanations on the tables, data and images exported from the database of the project (mDIS DOVE) as well as some basic explanations on identifiers used in ICDP, depths corrections and measurements that are integrated into the dataset.

Supplementary Material

DOVE-Phase 1 Scientific Team et al. (2023a) Drilling Overdeepened Alpine Valleys (DOVE) - Operational Report of Phase 1, <https://doi.org/10.48440/ICDP.5068.001>

DOVE-Phase 1 Scientific Team et al. (2023b) Drilling Overdeepened Alpine Valleys (DOVE) - Operational Dataset of Phase 1, <https://doi.org/10.5880/ICDP.5068.001>

Referencing Articles

Schaller, S., Buechi, M. W., Schuster, B. and Anselmetti, F. S. (2023). Drilling into a deep buried valley: A 252 m long sediment succession from a glacial overdeepening in northwestern Switzerland, *Scientific Drilling*, 32, <https://doi.org/10.5194/sd-32-27-2023>

Boreholes:

Borehole Combined-ID	Borehole IGSN https://doi.org/10.60510/	Latitude decimal WG 84	Longitude decimal WG 84	Year of Operational Phase	Cored length [m]
5068_1_A	ICDP5068EH50001	47.9998028	9.7486417	2021	0
5068_1_B	ICDP5068EH60001	47.9995528	9.7486111	2021	0
5068_1_C	ICDP5068EH70001	47.9995500	9.7490139	2021	164.25
5068_2_A	ICDP5068EH40001	47.6480956	8.7532566	2021	252
5068_3_A	ICDP5068EHC0001	47.9710190	11.460135	2017	198.8
5068_4_A	ICDP5068EHD0001	47.8628920	12.909791	2009	136
5068_5_A	ICDP5068EHE0001	47.6069711	13.7741043	1998	880
5068_6_A	ICDP5068EHG0001	47.8880460	9.7112920	2016	144

DOVE Phase 1 Science Team:

Anselmetti	Flavio S.	Institute of Geological Sciences and Oeschger Centre for Climate Change Research, University of Bern, 3012 Bern, Switzerland
Beraus	Sarah	Leibniz Institute for Applied Geophysics, 30655 Hanover, Germany
Buechi	Marius W.	Institute of Geological Sciences and Oeschger Centre for Climate Change Research, University of Bern, 3012 Bern, Switzerland
Buness	Hermann	Leibniz Institute for Applied Geophysics, 30655 Hanover, Germany
Burschil	Thomas	Federal Institute for Geosciences and Natural Resources, 30655 Hannover, Germany
Fiebig	Markus	Department of Civil Engineering and Natural Hazards, Institute of Applied Geology, University of Natural Resources and Life Sciences, Vienna (BOKU), 1190 Vienna, Austria
Firla	Gustav	Department of Civil Engineering and Natural Hazards, Institute of Applied Geology, University of Natural Resources and Life Sciences, Vienna (BOKU), 1190 Vienna, Austria

Gabriel	Gerald	Leibniz Institute for Applied Geophysics, 30655 Hanover, Germany and Institute of Geology, Leibniz University Hanover, 30167 Hanover, Germany
Gegg	Lukas	Institute of Earth and Environmental Sciences, University of Freiburg, 79104 Freiburg, Germany
Grelle	Thomas	Leibniz Institute for Applied Geophysics, 30655 Hanover, Germany
Heeschen	Katja	Department 4.2 Geomechanics and Scientific Drilling, GFZ German Research Centre for Geosciences, 14473 Potsdam, Germany
Kroemer	Ernst	Ref. 102 Landesaufnahme Geologie, Geogefahren, Bayerisches Landesamt für Umwelt, 95030 Hof, Germany
Lehne	Carlos	Leibniz Institute for Applied Geophysics, 30655 Hanover, Germany
Lüthgens	Christopher	Department of Civil Engineering and Natural Hazards, Institute of Applied Geology, University of Natural Resources and Life Sciences, Vienna (BOKU), 1190 Vienna, Austria
Neuhuber	Stephanie	Department of Civil Engineering and Natural Hazards, Institute of Applied Geology, University of Natural Resources and Life Sciences, Vienna (BOKU), 1190 Vienna, Austria
Preusser	Frank	Institute of Earth and Environmental Sciences, University of Freiburg, 79104 Freiburg, Germany
Schaller	Sebastian	Institute of Geological Sciences and Oeschger Centre for Climate Change Research, University of Bern, 3012 Bern, Switzerland
Schmalfuss	Clemens	Department of Civil Engineering and Natural Hazards, Institute of Applied Geology, University of Natural Resources and Life Sciences, Vienna (BOKU), 1190 Vienna, Austria
Schuster	Bennet	Institute of Earth and Environmental Sciences, University of Freiburg, 79104 Freiburg, Germany
Tanner	David C.	Leibniz Institute for Applied Geophysics, 30655 Hanover, Germany
Thomas	Camille	Institute of Geological Sciences and Oeschger Centre for Climate Change Research, University of Bern, 3012 Bern, Switzerland
Tomonaga	Yama	Eawag, Department of Water Resources and Drinking Water, 8600 Dübendorf, Switzerland
Wieland- Schuster	Ulrike	Regierungspräsidium Freiburg, Landesamt für Geologie, Rohstoffe und Bergbau, Referat 92 Landesgeologie, 79104 Freiburg i.Br., Germany
Wonik	Thomas	Leibniz Institute for Applied Geophysics, 30655 Hanover, Germany

Table of contents

1.	Introduction	2
1.1	ICDP Combined_ID.....	2
1.2	IGSN	3
1.3	Depths: drillers depth and depths corrections	3
1.4	mDIS data base scheme	3
2	Available data files	4
3	Meta Data Files (mDIS)	7
3.1	All Data	7
3.2	Expedition	7
3.3	Sites	8
3.4	Holes	8
3.5	Driller Reports	9
3.6	Cores	11
3.7	Sections.....	12
3.8	Core Section Reports	14
3.9	Split	14
3.10	Sample Requests.....	15
3.11	Samples.....	16
3.12	Cutting.....	17
3.13	Borehole Expansion Samples.....	18
4	Borehole Measurements	19
4.1	Preprocessing Site 1 (5068_1)	19
4.2	Preprocessing Site 2 (5068_2)	25
4.3	Borehole Logging Files	26
4.4	Borehole measurements available from the legacy Sites 3 through 6	26
5	Data Tables	27
5.1	Lithological Units and Core Description	27
5.2	Multi Sensor Core Logging (Sites 1 & 2)	27
5.2.1	MSCL data processing:.....	30
5.3	Water-content measurements (WACO) (Site 1 and 2).....	31
5.4	Carbon, Nitrogen and Sulfur Data (TNSC, ITC and Carbonate Content; CCOM) (Sites 1-6)	32
5.5	Undrained uniaxial compressive strength (POCK) and uniaxial shear strength (VANE) measurements	33
6	Images.....	33
7	References	34

1. Introduction

1.1 ICDP Combined_ID

The ICDP naming convention uses the hierarchical relation of a sample taken from a section split of a core run retrieved from a drill hole (Fig. 1). The convention uses relative depth, which is preferable because it will remain constant even after depth corrections possibly applied at a later stage. Deviating from the usual ICDP combine_ID, the DOVE project added an abbreviation for the analysis to the sample combined_ID, e.g.: ICDP_5068_1_A_550_3_WR_52-68:NOBE. See Chapter 2.

The ICDP expedition code for the DOVE project is 5068. At the time of this report (May 2023), the DOVE project has 6 sites with 1 hole each, except for site 1 (Tannwald) where holes A – B were drilled and only hole C was cored.

Core runs varied in length but the common length of a core section, which a core was cut into, is 1 m for better handling purposes. While only a few samples are taken on the full cylindrical core material (wholeroound, WR) most of the sampling and description was done after the section was split vertically into a working (W) and archive (A) half, with the latter commonly being used for nondestructive sampling only. The top and bottom of the sample (= interval) is expressed as the distance to the top of the section. An example for a combined_id of a cutting is: 5068_1_A_21_CUT, which is cutting (CUT) collected between 20 – 21 m from borehole 5068_1_A. An example of the combined_id of a borehole-expansion-sample is: 5068_2_A_1_BES, with 5068_2_A being the hole, _1 being the bottom depth and BES indicating the sample type.

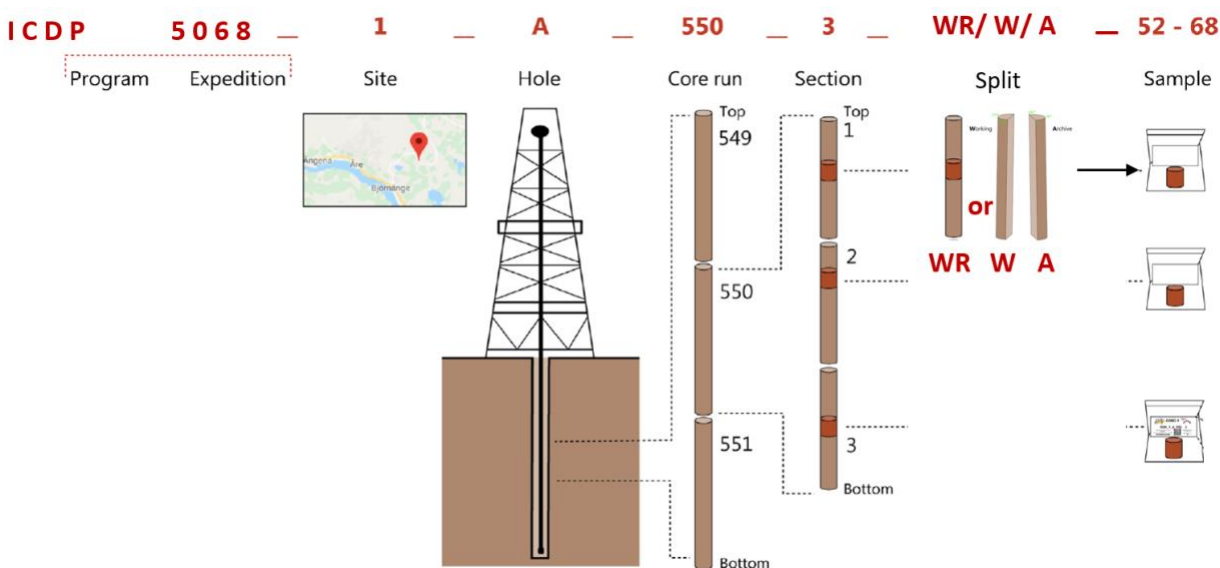


Figure 1 : Example for the common naming convention used in ICDP. The combined_id is used in ICDP to name any site, hole and drilled or cored material.

For legacy drill cores from sites 3 to 6, the original core length and core run number is unknown. Here each section is equivalent to a core run or vice versa there is only one section to each core run for all legacy.

1.2 IGSN

Following the FAIR data principle, each hole, core, section split, sample and cutting has a unique identifier, the so called International Generic Sample Number (IGSN). This number is registered through an agent and allows for the sample to be findable via the IGSN data base. For details on the ICDP – IGSN please see Conze et al. (2017) and <https://www.igsn.org/> (last visited 06/02/2023).

1.3 Depths: drillers depth and depths corrections

During the drilling operations, only driller's depth is documented. In the DOVE project, the drillers use the ground surface as their reference height, and no further depth correction has been made at the time of publication of the data set (August 2023). If you have to refer to total depth, use the depth given in column *mcd_depth*.

- In all depth-related datasets, usually, two or three different depths are stored:
 - The original driller's depth
 - Top and bottom depths, which are equivalent to the driller's depth corrected only by any difference between drillers reference height and surface (= 0 meter below surface (mbs))
 - Relative depth (to top of core or to top of section)
 - Corrected depth (=mcd_depth = meter corrected depths)

Throughout all datasets with measured values the metric unit system is used. It is recommended to use the MCD depth for any evaluation or visualization.

In the DOVE project an integrative depth matching between downhole logs and MSCL data show no significant differences in depth distribution. Thus, a depth correction based on downhole logging data will not be performed for any of the sites. A correction of the section lengths to match MSCL data and sample depths was performed for sites 5068_1 and 5068_2 but does not exceed 7 cm (see paragraphs on "Sections" for details).

1.4 mDIS data base scheme

The mobile Drilling Information System (mDIS) is a database management application developed by ICDP, using a MySQL relational data base in the backend. The relations of the separate tables often are hierarchical and set up to represent the combined_id (Fig. 2). mDIS uses so called "pseudo" fields, particularly helping to keep track of any depth changes. Apart from the driller's depth and any measured lengths, all depth information is calculated when data are called upon but is not stored in the database.

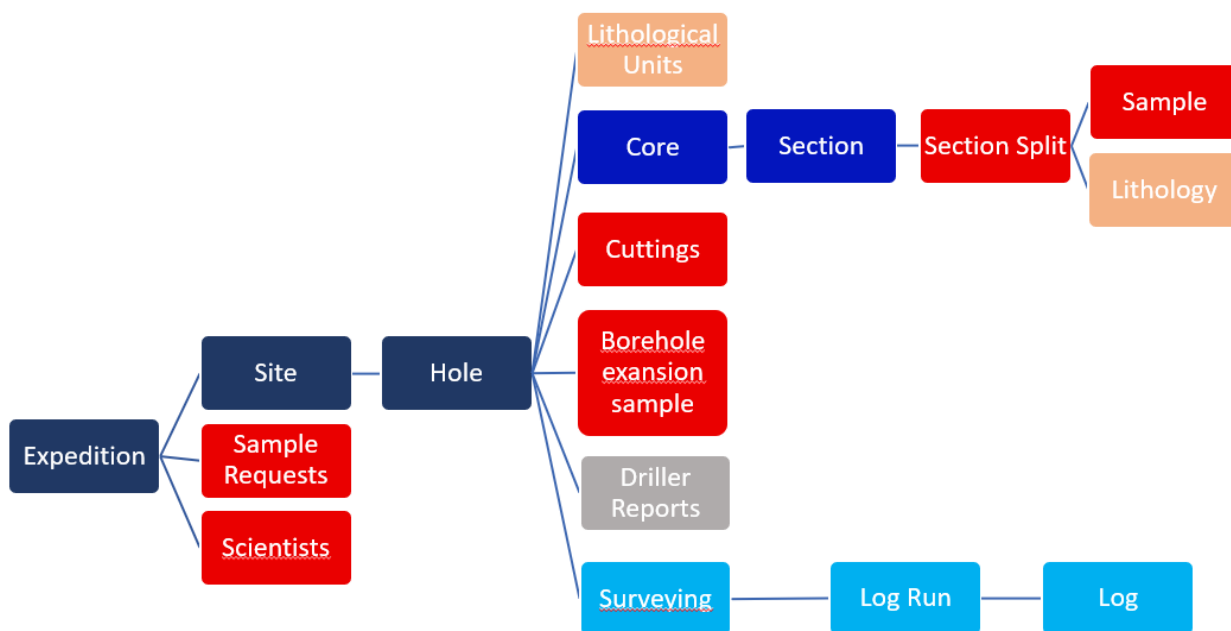


Figure 2: mDIS database relational hierarchy.

2 Available data files

The DOVE_5068 Dataset folder contains the curational datasets and 3 additional folders for files originating from borehole_logging, data measurements and imaging of the core material. Note that the data & images of the operational dataset are work in progress and will be updated at least two more time from now on (October, 2023) for the legacy drill sites.

DOVE_5068_Dataset

- Borehole_logging
- Data
- Images

Table 1: Available file containing reports & data from the DOVE Project Phase 1. Light gray files are still to come in a follow up version of the operational dataset once the data & reports are being produced.

	DATA	Description or Related Lists (pdf files)	DOVE Locations (xlsx, csv, zip)
1	All Data		All Data
2	Expedition		Expedition
3	Site Information		All Sites
4	Hole Information		All Holes
5	Cuttings (5068_1) & Borehole Expansion samples (5068_2_A)		5068_1_A 5068_1_B 5068_1_C 5068_2_A

6	Cores	CoreSection-Report_5068_1_C	5068_1_C
		CoreSection-Report_5068_2_A	5068_2_A
		CoreSection-Report_5068_3_A	5068_3_A
		CoreSection-Report_5068_4_A	5068_4_A
		CoreSection-Report_5068_5_A	5068_5_A
		CoreSection-Report_5068_6_A	5068_6_A
7	Core Sections		5068_1_C
			5068_2_A
			5068_3_A
			5068_4_A
			5068_5_A
			5068_6_A
8	Section Splits		5068_1_C
			5068_2_A
			5068_3_A
			5068_4_A
			5068_5_A
			5068_6_A
9	Samples	List of all Samples taken from Site 1 – 5 until 17 Aug 2023	5068_All Samples
10	Sample Request	All Requests for Samples taken in the field and during 1 st sampling party	5068_Sample Requests
11	Lithological Description of Section Units (Visual Section Logs)	this includes:	5068_1_C
		• mDIS records on lithology	5068_2_A
		• Table on Lithological Units	5068_3_A
		• Visual Core Description (VCD) Logs per Section (pdf)	5068_4_A
			5068_5_A
			5068_6_A
			Lithological Units
			SectionLogs_VCD Hole 1C
			SectionLogs_VCD Hole 2A
			SectionLogs_VCD Hole 3A
12	Driller Reports	Daily Drillers reports exported from mDIS Data Tables & scans of written reports for 5068_2_A	5068_1_A
			5068_1_B
			5068_1_C
			5068_2_A
13	Borehole Logging Data	Borehole Logging Data, Meta Data on Runs & Logs (csv) and Composite Logs (combined in 1 zip file for each hole); composite logs also as separate files	5068_1_BL_All Data
			5068_2_BL_All Data
			5068_3_BL_All Data
			5068_4_BL_All Data

			5068_1_BL_CompositeLogs 5068_2_A_BL_CompositeLog 5068_3_A_BL_CompositeLog 5068_4_A_BL_CompositeLog Logging Tools
14	Vertical Seismic Profile	All VSP Data Site 1 (zip file incl Read me)	5068_1_VSP
15	Auxiliary Tables	Sites 1 & 2	Borehole Diameter Casing Diameter
16	MSCL Data	Data Files Site 1 and 2 (zip) Calibration File (xlsx) (also see Explanatory Remarks)	5068_1_C 5068_2_A MSCL Calibration File
17	Additional Data	Carbon, Nitrogen, Sulfur, Water, Uniaxial Shear and Compressive Strength (files: CCOM, Watercontent, POCK, VANE,	5068_1_C 5068_2_A
18	Exp	External Link	https://doi.org/10.48440/ICDP.5068.002

Available images include

Table 2: Available image files from the DOVE Project Phase 1. Light gray files are still to come.

	DATA	Description	Locations/Holes
1	Hole Overview Reports	Image Hole Overview (pdf files)	5068_1_C 5068_2_A
2	Section Images	Slabbed Section Overviews (zip)	5068_1_C 5068_2_A
3	Cutting Images	Images (zip file with .jpg)	5068_1_B 5068_1_C
4	Core Overview	Image Core Overviews (pdf files)	5068_1_C 5068_2_A

- 1) **Section images** were taken from the archive half once the core was opened at the University of Bern (Sites 5068-1 & 2). Image file names begin with the abbreviation CS followed by the combined_id of the sections and are available in JPEG format.
- 2) **Cuttings images** taken at the drill site (Site 5068-1). The file names start with the abbreviation CU followed by the combined_id and are available in JPEG format
- 3) **Hole overview** reports showing images of all sections taken sorted after depths (exported from mDIS)
- 4) **Core overview** were taken from the archive half once the core was opened at the University of Bern (Sites 5068-1 & 2). Image file names begin with the abbreviation CS followed by the combined_id of the sections and are available in JPEG format.

3 Meta Data Files (mDIS)

3.1 All Data

This file contains all metadata exported from the mDIS database as described below

- Throughout all datasets the common naming convention used is Expedition, Site, Hole (the Expedition ID 5068 is used for DOVE)
- Throughout all datasets the common date and time format used is Year Month Day (Hours:Minutes:Seconds). Time is given in UTC.

3.2 Expedition

mDIS Table (1 File)

Name	Expedition		
ParentModel	ProjectProgram		
Column name	Data type	Column Label	Description
id	integer	Id	id (data base id)
program_id	integer	Program Id	parent id (database id)
name	string	Expedition Name	
expedition	string	Expedition Code	(ICDP: 4-digit number)
acr	string	Acronym	Abbreviation of project
chief_scientist	string_multiple	Chief Scientists	Name of Principle Investigators
start_date	dateTime	Start of Expedition	
end_date	dateTime	End of Expedition	
comment	string	Additional Information	
country	string_multiple	Country	Country in which the Drilling Takes Place
rock_classification	string_multiple	Rock Classification	Drilled Rock Types
geological_age	string_multiple	Geological Age	Age of Drilled Rocks
location_description	string	Location Description	
funding_agency	string	Funding Agency for Drilling	
name_alternative	string	Alternative name for expedition	
scientist_contact	string	Email chief scientist	
objectives	text	Objectives	Objectives listed in proposal
keywords	string_multiple	Keywords	Keywords other than geological age

3.3 Sites

mDIS Table Site (1 File)

Name	Site			
ParentModel	ProjectExpedition			
Column name	Data type	Column Label	Description	
id	integer	SKEY	id (data base id)	
expedition_id	integer	Expedition Id	parent id (database id)	
combined_id	string	Combined Id		
site	string	Site Number		
name	string	Name of Site	(if any)	
comment	string	Additional Information		
location_type	string	Location Type	e.g. land, sea, lake	
description	string	Description of site		
city	string	City nearby drill site		
state	integer	State		
county	string	County		
country	string	Country		

3.4 Holes

mDIS Table Hole (1 File)

The coordinate system for decimal latitude and longitude is WGS84. The platform type “R” stands for land-based drilling rig.

Name	Hole			
ParentModel	ProjectSite			
Name	Type	Label	Description	
id	integer	SKEY	id (data base id)	
site_id	integer	Site Id	parent id (database id)	

hole	string	Hole	Hole Identifier (one character A - Z)
combined_id	string	Combined Id	
latitude_dec	double	Latitude (decimal degrees)	
longitude_dec	double	Longitude (decimal degrees)	
coordinate_system	string	Coordinate System	WGS84
ground_level	double	Ground Level [m]	Height above Sea Level
depth_water	double	Water Depth [m]	below sea surface
elevation_rig	double	Elevation of Rig Floor [m]	Reference height for drillers depth
direction	string	Direction of Inclination	
inclination	double	Inclination [degree]	Degree of Inclination
start_date	dateTime	Start Date	Start of Drilling Operations
end_date	dateTime	End Date	End of Drilling Operations
comments	string	Additional Information	
drilling_depth_dsf	double	Drilled Depth Below Surface [mbs]	mbs = meter below surface; > 0
core_length	double	Core Length [m]	
comments_2	string	Additional Information	
igsn	string	IGSN	International Generic Sample Number
methods_in_hole	string_multiple	Methods In Hole	Measurements done in Hole
gear	string_multiple	Gear	Equipment Info; not applicable
comments_3	string_multiple	Comments 3	
drilling_method	string	Drilling Method	
platform_name	integer	Name of Platform	
platform_description	string	Description of Platform	
platform_type	string	Platform Type	
platform_operator	string	Platform Operator	
repository_name	string_multiple	Name of Repository	
repository_contact	string	Repository Contact	
moratorium_start	date	Start of Moratorium	
moratorium_end	date	End of Moratorium	
comment_4	string	Additional Information Repository	

3.5 Driller Reports

Metadata and scanned reports of the driller reports as written/filled in by the drillers are available for sites 5068_1 and 5068_2. The list is based on the most information given for one borehole – they vary considerably between different drilling companies.

Files: For each hole of sites 1 and 2, there is one .csv file exported from the mDIS table & a zip file containing the scans of the original – paper – drillers report. There is one zip file for each of the legacy drill sites where there are data available.

mDIS Driller Reports table

Name	DailyReport	
ParentModel	ProjectHole	

Name	Type	Label
id	integer	ID
hole_id	integer	Hole
report	integer	Report
date	date	Date
comission	string	Comission
site_manager	string	Site Manager
drill_manager	string	Drill Manager
drilling_rig	string	Drilling Rig
staff	integer	Staff
drilling_tool_typ	string	Drilling Tool Typ
drilling_tool_diameter	string	Drilling Tool Diameter [mm, inch]
water_level	double	Water Level [m]
last_depth	double	Last Depth [m]
daily_depth	double	Daily Depth [m]
completed_drilling_depth	double	Completed Drilling Depth [m]
casing_diameter	integer	Casing Diameter [mm]
casing_from	double	Casing from [m]
casing_to	double	Casing to [m]
comment_casing	string	Comment Casing
comment_drilling	string	Additional Comments by Drillers
fluid_content_1	string	Fluid Content 1
fluid_content_1_amount	integer	Fluid Content 1 [kg]
fluid_content_2	string	Fluid Content 2
fluid_content_2_amount	integer	Fluid Content 2 [kg]
density_drill_mud	double	Density of Drill Mud [kg/l]
az_raz	string	az/raz [sec]
temperature	double	Temperature of drilling fluid [°C]
conductivity	integer	Conductivity of drilling fluid [mS]
waz	double	WAZ [min]
ph	double	pH of drilling fluid
formation_1	string	Formation 1
formation_1_top	double	Formation 1 Top
formation_1_bottom	double	Formation 1 Bottom
formation_2	string	Formation 2
formation_2_top	double	Formation 2 Top
formation_2_bottom	double	Formation 2 Bottom

formation_3	string	Formation 3
formation_3_top	double	Formation 3 Top
formation_3_bottom	double	Formation 3 Bottom
formation_4	string	Formation 4
formation_4_top	double	Top of Formation 4
formation_4_bottom	double	Formation 4 Bottom
formation_5	string	Formation 5
formation_5_top	double	Top of Formation 5
formation_5_bottom	double	Bottom of Formation 5
formation_6	string	Formation 6
formation_6_top	double	Top of Formation 6
formation_6_bottom	double	Bottom of Formation 6
casing_2	integer	Diameter Casing 2 [mm]
casing_2_top	double	Top of Casing 2 [m]
casing_2_bottom	integer	Bottom of Casing 2 [m]
casing_3	integer	Diameter Casing 3 [mm]
casing_3_top	integer	Top of Casing 3 [m]
casing_3_bottom	integer	Bottom of Casing 3 [m]

3.6 Cores

A core or core-run is the complete geological material recovered from a single core barrel. The top depth of each core is the depth given by the drillers, not a cumulative depth of curated sections.

mDIS Table Core (one table for each hole)

Name	Core		
ParentModel	ProjectHole		

Name	Type	Label	Description
id	integer	SKEY	id (data base id)
hole_id	integer	Hole Id	parent id (database id)
core	integer	Core	core identifier
combined_id	string	Combined Id	
analyst	string	Curator	Initials of Data Curator
core_ondock	dateTime	Core on Deck (CoD)	
core_type	string	Core Type	Method of Drilling; R = Rotary Core Barrel (RCB); S = Ramming Drill Hammer, T = Triple Tube Core Barrel (TIR)
drillers_depth	double	Drillers Depth [mbrf]	Depth below Drillers Ref. Point (DOVE = ground surface = mbs)

drilled_length	double	Drilled Core Length [m]	
drillers_bottom_depth	pseudo	Drillers Bottom Depth [mbrf]	
top_depth	pseudo	Top Core Depth below surface [mbs]	mbs = meter below surface
bottom_depth	pseudo	Bottom Core Depth [mbs]	mbs = meter below surface
core_recovery	double	Core Recovery [m]	Length of Recovered Core
core_recovery_pc	double	Core Recovery (%)	$= \frac{([\text{core_recovery}] * 100)}{(\text{ABS}([\text{bottom_depth}] - [\text{top_depth}])))}$
core_loss_reason	string	Core Loss Reason	
continuity	string	Continuity	Continuity Between Cores or Sections
last_section	integer	Section Count	Number of Core Sections
core_diameter	string	Core Diameter [mm]	
oriented	boolean	Core Oriented?	1 = yes
rqd_abundance	string	RQD Abundance	RQD = Rock Quality Designation
comments	string	Additional Information	
igsn	string	IGSN	
fluid_type	string	Drilling Fluid Type	
bit_type	string	Bit Type	
barrel_length	double	Barrel Length [m]	
comments_2	string	Additional Information	
comments_3	string multiple	Comments 3	
comment_igsn	string	Comment IGSN	
core_splits	pseudo	Do splits exist?	Do Archive and/or Working Halves exist? (1 = yes)

3.7 Sections

The core is cut into sections that fit a corebox slot and can be handled in the laboratory. Since in the DOVE project each section is in a separate core box with a single slog, no core corebox information is needed.

The individual section depths are calculated based on the top depth of the core, the length of the individual sections, and the cumulative length of the sections of one core. The top of the first section of a core always corresponds to the top depth of the core. All following section tops are calculated using *core top depth [mbs] + section length [m]* of the preceding sections of the same core. Bottom depths are calculated from *section top depth [m] + section length [m]*. There is a very good depth correlation between the core logs and borehole logging data for Sites 5068_1 or 5068_2. All MCD offsets are zero.

In case of a difference between section length and curated length, commonly < 5 cm, small depth adjustment was carried out to plot MSCL logging data and lithology logs of the sections. As the liners were pre-cut to 1m length (+/- 1 cm), and the core catchers were pushed back into the liners, the length of a full liner was considered 1 m at the drill site. Only in the few cases when liners had to be cut, the length was measured by the driller (precision +/- 1 cm). Section overlengths of < 3 cm were accommodated using

the endcaps and were ignored for the section length but noted down in the curated length using MSCL logs and photos. In the few cases with a clear overlength (> 3 cm) a separate core catcher section was stored but considered as artificial overlength/ expansion/ backfall. These sections were not logged. Any curated overlength occurring in logs or sample depth was recalculated to fit the section lengths. For sites 1 and 2 a nominal section length is mentioned in the data files, which is the precut length of the black liners used in the field and closed immediately without inspection of the true cored length (recovery).

nominal section length = curated length, right

mDIS Table Section (1 file for each hole)

Name	Section		
ParentModel	CoreCore		

Name	Type	Label	Description
id	integer	Id	id (data base id)
core_id	integer	Core Id	parent id (database id)
section	integer	Section	Section number
combined_id	string	Combined Id	
top_depth	pseudo	Section Top Depth [mbs]	mbs = meter below surface
section_length	double	Section Length [m]	
bottom_depth	pseudo	Section Bottom Depth [mbs]	mbs = meter below surface
analyst	string	Curator	Initials of Data Curator
section_condition	string	Section Condition	Broken, whole...
curated_length	double	Curated Length [cm]	can differ from section length, e.g. due to sampling the whole round or degassing
comment	string	Additional Information	
mcd_top_depth	pseudo	Corrected Top Depth/MCD Top Depth [mbs]	mcd = meter corrected depth
mcd_offset	double	MCD offset for depth correction [m]	
core_catcher	boolean	Core Catcher	Is this section a core catcher? (yes = 1)
core_split	pseudo	Do Splits Exist?	
weight	double	Weight of section [kg]	including liner
filling_estimate	double	Estimate for filling of liner [%]	calculated using bulk density
pushed_cc	boolean	CC pushed back in section	yes = 1
noble_gas_sampling	boolean	Noble Gas Sampling	yes = 1
microbio_sampling	boolean	Deep Biosphere Sampling	yes = 1
onsite_split	boolean	Section splitted onsite	
bulk_density	double	Bulk Density [kg/m3]	Estimated Bulk Density of recovered Sediment

core_recovery	integer	Core Recovery (after opening) [%]	
onsite_lithology	string_multiple	Onsite Lithology	
comment_noblegas	string	Comment on Noble gas sampling	
comment_biosphere	string	Comment on deep biosphere sampling	
light_exposed	string	Light exposed	

3.8 Core Section Reports

The core section reports list all cores, including the related sections for the given borehole, their depths, length, comments and core recovery. There is one report for each hole.

3.9 Split

In mDIS a section is equivalent to a wholround section split (WR). The IGSN of the WR is inherited by the archive half (A) once the wholround is split into working (W) and archive (A) half. The working half gets a new IGSN assigned to it. All samples and lithological descriptions are related to the one of the splits WR, W or A in the database.

mDIS Table SectionSplit (1 file for each hole)

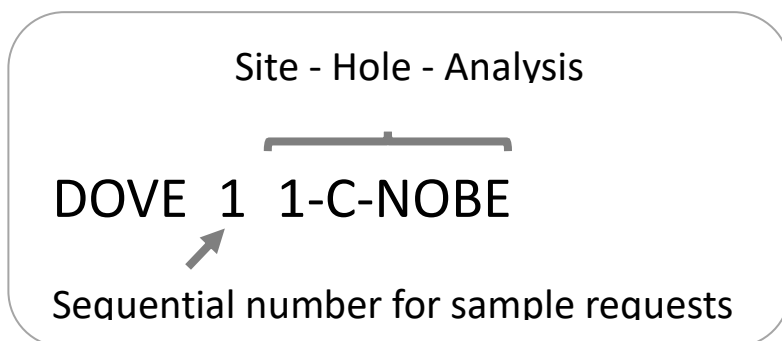
Name	SectionSplit		
ParentModel	CoreSection		

Name	Type	Label	Description
id	integer	ID	id (data base id)
section_id	integer	Section	parent id (database id)
origin_split_id	integer	Origin Split Id	Data base ID of the split before (further) splitting; usually the WR
origin_split_type	pseudo	Origin Split Type	
type	string	Type	Whole, Archive, Working (WR; W, A)
combined_id	string	Combined ID	
percent	integer	Percent [%]	Volume [%] of the original section
still_exists	boolean	Still exists	1 = yes
sampleable	boolean	Sampleable	Can samples be taken? 1 = yes
curated_length	pseudo	Curated Length [cm]	
curator	string	Curator	
mcd_top_depth	pseudo	MCD/Corrected Top Depth [mbs]	Top Depth + MCD offset
mcd_bottom_depth	pseudo	MCD/Corrected Bottom Depth [mbs]	= MCD_Top Depth + Section Length
comments	string	Additional information	
igsn	string	IGSN	Section IGSN needs to be new for working half

3.10 Sample Requests

Before sampling, a sample request needs to be approved by the principal investigators. The table contains all sample request_IDs collected before the publication of the basic data set. To find out who has the samples/who applied for a sample request, please contact the chief scientist of the expedition. Any personal data were deleted from the list, however, in the database every sample is assigned to a scientist/group of scientists by a sample request_IDs.

Sample Request Combined_ID



mDIS Table SampleRequests (1 file)

Name		SampleRequest	
ParentModel		ProjectExpedition	
Name	Type	Label	Description
id	integer	ID	id (data base id)
expedition_id	integer	Expedition	parent id (database id)
request_no	integer	Request No	
request_complete	string	Request Complete	Combined_ID of sample request
request_type	string	Request Type	Type of Sampling
purpose	string	Purpose	Purpose of sampling
request_date	date	Request Date	
approval_date	date	Approval Date	Date of Request Approval by PIs
completion_date	date	Completion Date	Date of Sampling
approved_by	string	Approved By	
comments	string	Additional Information	
sample_material	string	Sample Material	Kind of Sample Material
sample_size	double	Sample Size	Number only
sample_unit	string	Sample Unit	Unit of size of sample requested
amount_requested	double	Sample Volume Requested	Fraction of split section being requested [%]
number_samples	integer	Number of Samples requested	
destructive	boolean	Destructive	1 = yes; 0 = no
curator	string	Curator	
comments_2	string	Comments 2	

3.11 Samples

The main stock of cored material is described under Lithology and Cuttings. Some samples have already been taken on-site, mainly for microbiological and noble gas investigations. Samples taken from the legacy holes before the DOVE project are not included in the mDIS nor in the exported file.

Deviating from the usual ICDP combine_ID, the DOVE project added an abbreviation for the analysis to the sample combined_ID naming the split and the sampled depth interval, e.g., ICDP_5068_1_A_550_3_WR_52-68:NOBE.

Table on Analysis & Abbreviation

Abbreviation	Analysis
CCOM	Carbonate/organic matter analysis with CNS elemental analyzer of fine-grained lithologies
CLAS	Clast samples
COSM	Cosmo-samples, sand preferred
COTO	Computerized tomography (CT) scan
GEOT	Geotechnical samples for oedometer or other geotechnical analyses
GRSZ	Grain size analysis of mainly fine sections
GSPE	Gamma spectroscopy
LUMI	Luminescence dating
MBIO	Analysis of Microbiology in fine-grained lithologies
NOBE	Noble-gas porre water analysis of bulk sediment samples
PMAG	Paleomagnetic
PMEV	Paleomagnetic „Lachamps“ and „Blake“ Events
POCK	Pocket penetrometer measurements
POLL	Pollen screening in fine-grained lithologies
SMSL	Smear slide
VANE	Vane-shear measurements
WACO	Water content
XRFS	XRF-scanning

mDIS Table Sample (one file for all holes)

Name	Sample		
ParentModel	CurationSectionSplit		
Name	Type	Label	Description
id	integer	ID	id (database id)
section_split_id	integer	SectionSplit	parent id (database id)
sample_combined_id	string	DOVE Sample Combined ID	
sample	string	Sample number	
igsn	string	IGSN	
sample_date	date	Sample Date	
top	double	Sample Top Depth [cm]	Distance from Section Top Depth [cm]

interval	double	Sample Interval [cm]	Length of sampled area
bottom	pseudo	Sample Bottom Depth [cm]	Distance from Section Top Depth [cm]
curator	string	Curator/Analyst	
sample_material	string	Sample Material	
sample_size	double	Sample Size	Number only
sample_unit	string	Sample Unit	
fraction_of_split_taken [%]	double	Volume Taken	
request_no	string	Request No	Sample request number
scientist	String	Requesting scientist	
analysis	string	Analysis	Abbreviation for Analysis the sample was requested for; see Sample Requests, Table on Analysis & Abbreviation
sample_top_mbsf	pseudo	MCD/Corrected Sample Top Depth [mbs]	
sample_bottom_mbsf	pseudo	MCD/Corrected Sample Bottom Depth [mbs]	
comment	string	Additional Information	

3.12 Cutting

Cuttings were taken every meter during flush drilling at Site 5068_1_A and 5068_1_B and used to develop a crude lithological profile for these holes where there no coring took place. For details on the sampling please see the Operational Report of the DOVE Phase 1 project (DOVE-Phase 1 Scientific Team et al., 2023a).

mDIS Table Cuttings (1 file for each hole)

Name	Cuttings		
ParentModel	ProjectHole		

Name	Type	Label	Description
id	integer	ID	id (database id)
hole_id	integer	Hole	parent id (database id)
cuttings	string	Cuttings Complete ID	
cuttings_id	integer	Cuttings ID#	
igsn	string	IGSN	
curator	string	Curator	
sampling_datetime	dateTime	Sampling Date_time	
depth	double	Depth [mbs]	Average depth below surface
drillers_sieve	double	Drillers Sieve [mm]	Mesh width for mud sampling by drillers
comments_drillers	string	Comments Drillers	

sample_weight	integer	Sample Weight [g]	
ratio_rock_clasts	integer	Ratio Rock Clasts [%]	
ratio_mud_clasts	integer	Ratio Mud Clasts [%]	
max_diameter_rock_clasts	double	Max Diameter Rock Clasts [mm]	
max_diameter_mud_clasts	double	Max Diameter Mud Clasts [mm]	
sorting	string_multiple	Sorting	
comments_sample	string	Comments Sample	
petrography_coarse	string_multiple	Petrography Coarse	
fossiles_coarse	string_multiple	Fossils Coarse	
plant_remains_coarse	string	Plant Remains Coarse	
petrography_fine	string_multiple	Petrography Fine	
fossiles_fine	string_multiple	Fossils Fine	
plant_remains_fine	string	Plant Remains Fine	
accessory_minerals_fine	string_multiple	Accessory Minerals Fine	
internal_structures	string_multiple	Internal Structures	
smear_slide	boolean	Smear Slide	
consistency	string_multiple	Consistency	
inferred_lithology	string_multiple	Inferred Lithology	
clasts_roundness	string_multiple	Clasts Roundness	
fine_grains_roundness	string_multiple	Fine Grains Roundness	
colour_munsell	string_multiple	Color (Munsell chart)	
shape_clasts_coarse	string_multiple	Shape of Clasts	
surfacetexture_coarse	string_multiple	Surface Texture of Clasts	

3.13 Borehole Expansion Samples

Borehole expansion samples were taken at site 5068_2_A during the percussion drilling phase of the drilling operation from the excess material recovered after the casing had been advanced to the bottom depth of the previous core run. This excess material is a disturbed mix of the last core/casing interval, but the components are relatively original. They were stored in standard 5 l buckets as backup/additional bulk samples.

mDIS Table Borehole Expansion Samples (1 file)

Name		BoreholeExpansionSamples	
ParentModel	ProjectHole		

Name	Type	Label	Description
id	integer	ID	id (database id)
hole_id	integer	Hole	parent id (database id)

sample_number	integer	Expansion Sample Number	
combined_id	string	Borehole Expansion Sample Combined ID	
igsn	string	IGSN	International Generic Sample Number
top_depth_mbs	integer	Top Depth [mbs]	
bottom_depth_mbs	integer	Bottom Depth [mbs]	
weight	double	Weight [kg]	
sampling_date_time	dateTime	Sampling Date-Time	
lithology	string	Lithology	
curator	string	Curator	
comment	string	Additional Information	

4 Borehole Measurements

Chapters 3.1 and 3.2 describe in detail how the pre-processing of the DOVE data of the four measurement campaigns was done at Site 1 and Site 2. This includes, among other things, the matching of the depths of the individual measurements, the elimination of false measurement data, the splicing of measurement curves etc. With this knowledge it can be understood how to get from the raw data to the respective composite data set, which is e.g. the basis for the presentation of the measurements in respective PDF files.

For data files and details on the measurements please see the Operational Report of the DOVE Phase 1 project (DOVE-Phase 1 Scientific Team et al., 2023a). Not included in the preprocessing are BHTV and VSP data. The VSP data files for 5068_1 and 5068_2 are available as .seggy files, .jpg files for a better overview, coordinates in files for GIS software, a map as pdf and .txt files with the following columns: Source ID (SID), X, Y as can also be found in the .seggy header. There are no picks for VSP_Z_5068_1_B as they could cause confusion.

4.1 Preprocessing Site 1 (5068_1)

The following procedure was used to compile the raw data, which was mostly measured in two/three depth sections, into a composite file.

3.1.1 Campaign 1: 5068_1_A

Step 1:

Reference depth is the depth of the first measurement on 10.05.2021. If there is a risk of a borehole collapsing due to unconsolidated sediments, we start the logging program with the SGR probe in the drill pipe and/or casing. SGR (143-0 m) => GR = master curve for the depth!

This results in the following depth shifts for the remaining measurements by means of optical determination:

CAL = -0.3 m, DLL = 0 m, NN = -0.4 m, PE = -0.3 m, SGR (130-160 m) = 0.5 m, SONIC = 0.5 m, SUSZ+GR = 0.5 m, TEMPSAL+GR = 2.7 m.

Since the SUSZ and TEMPSAL probes also carried a GR sensor with each measurement, the depth difference between the respective measurements can be determined by comparing the SGR master curve and this data.

Step 2:

SGR in CH (cased hole) -> SGR in OH (open hole): Influence of drill string considered by factor 1.3 between 143 m and 43 m depth. Above 43 m depth, the SGR sonde measured through both the drill string and a casing. Therefore, a factor of 1.8 had to be applied here to eliminate the influence of both steel pipes.

Step 3:

Based on the cable tension (Tension curve) it can be determined when the probe lifted off from the lowest point of the borehole. Data registered before that are discarded.

Step 4:

Data that are affected by the casing are not used in the composite file (and in the figure). Examples: The SUSZ tool reacts to the piping approx. 1 m before it. Due to the design of the DLL probe, the drill string up to several metres disturbs resistivities before the tool reaches the drill bit/casing shoe.

The same applies to parameters that can only measure in liquid-filled boreholes: Data above the water level are not used (e.g., SALTEMP).

Step 5:

Determination of v_p from SONIC data: The first insertions of the two receivers near and far are picked in the full wave field display (dlis-file). From the time difference (far-near), the velocity v_p can be determined from the fixed distance between the two receivers (0.5 m for the LIAG SONIC probe).

Step 6:

Smoothing the porosity- and the v_p -curves with a 10 points average filter.

Step 7:

Determine splice points between each measurement of a parameter (optical determination):

SGR: 133 m.

3.1.2 Campaign 2: 5068_1_C

Step 1:

Reference depth is the depth of the first measurement on 11.11.2021. If there is a risk of a borehole collapsing due to unconsolidated sediments, we start the logging program with the SGR probe in the drill pipe. SGR => GR = master curve for the depth!

This results in the following depth shifts for the remaining measurements by means of optical determination:

DIP+GR = 0.4 m, DLL = -0.4 m, NN = -0.2 m, PE = -0.6 m, SONIC = -0.4 m, SUSZ+GR = 0.4 m, TEMPSAL+GR = 0.2 m.

Since for the DIP, SUSZ and TEMPSAL probes the same GR sensor was additionally included in the measurements, a comparison between the master SGR curve and these data can be used to determine the depth difference between the respective measurements.

Step 2:

SGR in CH (cased hole) -> SGR in OH (open hole): Influence of drill string considered by factor 1.3 between 164 m and 0 m depth.

Step 3:

Based on the cable tension (Tension curve) it can be determined when a probe lifted off from the lowest point of the borehole. Data registered before that are discarded.

Step 4:

Data that are affected by the casing/drill string are not used in the file (and in the figure).

Examples: The SUSZ tool reacts to the steel piping approx. 1 m before reaching it. Due to the design of the DLL probe, the drill string up to several metres disturbs resistivities before it reaches the drill bit.

The same applies to measurement parameters that can only measure in liquid-filled boreholes: Data above the water level are not used (e.g., SALTEMP, PE).

Step 5:

Determination of v_p from SONIC data: The first insertions of the two receivers near and far are picked in the full wave field display (dlis-file). From the time difference (far-near), the velocity v_p can be determined from the fixed distance between the two receivers (0.5 m for the LIAG SONIC probe).

Step 6:

Smoothing the porosity- and the v_p -curves with a 10 points average filter.

3.1.3 Campaign 3: 5068_1_A

Step 1:

Reference depth is the depth of the first measurement on 09.03.2022. We start the logging program with the SGR probe. SGR => GR = master curve for the depth!

This results in the following depth shifts for the remaining measurements by means of optical determination:

AIND+GR (0-97 m) = 0 m, AIND+GR (95-155 m) = -0.1 m, SONIC+GR = 0 m, SUSZ+GR = 0 m.

Since a GR sensor was also used in the measurements for the AIND, SONIC, and SUSZ probes, an additional comparison between the SGR master curve and this data is used to determine the depth difference between the respective measurements.

Step 2:

Based on the cable tension (Tension curve) it can be determined when a probe lifted off from the lowest point of the borehole. Data registered before that are discarded.

Step 3:

Data that are affected by the non-presence of liquid-filled boreholes are not used in the file (and in the figure), e.g., SONIC.

Step 4:

Determination of v_p from SONIC data: The first insertions of the two receivers near and far are picked in the full wave field display (dlis-file). From the time difference (far-near), the velocity v_p can be determined from the fixed distance between the two receivers (0.5 m for the LIAG SONIC probe).

Step 5:

Since the AIND probe of the LIAG can only measure resistivities up to a maximum of several hundred Ωm , only values up to 200 Ωm are shown in the corresponding pdf file.

Step 6:

Smoothing the v_p -curve with a 10 points average filter.

3.1.4 Campaign 3: 5068_1_B

Step 1:

Reference depth is the depth of the first measurement on 10.03.2022. We start the logging program with the SGR probe. SGR => GR = master curve for the depth!

This results in the following depth shifts for the remaining measurements by means of optical determination:

AIND+GR = 0.2 m, SONIC+GR = 0 m, SUSZ+GR = 0.2 m.

Since a GR sensor was also used in the measurements for the AIND, SONIC, and SUSZ probes, an additional comparison between the SGR master curve and this data is used to determine the depth difference between the respective measurements.

Step 2:

Based on the cable tension (Tension curve) it can be determined when a probe lifted off from the lowest point of the borehole. Data registered before that are discarded.

Step 3:

Data that are affected by the non-presence of liquid-filled boreholes are not used in the file (and in the figure), e.g., SONIC.

Step 4:

Determination of v_p from SONIC data: The first insertions of the two receivers near and far are picked in the full wave field display (dlis-file). From the time difference (far-near), the velocity v_p can be determined from the fixed distance between the two receivers (0.5 m for the LIAG SONIC probe).

Step 5:

Since the AIND probe of the LIAG can only measure resistivities up to a maximum of several hundred Ωm , only values up to 500 Ωm are shown in the corresponding pdf file.

Step 6:

Smoothing the v_p -curve with a 10 points average filter.

3.1.5 Campaign 3: 5068_1_C

Step 1:

Reference depth is the depth of the first measurement on 09.03.2022. We start the logging program with the SGR probe. SGR => GR = master curve for the depth!

This results in the following depth shifts for the remaining measurements by means of optical determination:

AIND+GR = 0 m, PE = 0 m, SONIC+GR = 0.4 m, SUSZ+GR = 0 m.

Since a GR sensor was also used in the measurements for the AIND, SONIC, and SUSZ probes, an additional comparison between the SGR master curve and this data is used to determine the depth difference between the respective measurements.

Step 2:

Based on the cable tension (Tension curve) it can be determined when a probe lifted off from the lowest point of the borehole. Data registered before that are discarded.

Step 3:

Data that are affected by the non-presence of liquid-filled boreholes are not used in the file (and in the figure), e.g., SONIC.

Step 4:

Determination of v_p from SONIC data: The first insertions of the two receivers near and far are picked in the full wave field display (dlis-file). From the time difference (far-near), the velocity v_p can be determined from the fixed distance between the two receivers (0.5 m for the LIAG SONIC probe).

Step 5:

Since the AIND probe of the LIAG can only measure resistivities up to a maximum of several hundred Ωm , only values up to 200 Ωm are shown in the corresponding pdf file.

Step 6:

Smoothing the v_p -curve with a 10 points average filter.

4.2 Preprocessing Site 2 (5068_2)

Step 1:

The data are corrected for depth on a daily basis. Reference is the depth of the first measurement on 26.10.2021.

26.10.2021: First measurement: SUSZ measurement incl. Gamma Ray => GR = master curve for the depth! This results in the following depth shifts for the remaining measurements by means of optical determination:

SUSZ = 0 m, SGR = -0.3 m, DLL = -1.3 m, PE = 0.2 m, NN = -1.0 m, CAL = -0.9 m, EBS = -0.5 m, SONIC = 0 m.

27.10.2021: SUSZ = -0.3 m, SGR = 0.1 m, DLL = -0.5 m, NN = 0.2 m, SONIC = 0 m.

28.10.2021: SUSZ = -0.3 m.

29.10.2021: SGR = 0 m, PE = -0.3 m, NN = 0.1 m, CAL = 2.6 m, SONIC = 0 m.

Step 2:

SGR in CH (cased hole) -> SGR in OH (open hole): Influence of steel piping considered by factor 1.3 above 104 m depth.

Step 3:

Based on the cable tension (tension curve) it can be determined when a probe lifted off from the lowest point of the borehole. Data registered before that are discarded.

Step 4:

Data that are affected by the casing are not used in the composite file and in the figure. Examples: The Susz curve reacts to the piping approx. 1 m before reaching it. Due to the design of the DLL probe, resistivities are disturbed by the pipe/drill string up to several metres before it reaches the pipe shoe.

Step 5:

Determination of v_p from SONIC data: The first insertions of the two receivers near and far are picked in the full wave field display. From the time difference, the velocity v_p can be determined from the fixed distance between near and far (0.5 m for the LIAG sonic probe).

Step 6:

Determine splice points between each measurement of a parameter (optical determination):

SGR: 122.1 m and 180 m, DLL: 180 m, PE: 177 m, Susz: 120 m and 180 m, NN: 121.5 m and 176.5 m, CAL: 177 m, Sonic: 119.4 m and 178.1 m.

For EBS only one measurement exists, because the probe showed a defect after the first measurement.

4.3 Borehole Logging Files

- The recorded field data are stored in ASCII files. The exception is the non-line data generated with the BHTV, Sonic and VSP probes. The extensive ultrasonic images of the borehole wall registered by the BHTV sonde are stored as TFD files for use e.g. with the WellCAD software. The complete wavefields registered by the SONIC sonde are stored as DLIS files. The VSP data are given in SGY format. All data are checked and edited.
- The preprocessed line data for each hole and campaign are summarized in a composite file (ASCII).
- Additionally, composite log plots (1:1000) are prepared as PDF documents to give a quick overview over the line data.

4.4 Borehole measurements available from the legacy Sites 3 through 6

Work in progress

5 Data Tables

5.1 Lithological Units and Core Description

The macroscopic lithological description (Visual Core Description VCD) is based on section units. Each core section has been described separately and the respective lithological sections units have been assigned to predefined LITHO_UNITS. These LITHO_UNITS have been defined within the DOVE project based on the encountered lithologies and a modified version of the definitions used by Krüger and Kjær (1999). This applies to all core material of DOVE Phase 1.

Files related to the lithological description comprise:

- list of LITHO_UNITS (1 file; csv)
- tables summarizing the depth distribution of the LITHO_UNITS for each section of a cored hole (csv; 1 for each hole)
- digitalized protocols of the VCD logs (zip file for each hole)
- a summarizing visual lithological column for each borehole (pdf)

5.2 Multi Sensor Core Logging (Sites 1 & 2)

For Site 1 (5068_1), p-wave velocity, wet bulk density, and magnetic susceptibility were measured on each core section using the GEOTEK-multi-sensor-core-logger (MSCL) (Geotek Limited, Daventry, Northants, UK) at the University of Bern. At Site 2 (5068_2) natural gamma radiation including K, Th, and U-Log was also measured. Here, the core sections were measured in the field laboratory using ICDP's GEOTEK-MSCL. The resolution was 5 mm. The same data processing was applied for both sites.

Before the first core was measured, all sensors were calibrated according to the instructions from Geotek, and a background measurement of the natural gamma radiation was done. Each measurement session started with calibration by measuring standards consisting of a mixture of aluminum and deionized H₂O (see construction scheme for further details, Fig. 3). The following table summarizes all parameters used to calibrate the raw log data, except the depth. The calibration was done with the integrated Geotek software for further information (see Geotek MSCL manual). Only the baseline correction of the magnetic susceptibility data was done during a separate step (see MSCL-data processing iv). The slope (B) and intercept (C) used for the gamma density processing was calculated with an external excel-file (5068_mscl_cal_density_file.xls). Due to a malfunction of the laser distance sensor pair for Site 2 cores, the core-diameter variation could not be detected for 5056_2, and a constant core diameter of 104 mm had to be assumed. For both sites, the p-wave data were of very poor quality, likely due to bad coupling between sensors, liner, and sediment. Therefore, the data were discarded.

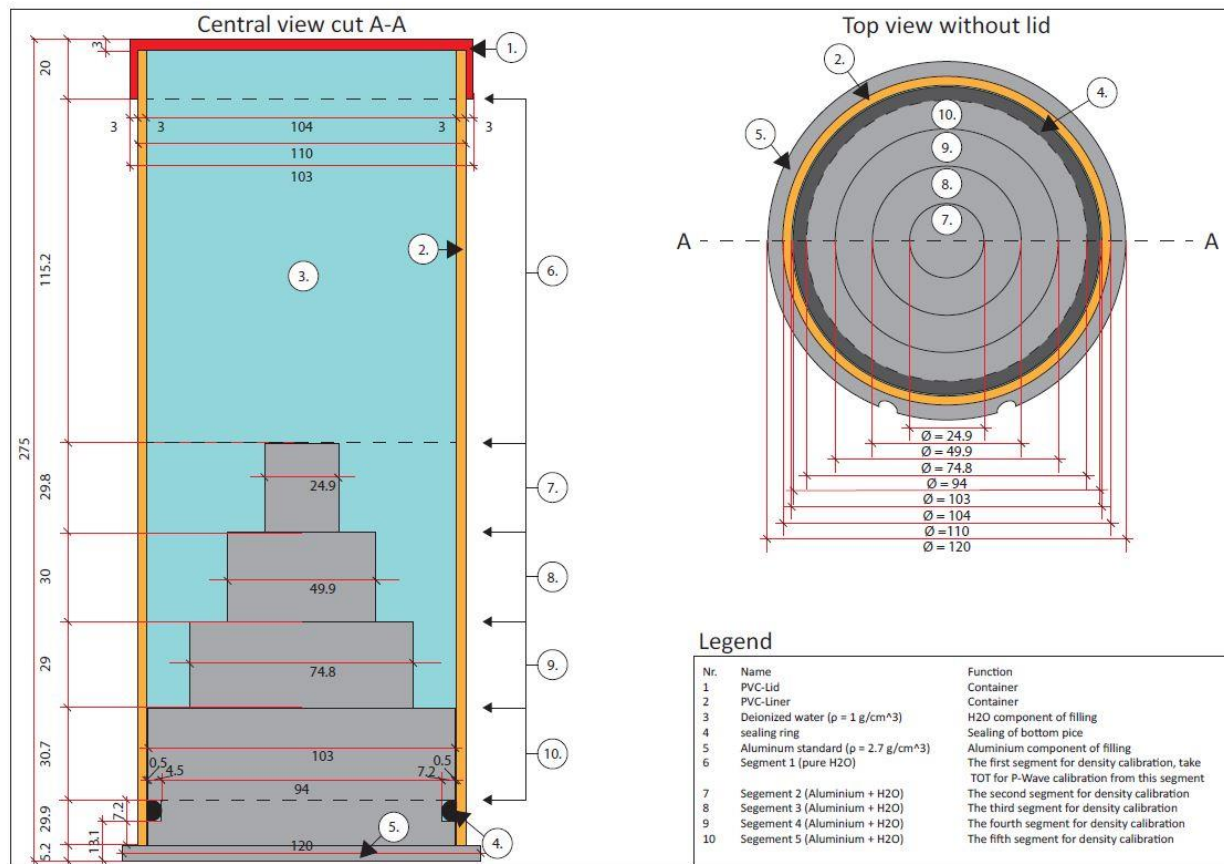


Figure 3: The construction scheme of the MSCL calibration piece was measured at the beginning of each measurement session.

- MSCL-calibration input parameter file: 5068_2_A_mscl_calibration_input_parameters.csv.
- Not described additional calibration file: 5068_mscl_cal_densety_file.xls (Slop and intercept of Gamma density)
-

Log	Parameter	Unit	mscl explanation
measurement ID	mes_id	/	Identifier of measurement/calibration cycle
Core Thickness (CT)	RCT [cm]	[cm]	Core diameter (input for 5068_mscl_cal_densety_file.xls)
	W [cm]	[cm]	Thickness of liner walls (2x thickness of wall, input for 5068_mscl_cal_densety_file.xls)
Gamma Density (Den1)	Segment 1 [cps]	[cps]	Intensity (average gamma counts from calibration section segment 1, raw calibration data, input for 5068_mscl_cal_densety_file.xls)
	Segment 2 [cps]	[cps]	Intensity (average gamma counts from calibration section segment 2, raw calibration data, input for 5068_mscl_cal_densety_file.xls)

	Segment 3 [cps]	[cps]	Intensity (average gamma counts from calibration section segment 3, raw calibration data, input for 5068_mscl_cal_densety_file.xls)
	Segment 4 [cps]	[cps]	Intensity (average gamma counts from calibration section segment 4, raw calibration data, input for 5068_mscl_cal_densety_pwave_file.xls)
	Segment 5 [cps]	[cps]	Intensity (average gamma counts from calibration section segment 5, raw calibration data, input for 5068_mscl_cal_densety_pwave_file.xls)
	A	/	Slope (if a correction second degree (ax^2+bx+c), is selected, default = 0)
	B	/	Slope (for a linear correction, calculated in an additional file: 5068_mscl_cal_densety_file.xls)
	C	/	Intercept (for linear correction, calculated in an additional file: 5068_mscl_cal_densety_file.xls)
Magnetic susceptibility (MS1)	A	/	Slope (for a linear correction, default = 1)
	B	/	Intercept (for linear correction, default = 0)
	Den	/	If set to 1, converted to mass-specific values; if set to 0, no mass conversion is applied; default = 0
	LD [cm]	[cm]	Diameter of the used Loop-sensor, if set to 0, no volume conversion is applied.
	bslc cal [Six10 ⁻⁵]	[Six10 ⁻⁵]	Calculated baseline correction
	bslc app [Six10 ⁻⁵]	[Six10 ⁻⁵]	Applied baseline correction value
	bslc orig	/	Explains the origin of the correction value: calculated from the calibration section 0-15 cm; manual input; calculation was < -0.5, converted to 0
Natural Gamma (NGAM)	B	[cps]	Background, gets subtracted from raw data
	Scale	/	Slope of conversion equation (since no conversion is applied, default = 1)
	Offset	/	Intercept of conversion equation (since no conversion is applied, default = 0)
k	Scale	/	Slope of conversion equation, [cps] -> [%], calculated by internal calibration of software/sensors
	Offset	/	Intercept of conversion equation
u	Scale	/	Slope of conversion equation, [cps] -> [ppm], calculated by internal calibration of software/sensors
	Offset	/	Intercept of conversion equation
Th	Scale	/	Slope of conversion equation, [cps] -> [ppm], calculated by internal calibration of software/sensors
	Offset	/	Intercept of conversion equation

5.2.1 MSCL data processing:

- i) Individual data files were loaded, and a measurement id was added to each measurement point. Calibration and measurement data were separated and combined in two separate files, and additionally, a core section id was added to each measurement point of the non-calibration data;
- ii) a quality class was appointed to each data point (0 = good; 1= possibly weakly disturbed; 2 = heavily disturbed; 3 = core loss; 4 = placeholder/core ends; 5 = artificial overlength);
- iii) data of empty sections of liners, representing core loss, were removed;
- iv) a baseline correction was applied to the corresponding magnetic susceptibility data to correct potential systematic shifts in the data (subtraction of the average of the calibration data between 0.5 and 15 cm of each measurement cycle, or by a manual set input);
- v) low-density data ($<1.5 \text{ g/cm}^3$), considered heavily disturbed sections, were excluded from the density log;
- vi) The overall data quality of the p-wave-data was very poor and the log excluded from data set;
- vii) the depth of the cleaned MSCL-logs was corrected based on the driller's depth. The corresponding driller depth served as the depth of the top data point, increasing by 0.5 cm with each further data point of the section. If the section is longer than the nominal section length, the data-point spacing is adjusted to meet the nominal section length. Such overlengths were considered as artificial/expansion;
- viii) the data from the upper- and lowermost cm in each section was considered likely disturbed; thus, the logs were excluded (converted to NaN's). This also prevented possible overlapping issues at the core ends.

There are two files available: i) File *data_cal* contains the combined data from the calibration section of all measurements; ii) File *data* contains the processed and cleaned data sets Filename:

- 5068_1_C_Combined_MSCL_data_cal.csv and 5068_1_C_Combined_MSCL_data.csv
- 5068_2_A_Combined_MSCL_data_cal.csv and 5068_2_A_Combined_MSCL_data.csv

Column name	Unit	Description
Composite_depth [cm]	cm	Corrected composited total depth
Rescaled SECT_DEPTH [cm]	cm	Corrected/rescaled in-section depth
SECT_NUM_MC	/	The number of measured sections starts at 1 at the beginning of each measurement session.
SECT_DEPTH [cm]	cm	Unaltered in-section depth
CT [cm]	cm	Core thickness
Dens [g/cc]	g/cm^3	Wet bulk density log (unfiltered)
Dens [g/cc] (pw and dens filtered)	g/cm^3	Wet bulk density log (filtered, $<1.5 \text{ g/cm}^3$ removed)
Mag_Sus	$\text{SI} \times 10^{-5}$	Magnetic susceptibility log (uncorrected)
Mag_Sus BS_cor	$\text{SI} \times 10^{-5}$	Magnetic susceptibility log (baseline corrected)
Nat_Gamma [cps]	cps	Natural gamma radiation log (sum of K, U, and Th logs)
K [%]	%	Potassium log
U [ppm]	ppm	Uranium log

Th [ppm]	ppm	Thorium log
core_quality	/	Quality of recovered sediment (0 = good; 1 = possibly disturbed; 2 = heavily disturbed; 3 = core loss/backfall; 4 = place holder/core ends; 5 = artificial overlength)
mes_ID	/	Measurement session id (the link between actual data and the corresponding calibration section)
section_ID	/	Measured core section

MSCL_data_cal file

Column name	Unit	Description
SECT_NUM_MC	/	The number of measured sections starts at 1 at the beginning of each measurement session.
SECT_DEPTH [cm]	cm	Unaltered in-section depth
CT [cm]	cm	Core thickness
Dens [g/cc]	g/cm ³	Wet bulk density log (unfiltered)
Mag_Sus [SI x 10 ⁻⁵]	SI x 10 ⁻⁵	Magnetic susceptibility log (uncorrected)
Mag_Sus BS_cor [SI x 10 ⁻⁵]	SI x 10 ⁻⁵	Magnetic susceptibility log (baseline corrected)
Nat_Gamma [cps]	cps	Natural gamma radiation log (sum of K, U, and Th logs)
K [%]	%	Potassium log
U [ppm]	ppm	Uranium log
Th [ppm]	ppm	Thorium log
mes_ID	/	Measurement session id (the link between actual data and the corresponding calibration section)

5.3 Water-content measurements (WACO) (Site 1 and 2)

Samples, with a sample length of 4 cm, were taken every 50 cm on sections from holes 1-C and 2-A whenever possible. Each sample was divided into three sub-samples for analyses: CCOM-, GRSZ-, and WACO-samples. All sub-samples were freeze-dried, and mean water content was derived from the three subsamples using the difference between wet and dry weight according to ISO 11465. A standard weight of 8.052 g was assumed for the empty container.

$$\frac{\text{Bruttowetmass} - \text{Bruttodrymass}}{\text{Bruttodrymass} - \text{Mass of empty container}} * 100$$

Data files for Water content (WACO)

Column name	Unit	Description
Section ID	/	Core section of origin
IGSN CCOM	/	IGSN of CCOM-subsample
IGSN WACO	/	IGSN of WACO-subsample
IGSN GRSZ	/	IGSN of GRSZ-subsample
Center Sample Depth [mcd bs]	m	Center of sample interval in composite depth
Distance from section top Depth [cm]	cm	Distance between the center of the sample interval and top of the core section
WC mean [Wt%]	wt%	Mean water content based on the water content of the three sub-samples
WC std [Wt%]	wt%	Mean water content standard deviation

5.4 Carbon, Nitrogen and Sulfur Data (TNSC, ITC and Carbonate Content; CCOM) (Sites 1-6)

Total carbon (TC), total nitrogen (TN), total sulfur (TS), and total inorganic carbon (TIC) were analyzed from the fine fraction (<63 μm) of the CCOM-subsamples. Total organic carbon (TOC) was derived as the differences between TC and TIC. The weight percent [wt%] of total carbonate (TCA; CaCO_3) and total organic matter (TOM) were calculated using a stoichiometrically simplified approach ($\text{TCA} = \text{TIC} \times 8.3$; $\text{TOM} = \text{TOC} \times 1.8$; Meyers and Teranes, 2001)

Available data files are *Filename: 5068_2_A_CCOM*,

Data Files: CCOM

Column name	Unit	Description
Sample ID	/	CCOM-sample-ID
IGSN	/	IGSN of CCOM sample
Center Sample Depth [mcd bs]	m	Center of sample interval in composite depth
Distance from section top Depth [cm]	cm	Distance between the center of the sample interval and top of the core section
TN [wt%]	wt%	Total nitrogen content
TC [wt%]	wt%	Total carbon content
TS [wt%]	wt%	Total sulfur content
TOC [wt%]	wt%	Total organic carbon content
TIC [wt%]	wt%	Total inorganic carbon content
TOM [wt%]	wt%	Total organic matter content
TCA [wt%]	wt%	Total carbonate content

5.5 Undrained uniaxial compressive strength (POCK) and uniaxial shear strength (VANE) measurements

Where applicable, undrained shear strength (c_u') and undrained uniaxial compressive strength (q_u') were measured at 25, 50, and 75 cm section depth with a pocket vane shear tester (Eijkelpamp, Model 14.10) and a pocket penetrometer (Impact Test Equipment Ltd, Model SL131). The measurements were executed according to the Swiss Norm: VSS 70 350a.

Filename: 5068_2_A_POCK

Column name	Unit	Description
Sample ID	/	POCK-sample-ID
IGSN	/	IGSN of POCK measurement
Center Sample Depth [mcd bs]	m	Center of sample interval in composite depth
Distance from section top Depth [cm]	cm	Distance between the center of the sample interval and top of the core section
Qu[kPa]	[kPa]	uniaxial shear strength (q_u')
Quality	/	Quality of measurement: 0 = good; 1 = invalid; 2 = out of scale but valid

Filename: 5068_2_A_VANE

Column name	Unit	Description
Sample ID	/	POCK-sample-ID
IGSN	/	IGSN of POCK measurement
Center Sample Depth [mcd bs]	m	Center of sample interval in composite depth
Distance from section top Depth [cm]	cm	Distance between the center of the sample interval and top of the core section
Cu[kPa]	[kPa]	undrained shear strength (c_u')
Quality	/	Quality of measurement: 0 = good; 1 = invalid; 2 = out of scale but valid

6 Images

- Digital images of section splits are available for holes 5068_1_C and 5068_2_A (jpg files)
- For all cored holes, hole overview reports are available. They contain all section images of one core (pdf).
- Selected images of CT-scans, used in Schaller et al. 2023 are available (jpg files).
- Where applicable, images of the cuttings (Holes 5068_1_A, 5068_1_B) are available (jpg).

7 References

Conze, R., Lorenz, H., Ulbricht, D., Elger, K., & Gorgas, T. (2017). Utilizing the International Geo Sample Number Concept in Continental Scientific Drilling During ICDP Expedition COSC-1. In *Data Science Journal* (Vol. 16). Ubiquity Press, Ltd. <https://doi.org/10.5334/dsj-2017-002>

DOVE - Phase 1 Scientific Team; Beraus, S., Buechi, M. W., Bunes, H., Burschil, T., Fiebig, M., Firla, G., Gabriel, G., Gegg, L., Grelle, T., Heeschen, K., Kroemer, E., Lehne, C., Lüthgens, C., Neuhuber, S., Preusser, F., Schaller, S., Schmalfuss, C., Schuster, B., Tanner, D. C., Thomas, C., Tomonaga, Y., Wieland-Schuster, U., and Wonik, T.: Drilling Overdeepened Alpine Valleys (DOVE) - Operational Dataset of DOVE Phase 1. GFZ Data Services. <https://doi.org/10.5880/ICDP.5068.001>, 2023

DOVE-Phase 1 Scientific Team, Anselmetti, F. S., Beraus, S., Buechi, M. W., Bunes, H., Burschil, T., Fiebig, M., Firla, G., Gabriel, G., Gegg, L., Grelle, T., Heeschen, K., Kroemer, E., Lehne, C., Lüthgens, C., Neuhuber, S., Preusser, F., Schaller, S., Schmalfuss, C., Schuster, B., Tanner, D. C., Thomas, C., Tomonaga, Y., Wieland-Schuster, U., and Wonik, T.: Drilling Overdeepened Alpine Valleys (DOVE) – Operational Report of Phase 1. ICDP Operational Re-ports. GFZ German Research Centre for Geosciences. <https://doi.org/10.48440/ICDP.5068.001>, 2023

Krüger, J. and Kjær, K. H.: A data chart for field description and genetic interpretation of glacial diamicts and associated sediments - with examples from Greenland, Iceland, and Denmark, *Boreas*, 28, 386–402, <https://doi.org/10.1111/j.1502-3885.1999.tb00228.x>, 1999.

Meyers, P. A. and Teranes, J. L.: Sediment Organic Matter, in: *Tracking Environmental Change Using Lake 474 Sediments: Physical and Geochemical Methods*, edited by: Last, W. M. and Smol, J. P., Springer Netherlands, 475 Dordrecht, 239–269, https://doi.org/10.1007/0-306-47670-3_9, 2001.

Schaller, S., Buechi, M. W., Schuster, B. and Anselmetti, F. S. (2023). Drilling into a deep buried valley: A 252 m long sediment succession from a glacial overdeepening in northwestern Switzerland, *Scientific Drilling*, 32, <https://doi.org/10.5194/sd-32-27-2023>

Erklärung

gemäss Art. 18 PromR Phil.-nat. 2019

Name/Vorname: Schaller Sebastian

Matrikelnummer: 15-114-119

Studiengang: PhD in Erdwissenschaften

Bachelor ☐

Master ☐

Dissertation ☒

Titel der Arbeit: ICDP DOVE Project:
Investigating the erosion and infilling of overdeepened Alpine valleys
by combining scientific drilling with geophysical exploration

LeiterIn der Arbeit: Prof. Dr. Flavio S. Anselmetti
Dr. Marius W. Buechi

Ich erkläre hiermit, dass ich diese Arbeit selbständig verfasst und keine anderen als die angegebenen Quellen benutzt habe. Alle Stellen, die wörtlich oder sinngemäss aus Quellen entnommen wurden, habe ich als solche gekennzeichnet. Mir ist bekannt, dass andernfalls der Senat gemäss Artikel 36 Absatz 1 Buchstabe r des Gesetzes über die Universität vom 5. September 1996 und Artikel 69 des Universitätsstatuts vom 7. Juni 2011 zum Entzug des Dokortitels berechtigt ist. Für die Zwecke der Begutachtung und der Überprüfung der Einhaltung der Selbständigkeitserklärung bzw. der Reglemente betreffend Plagiate erteile ich der Universität Bern das Recht, die dazu erforderlichen Personendaten zu bearbeiten und Nutzungshandlungen vorzunehmen, insbesondere die Doktorarbeit zu vervielfältigen und dauerhaft in einer Datenbank zu speichern sowie diese zur Überprüfung von Arbeiten Dritter zu verwenden oder hierzu zur Verfügung zu stellen.

Bern, 19.12.2024

Ort/Datum


Unterschrift